



Title Tectonics and mineralization of Wadi
Allaqi, south Eastern Desert, Egypt

Name Yahia Abbas Hamed Abdalla El Kazzaz

This is a digitised version of a dissertation submitted to the University of Bedfordshire.

It is available to view only.

This item is subject to copyright.

**Tectonics and Mineralization of
Wadi Allaqi,
south Eastern Desert,
Egypt**

Yahia Abbas Hamed Abdalla (El Kazzaz)

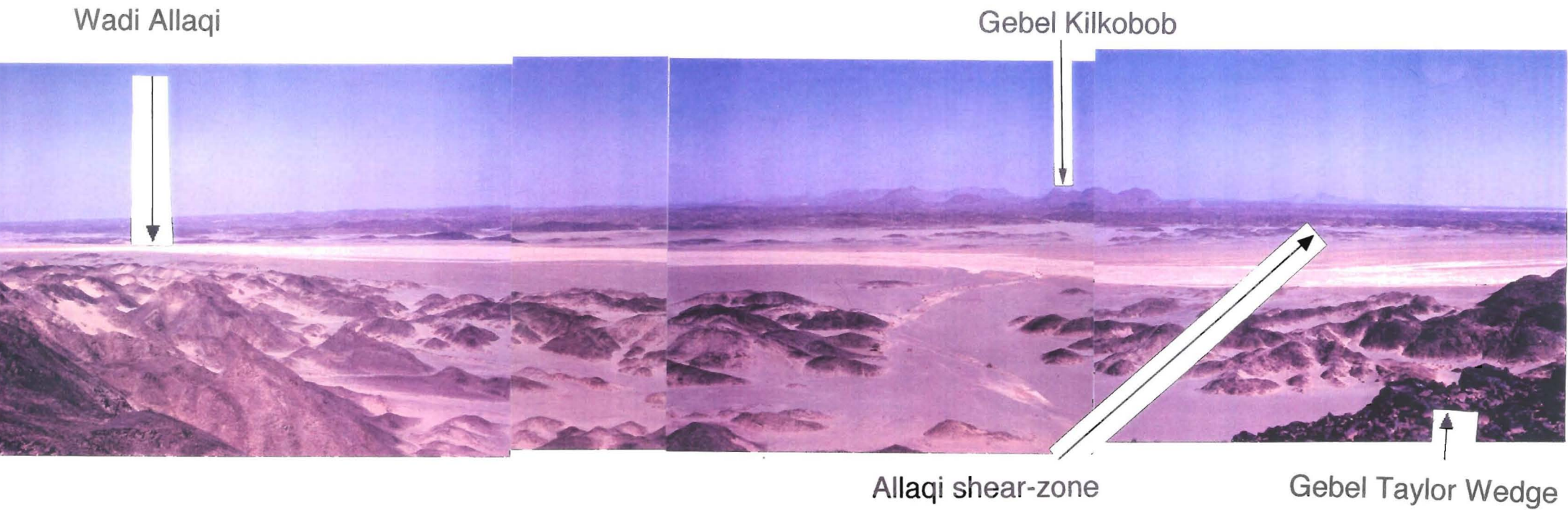
**A thesis submitted to the Faculty of Science
& Computing, University of Luton, in partial
fulfilment of the requirements for the degree
of Doctor of Philosophy**

Collaborating Institution : Egyptian Geological Survey and Mining Authority

August 1995

Reference UNIVERSITY OF LUTON PAULINE L. LINDSEY	
3601482537	
551.80962	
EL	ENQUIRY DESK

**I dedicate this thesis
to the memory of my Father**



Frontispiece: a panoramic view of the northern part of the study area; taken from Gebel Taylor and surveying the complex thrust duplex below the Allaqi shear-zone

Acknowledgements

I wish to express my sincere thanks and deepest gratitude to my supervisors Dr W. E. G. Taylor, my director of studies, Dr. R. D. Young and Dr. A. A. Rashwan. Thanks are due to the Egyptian Geological Survey and Mining Authority, in particular Drs. A. A. Dardir and A. A. Hussein for their support and encouragement, to Professor S. El Gaby for drawing my attention to Wadi Allaqi as an area ripe for study, and to my colleague Mr H. Mahmoud for assisting me during the preparation of this thesis. The University of Luton, which supported this study by the award of a research studentship, and those colleagues of mine at Luton, who kindly assisted me during the progress of this investigation and in particular Miss Donna Bakewell, are especially acknowledged. Several people, external to Luton who provided material assistance during this investigation, are gratefully acknowledged especially : Mr T. T. Turner (Military Survey Geodetic Support Branch UK Universal Transverse Mercator (UTM) grid referencing system), Dr. N. Walsh (Royal Holloway College - major and trace element analyses), Dr. K. Jarvis (now Imperial College, London - gold analyses), Professor A. Rankin (Kingston University - fluid inclusion analyses), Dr. A. E. Fallick (Scottish Universities Research and Reactor Centre (SURRC), East Kilbride - stable isotope analyses), Dr. A. Kearsley (Oxford Brookes University - electron microprobe analyses), and Dr E. A. O'Connor (British Geological Survey - Thematic Mapper satellite Imagery; Figs. 2.1 & 5.3).

Preface

Arabic place names translated into English can have variations in spelling. Throughout the text of this thesis spelling of place names is consistent but variations do occur in the list of references which reflect the preferences of other authors at various times in the past. Text-figure 1.2 shows the location of the main geographical places in central Wadi Allaqi. The symbols for rock-forming minerals recommended by Kretz (1983) are used in text-figures and Appendix A. Use of other non-standard abbreviations have been kept to a minimum and are given in full where they first occur in the text. A list of abbreviations used follows this preface.

A ten-figure Universal Transverse Mercator (UTM) grid system has been applied for the first time in the Eastern Desert of Egypt in the referencing for geological maps and UTM grid references have been used instead of longitude and latitude (Figs. 1.3a,b), geological localities and samples in the text and appendices throughout this thesis (the methodology is outlined in Appendix F). The Thematic-Mapper satellite images, which used for this study, were produced at the British Geological Survey (BGS) in collaboration with Egyptian Geological Survey and Mining Authority (EGSMA).

The terminology and usage for lithostratigraphic units in strongly-faulted zones of the Earth's Lithosphere are not yet firmly established. Throughout this thesis an informal tectonic-stratigraphy nomenclature (in the sense of Soper & England 1995) has been developed and used. This informal nomenclature is explained in chapter three. Major Precambrian stratigraphic terminology, as recommended by the International Union for Geological Sciences (Plume 1991), is followed throughout. The colours of rocks and minerals are described using the Rock-Color Chart of the American Geological Society (1970).

Standard structural terminology is used throughout this study (*e.g.*, Boyer & Elliott 1982; Dunnet 1969; Dunnet & Siddans 1971; Hammer & Passchier

1991; Lisle 1979, 1985; Ramsay 1967; Ramsay & Huber 1983, 1987; Simpson 1988). In this study the modified (White 1982) fault classification of Sibson (1977) is used. Azimuths of structures are given either by using the cardinal points of the compass or in degrees from north (0°) to south (180°) in a *clockwise* rotation.

Standard fluid inclusion and stable isotope terminology is used (*e.g.*, Roedder, 1984; Shepherd *et al.* 1985).

The thesis is arranged in six chapters with appendices and large text-figures (Figs. 1.3a,b & 1.4) in a pocket at the back. *Chapter one* describes the purpose, background and methodology for the investigation. *Chapter two* deals with the structures of the central Wadi Allaqi area with an emphasis on the shear-zones and the structural history which provides a basis for other studies. *Chapter three* documents the tectonic-stratigraphy and the geochemical signatures of the rocks. *Chapter four* is concerned with the granitic and late basaltic intrusions including their relative times of emplacement. *Chapter five* describes the gold mineralization and discusses the evidence for the processes which formed the mineralization. In *chapter six* the significance of the results of the investigation are discussed, conclusions reached and suggestions for further investigations are made.

list of abbreviations used in the thesis

AF	Atshani Formation
ande-basalt	andesitic-basalt
AST	axial-surface-trace
ASZ	Allaqi Shear-zone
AtG	Atshani Granite
Au	gold
CSst	Calcareous siltstone
D1, D2, D3, D4, D5	successive Pan-African deformation phases
DSDP	Deep-Sea Drilling Project
F1, F2, F3, F4	minor folds of successive deformation phases
FerVc	Ferruginous sandstone volcanoclastic
FG	Filat Granite
FI	fluid inclusion
Fm	Formation
FS	Filat Succession
GBF	Granite Boulder Formation
Gp	Group
GR	Grid Reference following by a ten-figure number with easting followed by northing
Gr	granite
GTW	Gebel Taylor Wedge
H ₂	hydrogen
H ₂ O	aqueous water
ICP-AES	Inductively coupled plasma-atomic emission spectrometry
ICP-MS	Inductively coupled plasma-mass spectrometry
KF	Kazzaz Formation
KG	Kilkobob Granite

Kh	Kholoud Formation
KS	Kilkobob Succession
L1, L2	fluids in fluid inclusions
L1, L2, L3	lineations of successive deformation phases
M & T any	major and trace analyses
m	metre
Mbm	Meta-basaltic member
Mbr	Member
MCM	Metaconglomerate Member
MF	Murra Formation
MGU	Meta-gabbro unit
MLF	Meta-limestone Formation
Mod	modal analyses
NERC	Natural Environment Research Council
NF	Neiqit Formation
PBF	Pyroclastic breccia Formation
PC M	Polymict Conglomerate Member
PCM	Pyroclastic and conglomerate Member
Peb	Pebble
Ref Lt	reflected light
S1, S2, S3, S4	foliation planes of given deformation phases
SMOW	Standard Mean Ocean Water
Sp. No.	Specimen number
Sst	Siltstone
T _e	freezing temperature
Tect-strat	Tectonic-stratigraphy
T _m	melting temperature
TS	thin section
URG	Um Relan Granite

URS	Um Relan Succession
Vc	Volcaniclastics
XRF	X-ray fluorescence
‰	parts per thousand

Abstract

Neoproterozoic volcanic, sedimentary and volcano-sedimentary rocks of central Wadi Allaqi were deformed and metamorphosed to greenschist facies during the Pan-African orogeny. Three major, geochemically and lithostratigraphically distinct, tectonic-stratigraphic Successions with an intermediate tectonically-emplaced unit of ophiolitic rocks (Gebel Taylor Wedge), which have been metamorphosed to blueschists facies prior to emplacement, are recognised. The tectonic pile has been intruded by four granitic plutons and basic igneous sills, which were emplaced at various stages in the tectonic history.

A series of large-scale thrust duplexes with a few major nappe-like folds and shear-zones, the most conspicuous of which is the Allaqi Shear-zone, structurally dominate the area. A complex polyphase structural history has been deduced consisting of earlier ductile and late more brittle deformation phases and this has been related to the regional metamorphic development.

A gold mineralized quartz vein system was emplaced syn-tectonically along the first deformation (D1) shear-zones. Data from structures, petrography, fluid inclusions and stable isotopes of oxygen and hydrogen tend to support a metamorphic provenance for the auriferous fluids.

The petrological, geochemical and structural evidence strongly support a back-arc basin environment for the sedimentary development of central Wadi Allaqi before the Pan-African Orogeny. A single Wilson Cycle is proposed for the evolution of the area, in which following an extensional phase, during which the marginal elements of the ancient *Mozambique Ocean* (in the sense of Dalziel 1991) were developed. Back-arc sedimentary rocks and volcanoclastic rocks were metamorphosed and transported as a thrust-duplex system northward over the Nile Craton and any associated marginal sedimentary sequence.

Contents

1. Introduction	1
1.1 Purpose of this investigation	1
1.2 Concurrent investigations	5
1.3 Methodologies employed for this study	5
2. Structural Geology	7
2.1 Introduction.	7
2.2 Large-scale structures	7
2.3 The deformation history	9
2.4 D1 deformation phase	9
2.4.1 Minor structures	16
2.4.2 Strain analysis	20
2.5 D2 deformation phase	24
2.6 D3 deformation phase	29
2.7 D4 deformation phase	29
2.8 D5 deformation phase	29
2.9 The Allaqi Shear-zone.....	35
2.10 Metamorphic history in relation to the tectonic history	42
2.11 Summary	45
3. Tectonic-stratigraphy	48
3.1 Introduction	48
3.2 Earlier Classifications	51
3.3 Filat Succession	53
3.3.1. General characteristics.....	53
3.3.2 The Neiqit Formation	53
3.3.3 The North Allaqi Group	54
3.4 Um Relan Succession	68
3.5 Kilkobob Succession	74

3.5.1 Pyroclastic Breccia Formation	76
3.5.2 Murra Formation	76
3.5.3 Meta-limestone Formation.....	78
3.6 Gebel Taylor Wedge.	80
3.7 Summary	86
4. Igneous Intrusions	88
4.1 Introduction	88
4.2 The granitic plutons	88
4.2.1 Atshani Granite	88
4.2.2 Um Relan Granite.....	94
4.2.3 Filat Granite	96
4.2.4 Kilkobob Granite.	96
4.2.5 Petrochemistry of the granitic bodies	100
4.3 Late basaltic sills and dykes.....	102
4.4 Late aplitic dykes.....	104
4.5 Discussion of the tectonics of the granites	104
4.6 Summary	105
5. Gold mineralization and its tectonic setting.....	106
5.1 Background	106
5.2 Objectives of this investigation	106
5.3 Structural setting	109
5.4 Gold geochemistry	112
5.5 Petrography of the mineralized zones.....	112
5.6 Fluid inclusions.....	120
5.7 Stable isotopes.....	124
5.8 Paragenesis	126
5.9 Summary	130
6. Discussion and Conclusions	133
6.1 Broader considerations	133

6.2 Tectonic evolution and setting	135
6.2.1 Limits of the Nile Craton and the Arabian-Nubian volcanic pile	135
6.2.2 Ophiolite belts.....	136
6.2.3 Suture zones / shear-zones and their sense of movement in Wadi Allaqi	139
6.2.4 Regional sense of movement.....	142
6.2.5 Radiometric dating of the Pan-African Orogeny	144
6.2.6 Reconstruction of the assembly of Gondwana	144
6.3 A model for the development of the central Wadi Allaqi.....	147
6.4 Outcomes and Conclusions	151
6.5 Suggestions for further work	153
References.....	155
APPENDICES	183
Appendix A List of samples	184
Appendix B Geochemical methodologies and data	197
Appendix C Strain data	206
Appendix D Fluid inclusion methodology and data	216
Appendix E Stable isotope methodologies and data	218
Appendix F UTM co-ordinate methodology.....	219

List of figures

Frontispiece: a panoramic view of the northern part of the study area.

1.1 African cratons and the Pan-African mobile belt showing location

of the area 2

1.2 The main geographical locations for central Wadi Allaqi 4

2.1 Thematic Mapper(TM)-imaged mosaic of the area 8

2.2 Polyphase deformation within the meta-limestone, Um Relan 11

2.3 Style of D1 mesoscopic structures 12

2.4 Examples of D1 duplexes and thrusts 13

2.5 Synoptic map of the D1 thrusts 14

2.6 The Gazira D1 recumbent fold 15

2.7 Map of the structural domains 17

2.8 Synoptic map showing geometrical variation of S1 & L1 18

2.9 Photomicrographs illustrating D1 fabrics 19

2.10 (a) Examples of strain data (Flinn diagram) 21

2.10 (b) Examples of strain data (R_f / ϕ diagram) 22

2.11 Map of regional strain 23

2.12 Block diagram demonstrating the movements along the thrusts 25

2.13 Style of D2 and D3 mesoscopic structures 26

2.14 Aerial photograph of Kilkobob D2 large-scale folds 27

2.15 Map showing geometrical variation of S2 and L2 28

2.16 Map showing geometrical variation of S3 and L3 30

2.17 Style of D4 mesoscopic structures 31

2.18 Map of D5 structures 33

2.19 Analyses of the late-stage D5 faults 34

2.20 Criteria for sense of shear 37

2.21 Sense of shear within shear-zones 38

2.22 Photomicrographic evidence for sense of shear 39

2.23 Map comparing the structures of D1 and Allaqi Shear-zone	41
2.24 Evidence for the metamorphic history	43
2.25 Metamorphic history	44
3.1 Summary of Facing directions within the Successions	49
3.2 Field evidence of facing directions	50
3.3 Tectonic and balanced cross-sections for the middle part of the Filat Succession	55
3.4 (a) Neiqit Formation of the Filat Succession	56
3.4 (b) Kazzaz and Granite Boulder Formations of the Filat Succession	57
3.4 (c) Atshani and Kholoud Formations of the Filat Succession	58
3.5 Filat Succession lithologies	59
3.6 Textures of Filat Succession lithologies	60
3.7 Modal analyses of the volcanoclastic rocks	62
3.8 Discrimination diagram for the volcanoclastic rocks	63
3.9 Geochemical signature of the Filat Succession	65
3.10 The Um Relan Succession	69
3.11 Alternative explanations for the stratigraphical relationship of the North Allaqi Group to the Um Relan Succession	70
3.12 Um Relan and Kilkobob Successions lithologies	72
3.13 textures of the Um Relan lithologies	73
3.14 Geochemical signature of the Um Relan Succession	74
3.15 The Kilkobob Succession	75
3.16 Textures of the Kilkobob Succession lithologies	77
3.17 Geochemical signature of the Kilkobob Succession	79
3.18 Gebel Taylor Wedge	81
3.19 Field relations of the Gebel Taylor Wedge lithologies	82
3.20 Metamorphic textures from Gebel Taylor Wedge	83
3.21 Geochemical signature of Gebel Taylor Wedge components	85

4.1 Outcrops of the Granites	89
4.2 Field relations of the Atshani, Um Relan and Filat Granites	90
4.3 Atshani Granite	92
4.4 Modal data for the Granite Plutons	93
4.5 Um Relan Granite	95
4.6 Filat Granite.....	97
4.7 Field relations of Kilkobob Granite and late basalt intrusions	98
4.8 Kilkobob Granite	99
4.9 Geochemical signatures of the Granite Plutons.....	101
4.10 Petrography and geochemical signature of late basaltic sills	103
5.1 Gold occurrences and production in the Eastern Desert	107
5.2 Wadi Allaqi mineralized occurrences and former mines	108
5.3 Thematic Mapper imagery showing shear-zones and target mineralized zones	110
5.4 Field relations of mineralized zones.....	111
5.5 Mineralization development in the quartz vein system	113
5.6 Mineralization in the Atshani Granite	114
5.7 Early mineralization petrography	115
5.8 Petrography of quartz-veins formed during the early mineralization	116
5.9 Petrography of the late mineralization and residual / diagenetic events.....	118
5.10 Wall-rock petrography	119
5.11 Photomicrographs of fluid inclusion types	121
5.12 Th data for the fluid inclusions	123
5.13 Summary of the stable isotope data.....	125
5.14 History of mineralization	127
6.1 The distribution of the ophiolitic rocks of the Pan-African belt	137

6.2 Map showing the generally accepted division between the Nile Craton and the rocks of the Pan-African belt, and the tectonic windows	138
6.3 Thematic Mapper image of the western Wadi Allaqi area	140
6.4 Postulated terrane boundaries and "sutures" of the eastern Egyptian	143
6.5 Reconstructions of the continent dispositions at 700 Ma and 500 Ma	146
6.6 Model of the development of the Pan-African rocks, central Wadi Allaqi	150

List of tables

2.1 A summary of the deformation history of the area.	10
2.2 Tectonic evolution of the mountain belts.....	46
3.1 Terminology for Tectonic-stratigraphical units used in this thesis.....	51
3.2 Previous divisions of the Precambrian rocks of Egypt.....	52
4.1 Composition of Granite Plutons	93
5.1 Fluid inclusion types.....	122

Chapter One

Introduction

1.1 Purpose of this investigation

The Wadi Allaqi area is of critical importance in our understanding of the evolution of the Neoproterozoic East African Orogeny (in the sense of Stern 1993, 1994) since the area occurs close to a complex shear-zone formed during the Pan-African tectono-thermal events. The term *Pan-African* was introduced by Kennedy (1964) to describe continent-wide tectono-thermal events which affected much of Africa including the Arabian and Nubian Shields in a period of the Neoproterozoic from 950-450 Ma (Kröner 1984; Shackleton 1986, and Fig. 1.1), although Kennedy originally believed that the time of the events was 500 ± 100 Ma. Previous authors have referred to the putative tectonic setting of Wadi Allaqi as: a suture-zone between the Aswan and Gabgaba terranes (Greiling *et al.* 1994; Kröner *et al.* 1987), a possible westward extension of the Heiani-Onib-Sol Hamed ophiolite belt (Stern *et al.* 1989, 1990; Sultan *et al.* 1992; Abdelsalam & Stern 1993a,b), a foreland basin in which a thick pile of molasse sediments accumulated above shelf sediments containing limestone layers (El Gaby *et al.* 1988, 1990), and a major fault-zone (Morgan 1990).

The main aims of the project were to deduce the structural history of the central Wadi Allaqi area (Figs. 1.3a and 1.4), south Eastern Desert, Egypt, and the position of the gold mineralization.

The specific objectives of the investigation were:-

1. to produce a framework for the historical development of the rocks in the area including a detailed structural analysis, a tectonic-stratigraphy and evidence for the relative ages of granite emplacement,
2. to obtain evidence for the tectonic setting for the rocks of the area,
3. to relate the gold mineralization to the tectonic history.

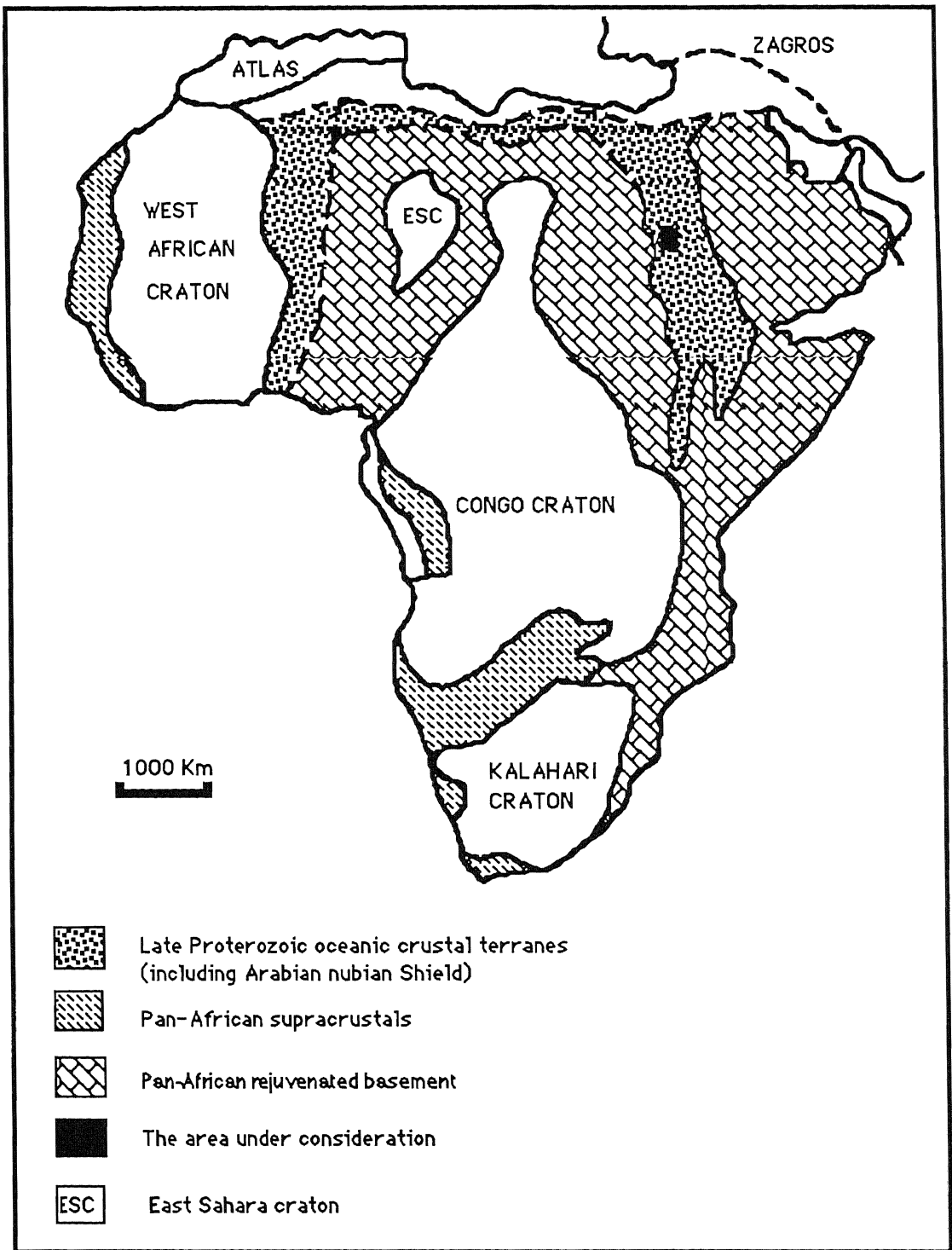


Fig. 1.1 African cratons and the Pan-African mobile belt showing location of the area (compiled from Pohl 1984; Vail 1990)

The study area (Fig. 1.1 & 1.2) covers 1000 km² and is bounded by latitude 22°19'N to 22°36' N and longitude 33°30'E to 33°47' E. The area is found on the Elba topographic sheet (12, scale 1:250,000) of the Survey of Egypt (1945), some 250 kilometres south-south-east of Aswan. Access to the area is by an asphalt road from Aswan to the western edge of Wadi Allaqi but within the area the physiography (see Frontispiece) restricts access to four-wheel drive vehicles along the main wadis. Although some workers have made passing reference to the Wadi Allaqi area (*e.g.*, Hume 1934, 1935, 1937; Stern *et al.* 1990) there have been no previous detailed investigations of the geological, structural and mineralization processes in the area and none of the regional investigations have attempted to integrate the structural evolution of the area with mineralization. For example Hunting Geology & Geophysics Ltd (1967) produced a generalized lithological map which included the area, on a scale of 1:5,000,000 in which the rocks of the area are designated as *geosynclinal metasedimentary and metavolcanic types*. El Ramly (1972; see Table 3.2) assigned all the rocks of the area to the geosynclinal Shadli metavolcanic group which was intruded by a metagabbro-diorite complex and granitoids. The Egyptian Geological Survey and Mining Authority (EGSMA) produced a coloured geological map of Egypt on the scale of 1:2,000,000 (1981) and Conoco (1987) produced a geological map which included this part of Egypt on the scale of 1:500,000 (*NF 36 : NE Bernice*) designating the rocks of this area as *geosynclinal metasedimentary schists and greywacke*. The United Nation Department of Technical Co-operation For Development (UND) provided assistance to the Geological and Mining Centre in Aswan for both the formulation and execution of an integrated preparatory project covering the southern Egypt and northern Sudan and bounded by latitudes 20°-24°N. and longitudes 30°-34°E. UND (1986) concluded that the greatest potential for metals is in the Precambrian rocks of volcano-sedimentary affinities, that the geological

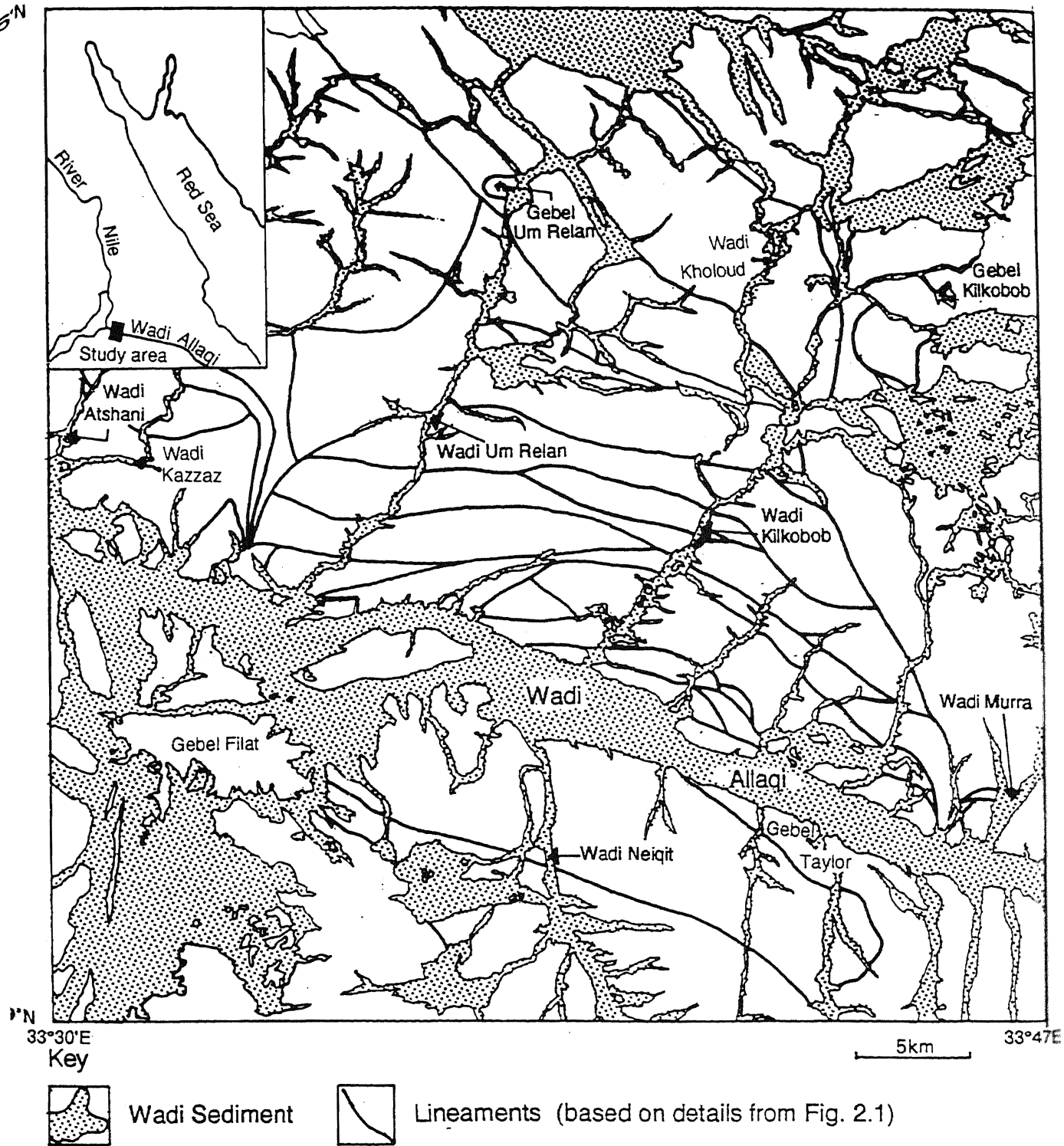


Fig. 2.1 The main geological locations of the central Wadi Allaqi area to which reference is made in the text, inset shows location of the central Wadi Allaqi area

structure was the key to the understanding of the origin of the mineral deposits, and that there was justification for a thorough study of the structure of the entire Precambrian basement complex.

1.2 Concurrent investigations

There are a few projects in hand which are adjacent to the area. An EGSMA-BGS project involving the remapping of the central and parts of the southern Eastern Desert on a scale 1:250,000 is nearly complete. Sultan (University of Missouri in collaboration with EGSMA) is carrying out selected tectonic studies and isotopic radiometric dating investigations in the central Eastern Desert and north Sudan. Sadek (University of Ein Shams) is carrying out tectonic investigations of the Abu Fas area which is situated some 10 km to the south-east of the present area and part of the results of this investigation have been incorporated within Greiling *et al.* (1994).

1.3 Methodologies employed for this study

This investigation is primarily concerned with the detailed tectonic-stratigraphy and structural analysis of the Pan-African rocks, supported by petrological and geochemical studies. The following methodologies and approaches have been followed for this study:

(a) *Standard geological field techniques and photogeology*; hard-copy photographs of remote-sensed images (*e.g.*, Fig. 2.1) which were produced in collaboration with the BGS on an original scale of 1:100,000, and black and white aerial photographs (on a scale of 1:40,000) were used to produce a base-map for the field observations and a geological map, at a scale of 1:58,000, (Fig. 1.3). Selected critical areas were mapped on various scales down to 1:10. Evidence for the tectonic-stratigraphy, the structural history, the tectonic provenance, and the mineralization were documented. The field-work of some 60 weeks was done from 1988-1992.

(b) Structural analysis; in addition to deducing a structural history in the field, some 3500 structural measurements of planar and linear elements have been made in order to obtain both information on the geometry of the deformation phases and the regional directions of the major thrust movements. Strain analyses from 6 localities have been carried out in order to quantify the deformation

(c) Petrographical and mineralogical analysis; some 700 thin-sections of the collected specimens have been studied in order to deduce both the mineral assemblages (and hence the degree of metamorphism) and any residual volcanic- and sedimentary-textures of the tectonic-stratigraphy. Polished-discs and polished thin-sections have been used to study the opaque minerals and mineralization. Electron-microprobe technique have been used to identify specific mineral species.

(d) Geochemical analysis; the purposes of the geochemical investigation were : (i) to use Inductively Coupled Plasma-Atomic Emission Spectroscopy (ICP-AES) and X-ray fluorescence (XRF) in order to obtain major and minor element analyses from 48 selected samples from both the Neoproterozoic tectonic-stratigraphy and igneous intrusions for deducing the tectonic provenance; (ii) to use the Inductively Coupled Plasma-Mass Spectroscopy (ICP-MS) to obtain analyses of gold of a suitable number of specimens of the mineralized rocks, including some traverses across mineralized zones.

(e) Fluid inclusions within mineralized specimens; a preliminary study of selected specimens has been made at Kingston University to determine T_H

(f) Stable isotopes of mineralized specimens; preliminary analyses of the isotopes of oxygen and hydrogen (deuterium) were made for selected samples at the Scottish Universities Research and Reactor Centre, East Kilbride.

Chapter Two

Structural Geology

2.1 Introduction.

The geometry of the structures, sequence of deformation, strain, and kinematics, especially sense of movement, within the shear-zones will be described in this chapter. Earlier investigations did not recognise the complex faulting in the area, *e.g.*, Hunting Geological & Geophysical Ltd (1967) interpreted the structures of the area as consisting of an earlier set of NW-SE-trending close folds superimposed by later northwesterly plunging co-axial folds which had an open geometry in the north becoming more intense to the south. Most of the rocks in the area have undergone low greenschist facies metamorphism.

2.2 Large-scale structures

Both Landsat satellite thematic mapper (TM) imagery (Fig. 2.1) and detailed field-mapping (Figs. 1.3a, 1.4) have been used to investigate the large-scale structures. Complex WNW-ESE-trending thrust duplex structures (which form strong lineaments, see Figs. 2.1, 2.5) with predominant facing directions toward the north dominate the area which has a multi-deformational history. The most significant of these movement zones is the 3 km-wide *Allaqi Shear-zone* (see section 2.9). The major linear high-strain shear-zones have been used to divide the area into seven homogeneous tectonic domains for analysis (*e.g.*, Fig 2.7). Major folds are not common but a particularly well-developed recumbent nappe-fold (the Gazira fold) can be demonstrated to the south of Wadi Allaqi (Fig. 2.6).

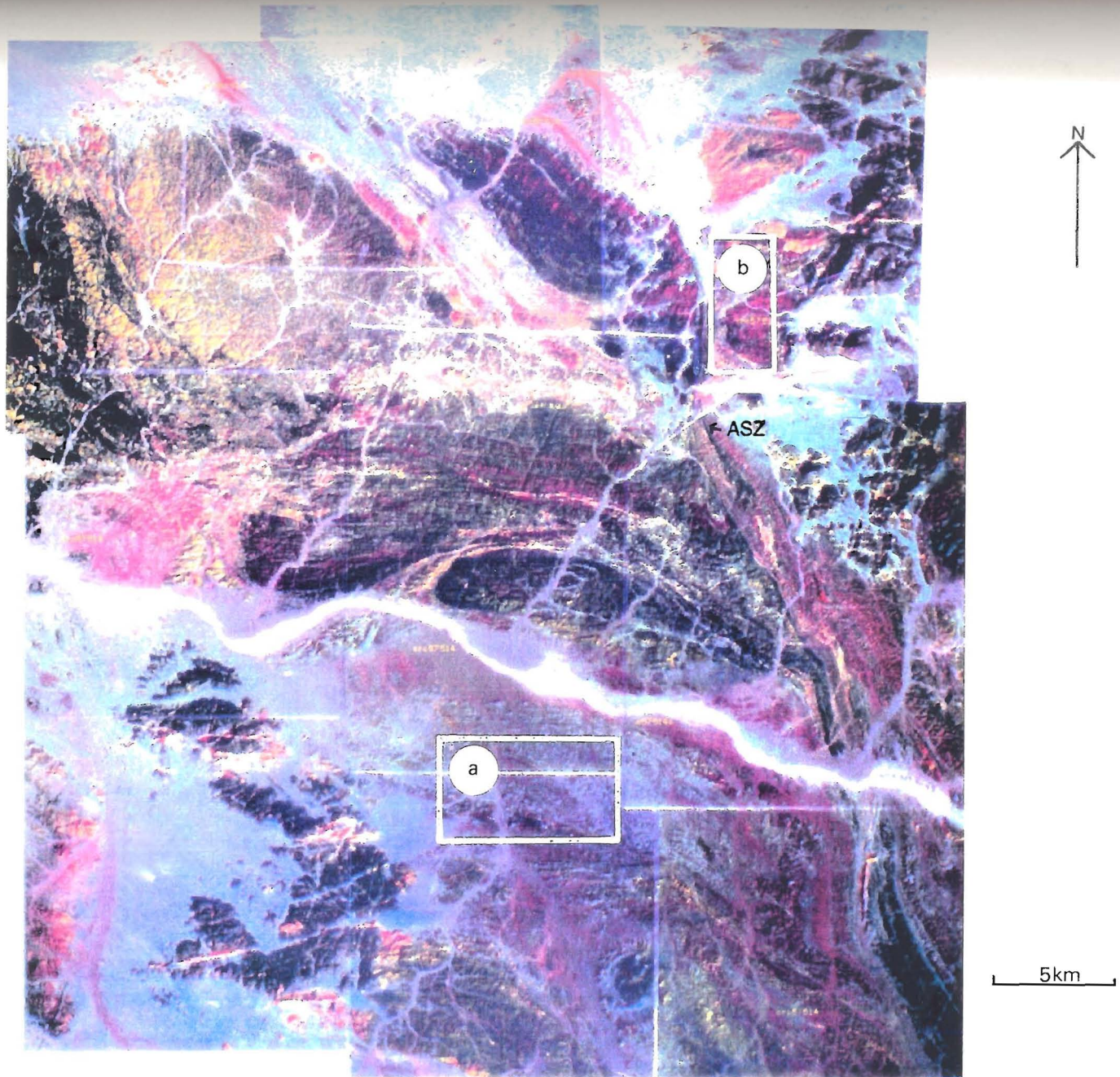


Fig. 2.1 Thematic Mapper (TM)-imaged photomosaic of the area; Allaqi shear-zone is indicated.
(a) outline of Fig. 2.6a, (b) outline of Fig. 2.14

2.3 The deformation history

Using minor structures (Figs 1.3a & 1.4) and superimposed relationships a complex polyphase deformational history has been deduced (Table 2.1). Examples of the evidence for the polyphase structural history are shown in text-figures 2.2, 2.3, 2.13, and 2.17. The history is interpreted as being contained within a single Pan-African orogenic cycle with initially ductile phases giving way to later brittle phases. The small-scale structures generally reflect the pattern of large-scale structures (see Fig. 2.18). The structural pile has been intruded at various times by four granitic plutons (see chapter 4).

2.4 D1 deformation phase

D1 minor and major structures are the most pervasive in the area and are recognised by conspicuous shear-zones (*cf.* Bak *et al.* 1975, Watterson 1979; Figs. 2.1, 2.4) on all scales which are approximately parallel (Figs. 1.3a, 2.5) to a prominent steep- to moderately-dipping, generally NW-SE-trending penetrative foliation (S1) and associated with an approximately north-east plunging lineation (L1) (Figs. 2.3c, 2.8 & 2.9). Analysis of the movement criteria (Figs. 2.4, 2.8, 2.20, 2.21 & 2.22) within the major shear-zones indicates that the original dip of the fault planes was gently towards the south giving a thrust geometry in a series of duplexes although there is some evidence of local lateral movement (Fig. 2.22c,d,e,f). North of Wadi Allaqi the thrust faults now consistently dip to the north (Fig. 2.5) giving, at present, a lag geometry since the hanging-wall block moved down in a northerly direction (Fig. 1.4). This is because most of the rocks in this region form the northern limb of a major D2 antiform (Fig. 1.4, 2.3a) and have been rotated from a near horizontal position through an angle of up to 70° (Fig. 2.5, 2.8, 2.12). Although thrusting occurs on all scales (Figs. 2.3e,f, & 2.4), the criteria for recognising major thrusts depended very much upon the

Table 2.1 A summary of the deformation history of the area.

PHASE	Filat Succession	Um Relan Succession	Kilkobob Succession	Major Intrusions	Metamorphism
Localized Blue schist facies					
"MAIN TECTONIC PHASES"	D1	To N.: Thrust Duplexes movement to NE; & S1 foliation	Lower limb of a Fold-thrust Nappe-facing to N.; & S1 foliation	Fold-thrust nappes facing N & S1 foliation	Green-schist facies
		To S.: Fold-thrust nappes-facing to N; & S1 foliation		Atshani Granite	
Allaqi Shear-zone formed.					
	D2	Upright E-W-trending folds. & S2 crenulation foliation.	Upright E-W trending folds; & S2 crenulation foliation.	Upright E-W trending open folds	Um Relan Granite facies
"LATE TECTONIC PHASES"	D3	NNE-trending & mainly, steeply-plunging kink bands.	NNE-trending & mainly, steeply-plunging kink bands.	Filat Granite	Contact metamorphism
	D4	NW-SE-trending & mainly gently-plunging kink bands	NW-SE-trending & mainly gently-plunging kink bands	Kilkobob Granite	
	D5	(a) E-W-trending strike-slip faults post-dating the intrusion of the Kilkobob granites at the late stage of Pan-African events (b) NE-SW trending strike-slip faults post-dating of the intrusion at the late stage of Pan-African events			

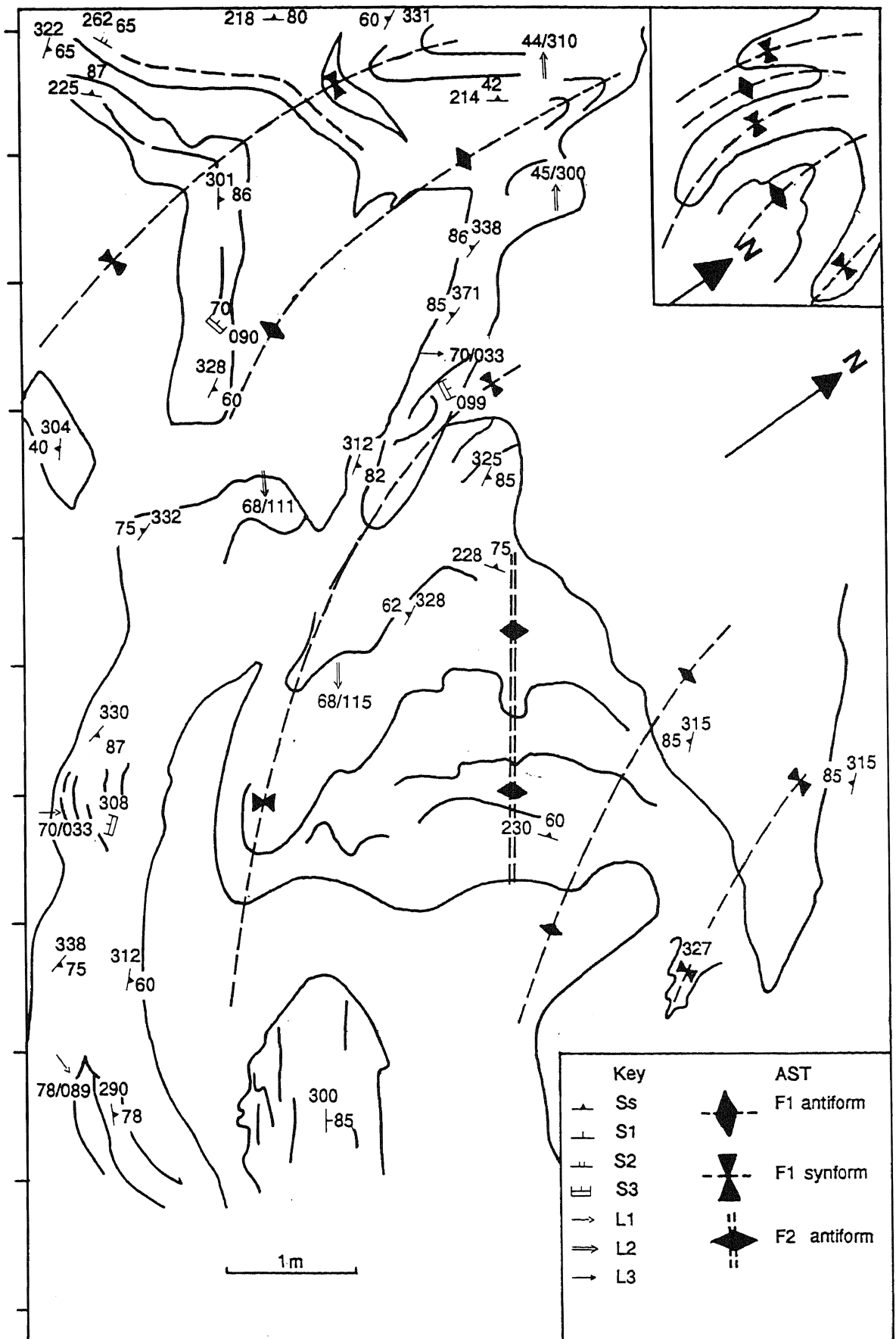


Fig. 2.2 Map showing evidence for polyphases deformation within the meta-limestone of the Um Relan Succession at (GR 6700980023). AST-axial-surface trace. The inset sketch map summarizes the polyphases structural geology of the area in which F1 folds are refolded by F2 folds and indicates that the F1 folds are situated on the upper limb of the southward-closing recumbent structure

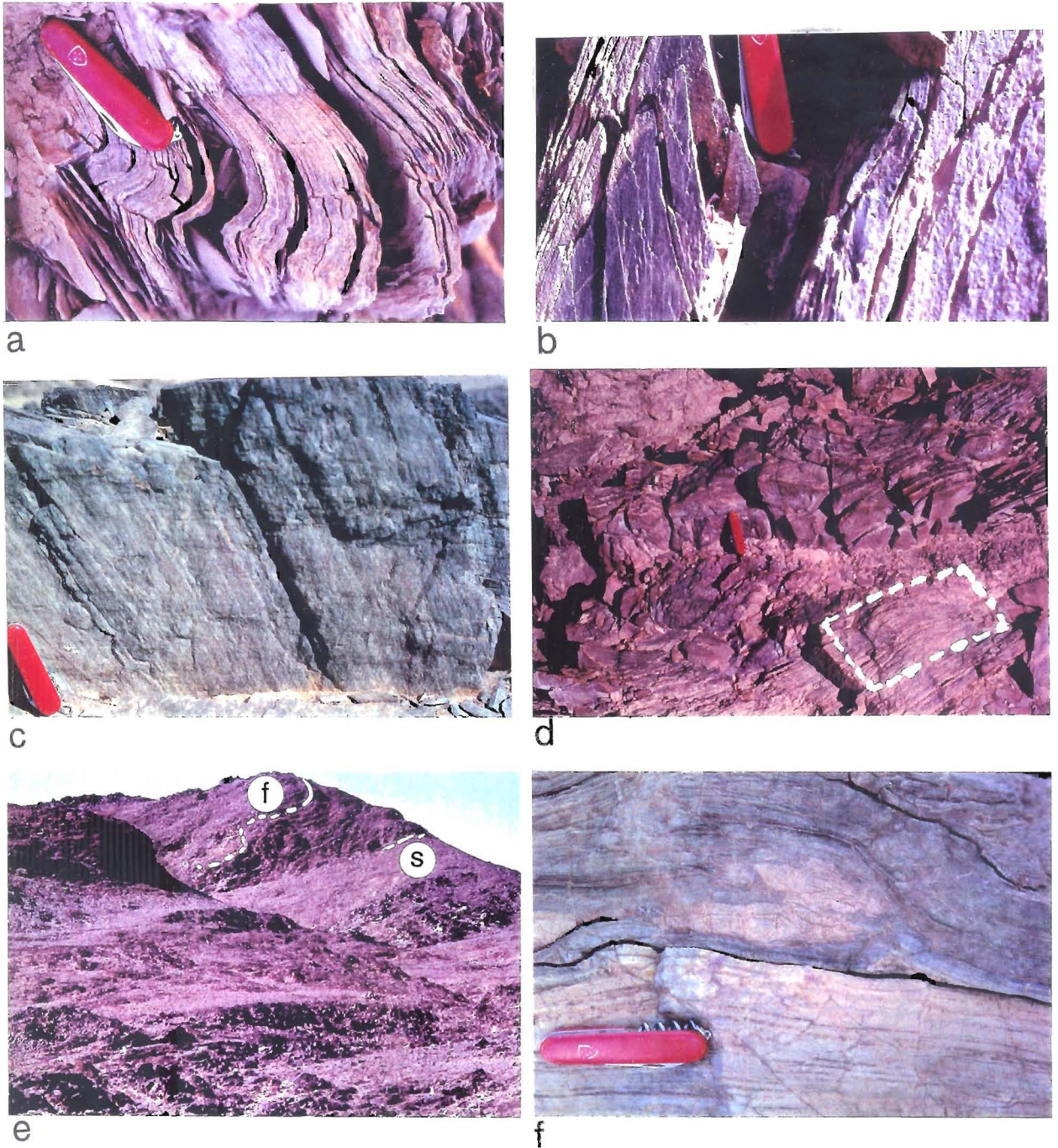
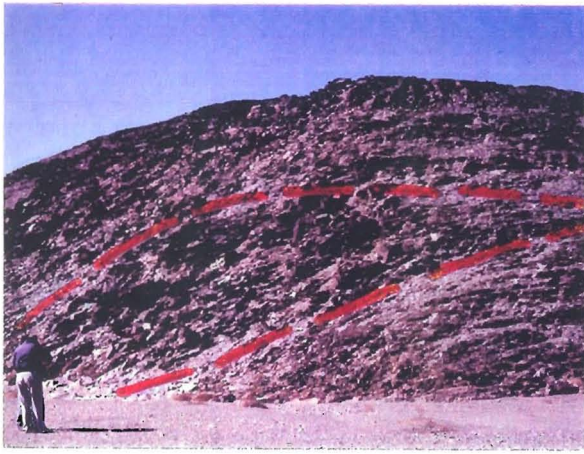


Fig. 2.3 Style of D1 structures

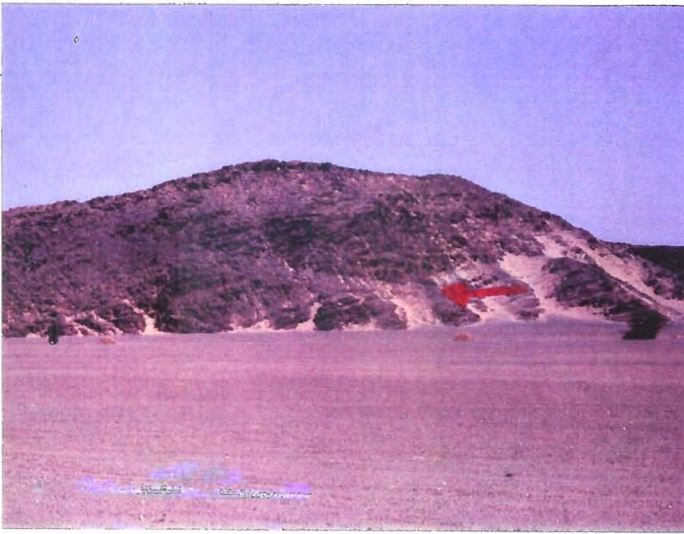
- (a) asymmetric close steeply-plunging F2 fold refolding S1 foliation, Metakalimestone Formation, Um Relan Succession (GR 6700890023)
- (b) inverted graded-bedded volcanoclastic rocks showing inclined (top right to bottom left) S1 foliation and bedding (Ss) and near vertical refracted S2 spaced cleavage, Neiqit Formation (GR 6680472738)
- (c) L1 stretching lineation on S1 foliation, Allaqi Shear-zone (GR 7888178354)
- (d) F2 fold with axial-surface-trace refolding D1 structures (location as for (a). area of (f) outlined)
- (e) large-scale cascade of F1 recumbent folds (f) divided by high strain shear-zones (s), Allaqi Shear-zone (GR 7812479460), height of the hill is 8m.
- (f) small-scale D1 ramp and flat structures (location as for d).



a



b



c



d

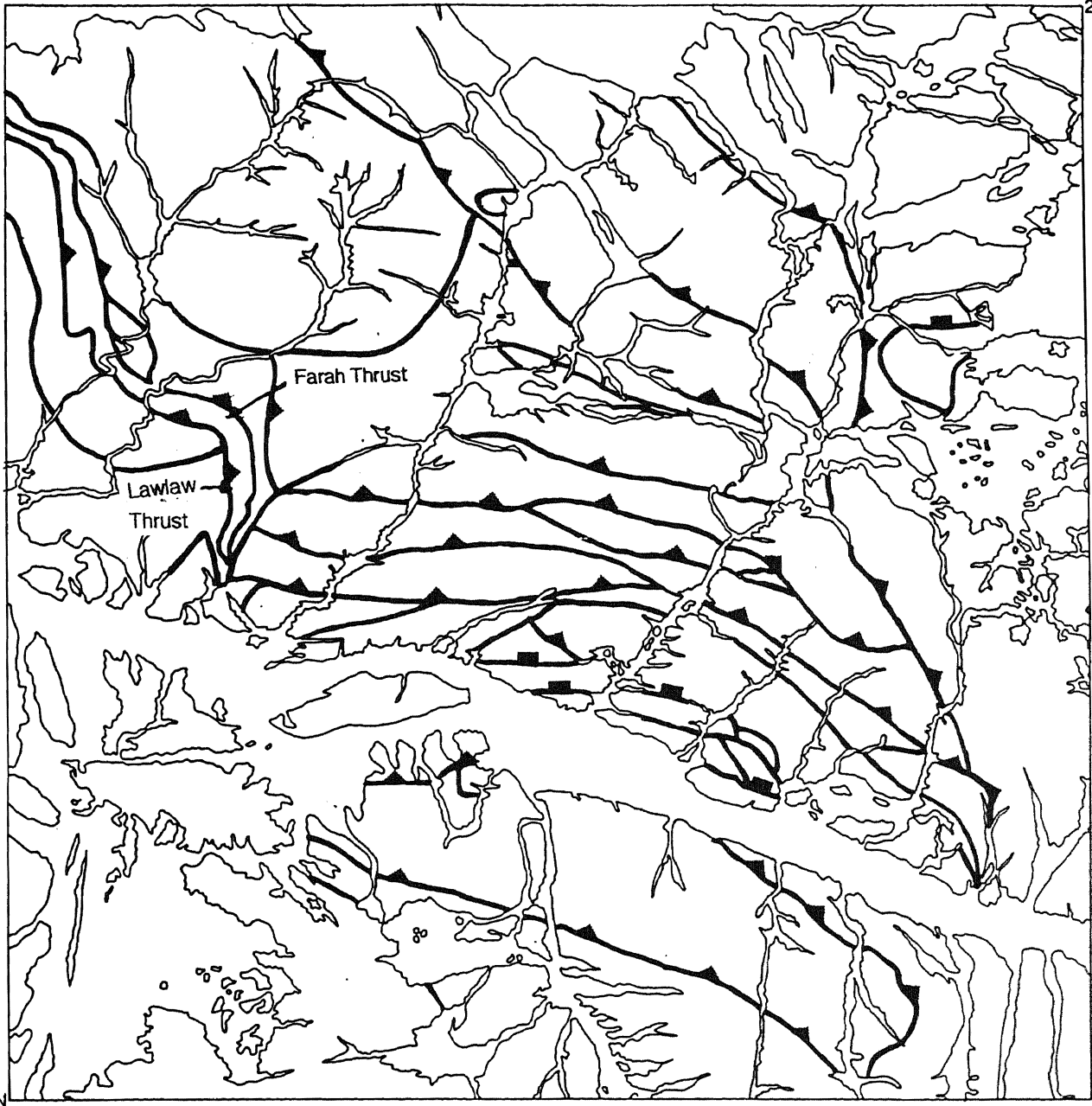
Fig. 2.4 Examples of the D1 duplexes and thrusts

(a) strong S1 foliation with duplex structure outlined by weak upright S2, North Allaqi Group (GR 6369086415)

(b) D1 duplex in North Allaqi Group (GR 7649477598)

(c) D1 ramp thrust fault in Neiqit Formation (GR 6604874426), the height of the hill is 13m.

(d) close-up of incipient D1 ramp in North Allaqi Group, notice the cut-off of the underlying laminated volcanoclastic rocks (GR 7640776375).



33° 30' E

33° 47' E

Key

5km



"Thrust" fault with dip of 20° - 30°



"Thrust" fault with dip of 45° - 75°

Fig. 2.5 The traces of the major D1 "thrusts". In all examples the movement of the hanging walls is downwards and toward the northeast giving a lag fault geometry at present, but if the effects of the later phases (particularly D2) are removed the restored sense of movements indicate that the present hanging walls moved upwards and to the northeast

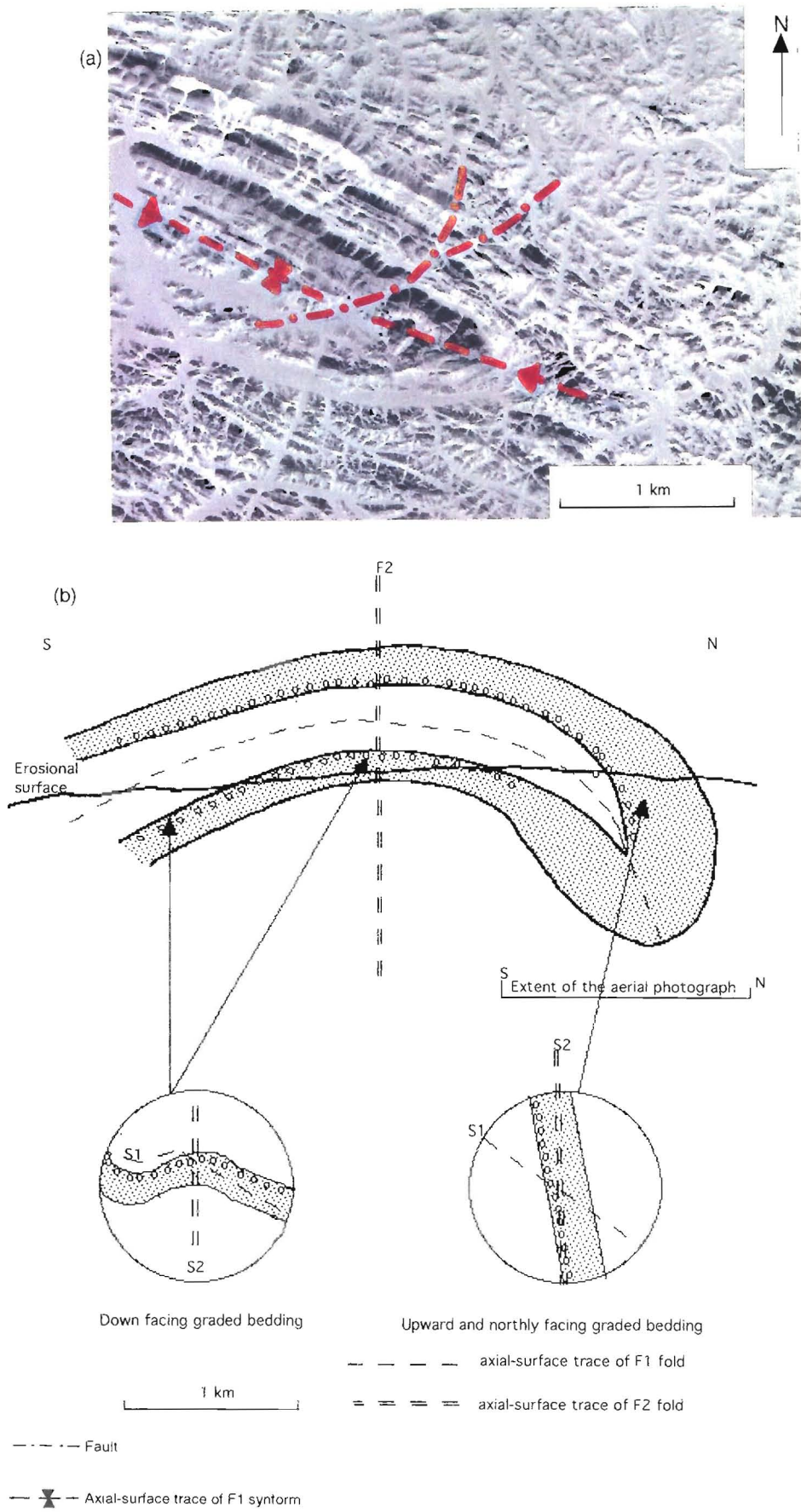


Fig. 2.6 The Gazira D1 recumbent fold
 (a) axial-surface-trace of the fold in the down-turned nose on an aerial photograph, south Wadi Allaqi in the Neiqit Formation (see Fig. 2.1)
 (b) structural cross-section of the fold with an indication of the extent of the aerial photograph (see Figs. 1.3a, 1.4)

types of lithologies present. Initially potential shear-zones were identified using TM imagery (Fig. 2.1). Then these were investigated in the field either to confirm their status or to add other probable major thrusts. Criteria such as the presence of relatively narrow zones of intense shearing with high strain along parallel structural planes (Fig. 2.4a,b), discordance of bedding structurally above the thrust plane (Fig. 2.4c,d), and distinctive lithological units truncated when traced laterally (Fig. 1.3b) have been used to deduce major thrusts which are always contained within shear-zones (see Figs. 1.3a, 1.4). Some of the major thrusts run on both the top and bottom junctions of relatively thick rudaceous lithological units (Figs. 1.3a,b); they form tectonic boundaries to the calcareous, siliceous and pelitic units of the Um Relan Succession which occurs within the Allaqi Shear-zone. Estimates of the amounts of displacement from balanced cross-section (Woodward *et al.* 1989) for the middle part of the Filat Succession (Fig. 3.3b) indicate values of about 16 km for both Farah and Lawlaw thrusts (Fig. 2.5)

South of Wadi Allaqi the nose of the major Gazira recumbent north-facing F1 fold, which is refolded by a phase 2 open fold (Figs. 2.6 & 1.4), is exposed. Tight, north-easterly facing recumbent F1 folds within a sequence of phyllites, meta-limestones and quartzites (Figs. 2.3e, 2.6; see section 2.9) are exposed within the Allaqi Shear-zone at the south-east of the central Wadi Allaqi area. These latter folds represent the vestiges of an early compressional stage in the development of the Allaqi Shear-zone. To the north a type 2 interference pattern (Ramsay 1967, p 527) in the lithological units has been formed from the refolding by upright F2 folds of a tight, easterly-facing overturned major F1 fold (the Kilkobob Synform; Fig. 1.4). This latter fold in all probability was nearly recumbent during the D1 phase.

2.4.1 Minor structures: The S1 foliation varies from a phyllitic cleavage (Fig. 2.4a) to a mylonitic fabric (Fig. 2.9a,b) in the high-strain zones (especially in the Allaqi Shear-zone, see section 2.9) to a schistosity (in the

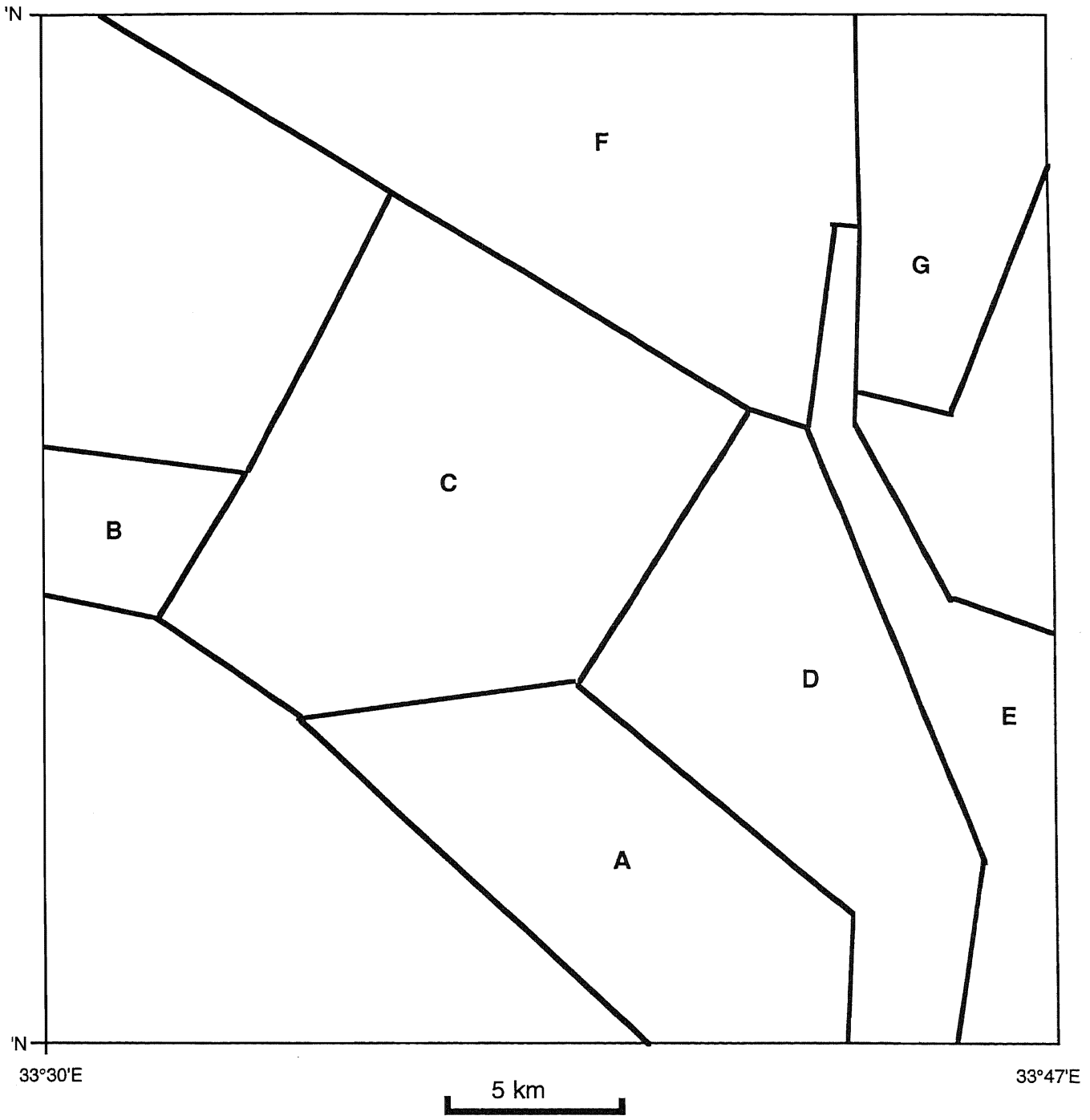


Fig. 2.7 Map showing domains using in the structural analyses

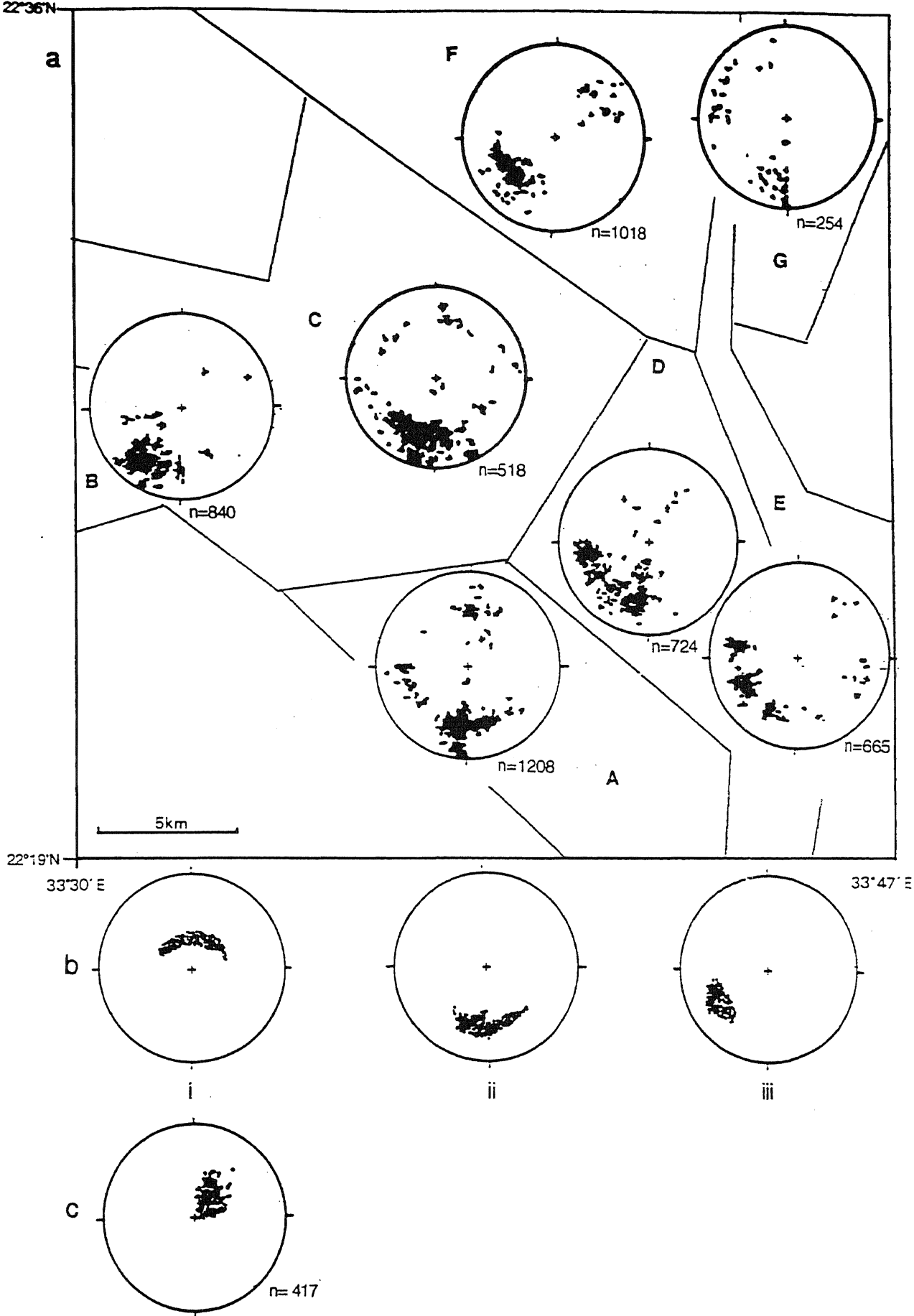


Fig. 2.8 (a) Synoptic map showing geographical variation of S1 (poles to S1 plotted on equal-angle projection). (b) Stereogram plots of 'ideal' deformation behaviour. (i) original S1 poles, note that the plots are related to curved foliations associated with the thrust planes (e.g. domains A, C) (ii) distribution of S1 poles after D2 deformation, note weak N-S girdle with a tendency to cluster in the south since the major D2 structure is a north limb of an antiform (e.g. domains A, F, G). (iii) distribution of S1 poles after both D2 & D3 deformation, note that a weaker N-S girdle is present but there is an increase in clustering in the SW quadrant (e.g. domains B, D, E). (c) Synoptic L1 diagram showing a moderate to steep plunge towards NE.

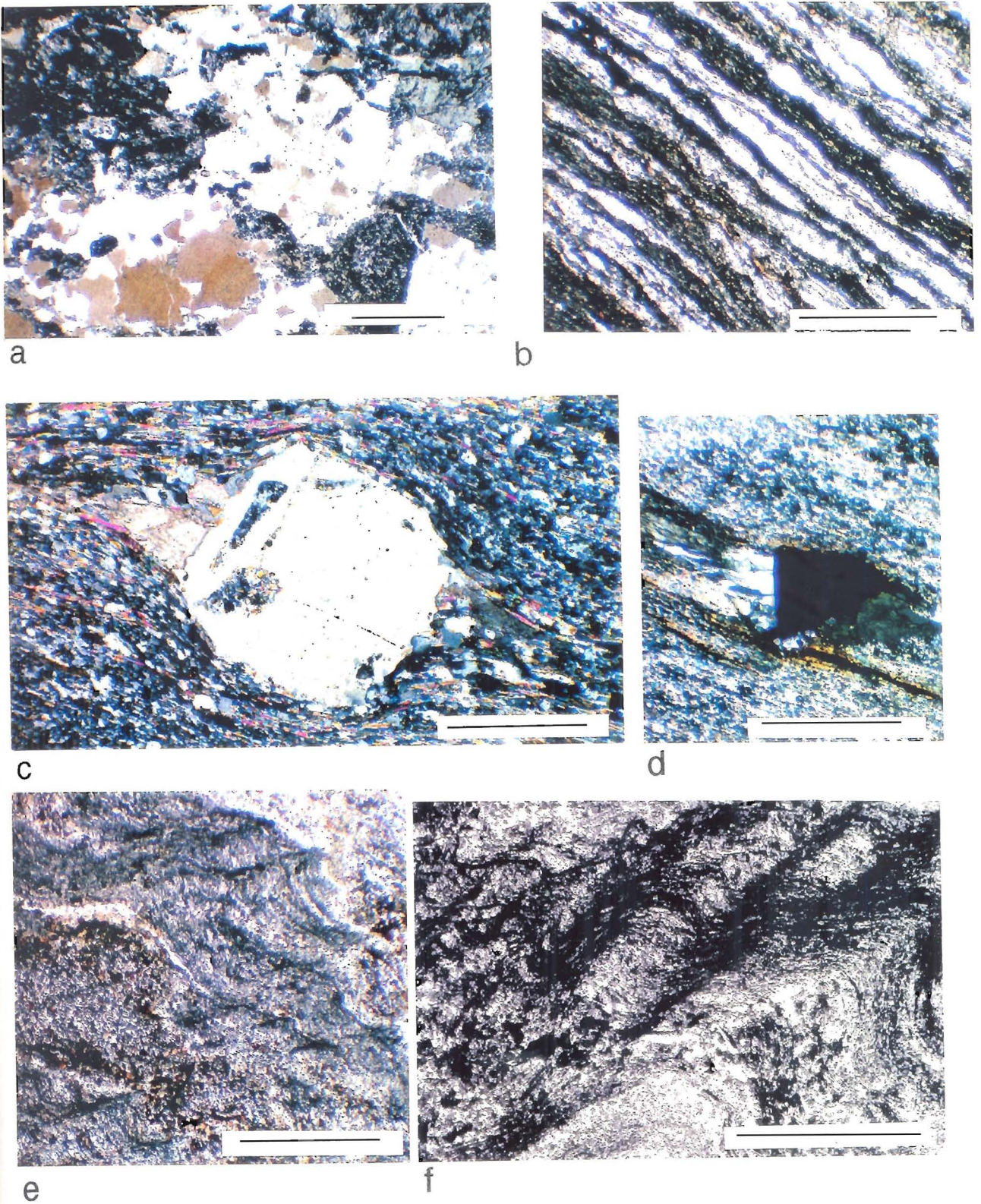


Fig. 2.9 Photomicrographs illustrating D1 fabrics

- (a) protomylonite showing S1 granulation of quartz, volcaniclastic rocks, Um Relan Succession [cross-polarized light; GR 6261494185; scale bar 0.1 mm]
- (b) mylonitic S1 fabric from the Allaqi Shear-zone showing alternating bands of stretched quartz (light) with chlorite and epidote (dark) [plane-polarized light; GR 7405086269; scale bar 1 mm]
- (c) white mica and quartz S1 foliation wrapped around quartz porphyroclast, phyllite, Um Relan Succession (cross-polarized light; GR 6494292206; scale bar 1 mm)
- (d) quartz pressure-fringes developed against a pyrite crystal showing obliquity to S1 foliation, phyllite, Um Relan Succession (cross-polarized light; GR 6578691769; scale bar 1 mm)
- (e) asymmetrical S1 chlorite-quartz fabric folded by D2 minor folds forming a crenulation cleavage (S2) in phyllite, Allaqi Shear-zone (plane-polarized light; GR 7681587026; scale bar 0.1 mm)
- (f) S1 folded by symmetrical and asymmetrical D2 folds with crenulation cleavage (S2) in phyllite, Allaqi Shear-zone. (plane-polarized light; GR 7736780333; scale bar 0.5 mm)

Gebel Taylor area, Figs. 1.3a, 2.9 & 3.17). The minor structures within a particular shear-zone always demonstrate variable rheology, *e.g.*, in the Allaqi Shear-zone D1 deformation phase mylonitic foliations (Fig. 2.9b), phyllitic cleavages (Figs. 2.8e,f, 3.10b) and fractures (Fig. 2.22d,f) are often juxtaposed, but the predominant style is brittle-ductile (using the criteria of Ramsay 1980, Ramsay & Huber 1987). L1 is defined mainly by elongated pebbles, a stretching mineral alignment (Fig. 2.3c), and a bedding/foliation (Ss/S1) intersection (Fig. 2.3b). Tight minor folds (F1) with a NW-SE trending axial-surface-trace (Fig. 2.3a) and an axial-plane cleavage (S1) are not common outside the Allaqi Shear-zone. The data for S1 (Fig. 2.8) shows a north-south girdle indicating refolding about an east-west axis (*i.e.*, F2 folds), and limited spread of L1 with a mean vector plunge at about 60° towards the NE. There is surprisingly little variation from sub-area to sub-area in this overall synopsis (Fig. 2.8).

2.4.2 Strain analysis: The deformed pebbles and boulders within a few lithostratigraphic units have been investigated for strain using both direct measurements and enlarged photographs. The R_f / ϕ method (Dunnet 1969; Lisle 1985) and Flinn (1962) methods were used in the analysis of the raw data. Granitic boulders and pebbles, set in a wacke sandstone matrix, were extracted from the Granite Boulder Formation (see Figs. 3.4b and 3.5 for more details) and yielded a strain ratio ($R_{s_{xy}}$) of 3.6 (Fig. 2.10b). Volcanic rock clasts set in a fine-grained volcanoclastic matrix from the Pyroclastic and Conglomerate Member of the Kilkobob Succession gave a lower strain ratio ($R_{s_{xy}}$) of 1.6 (Fig. 2.10b). Data from volcanic rock clasts set in a fine-grained volcanoclastic matrix at a further four locations (GR 7399282341, 6121782254, 5909381206 & 5833680508) from the Metaconglomerate Members within the Kazzaz and Atshani Formations of the Filat Succession indicate that most of the pebbles lie within the field of flattening (Fig. 2.10a) and are parallel to S1. However at another locality (328, GR

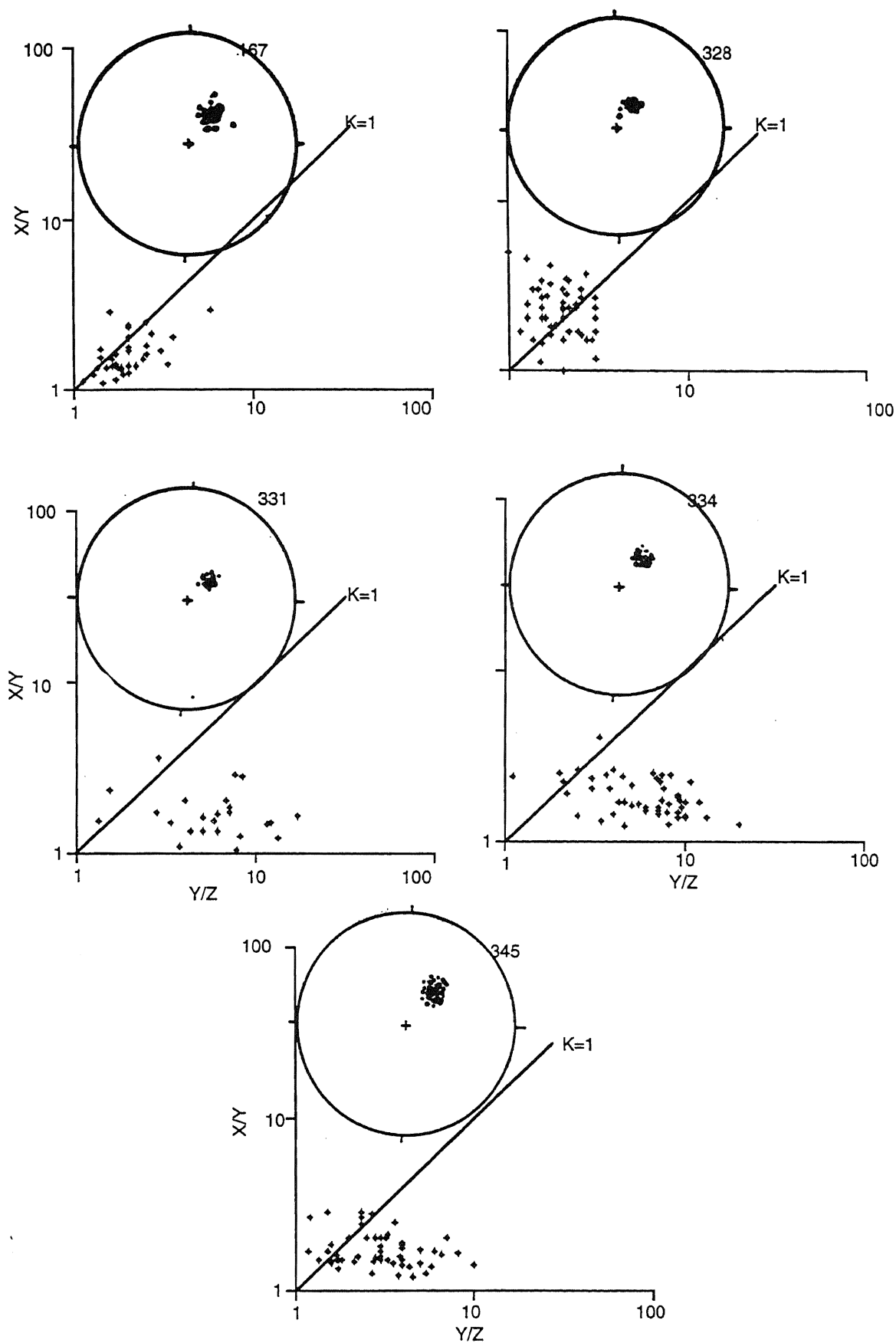
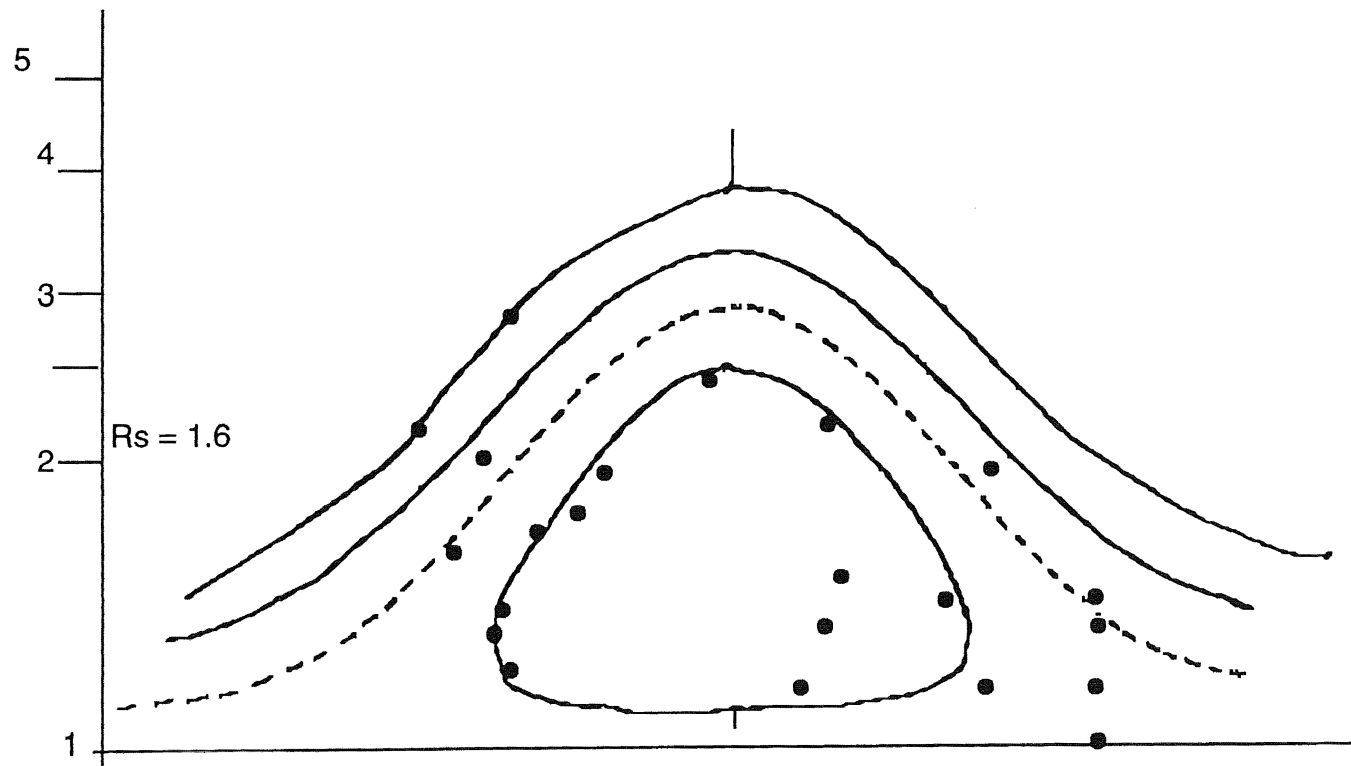
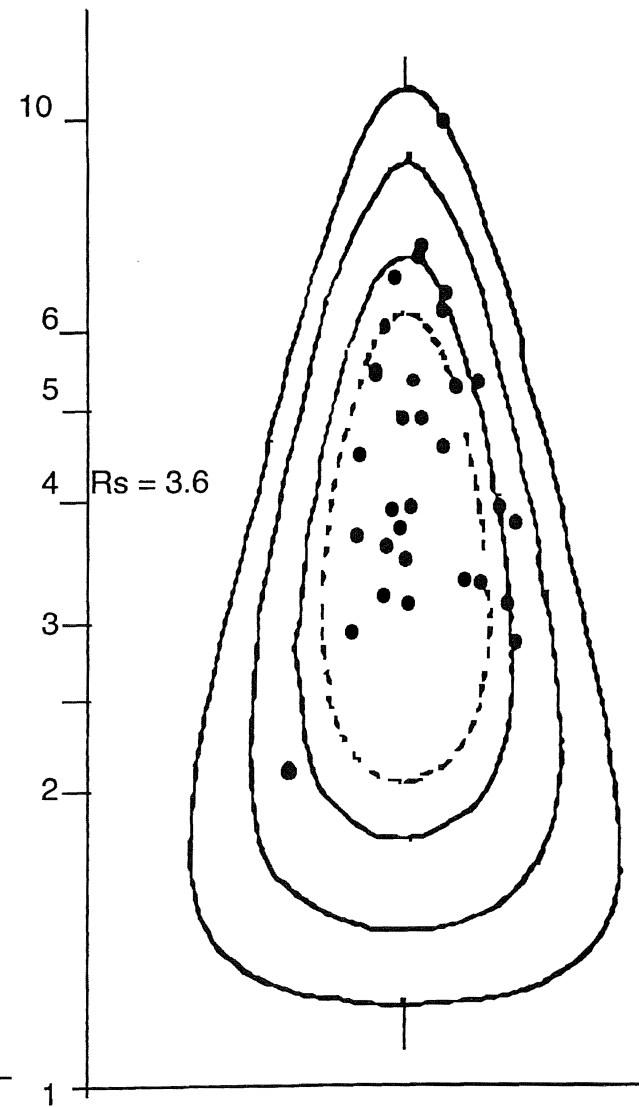


Fig. 2.10a Examples of Flinn plots (1962) for the strain results (sample locations 167 (GR 7399282341); 328 (GR6622288161); 331 (GR 6121782254); 334 (GR 5909381206); 345 (GR 5833680508) which indicate most of the data plot in the field of flattening. Type of pebbles are volcanic rocks except sample 167 from the Granite Boulder Formation. Circles are equal-angle stereonet which indicate general trend of elongation pebbles



a



b

Fig. 2.10b An examples of Rf/ϕ analyses

(a) volcanic pebbles from Kilkobob Succession (GR 7533091042)

(b) granite pebbles from Granite Boulder Formation (GR 7399282341)

The pebbles are flattened in the XZ plane and elongated parallel to Y which is alligned NE-SW

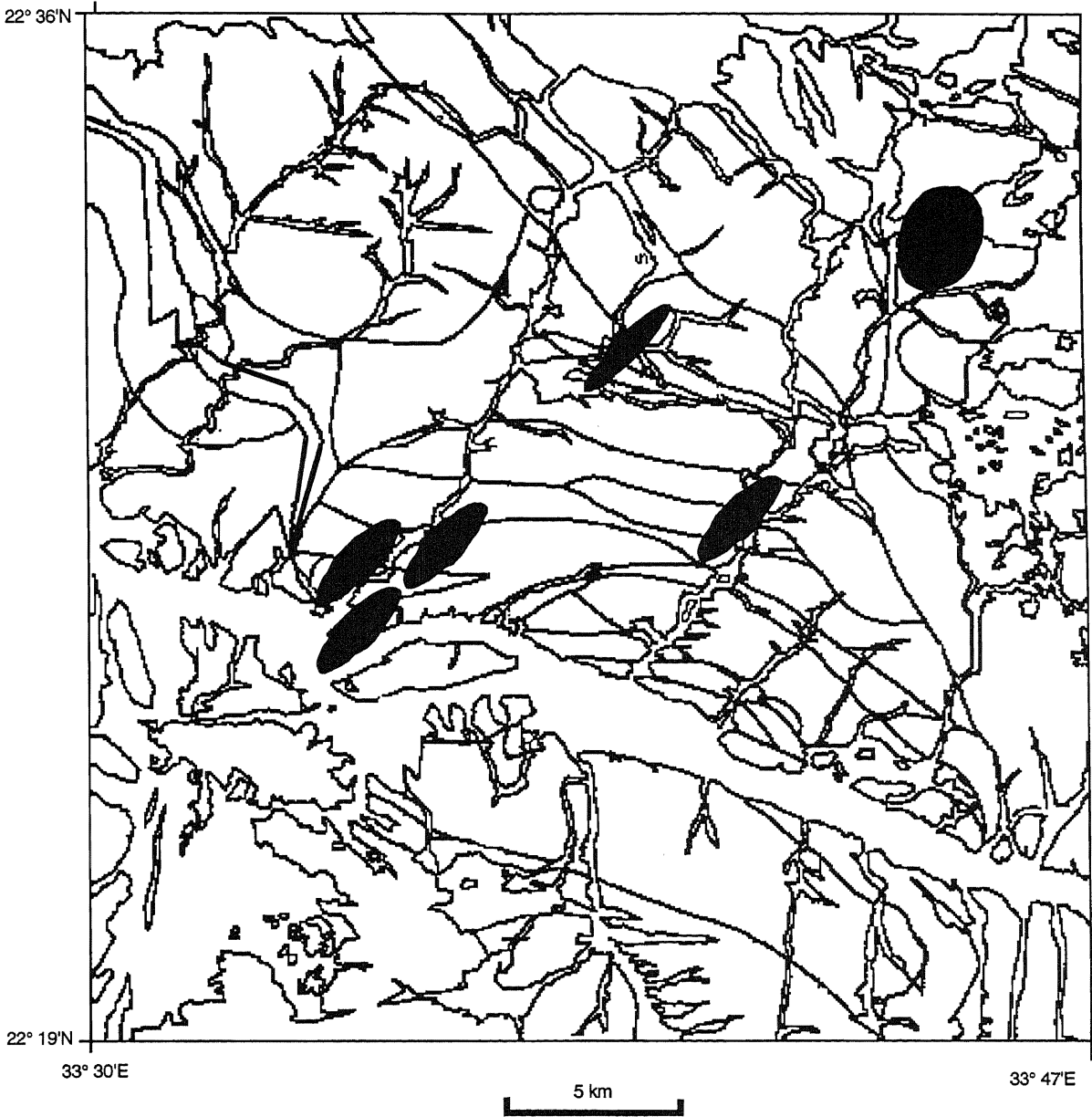


Fig. 2.11 A strain map within the Filat Succession, with the strain ellipsoid projected onto the map surface, indicating elongations predominantly towards the NE, and an increase in strain towards the ASZ. Note the lower strain to the north-east of the ASZ within the Kilkobob Succession.

6622288161; Figs 2.10a and 2.11), in the Atshani Formation, the data from the pebbles indicate a predominance of elongation.

In summary, the strain data demonstrates a gradual increase in elongation and amount of strain from the south to the north towards the Allaqi Shear-zone. Then there is a sudden diminution of strain in the rocks of the Kilkobob Succession, which structurally overlies the Allaqi Shear-zone and the Filat Succession. This is related to a change in tectonic régime from the intense shearing along the lower limb (*i.e.*, the Allaqi Shear-zone) of a north-facing and south-closing recumbent fold contained within the rocks of the Kilkobob Succession (Fig. 1.4) to a less strained environment.

2.5 D2 deformation phase

The attitudes of the D1 structures are mainly related to subsequent deformation by a major open, E-W-trending and upright antiformal fold of the D2 phase of which only the northern limb with associated parasitic folds is exposed in the central Wadi Allaqi area (Fig. 1.4). Two close to open large-scale antiforms with intervening synforms (Figs. 1.4, 2.14) have been deduced in the Kilkobob Succession adjacent to the northern part of Allaqi Shear-zone (Fig. 2.13a, b, c) where S1 has been refolded (sub-area G in Fig. 2.8, Fig. 2.23).

S1 is commonly deformed by minor, upright, open folds (F2; Figs. 2.2, 2.13 & 2.14). Small-scale E-W trending moderate to subvertical crenulation cleavage (S2) has developed parallel to the axial-surfaces of minor tight upright folds (F2) (Fig. 2.13). Rare lineations (L2) are formed by the intersection of S1/S2 (Fig. 2.3b). The data for S2 (Fig. 2.15) give concentrations indicating only limited later deformation of the structure. The L2 is intersection of S1/S2 and plunges to about 20° towards the NW and L2 is not common.

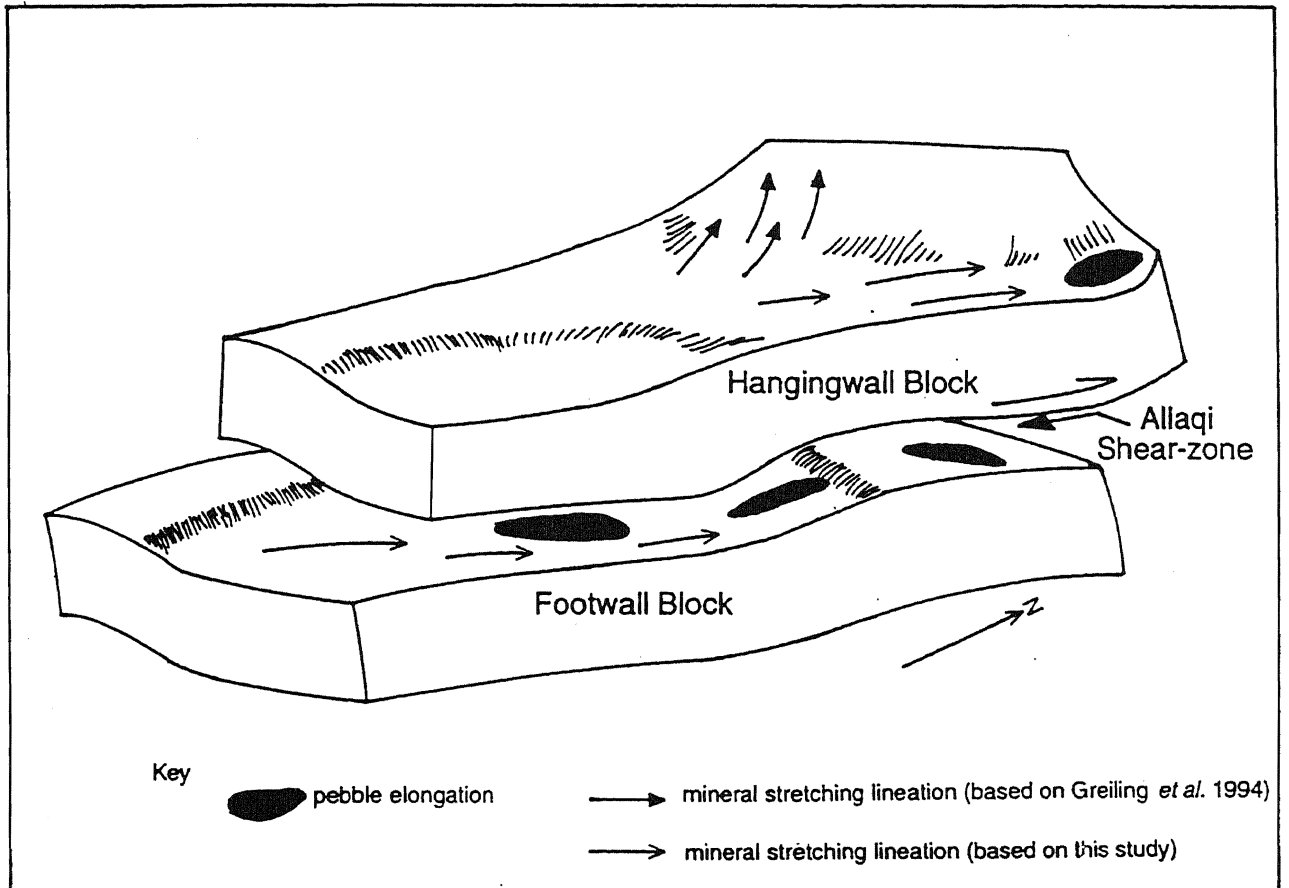
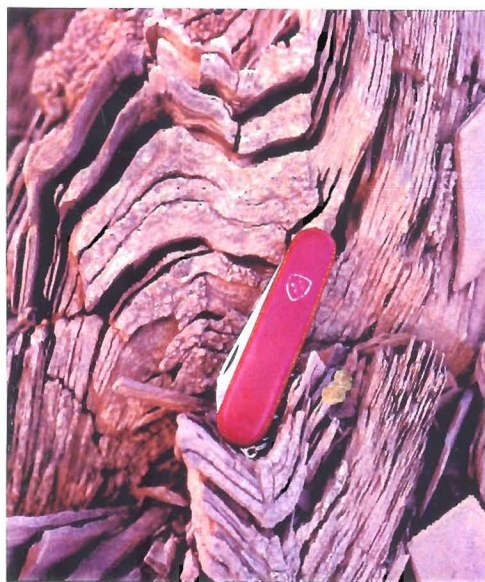


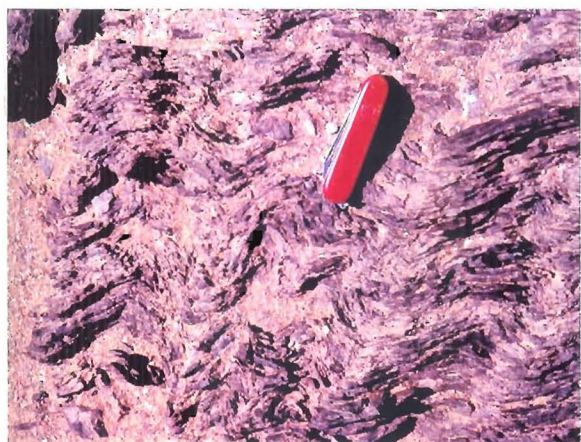
Fig. 2.12 A block diagram reconstructing the original movements along the Allaqi Shear-zone, as a typical D1 thrust, suggesting frontal and lateral ramping in the central Wadi Allaqi area (to the NE and NW respectively)



a



b



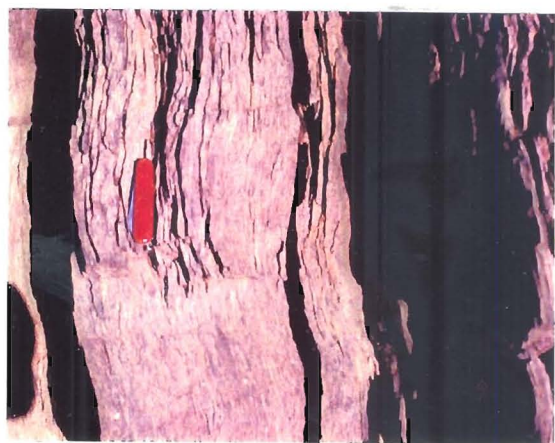
c



d



e



f

Fig. 2.13 Style of D2 and D3 mesoscopic structures

(a) upright F2 fold in quartzose phyllites of the Um Relan Succession (GR 6735790431)

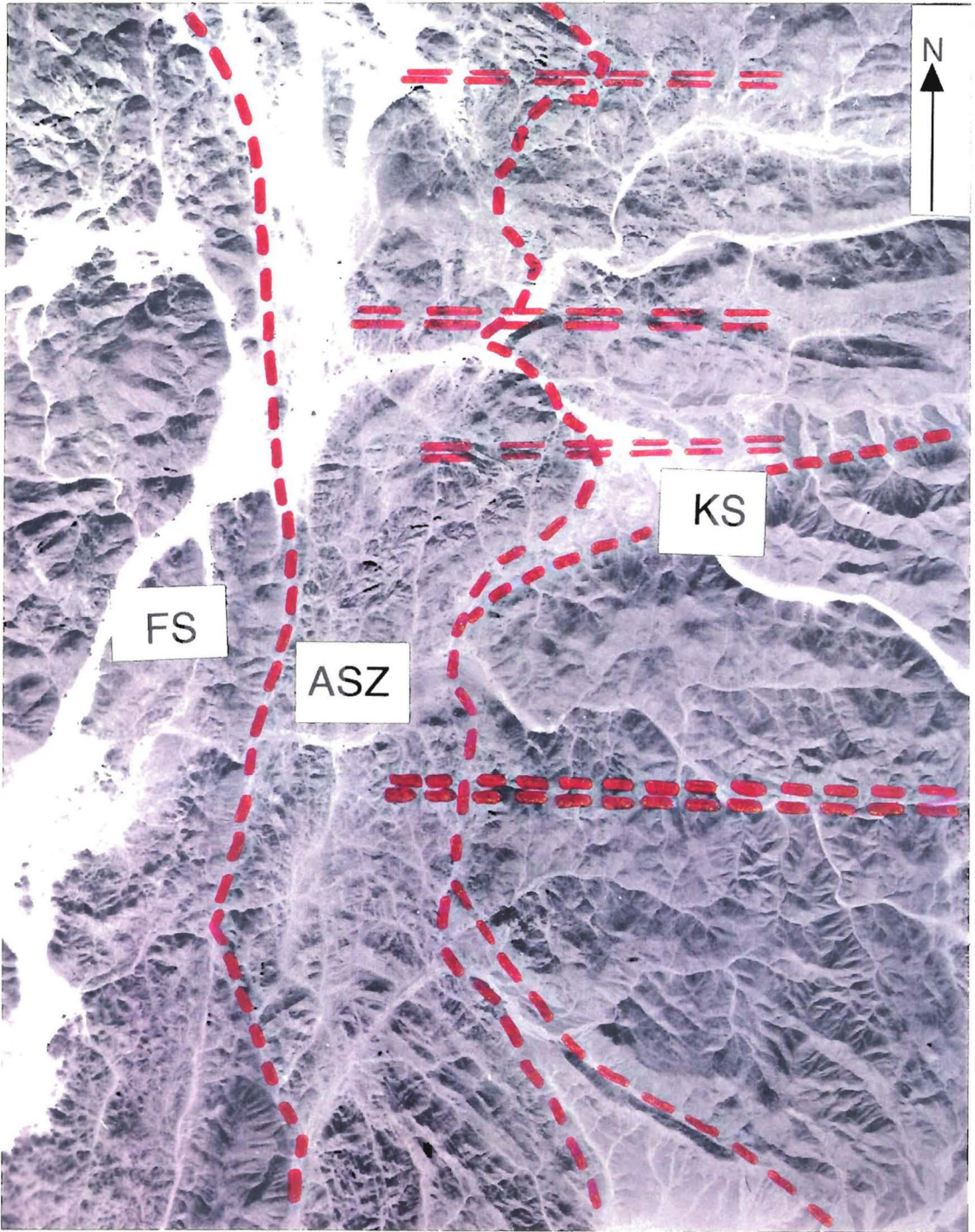
(b) upright close F2 fold in meta-limestone, Um Relan Succession (GR 6700890023)

(c) close, upright F2 folds in phyllitic volcaniclastic rocks of the Filat Succession (GR 6313880217)

(d) vertically plunging D3 kink band, Um Relan Succession location for (b)

(e) vertically plunging D3 conjugate kink band, Allaqi Shear-zone (GR 7864878529)

(f) steeply plunging D3 kink band, deformed S1, Um Relan Succession (GR 6788190838)



Key



-  S1 foliation traces
-  Axial-surface trace of F2 fold
- FS Filat Succession
- ASZ Allaqi Shear-zone
- KS Kilkobob Succession

Fig. 2.14 Annotated aerial photograph, showing D2 large-scale folds within the Kilkobob Succession (see Fig. 2.1)

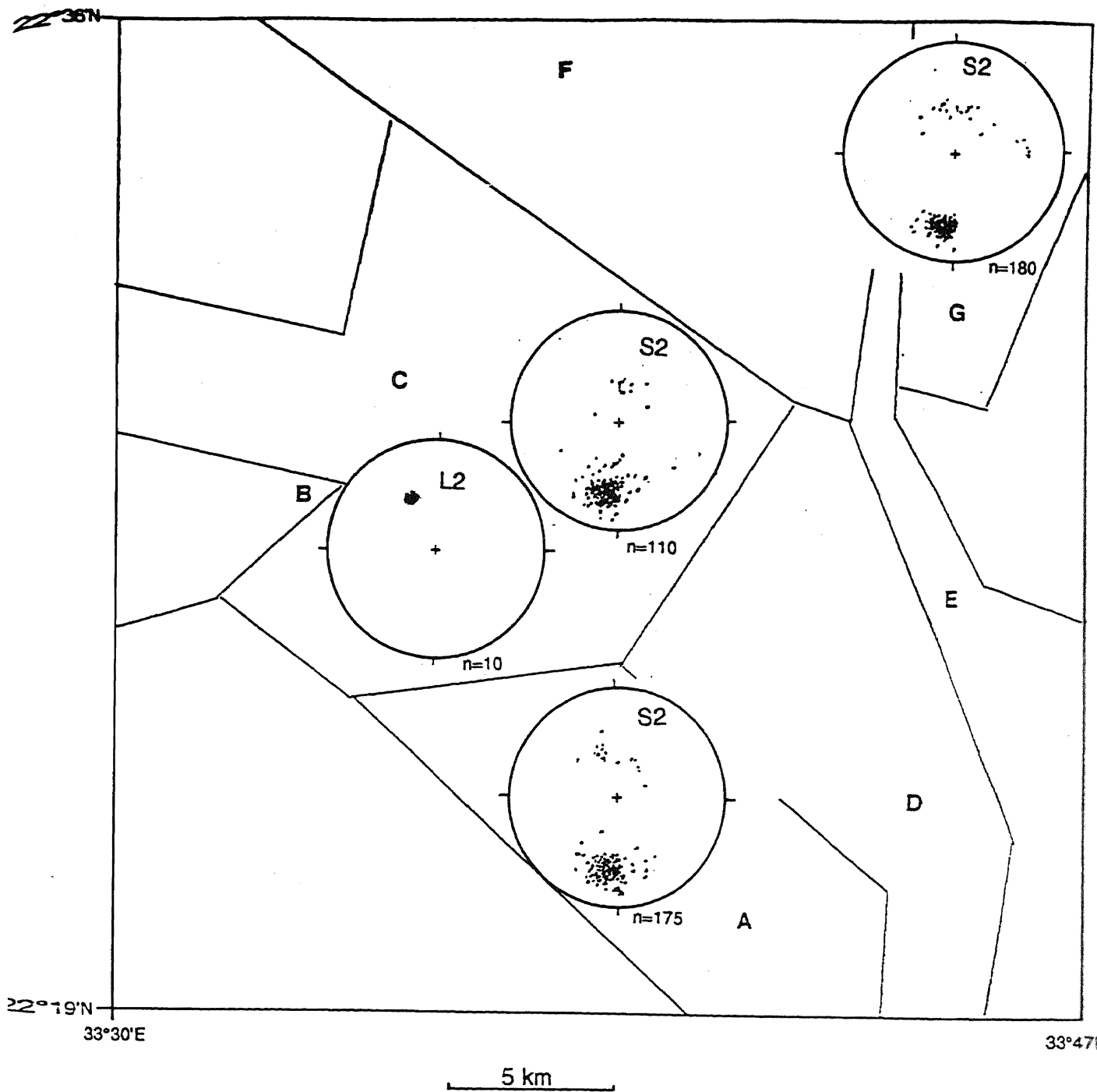


Fig. 2.15 Geographical variation of S2 and L2, shown for example in subdomains A, C & G (see text for discussion & Fig. 5.7)

2.6 D3 deformation phase

Large-scale fold structures of this phase of deformation are conspicuous in the Allaqi Shear-zone (Figs. 1.3a, 2.23) and in the Filat (Fig. 1.3a) and Um Relan Successions (Fig. 1.3a). On a small-scale the phase is distinguished by NE-SW-trending, brittle-ductile kink-bands/folds (F3; Fig. 2.13d, e, f), often occurring in conjugate systems (Fig. 2.13e,f), in which the bounding surfaces (S3) are steeply-dipping (Fig. 2.16). A crude hinge-line lineation (L3) has a generally steep plunge towards the NE (Fig. 2.16) .

Assuming that the maximum compressional stress (σ_1) was sub-parallel to the predominant foliation (S1; Ramsay 1967, p 452) and oriented horizontally at 320° , the minimum principal normal stress (σ_3) would be oriented horizontally at 050° and the intermediate stress would be vertical. This indicates a régime with approximately NW-SE oriented shortening in more brittle circumstances.

2.7 D4 deformation phase

D4 structures do not appear to have had a significant effect on the overall disposition of the lithological units (Fig. 1.3b). The minor structures are sub-horizontal kink-bands (F4) and conjugate fractures (Fig. 2.17a) which trend NW-SE (Fig. 2.17b). These brittle structures are probably related to gravitational collapse of the volcanic pile since the maximum principal normal stress (σ_1) was horizontal and extensional (Fig. 2.17a) and the minimum principal normal stress (σ_3) was compressional and vertical (*cf* Ramsay 1967, p 293).

2.8 D5 deformation phase

Major late-stage brittle structures, which were formed in the waning stages of the Pan-African orogeny since they not recorded in post-Pan-African rocks to the west, are represented by a set of NNE-SSW-trending left-lateral

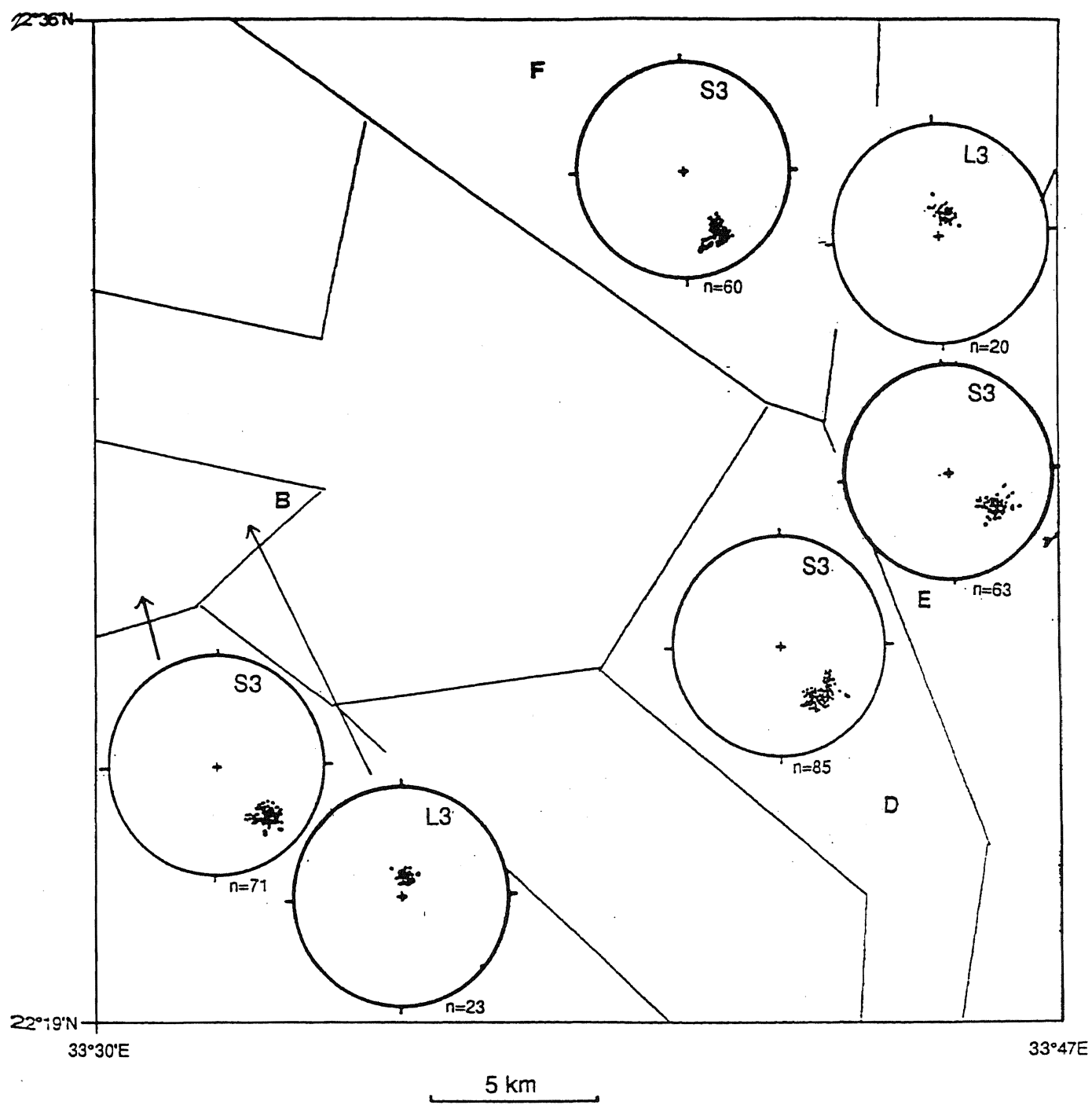
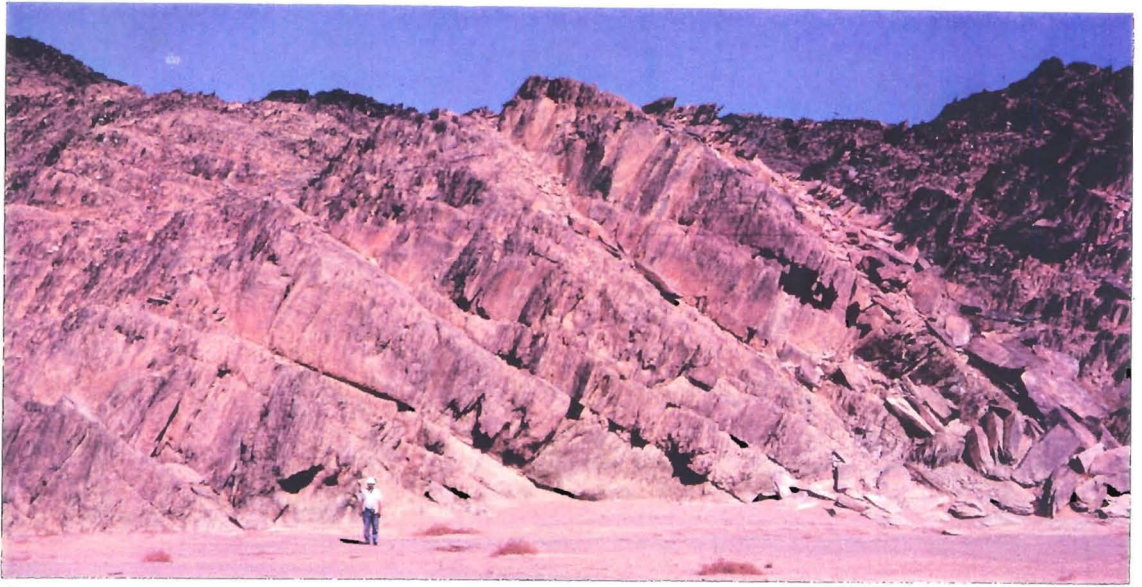
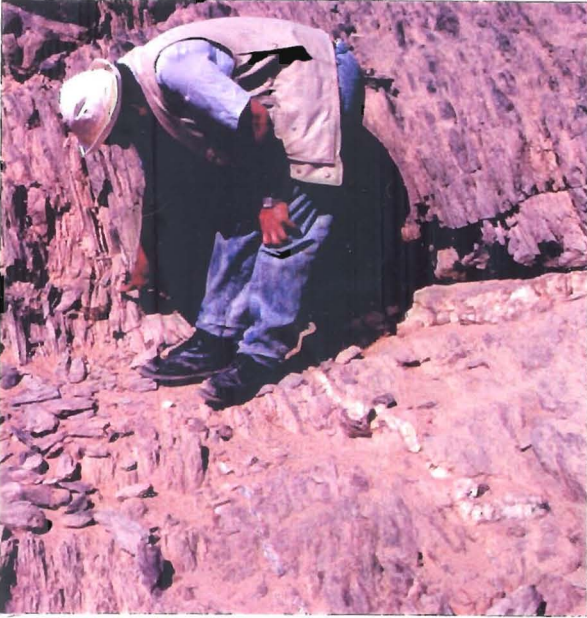


Fig. 2.16 Geographical variation of S3 and L3 data for example in subdomains B, D, E & F (see Fig. 5.7)

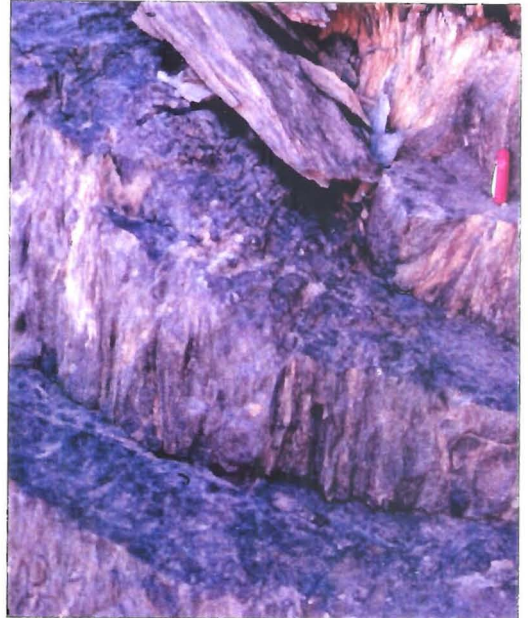
(i)



a



b



c

(ii)

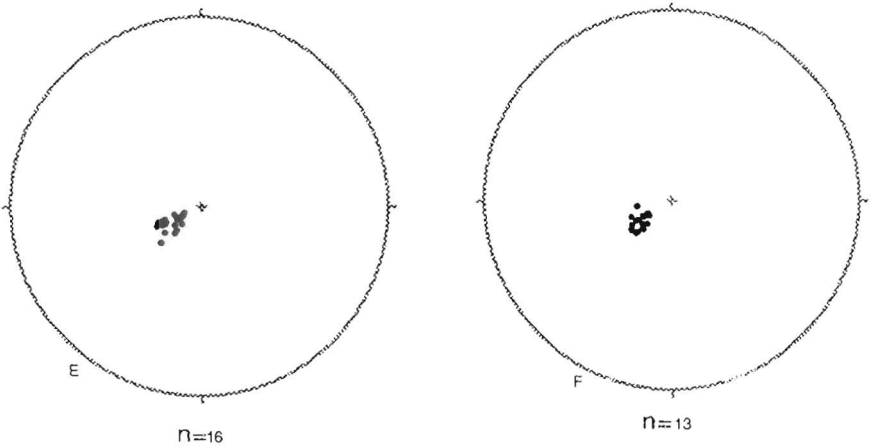


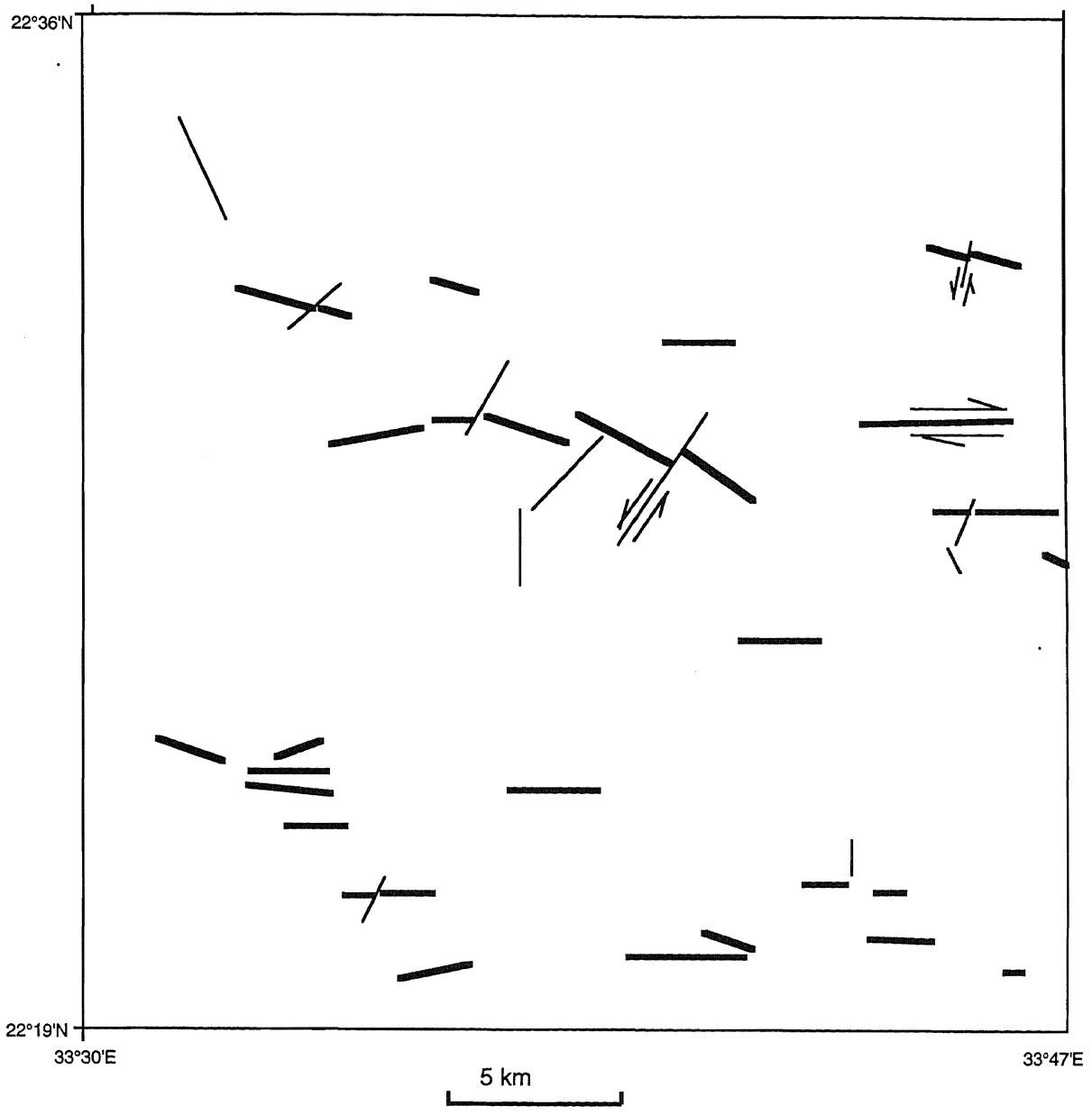
Fig. 2.17 (i) Style of D4 mesoscopic structures
 (a) large-scale northerly dipping D4 kink-bands, North Allaqi Group (GR 6628088103)
 (b) a nearly horizontal D4 kink-band S4 intersecting S1 and barren quartz vein (GR 5461188219)
 (c) close-up of D4 kink-band near to location of (a) indicating the curved inclination of the band surface
 (ii) Data for S4 mesostructures for subareas E and F (poles to the plane)

strike-slip faults (D5b) which displace earlier E-W-trending right-lateral strike-slip faults (D5a). Text-figure 2.18 shows the orientation of these structures. No obvious minor structures are associated with either set of large-scale faults.

D5a right-lateral strike-slip faults are readily recognized in the TM imagery (Fig. 2.1) and post-date all granitic intrusions of the region (Fig. 2.19a). In one example a 2 km displacement of the Kilkobob Granite and the nearby Allaqi Shear-zone can be demonstrated (Figs. 1.3, 1.4, 2.18). Trend data shown on a rose diagram and a cumulative curve of fault lengths (Fig. 2.19a) indicate both the predominance of the E-W trend and a close approximation to an exponential power fractal law with a value of 1.65 (Peacock 1991).

D5b left-lateral strike-slip faults (Fig. 2.19b) have variable displacements from about 100m to only a few metres and can be extrapolated outside the study area, for example with the conspicuous left-lateral strike-slip fault in Wadi Murra (which can be resolved with difficulty in the central part of Fig. 6.1). Data plotted on a rose diagram and cumulative curve of fault lengths (Fig. 2.19b) demonstrate a predominant NE-SW trend with a minor general N-S trend and a close approximation to an exponential power law with a value of 1.4.

If the *D5a* faults were formed as master shears and the *D5b* faults represent a complementary set of antithetic Riedel shears then the major extensional stress would be oriented approximately NE-SW and would have to be accompanied by an approximately NW-SE compression (*cf.* Ramsay & Huber 1987, p530). Alternatively if the *D5a* faults were formed in a separate and distinct phase from the *D5b* faults then the stress field would need to undergo considerable change and orientation. There is insufficient data to support the latter interpretation which would involve a complicated mechanism.



Key


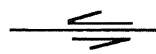
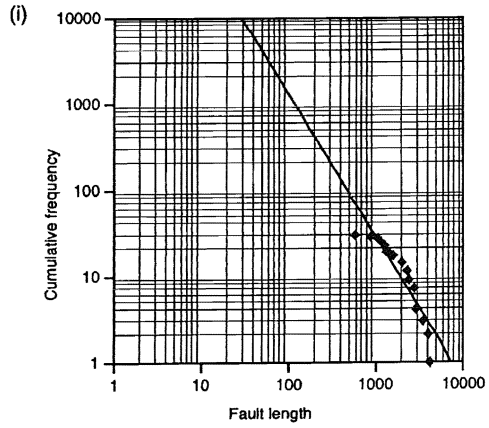
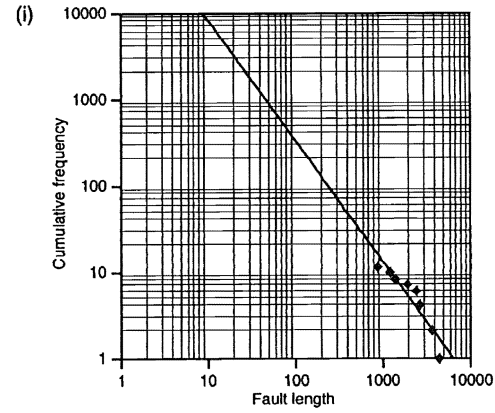
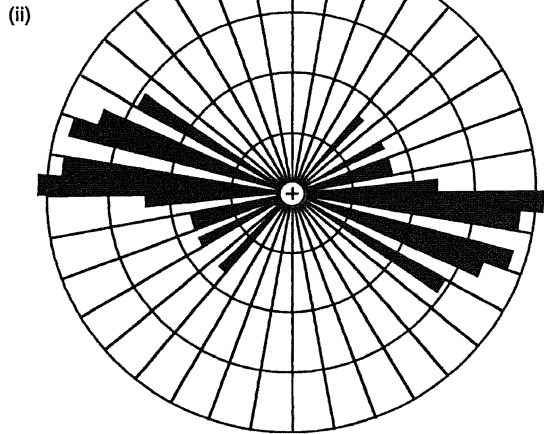
-  D5a dextral strike slip-fault
-  D5b sinistral strike slip-fault

Fig. 2.18 Traces of late-stage D5 faults, based upon field observation and remote sensed image (Fig. 2.1)



N



N

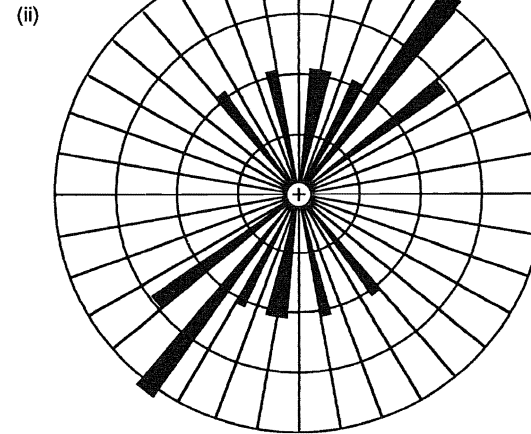


Fig.2.19 Analyses of the late-stage faults, (a) D5a faults
 (i) fault length against cumulative frequency for 29 right-lateral strike-slip faults with a power-law exponent of 1.65 (Peacock 1991)
 (ii) rose diagram showing general trend for 29 right-lateral strike-slip faults

Fig.2.19 Analyses of the late-stage faults, (b) D5b faults
 (i) fault length against cumulative frequency for 11 left-lateral strike-slip faults with a power-law exponent of 1.4.
 (ii) Rose diagram showing general trend for 11 left-lateral strike-slip faults

2.9 The Allaqi Shear-zone.

This conspicuous shear-zone is a fundamental large-scale structure in the south Eastern Desert (Fig. 6.1). The Allaqi Shear-zone, in the central Wadi Allaqi (Fig. 2.1, 2.23), is variable in width, but in places exceeds 3 km, and is composed largely of metasedimentary lithologies from the Um Relan Succession (see section 3.4) with a sliver, about 70 m long and 4 m wide, of serpentinite (GR 7847378762). Metre-wide bands of protomylonite occur in the volcanoclastic rocks of the Um Relan Succession (GR 6261494185) and consist of quartz, plagioclase, chlorite, epidote, zircon and goethite. The minerals show a complex mixture of ductile and brittle deformation; quartz show slight stretching and granulation; plagioclases are broken, and chlorite shows ductile stretching (Fig. 2.9a). Mylonites are rare but a quartz-plagioclase-chlorite-sericite-calcite variety (GR 7736780333) with quartz flaser structures and a chlorite-quartz-graphite-calcite-plagioclase-epidote variety (GR 7737080336) display D1 banded structures (Fig. 2.9b). In both examples plagioclase shows deformed lamellar twinning, the calcite occurs either as disseminated xenomorphic crystals and porphyroclasts or as veinlets which show pinch and swell structures parallel to the S1 schistosity (Fig. 2.9b).

The four earliest phases of deformation (D1-D4) are recognised from the minor structures within the Shear-zone and have similar styles to those minor structures outside the Shear-zone. The earliest structures in the Allaqi shear-zone are tight, asymmetric, overturned, and occasionally recumbent, N-S-trending folds (F1) which face and verge to the ENE (Fig. 2.3e). Usually the bottom limbs of easterly-closing folds are intensely sheared. The intensely penetrative S1 foliation is occasionally distinguished as mylonitic banding (Fig. 2.9b). Shear-zones are known as either brittle or ductile, according to whether the dominant deformation mechanism is by cataclasis or by crystal plastic processes (Fig. 2.9a,b).

A detailed analysis of the sense of shear during the D1 phase has been made from several independent criteria and from an understanding of the relationships between various microstructural elements. A range of independent mesoscopic and microscopic kinematic indicators (Fig. 2.20) (Simpson 1986; Simpson & Schmidt 1983; White *et al.* 1986) used and related to a single kinematic framework (Figs. 2.21, 2.22 and 2.23). There are two types of *C-S fabrics* (Berthe *et al.* 1979, Blenkinsop & Treloar 1995). Type 1 fabrics are found in the Allaqi Shear-zone and comprise of narrow spaced C-surfaces transecting a mylonitic foliation (S-surfaces) with a persistently left-lateral sense of movement (Fig. 2.21, 2.22a). Type 2 mica fish fabrics (Lister & Snoke 1984) have not been recorded in the area. *Displaced fractured grains* as domino-like microstructures are found in quartz and plagioclase crystals (Fig. 2.22b,f). Occasionally some displaced fractured grains can give an apparent opposite overall shear-sense to that of the majority of adjacent examples (Fig. 2.22f). Shear-sense may be deduced from two types of pull-aparts. First, *parallel pull-aparts* which are formed when the direction of movement is nearly normal to the fracture plane causing the development of gaps between the fragments (Mandal & Khan 1991; Fig. 2.22e). These occur when there is a competency contrast and the more competent layer can not accommodate strain by a plastic mechanism. Brittle fractures develop which are oriented approximately perpendicular to the axis of maximum extension (Sudgen 1987); Fig. 2.22e). Secondly, "*V*"-pull-aparts (Hippertt 1993) in which the fracture plane is not normal to the direction of movement (Fig. 2.22c,f). The sense of movement can be determined from the relative orientation of the fracture walls of the two adjacent co-genetic fragments. The fragment with the fracture edge inclined with a lower angle to the foliation (shear-band [S]), usually the smaller fragment, is rotated in the direction of movement with respect to the top of the 'V' (Urai *et al.* 1991; Fig. 2.22c,f). A characteristic of the gaps

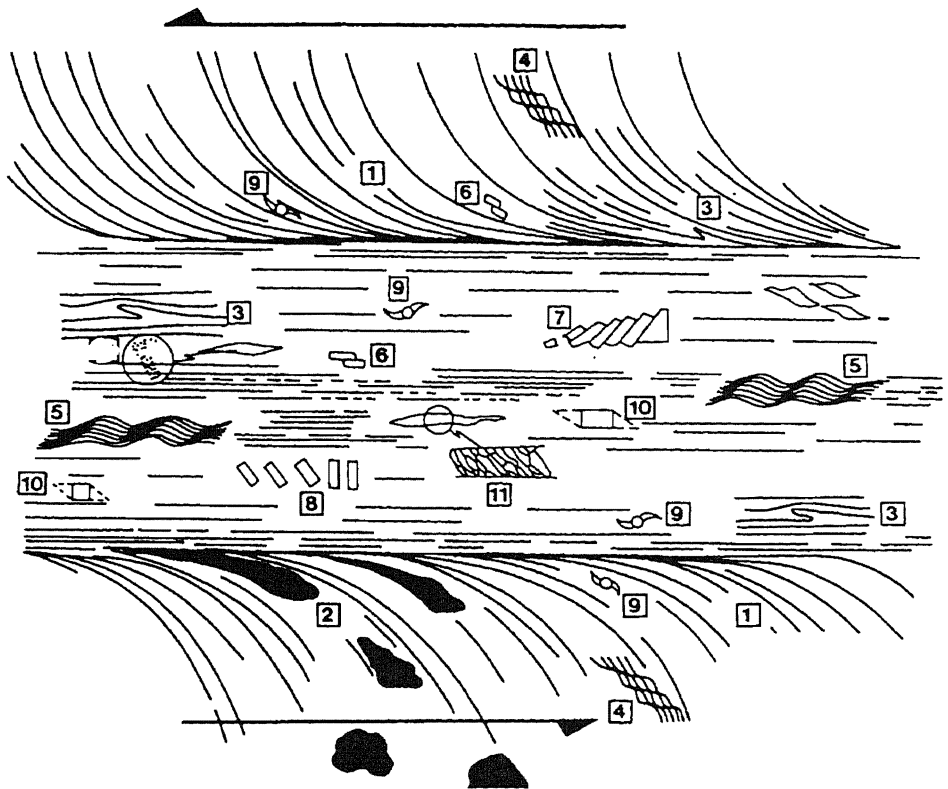
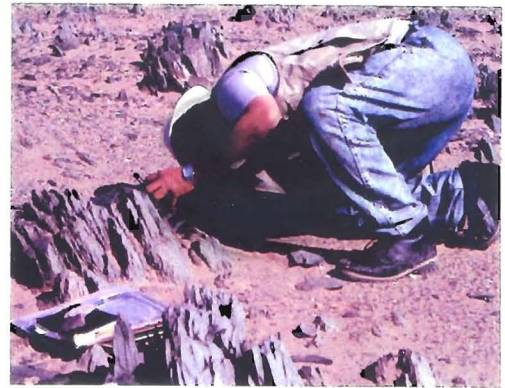


Fig. 2.20 Criteria for sense of shear used in central Wadi Allaqi (after White *et al.* 1986)

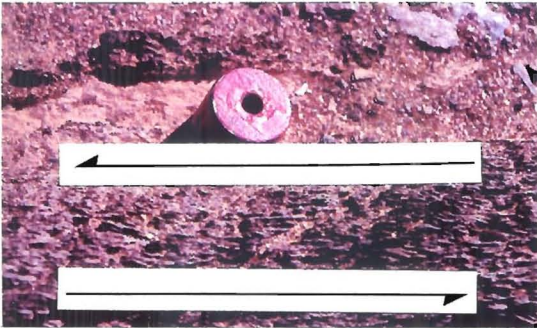
1. rotation of pre-existing or generated foliation;
2. rotation of deformed markers;
3. asymmetry of intrafolial folds;
4. microshears or C-bands;
5. shear bands or S-bands;
6. sheared porphyroclasts;
7. rotation of fragments owing to shear fractures;
8. rotation of fragments owing to tensile fractures;
9. asymmetry of trails growing around rotating clasts;
10. asymmetry of trails growing around non-rotating clasts;
11. asymmetry of elongate recrystallized quartz grains;



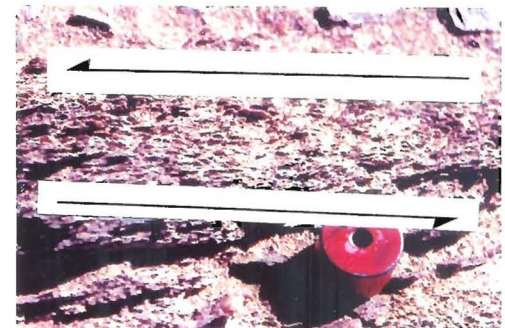
a



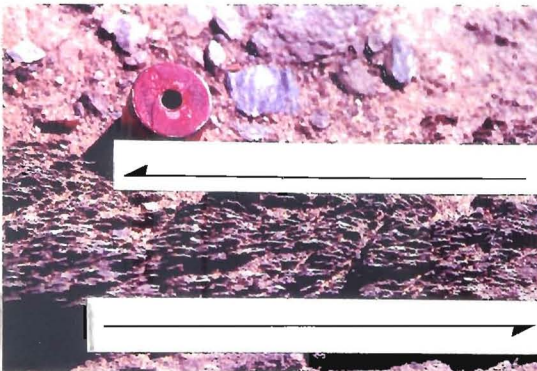
b



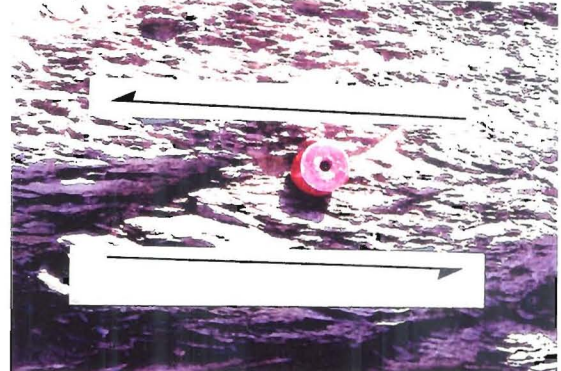
c



d



e



f

Fig. 2.21 Sense of shear within shear-zones
 (a) Allaqi Shear-zone showing upright S1 mylonite foliation (GR 7582586357), the height of the rock face is 15m
 (b) steeply inclined mylonite foliation (S1) within the Allaqi Shear-zone showing the sigmoidal shape of the foliation (GR 7998680100)
 (c), (d), (e) and (f) C-S structures in the mylonite of the Allaqi Shear-zone all indicated sinistral shear: photographs taken normal to S1 foliation (left to right) and approximately normal to L1 intersection lineation (GRs (c) 7556386619), (d) 7789179926, (e) 7888178354, (f) 7847378762)
 Circular magnet scale is 1 cm in diameter

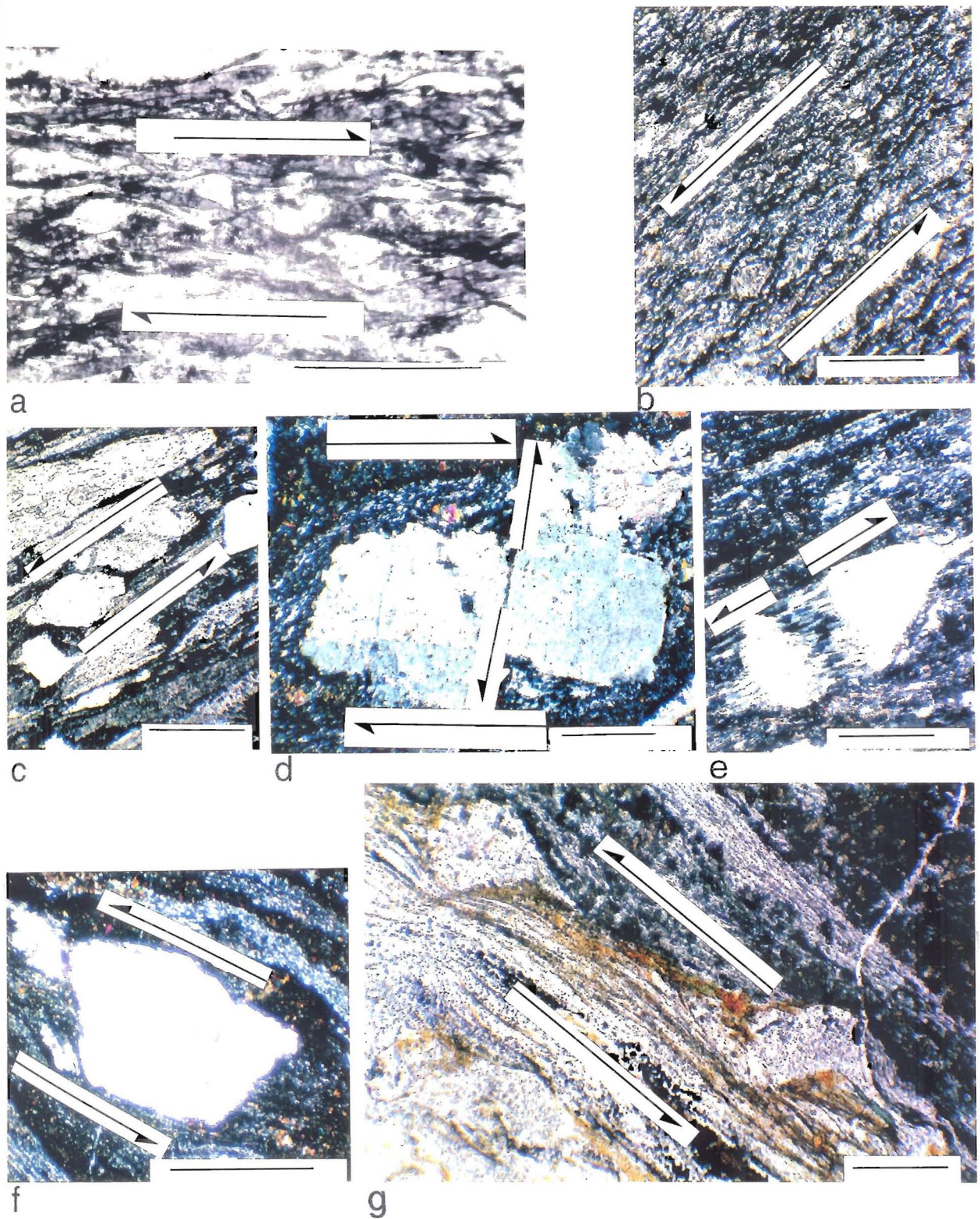


Fig. 2.22 Photomicrographic evidence for sense of shear

- (a) micro C-S fabrics indicating dextral sense of shear in tremolite-actinolite schists, Filat Succession (plane polarized light; GR 6919087288; scale bar 0.5 mm)
- (b) micro C-S fabrics indicate sinistral sense of shear in phyllite, Allaqi Shear-zone (plane-polarized light; GR 7405086269; scale bar 0.1 mm)
- (c) domino-like structures displaced dextrally (antithetic shear) in mylonite showing overall sinistral sense of shear, Allaqi Shear-zone (plane-polarized light; GR 7405286271; scale bar 0.1 mm)
- (d) sinistrally-displaced fracture in plagioclase grain indicating overall dextral sense of shear in mylonite, Allaqi Shear-zone (cross-polarized light; GR 7404986267; scale bar 0.1 mm)
- (e) parallel pull-apart structure in phyllite, Um Relan Succession; gap filled with fibres of quartz and mica (plane-polarized light; GR 6494292206; scale bar 1 mm)
- (f) V-shaped pull-apart structure in plagioclase showing a smaller fragment separated from a larger fragment indicating sinistral sense of shear in a mylonite, Allaqi Shear-zone (plane-polarized light; GR 7405086269; scale bar 1 mm)
- (g) $\sigma\alpha$ porphyroclast system indicating sinistral sense of shear in a mylonite, Allaqi Shear-zone (plane polarized light; GR 7405086269; scale bar 0.1 mm)

associated with pull-aparts is that infillings occur of quartz fibres or fine-grained mica-quartz aggregates between the separated fragments during greenschist facies metamorphism (Ramsay 1980; Cox & Etheridge 1983,1989; Fig. 2.22e). The sense of movement of rigid objects along microfractures depends mainly on the initial orientation of these fractures relative to the kinematic framework (Simpson & Schmidt 1983; Simpson 1986). The most widely applied kinematic indicators of this type are *porphyroclasts* (Passchier & Simpson 1986) which are divided into either σ or δ -types on the basis of the geometry of the tails. The former types have median lines on opposite sides of reference plane parallel to the tail and containing the symmetry axis for the system. σ -types are further subdivided into a σ_a -types (Fig 2.22d), in which the porphyroclast is isolated in a relatively homogeneous matrix, and σ_b -types, in which porphyroclast system is associated with a shear-band foliation in the matrix. δ -types of porphyroclast display characteristic bends and short tails.

The relationship of small-scale kinematic inferences to the large-scale is rarely a straightforward matter since natural deformation processes are normally heterogeneous and antithetic movements are common phenomena because most shear-zones have a component of pure shear acting perpendicular to the mylonitic foliation which leads to back rotation of the porphyroclast, opposite to the overall sense of shear (Simpson & Schmidt 1983, Passchier & Simpson 1986). Regional analysis (Fig. 2.23) of the Allaqi Shear-zone has involved the use of as many kinematic criteria as possible. Many scales have been used and the criteria have been related to known regional structures. σ_b - and δ -types of porphyroclasts have not been recognized in the Allaqi Shear-zone. The axial-surface-traces of the F1 folds are presently aligned in a N-S direction (Fig. 2.23) and the folds often occur in sigmoidal shear-pods. Microtextural evidence (*e.g.*, quartz pressure fringes in Fig. 2.9d) supports a simple anticlockwise rotation (less than 25°)

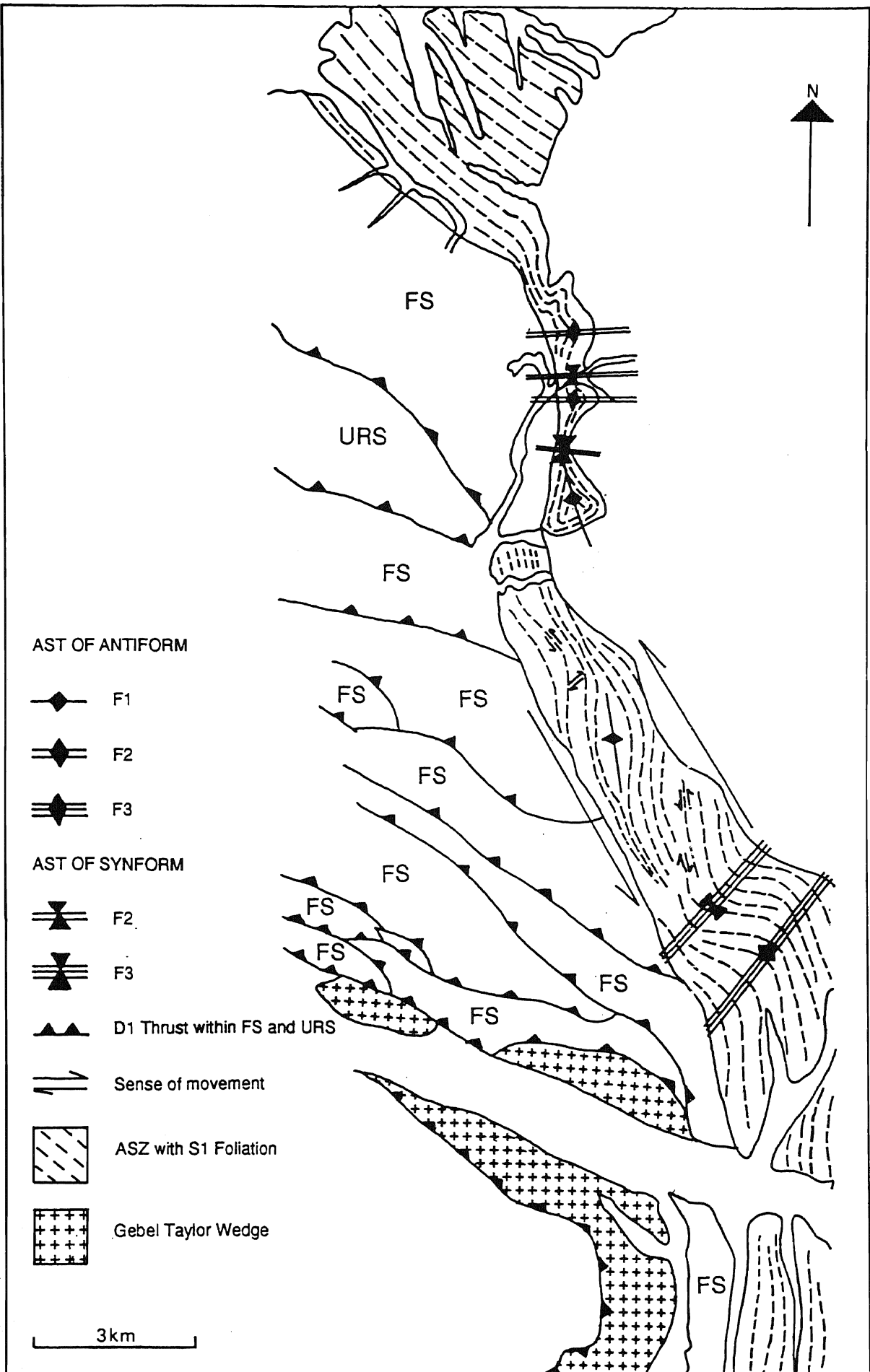


Fig. 2.23 Synopsis of the structures in the Allaqi Shear - zone (ASZ) .
 AST - axial-surface trace; FS - Filat Succession;
 URS - Um Relan Succession

of the structures during D1; and the F1 folds developed obliquely to the shear direction and during progressive deformation rotated to a N-S alignment. This would mean that the axial-surface-traces originally trended NNE-SSW.

Collation of the various data (Fig. 2.23) show that the Allaqi Shear-zone:

- (a) has a complex progressive deformation history which commences with the formation of NNE-SSW-trending recumbent-type folds (F1)
- (b) is a major D1 structure and related to the large-scale thrust duplex structures found in rocks outside
- (c) exhibits an overall sense of sinistral and oblique shear
- (d) is a brittle-ductile shear (Ramsay & Huber 1987)
- (e) was principally deformed by a mechanism of softening processes (e.g. Rutter 1976; White *et al.* 1980, 1986)

2.10 Metamorphic history in relation to the tectonic history

Apart from the rocks of the Gebel Taylor Wedge (see section 3.6) the largely metabasic rocks of the area have been metamorphosed to a low-grade greenschist facies (*i.e.*, 2-3 kilobars pressure and 260-300°C temperature, Barker 1990 p.149). Chlorite, tremolite-actinolite amphibole, and epidote (Fig. 2.24) are typical indicators of the grade of metamorphism and relic plagioclases of an originally labradorite composition are frequently altered to albitic-rich varieties. Evidence from north of the Wadi Allaqi area about 10 km toward the north (Allaqi White Marble Quarry, west of Wadi Shilman), where almandine garnets and fibrolitic sillimanite have been observed (Fig. 2.24e,f) in pelitic bands, indicates that there is an increase in the grade of metamorphism from south to north (Fig. 2.24). This observation has been corroborated by others (*e.g.*, Prof. El Gaby, personal communication).

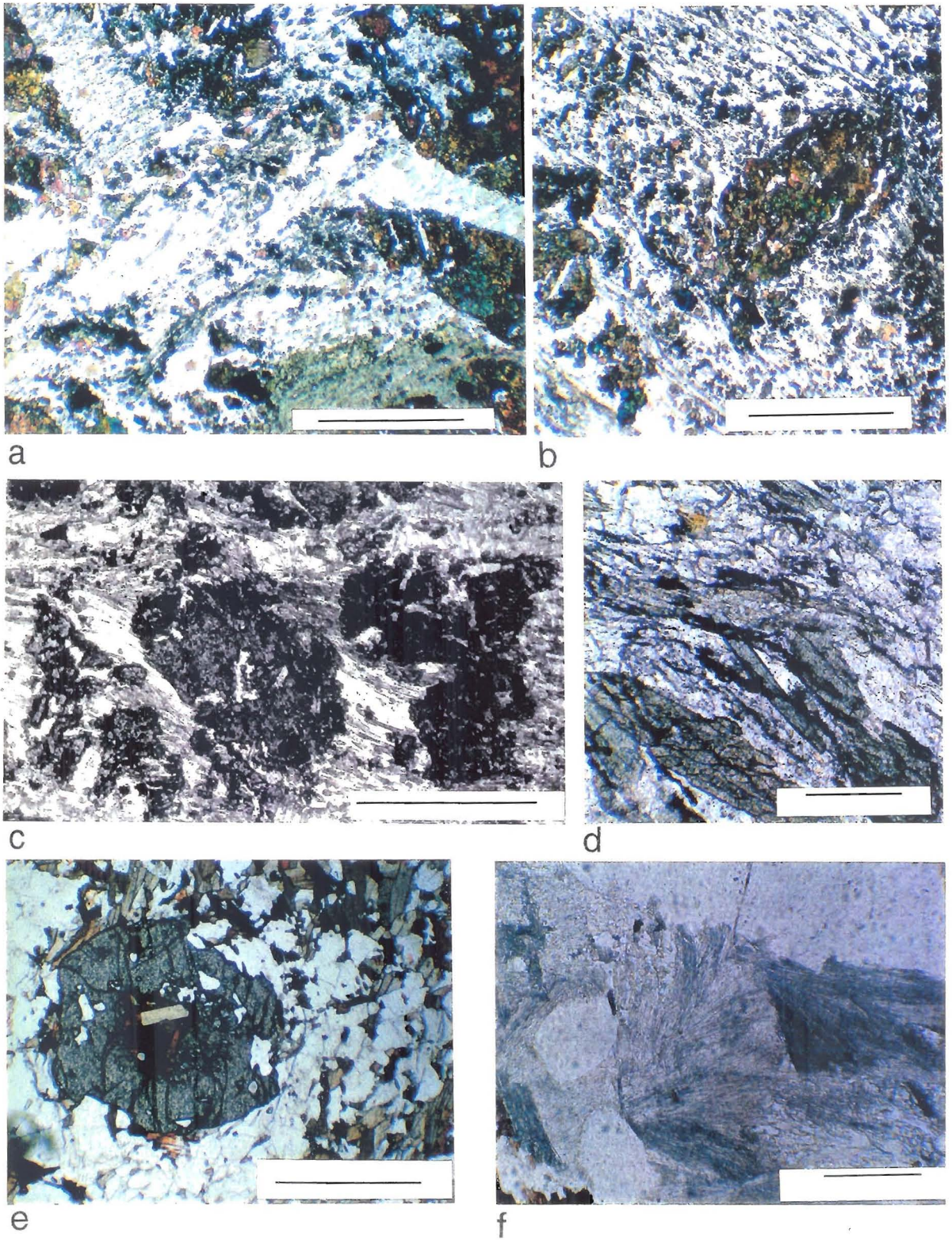


Fig. 2.24 Evidence for the metamorphic history

- (a) chlorite (Chl) developed parallel to S1; statically grown epidote (Ep) disrupted during D2 in volcaniclastic rocks, from Kholoud Formation (plane-polarized light; GR 6700893923; scale bar 1 mm)
- (b) smaller syn-D1 epidote (Ep1) grown parallel to S1 in volcaniclastic rocks from Kholoud Formation (plane-polarized light; GR 6700893923; scale bar 1 mm)
- (c) statically-grown epidote (Ep) on S1 phyllosilicates, which are folded by F2 microfolds syn-D2 disruption of epidote in volcaniclastic rocks, Kholoud Formation (plane-polarized light; GR 6700893923; scale bar 0.5 mm)
- (d) tremolite-actinolite developed parallel to S2 and inclined to S1 in volcaniclastic rocks, Atshani Formation (plane-polarized light; GR 6133386677; scale bar 0.1 mm)
- (e) zoned garnet porphyroblast developed at the expense of biotite parallel to S1 in pelitic schist, 10 km due north of the NW extremity of north of central Wadi Allaqi (plane-polarized light; scale bar 0.1 mm)
- (f) fibrolitic sillimanite aggregates replacing biotite fabric (S1) in pelitic schist, 10 km due north of the NW extremity of north of central Wadi Allaqi (plane-polarized light; scale bar 0.1 mm)

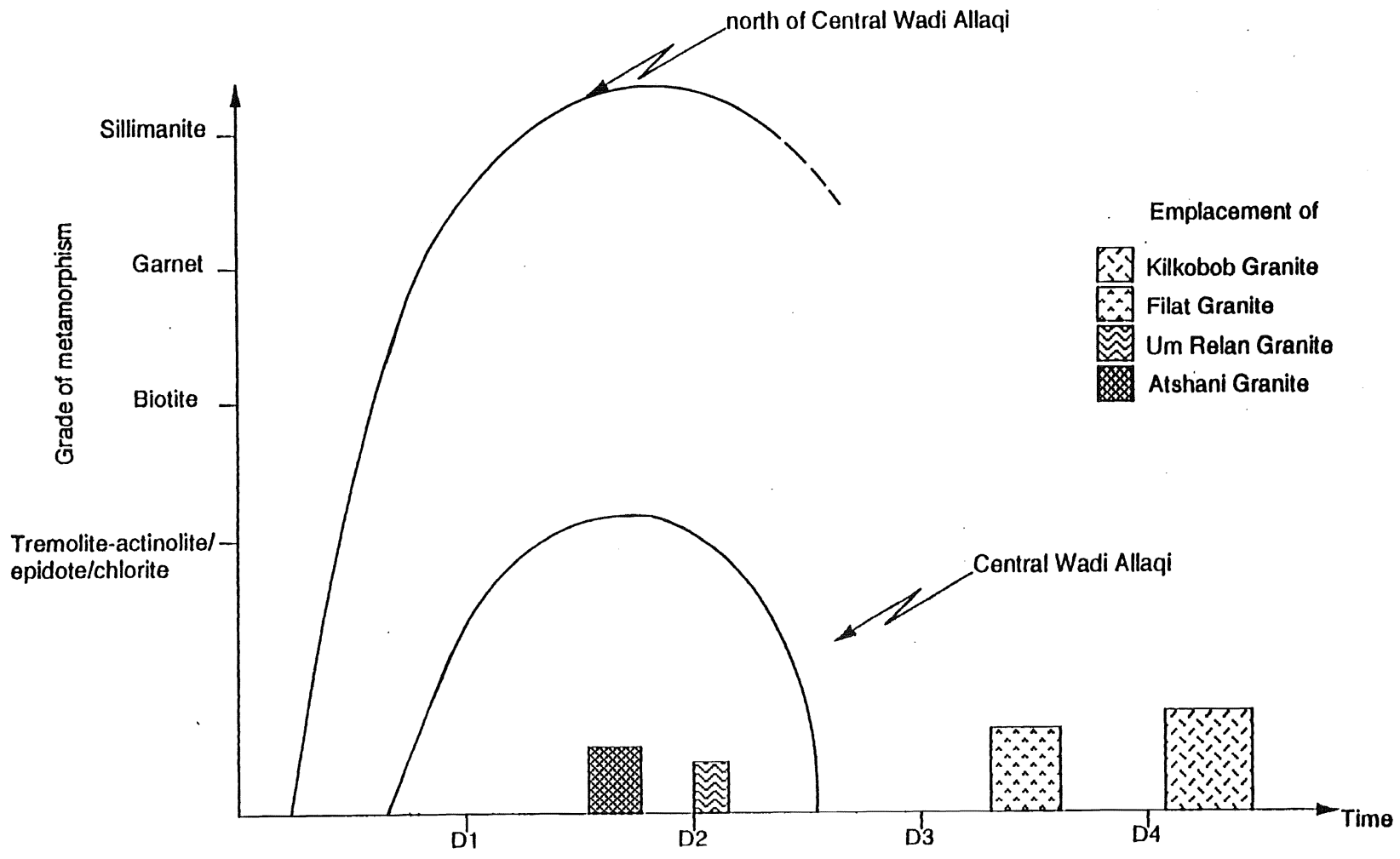


Fig. 2.25 Summary of the metamorphic history in central Wadi Allaqi

Textural studies (Figs. 2.24, 2.25) indicate that the acme of regional metamorphism in the area was maintained from early-D1 until D2 times. Initial metamorphic mineral growth in the volcanoclastic rocks (*e.g.*, epidote in Fig. 2.24a,b,c,d) occurred before the formation of the S1 foliation which was associated with the predominant thrusting. Chlorite, probably formed from biotite of an igneous origin within the Atshani Granite (see section 4.2.1), with its, now deformed, quartz inclusions is aligned parallel to S1 (Fig. 4.3d).

However most minerals grew in syn-D1 and post-D1-pre-D2 times (Fig. 2.24) and the grade of metamorphism must have been maintained for a considerable length of time. This conclusion is not in agreement with a more generalized account of the rocks of the Eastern Desert (Greiling *et al.* 1990) which has concluded that all metamorphic growth occurred prior to the deformation.

In the schistose basic igneous rocks of the Gebel Taylor Wedge original olivine has been altered to serpentine with the occasional production of talc and chlorite. Relict glaucophane, which has been deformed by D1 structures, has been recorded from one sample (Fig. 3.20d) and a metamorphic event of blueschist facies appears to have been overprinted by the prolonged regional greenschist facies metamorphic event.

2.11 Summary

The deformation history and kinematic analysis indicate that the central Wadi Allaqi rocks are allochthonous relative to the Nile Craton. The structural history shows some similarity to the tectonic evolution model of mountain belts proposed by Dewey (1988) and Greiling *et al.* (1994), partly based on my work (see Taylor *et al.* 1993), have recognised elements of this model for the Pan-African orogeny (Table 2.2). Earlier ductile events (D1 and D2) are succeeded by more brittle events (D3, D4, and D5).

Table 2.2 A comparison between the development of the Pan-African orogeny in the central Wadi Allaqi and the tectonic evolution of mountain belts as summarized by Dewey (1988) [TBCL thermal boundary condition layer; HT-high temperature; HP/LT-high pressure/low temperature; ED-Eastern Desert]

Phase	Tethyan orogeny (Dewey 1988)	Pan-African, ED (Greiling <i>et al.</i> 1994)	central Wadi Allaqi Present study
5	post-extensional thermal recovery, thickening of TBCL, eventual retrograde metamorphism, marine transgression	subsidence (530 Ma)	D5
4	convective TBCL thinning, mantle partial melting, mafic magmatism, minimum-melting granite suites, HT mantle diapir, rapid subsidence, extensional basin, Verrucano-type deposits	subsequent thrust stacking (575 Ma) accelerating extensional collapse, (radial) extension, development of metamorphic core complexes, little relationship between, displacement vectors and bounding plate slip vectors (595 Ma)	D4 Kilkobob Granite emplacement D3
3	catastrophic erosion of the TBCL, rapid uplift, pro-grade HT metamorphism, post-tectonic granite suites	beginning extension (600 Ma)	Filat Granite emplacement
2	post-or slow-convergence, slow uplift, 40 Ma to few Ma thermal reequilibration, slow thinning of TBCL, minor alkaline to silicic granites	thrust and strike-slip structures, strong direct relationship between shortening structures and plate slip-vector (615 Ma)	D2 Um Relan Granite emplacement Atshani Granite emplacement
1	lithospheric/crustal shortening and thickening, HP/LT blueschist and kyanite bearing metamorphic assemblages, continental collision, rift inversion, compressive continental margin arc		D1 subduction associated with HP/LT blueschist metamorphism of Gebel Taylor Wedge

Quantitative estimates of the amount of deformation during D1 indicate significant differences between rocks found to the south and west of the Allaqi Shear-zone from those which crop out east and north of the Shear-zone. The Allaqi Shear-zone was formed initially during D1 with a bulk sinistral shear-sense and movements towards the north. Estimates of the amount of horizontal translation indicates that the hanging wall for each major thrust was moved as much as 16 km. Since there were seven major thrusts within Filat Succession the total bulk movements must have been in excess of 100 km.

The mineral assemblages in most of the constituent rocks indicate that greenschist facies metamorphism occurred during the early stages of deformation and was developed over the period of the D1 and D2 events, although there is some evidence of a relict blueschist facies event earlier than the syn-D1 metamorphism in the allochthonous Gebel Taylor Wedge rocks. The history of metamorphism is relatively simple and, based upon evidence outside the central Wadi Allaqi area, the metamorphic grade increases towards N.

Chapter Three

Tectonic-stratigraphy

3.1 Introduction

As can be seen from chapter two the rocks which crop out in the area have been affected by strong and complex deformation and low-grade metamorphism. So it is unlikely that a complete and continuous stratigraphic sequence is present in the area. Moreover there are very few marker bands in the sequences to aid correlation of lithological units. Most of the succession is made up of ancient volcanoclastic rocks which are notoriously difficult to interpret unambiguously (Cas & Wright 1987, p 355) so the non-genetic classification and terminology of Cas & Wright (1987, tables 12.7 and 12.8) has been adopted for this thesis. Original sedimentological and igneous textures are often preserved and there is abundant facing evidence with well-preserved original bedding (Figs. 3.1 & 3.2). None of the original stratigraphical boundaries of the major lithostratigraphic units are preserved, because the units are juxtaposed through tectonic processes, so a quasi-formal terminology was devised to classify the tectonic-stratigraphy units (Soper & England 1995; table 3.1). The term tectonic-stratigraphy is used in the sense of stratigraphy disrupted by thrusts and is preferred to tectono-stratigraphy which has been used ambiguously by some authors (Holdsworth *et al.* 1994; Howell 1995) and not in terms of tectonic controls on sedimentation (Bates & Jackson 1987; Surlyk 1991). This represents the first attempt to apply rigorous tectonic-stratigraphical nomenclature to the Neoproterozoic rocks of the Eastern Desert and the methodology involves a mixture of standard lithostratigraphical techniques (*e.g.*, Tucker 1986; Whittaker *et al.* 1991) combined with an intimate knowledge of the structural geology. The tectonic thicknesses of the units were estimated using the method of Taylor (1966), in which an estimate of the thickness of lithological

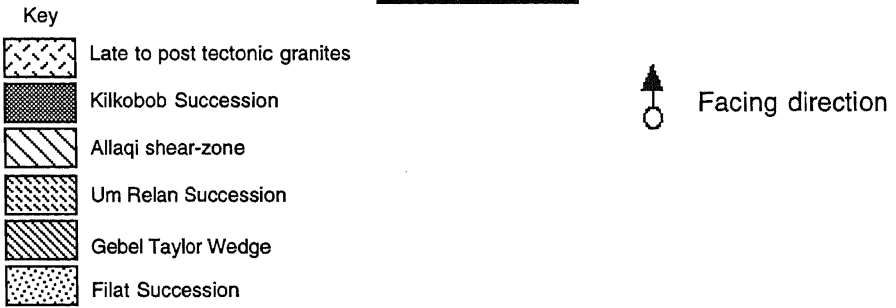
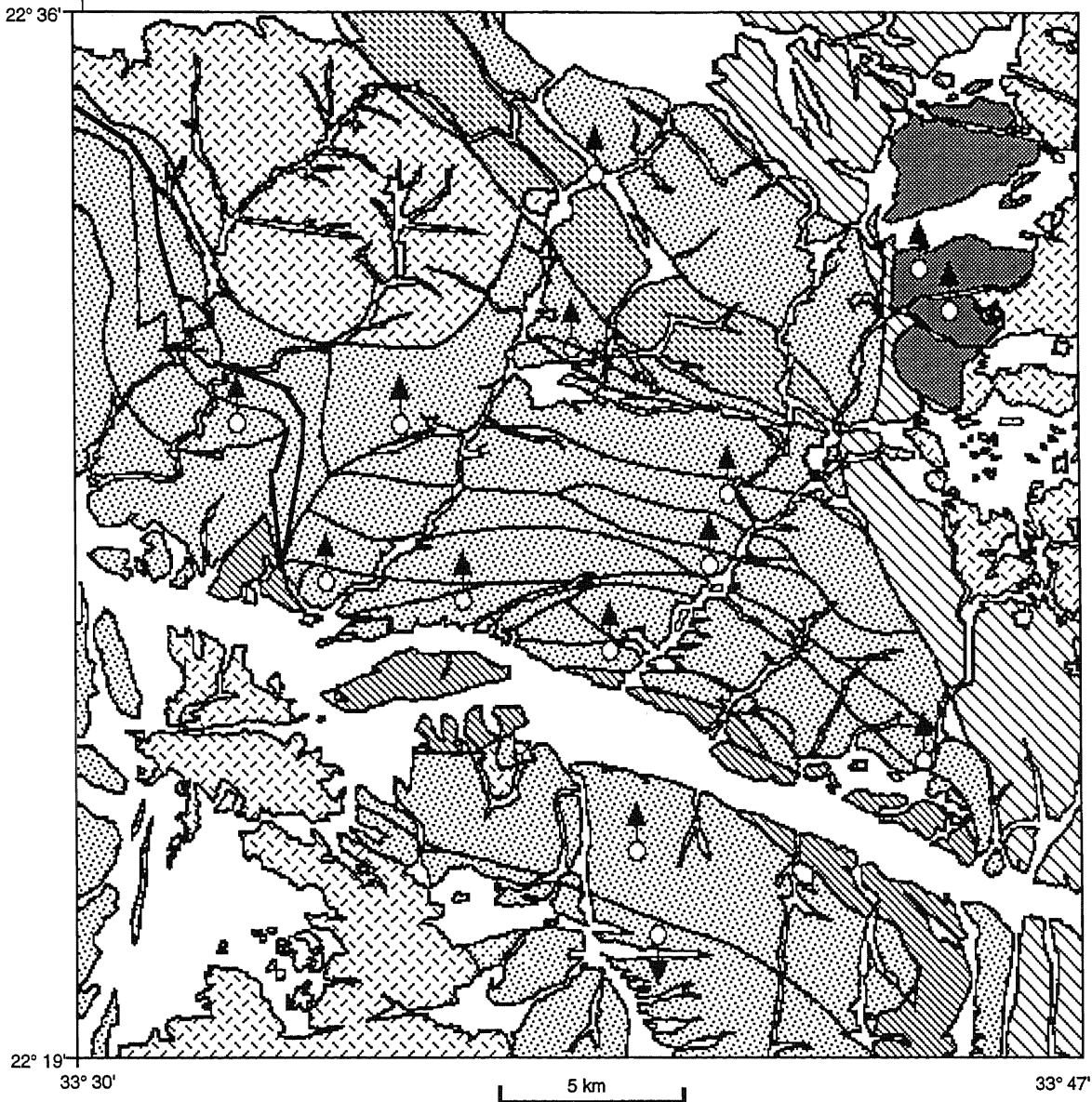
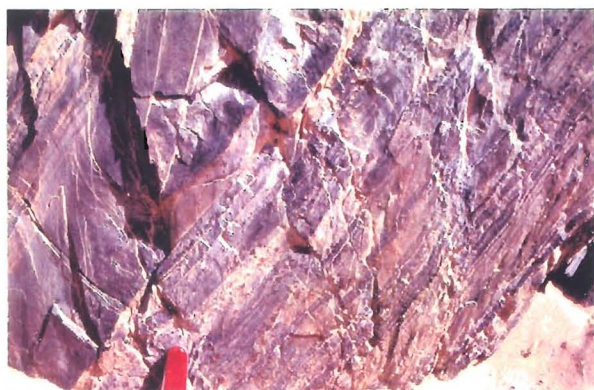
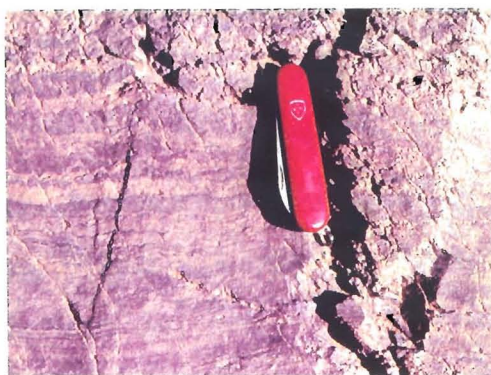


Fig. 3.1 General lithological map with facing directions



a



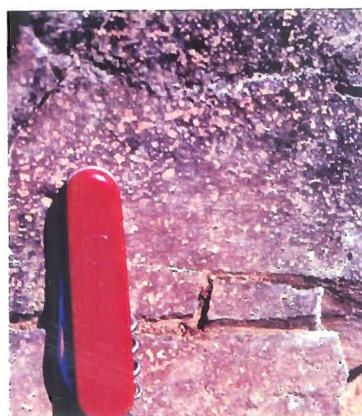
b



c



d



e

Fig. 3.2 Evidence for facing direction

(a) downward graded bedding in Neiqit Formation (see also Fig. 2.3b, (GR 6680472738)

(b) crenulated lamination crossed by S₂, Neiqit Formation (GR 6680472741)

(c) downward-facing convolute lamination, Neiqit formation (GR 6679872736)

(d) upward-facing scoriaceous basaltic lavas with weathered blocky tuff in Kazzaz Formation (GR 5478685687)

(e) vesicular lava in Kazzaz Formation (GR 6459379198)

unit in a area of structural complexity may be obtained from the trigonometrical relationship of the inclination of the enveloping surface and its outcrop width, combined with strain data and balanced sections.

Three major and lithologically-distinct tectonic-stratigraphical Successions have been recognised, Filat, Um Relan and Kilkobob Successions and are separated by structural zones of relatively high tectonic strain (Fig. 3.1). An allochthonous unit consisting of schists and basic & ultra-basic intrusive rocks, the Gebel Taylor Wedge, is emplaced within the structurally lower Filat Succession. The tectonic pile has been intruded by granitic bodies (see chapter 4) and late-stage basic igneous sills.

Table 3.1 Terminology for Tectonic-stratigraphical units used in this thesis

Tectonic-stratigraphical unit	Definition
Succession	a relatively consistent and thick rock unit of two or more than two groups (cf. Long & Max 1977)
Group	two or more formations
Formation	homogeneous mappable unit
Member	subdivision of formation (usually lens or wedge)

3.2 Earlier Classifications

Earlier subdivisions of the Neoproterozoic rocks of the Eastern Desert are shown in Table 3.2. Hume (1934) classified the rocks into four major divisions which have more or less been followed since (e.g., El Ramly & Akaad 1960; Akaad & El Ramly 1960; El Shazly 1964; Sabet 1972; El Ramly 1972; Akaad & Noweir 1980), although Schurman (1953) attempted to add the Shaitian granite as a new division to the classification but, subsequently, it was shown that the Shaitian granite was a deformed older granite (Akaad & El Ramly 1963; Akaad & Moustafa 1963). Recent workers

Table 3.2 Previous classifications of the Neoproterozoic succession of the Eastern Desert of Egypt

Hume (1935)		El Ramly (1972)	El Gaby <i>et al</i> (1988)	Hassan & Hashad (1990)	Approx. dates (after Stern 1994)
(Gattarian)	Igneous intrusions Alkali Granite felsite & dolerite dykes Red granite	Alkali granite & syenite intrusions	Subalkaline to per-alkaline silicic igneous rocks	Peralkaline granite intrusions	Phanerozoic
	Bt & Hbl-granites Diorite Peridotite	Younger granites Gabbro Post-Hammamat felsite	"Cordilleran stage" Calc-alkaline granites (G1 & G2) and their volcanic suit (Dokhan); pencontemporaneous molass sediments (Hammamat) and Iherzolite-gabbro- diorite intrusions	Felsic calc-alkaline to peralkaline volcanism and molasse type sedimentation	
(Eparchean)	Hammamat or Upper para- schist Dokhan volcanic rocks	Hammamat Group Dokhan volcanic rocks			
(Metarchean)	Shadli or Middle paraschists	Metagabbro-diorite Serpentinities Geosynclinal Shadli metavolcanic rocks Geosynclinal metased- imentary rocks	"Island Arc stage" Island arc assemblage: intermediate metavolc- nic rocks, tuffs & volcanogenic greywa- ckes. Ophiolite: Metabasalts, metadolerites, metaga- bbro and serpentinite.	Oceanic and island arc volcanism and sedimentation Intermediate and acid igneous intrusions of various ages.	----- 700 Ma -----
	Shait granite (Shurman 1953) Fundamental gneiss	Migif-Hafafit paragneiss and migmatites	Granites (including Shait granite) and high grade Schist and gneiss, (largely mylonitized or remobilized during the Pan-African orogeny).	"Pre-Pan-African" psammitic schist and gneisses.	----- 850 Ma ----- ----- 1000 (?) Ma -----

have attempted to place the sequence into a plate tectonic context (Table 3.2; El Gaby *et al.* 1988, 1990; Hassan & Hashad 1990) with limited success. The foregoing account supersedes and up-dates a preliminary subdivision of the area by Taylor *et al.* (1993).

3.3 Filat Succession

3.3.1. General characteristics

The Succession is an at least 15 km thick pile of various types of volcanoclastic rocks from fine-grained to coarse-grained with basaltic to andesitic affinities, coeval sub-volcanic intrusions, and rare thin meta-limestones. Rocks of the Succession crop out over the majority of the study area (Figs. 3.4, 3.5). The lowermost boundary of the Succession is not exposed in the area. The allochthonous Gebel Taylor Wedge (section 3.5) allows a separation of the Succession into the North Allaqi Group (Fig. 3.4b & c) and Neiqit Formation (3.4a). To the north-east a relatively small outcrop of Kholoud Formation is sandwiched by the bifurcating outcrops of the Allaqi Shear-zone and occurs in the core of a thrust horse (Figs. 1.3b, 1.4). All three main tectonic-stratigraphical units are considered a single tectonic stratigraphical Succession because they share broadly similar tectonic histories and characteristics.

3.3.2 The Neiqit Formation

This Formation, with minimum thickness of 2 km, occurs within a north-facing (Shackleton 1958), faulted recumbent D1 fold which has been arched into a large-scale D2 antiform (Figs. 1.4, 2.6b, 3.4a) and is distinguished from the North Allaqi Group by the absence of rudaceous units and the rarity of lavas and sub-volcanic intrusions. The type-section for the Formation was measured in Wadi Neiqit (Fig. 3.4a). Medium-grained grey volcanoclastic rocks form the bulk of the sequence with no distinct marker bands, although rare, impersistent, thin (2-3 m), lens-like intercalations of meta-limestones

and lavas occur, further subdivision of the unit could not be achieved. Graded-bedding and convolute lamination (Fig. 3.2) is frequently observed throughout the Formation but attempts to establish *Bouma* sequences were not successful.

In thin-section (Fig 3.6) the volcanoclastic rocks show sedimentary textures particularly in the coarser-grained fraction. The matrix to the clasts is usually greater than 80%. The mineral composition is normally feldspar-quartz-chlorite-white mica-epidote. Chemical analyses of the volcanoclastic rocks (Appendix B) plot in the field of andesite-basalt (Winchester & Floyd 1977, Fig. 3.9) and have higher enrichments in light-rare earth elements (LREE) (Fig. 3.9). These rocks are epiclastic reworked volcanoclastic sandstones and siltstones (Cas & Wright 1987; Fisher 1961) and the reworking was at an early stage since the detrital material is chemically close to calc-alkaline affinities of island arc material (Fig. 3.8) because they are characterized by high $\text{Fe}_2\text{O}_3 + \text{MgO}$ (8 to 14%) and high $\text{Al}_2\text{O}_3/\text{SiO}_2$ (0.24 - 0.33%).

At the northern part of this formation a single iron-stained *meta-limestone* lens (about 2 m thick and 50 m long) is intercalated within the volcanoclastic rocks. The main constituents are calcite, quartz and limonite.

3.3.3 The North Allaqi Group

The outcrop of the entire Group lies within a thrust duplex complex in which seven major thrusts are recognised north of Wadi Allaqi (Fig. 2.5). A total horizontal movement in the order of 100 km can be established for movements within the Kazzaz Formation of the Filat Succession (Figs 3.3a,b) by using sectional balancing techniques (see section 2.11). The Group consists of about 13 km of mainly volcanoclastic rocks and may be divided into four formations, *viz.*, Kazzaz Formation, Granite Boulder Formation, Atshani Formation and Kholoud Formation.

The type-section for the **Kazzaz Formation** is just to the east of the southern part of Wadi Um Relan (Fig. 3.4b) where c.5 km of almost

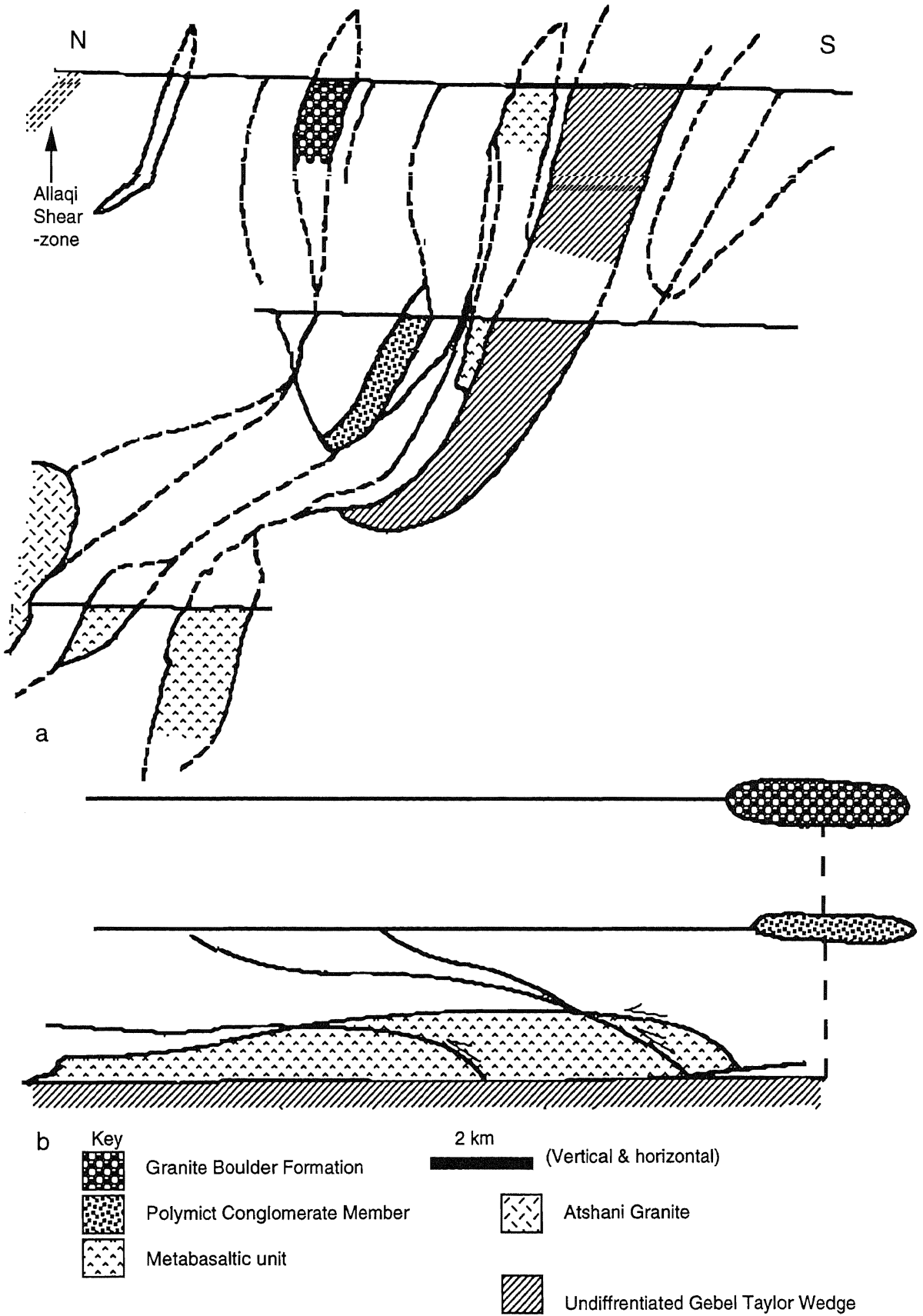


Fig. 3.3 (a) Tectonic cross-section of part of the Filat Succession (Unshaded above)
 (b) A balanced cross-section of the Kazzaz Formation using upper thrust surface of Gebel Taylor Wedge as a base line

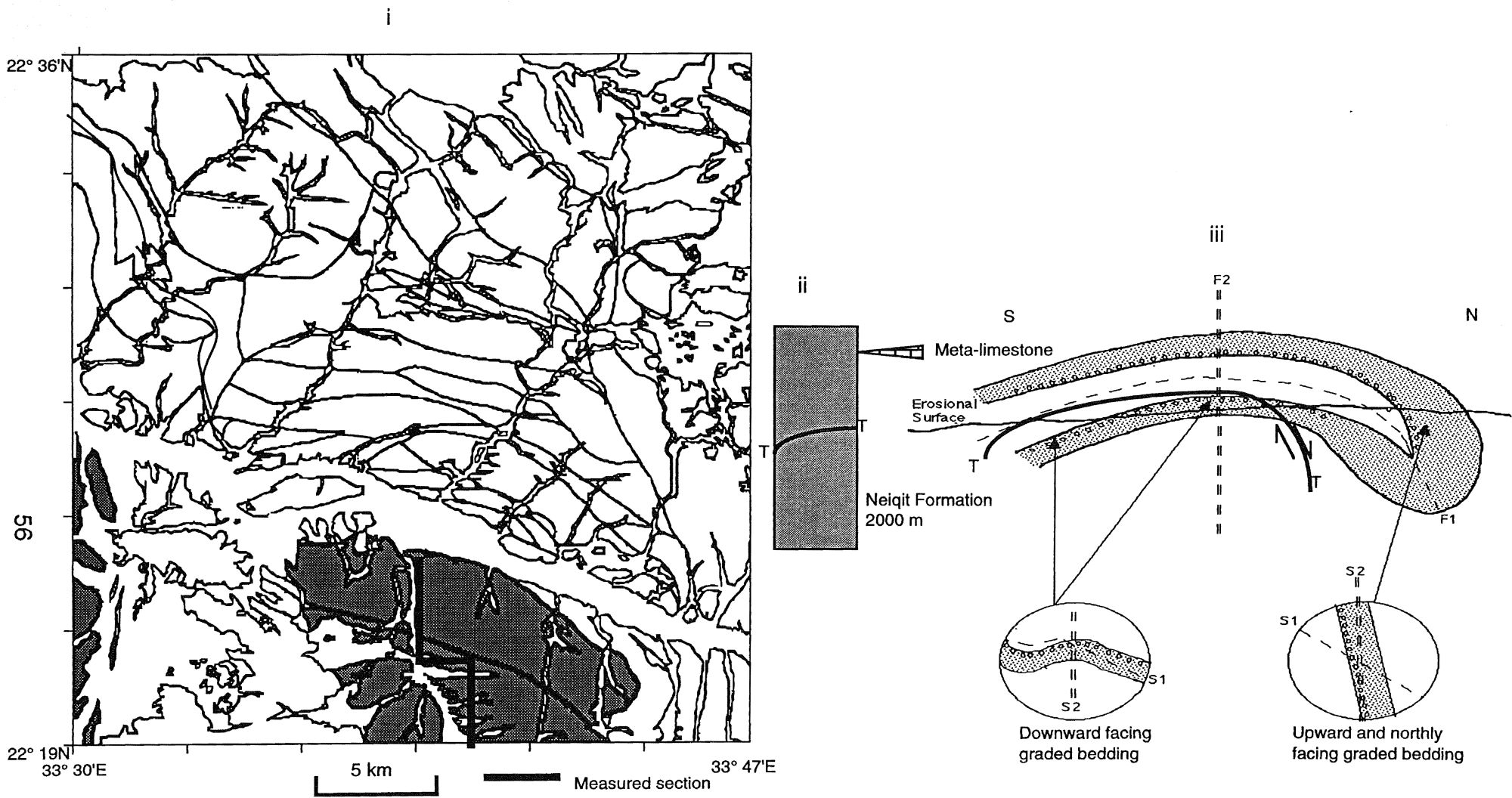


Fig 3.4a (i) The Neiqit Formation outcrop; (ii) stratigraphic column ; (iii) refolded recumbent fold involving the Neiqit Formation, note F1 is axial-surface trace of D1 fold, F2 is axial-surface trace of D2 fold (from Fig.2.6)

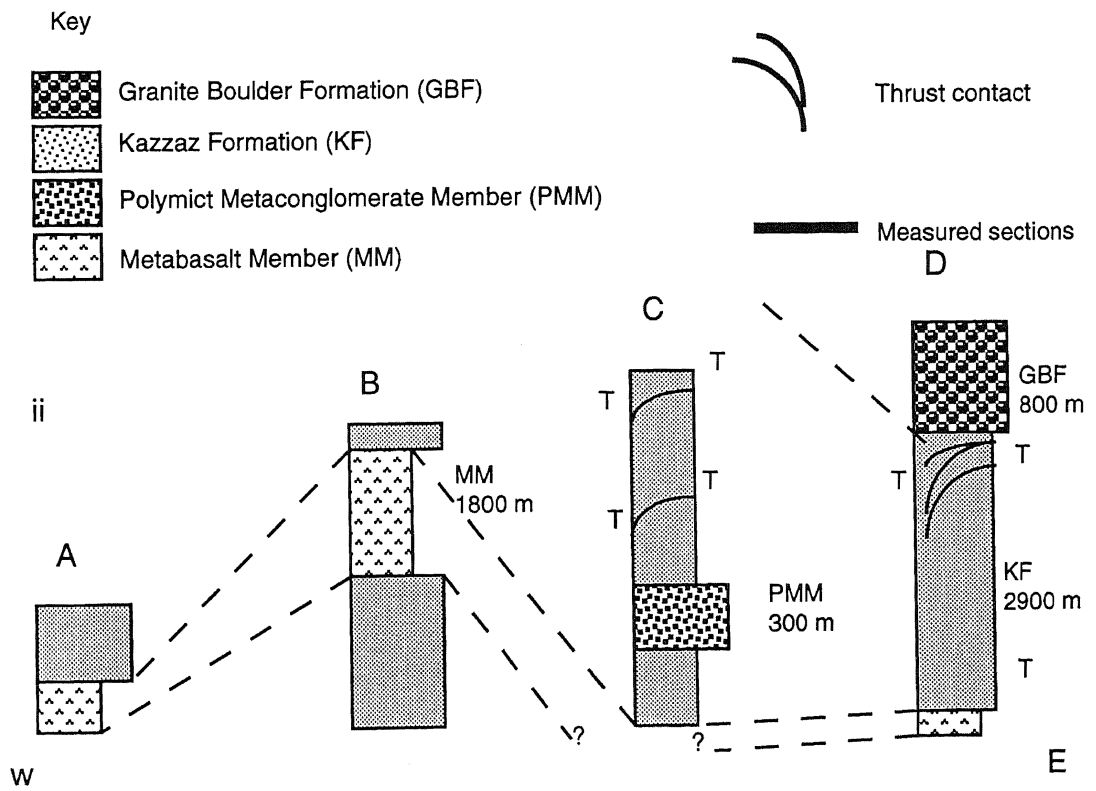
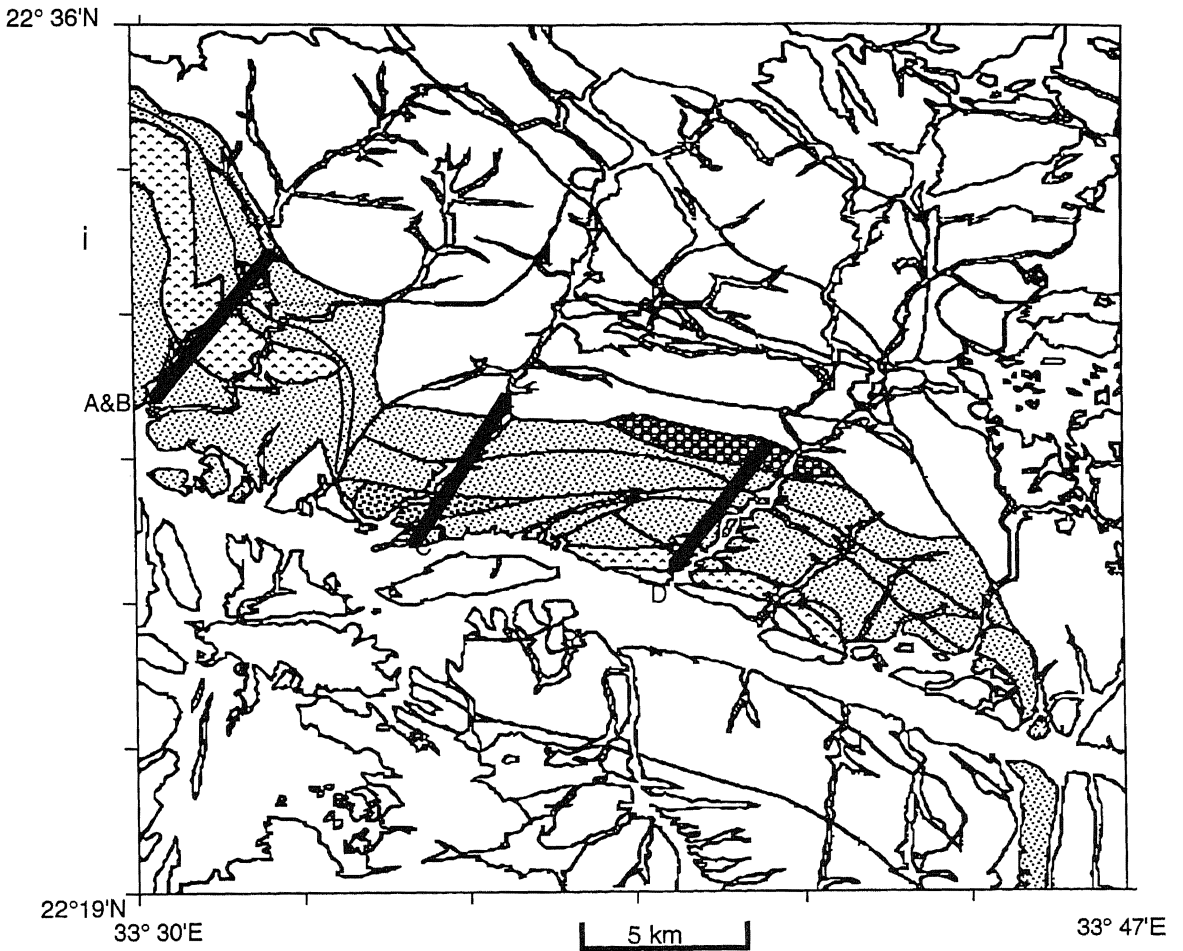


Fig. 3.4b (i) Kazzaz Formation and Granite Boulder Formation outcrop and (ii) stratigraphic columns of the Kazzaz Formation and Granite Boulder Formation

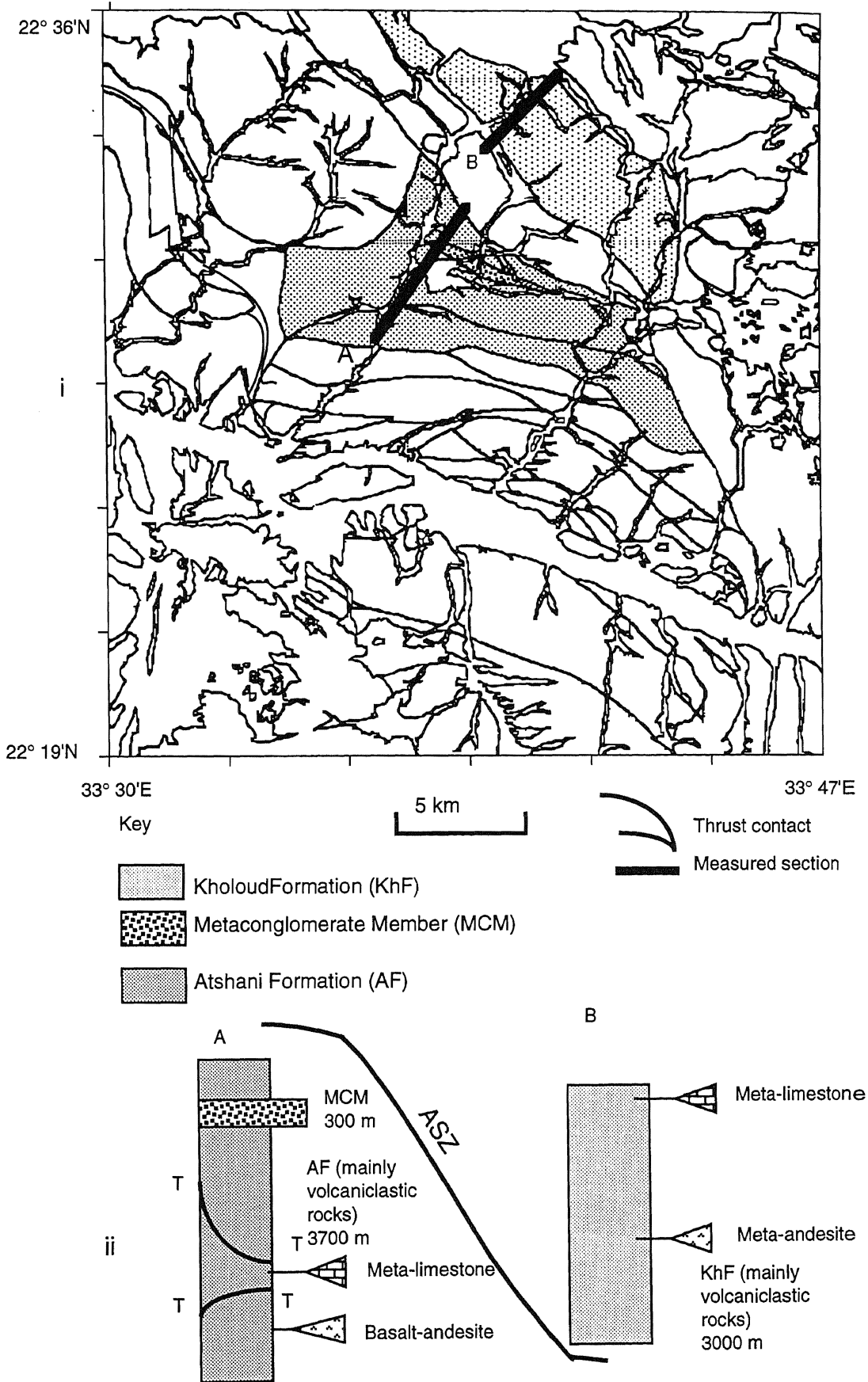
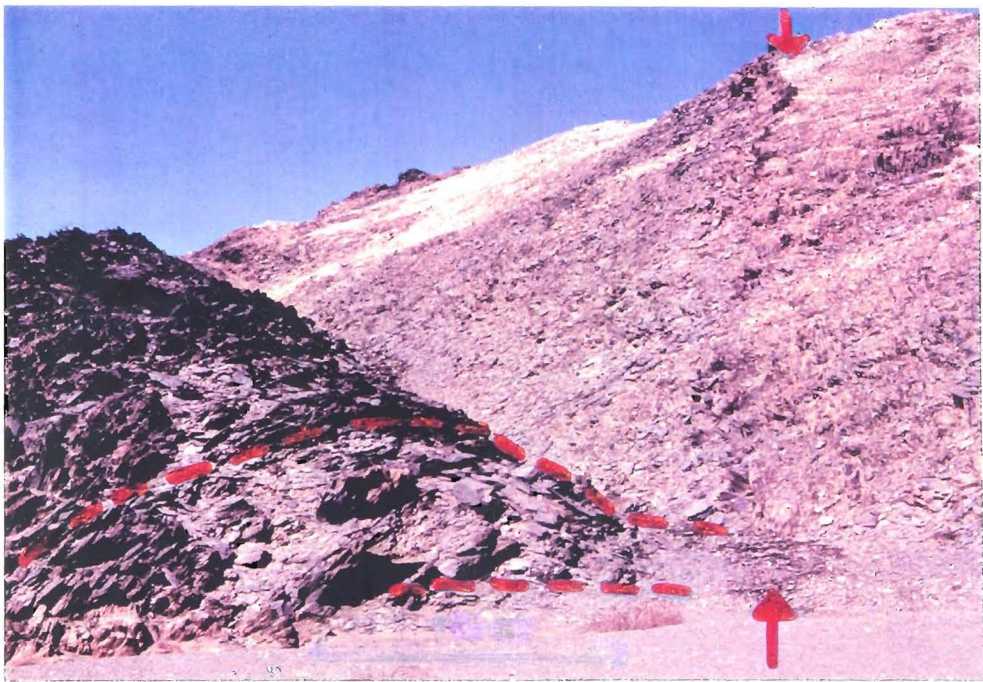
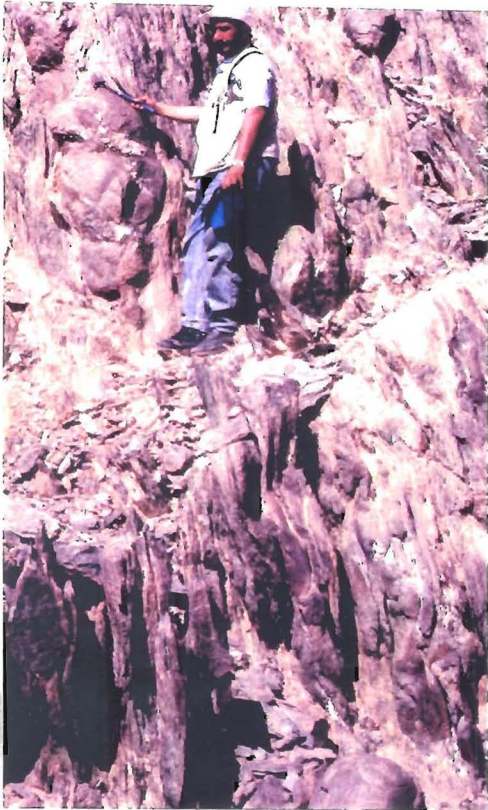


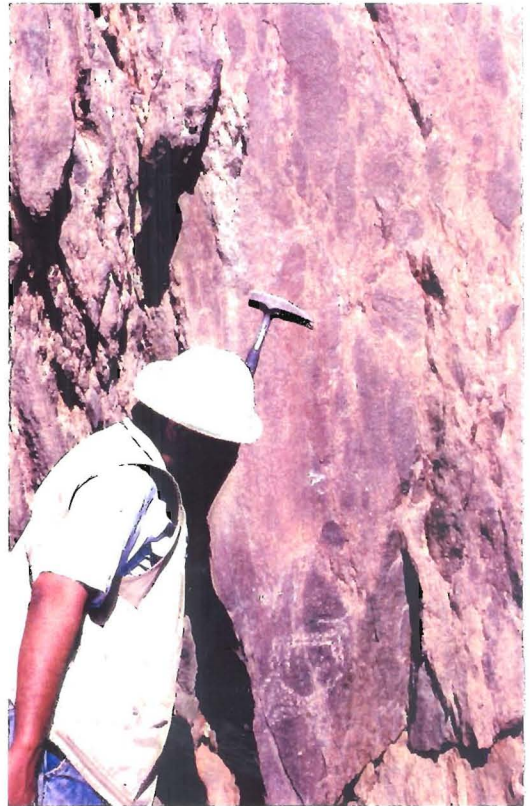
Fig. 3.4c (i) Atshani and Kholoud Formations outcrops
(ii) stratigraphic columns of Atshani Formation (A) and Kholoud Formation (B)



a



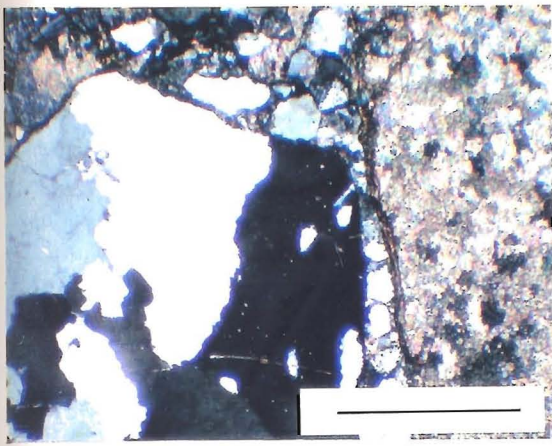
b



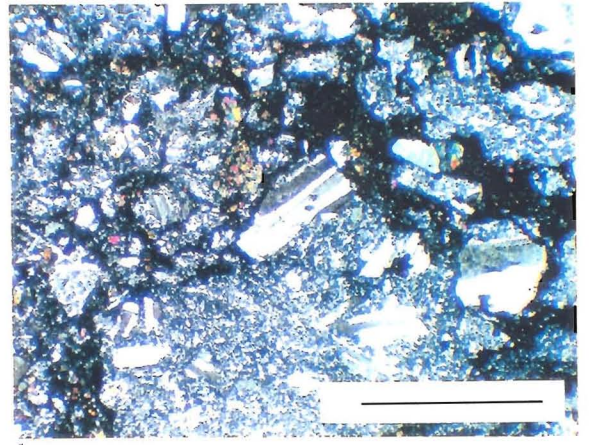
c

Fig. 3.5 Filat Succession Lithologies

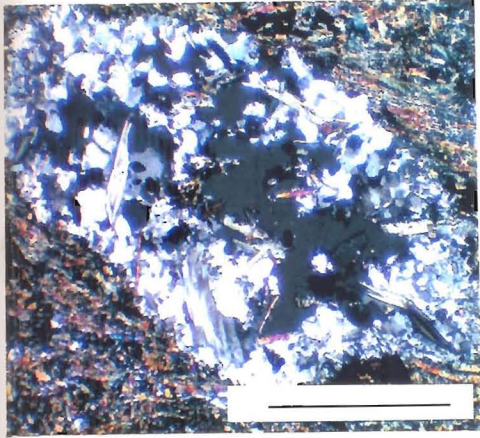
- (a) fine-grained volcaniclastic phyllites with poor bedding but strong S1 in a partial duplex horse structure in the Kazzaz Formation, looking west (GR 7533091042), height of the hill is 10m.
- (b) Granite Boulder Formation with conspicuous boulder extended parallel to S1 (GR 7399282341)
- (c) Volcaniclastic conglomerate, cobblestone, elongation parallel to S1 in the Atshani Formation (GR 7399582337)



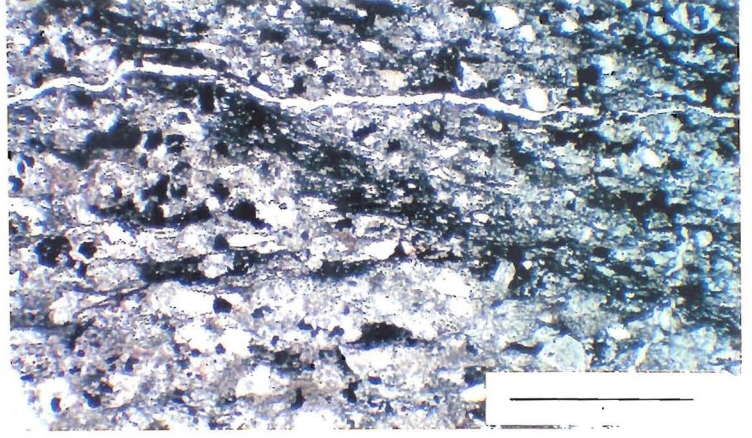
a



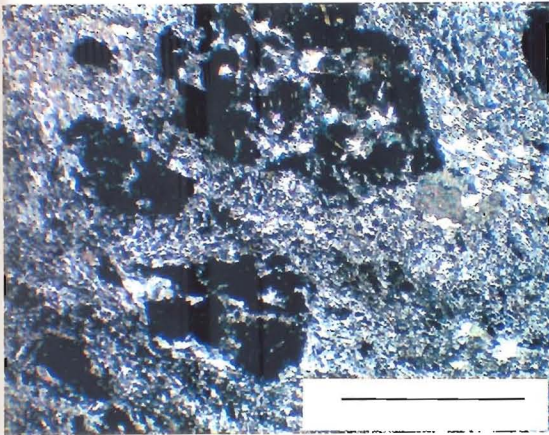
b



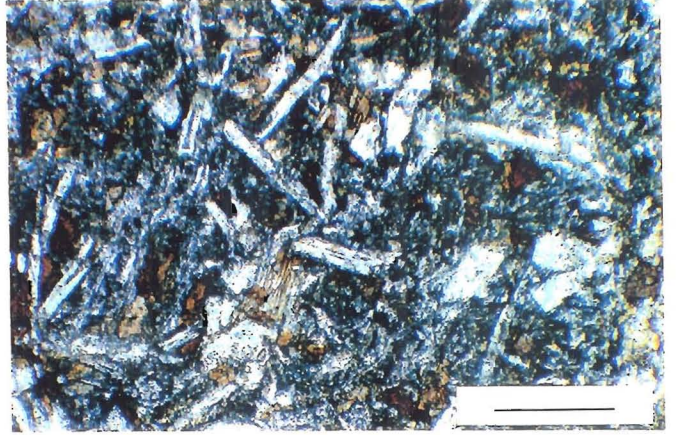
c



d



e



f

Fig. 3.6 Textures of Filat Succession lithologies

(a) poorly-sorted quartz and meta-limestone lithic fragments embedded in a fine-grained groundmass of quartz and chlorite in a wacke of the Metaconglomerate Member of the Kazzaz Formation (cross-polarized light; GR 5865680828; scale bar 1 mm)

(b) poorly-sorted quartz, plagioclase and porphyritic lithic fragments embedded in a fine-grained groundmass of quartz and chlorite in greywacke, Kazzaz Formation (cross-polarized light; GR 5932580857; scale bar 1 mm)

(c) quartz filled vesicles within fine-grained tremolite-actinolite and plagioclase groundmass of a meta-basalt, Meta-basaltic unit of the Kazzaz Formation (cross-polarized light; GR 4575786269; scale bar 1 mm)

(d) bedding lamination oblique to the cleavage S1 in wacke, Atshani Formation (plane polarized light; GR 6133386677; scale bar 1 mm)

(e) altered relict plagioclase phenocrysts embedded in a fine-grained quartz, plagioclase and chlorite groundmass of a metamorphosed dacitic dyke intruded into Kazzaz Formation. The dykes were affected by metamorphism during the D1 phase (cross-polarized light; GR 7148980100; scale bar 1 mm)

(f) relict porphyritic texture with plagioclase and chloritized biotite laths in andesitic dyke intruded into Kazzaz Formation. The dykes were affected by metamorphism during the D1 phase (cross-polarized light; GR 5792980944; scale bar 0.1 mm)

continuously exposed, north-north-easterly steeply-dipping, pale-grey to greenish-grey, coarse- to medium-grained volcanoclastic rocks with occasional basaltic lavas, agglomerates and dykes are found. Rare greenish-grey phyllites are intercalated within the volcanoclastic rocks and are composed mainly of quartz, plagioclase, chlorite, epidote with subordinate amounts of opaque minerals, calcite, apatite and titanite. The sequence is punctuated by five major thrusts (Fig. 1.4) and the base of the Formation is formed by the tectonic upper thrust of the Gebel Taylor Wedge (see section 3.5 below). The vast bulk of the Formation is made up of moderately-bedded (10-15 cm thick) and massively-bedded (c.50 cm thick) epiclastic reworked volcanoclastic sandstones and siltstones within which rare graded-bedding and poorly preserved cross-lamination structures occur. Occasional irregular pebbly pockets, with mainly sub-rounded, ellipsoidal clasts, up to 5 cm in length, composed of microgranitic, volcanic, and quartzitic rock types, are found throughout the Formation. Fine-grained pyroclastic units have not been distinguished within the Formation.

In thin-section the volcanoclastic rocks commonly show metamorphic effects mainly related to the syn-D1 phase (section 2.9); presence of tremolite-actinolite, epidote grains, saussuritization of plagioclase, chloritization of pale-green hornblende and quartz with wavy extinction. The lithic fragments, forming up to 60 % of the rock, are mainly subangular volcanoclastic psammitic types. Meta-limestone and quartzite clasts are common (Fig. 3.6a,b). The groundmass is composed chiefly of microcrystalline quartz, feldspar, carbonate, sericite, chlorite, epidote and pyrite.

Modal analyses (Fig. 3.7) demonstrate that the clastic rocks can be classified as greywackes (after Pettijohn 1975), in which the matrix ranges from 11 to 42% of the rock with a mean of 25.3%, and that they plot in the 'recycled-orogen' field (Dickinson & Suczek 1979, Busby & Ingersoll 1995). Typically the greywackes form the matrix of other rudaceous lithologies.

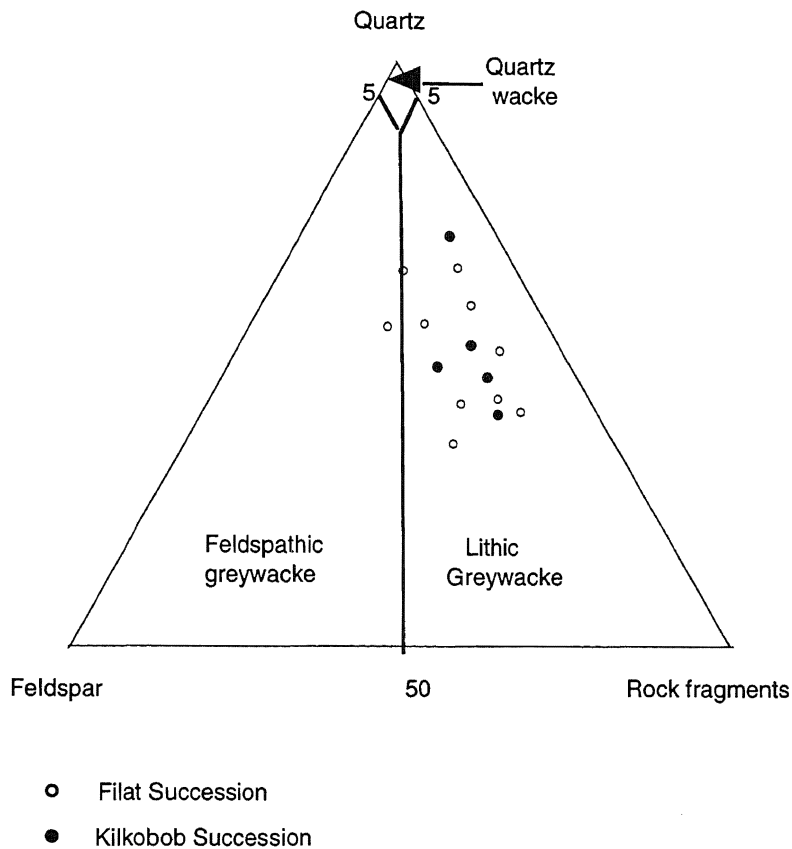


Fig. 3.7 modal plot (after Pettijohn 1975) of volcaniclastic rocks from Filat and Kilkobob Successions. Most of the samples plot in the greywacke field

The majority of the chemical analyses of the volcaniclastic rocks from this Formation (Appendix B) plot in the field of andesite using the $Zr/TiO_2 - Nb/Y$ diagram (Winchester & Floyd 1977) although other samples plot in adjacent fields viz., andesite-basalt, rhyolite and the boundary between subalkali-basalt and alkali basalt, (Fig. 3.9). By using Al_2O_3/SiO_2 vs $Fe_2O_3 + MgO$ (Fig. 3.8; Bhatia 1983) to discriminate the tectonic setting of the volcaniclastic rocks, most of the data plot in and around island arc field and are characterized by high $Fe_2O_3 + MgO$ (8-14%) and high Al_2O_3/SiO_2 (0.24-0.33%).

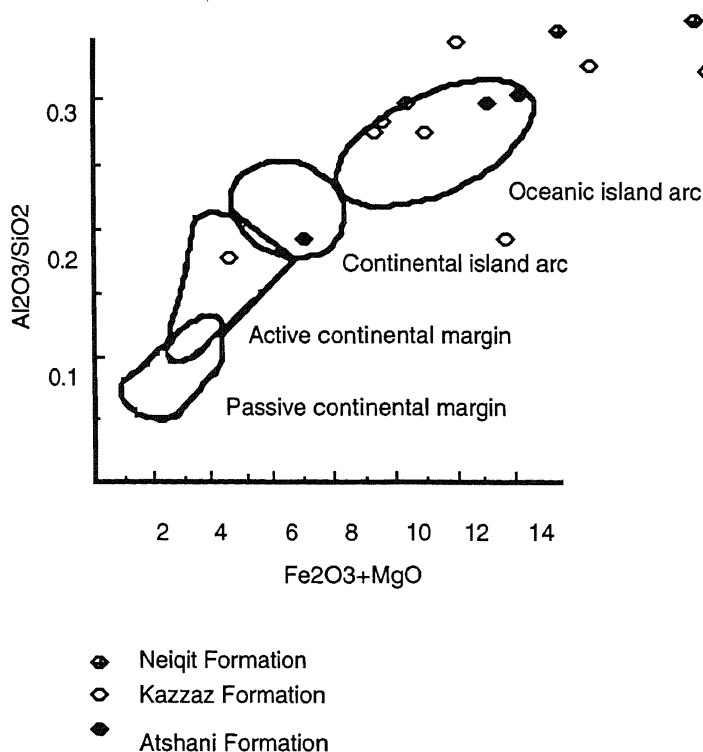


Fig. 3.8 discrimination diagram (Bhatia 1983) for Volcaniclastic rocks of Filat Succession. Most of the samples fall within and around the field of oceanic island arc

Rare, thin metamorphosed dykes invade the volcaniclastic rocks. Basaltic (GR 7038382923), dacitic (GR 5792980944) and andesitic (GR 7148980100) types have been distinguished by chemical analyses (Figs 1.3b, 4.10ii). Petrographically the dacitic and andesitic varieties are porphyritic and are composed of sub-hedral plagioclase phenocrysts, set in fine-grained groundmass mainly of plagioclase, quartz, epidote, chlorite, pyrite and limonite (Fig. 3.6e,f). The plagioclase, of both the phenocrysts and groundmass, is commonly altered to epidote and sericite (Fig. 3.6e,f).

A few distinctive stratigraphic units worthy of more detailed consideration. The distinctive *Basic Lava Member* occurs near the base of the Formation in three dismembered thrust horses (Figs 1.3b, 1.4). Restoration by cross-section balancing (Woodward *et al.* 1989; Fig. 3.3b) indicates that the original maximum thickness of the member was in the order of 1.8 km. Typically, the rock is a hard, massive, fine-grained, greyish-green to dark-

green basalt. The upper part of the easterly segment of the member contains carbonate- and quartz-filled vesicles with a fragmented surface which indicates a north-facing orientation (Fig. 3.2d,e). Pyroclastic rocks are intimately associated with the lavas. For instance, in the Wadi Atshani (GR 5478685687) blocky agglomerates, up to 2m in thickness, occur as both lenses within the lava and as layers at the base of the lava. The latter agglomerates grade upwards into breccias and lapilli tuffs. Under the microscope, the meta-basalt is composed of sericitized plagioclase phenocrysts set in fine-grained groundmass of mainly plagioclase, tremolite-actinolite and chlorite with accessory amounts of zoisite, goethite, apatite and titanite. Amygdales, where present, are commonly ovoid with maximum dimension up to 1.5 mm and filled with quartz, calcite, epidote and chlorite (Fig. 3.6c). Relict igneous textures (comparable to sub-ophitic type) are formed by altered plagioclase laths with tremolite-actinolite, carbonate, epidote and chlorite filling the interstices. Actinolite forms pale-green prismatic crystals up to 0.3 mm in length. Major and minor elemental analyses of the meta-basalts (Appendix B) have been plotted on a total alkali-silica (TAS) diagram (Fig. 3.9; Sabine 1989 modified from Le Maitre 1984; Sabine *et al.* 1985; Le Bas *et al.* 1986) since Sabine *et al.* (1985) showed that this diagram can classify altered and low-grade metavolcanic lavas satisfactorily. All samples plot in the basalt field. Also the TiO₂-Zr discrimination diagram (Pearce 1980) indicates that the meta-basalts lie within the arc-lava field (Fig. 3.9). Spider diagrams (Pearce 1983) for the meta-basalts gives a typical LREE enriched pattern of back-arc basalts (Fig. 3.9; *cf.* Saunders & Tarney 1979, Hickey & Frey 1982; Wilson 1989) which are of calc-alkaline type. Trace elements show similar patterns (Fig. 3.9 for typical spider diagram patterns of island-arc basalt (Thompson *et al.* 1984). The Ti-Zr-Y discrimination diagram (Pearce & Cann 1973) confirms this classification of the meta-basalts.

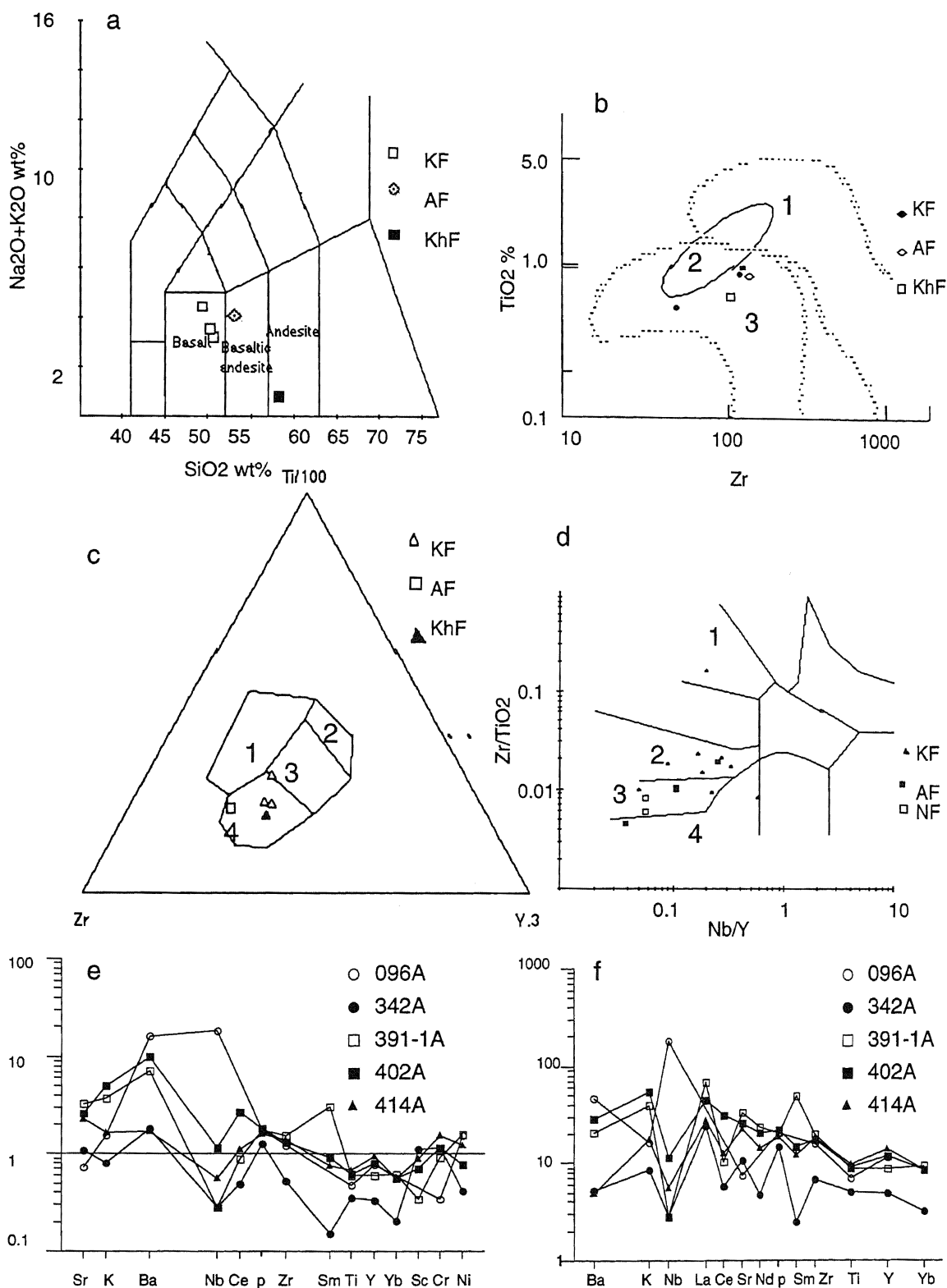


Fig. 3.9 Geochemical signature of rocks of the Filat Succession

- (a) composition of analysed lava (Sabine 1989). Kazzaz Formation (KF); lava, Atshani Formation (AF); lava from Kholoud Formation (KhF)
- (b) TiO₂-Zr diagram (Pearce 1980) shows the fields of within-plate basalt (1), mid-ocean ridge basalt (2) and arc lava (3). All samples fall in the field of arc lava.
- (c) discrimination diagram (Pearce and Cann 1973) of within-plate basalt (1) low K-Tholeiites (2), ocean floor basalt+ low K-tholeiite + calc-alkaline basalt (3) and calc-alkaline basalt (4). All samples plot in the field of calc-alkaline basalt.
- (d) diagram to classify volcanoclastic rocks (Winchester and Floyd 1977). Rhyolite (1), andesite (2), andesite-basalt (3) and sub-alkali-basalt (4), Kazzaz Formation (KF), Atshani Formation (AF) and Neiqit Formation (NF)
- (e) MORB-normalized trace element diagram (Pearce 1983); KF(342A, 402A, 414A), AF (391-1A) and KhF (96A).
- (f) chondrite-normalized trace elements (Thompson *et al.* 1984); KF(342A, 402A, 414A), AF (391-1A) and KhF (96A).

The *Polymict Metaconglomerate Member* is best exposed in the southern part of Wadi Um Relan as a lens with a maximum thickness of 300m. Clasts consisting of quartzite, volcanoclastic rocks, granites and very rare meta-limestone are normally less than 4 cm in length but occasional clasts of up to 10 cm in length have been recorded for volcanoclastic rocks and meta-limestone clasts (Fig. 3.6a). The matrix is typically of greywacke.

The best exposures of the ***Granite Boulder Formation*** are found in Wadi Kilkobob (Fig. 3.4b). The Formation is a poorly-bedded lensoid unit with a maximum thickness of 800m which is bounded at its upper and lower junction by thrusts. Boulders and cobbles of granite (>85% of the total), quartzite, and volcanoclastic rocks are set in a matrix of volcanoclastic material. The deformed, coarse-grained, and tonalitic granite boulders are particularly conspicuous and are composed of plagioclase, quartz, epidote and chlorite in the main. A chemical analysis (Appendix B) of one granitic pebble (Fig. 4.4) indicates that the parent rock is tonalite (Le Bas & Streckeisen 1991), plots in the field of "I" type granites (Fig. 4.9a, Hine *et al.* 1978), has calc-alkaline affinities (Fig. 4.9b, Wright 1969) and occurs within the volcanic-arc field (Fig. 4.9d, Pearce *et al.* 1984).

The significance of Granite Boulder Formation represents both rapid erosion and the unroofing of a granitic pluton which has the same characteristics as the Atshani granite (see chapter 4) although similar tonalites do occur throughout the Eastern Desert, Sudan and Saudi Arabia. Attempts to match the granitic pebbles to exposed granites and to locate the exact place of derivation have not been successful. Clearly if the original position of derivation could be established this would enable an estimation of the direction and distance of travel with a fair degree of precision.

Atshani Formation (Fig. 3.4 c) is estimated to be about 4 km in thickness and may be distinguished from the Kazzaz Formation by having more finer-grained volcanoclastic rocks, more thinly-bedded lithological units (Fig. 3.6d),

the occurrence of meta-limestones, lava units, and those, which do occur, have basalt-andesitic affinities (Fig. 3.9). The top and bottom of the formation are defined by thrusts. Primary structures are rare and when found consistently show a north-north-east facing direction. Under the microscope the volcanoclastic rocks are composed mainly of crystal and lithic sand-size fragments in a matrix of quartz, plagioclase, chlorite and epidote. Chemically these rocks fall in the adjacent fields of andesite-basalt and subalkali-basalt (Fig. 3.9). Samples plot in the island arc field and active continental margin field (Fig. 3.8).

A distinctive Metaconglomerate Member, with an estimated thickness of at least 200m, is well exposed in Wadi Um Relan (Figs 1.3b, 3.4c). The top and bottom of the Member are bounded by thrusts. The Member is composed of volcanoclastic clasts up to 4 cm in diameter set in greyish-green fine-grained greywacke matrix composed of up to 70% sub-rounded to sub-angular quartz fragments.

Kholoud Formation is best exposed in the northern part of Wadi Allaqi (Fig. 3.4c) the thickness is about 3 km and occurs in a thrust horse, sandwiched by structurally lower Um Relan Succession to the south and the structurally higher Allaqi Shear-zone to the north. This Formation is distinguished from the Atshani Formation by even finer-grained volcanoclastic rocks, the presence of rare lava of andesitic composition (Fig. 3.9), and fewer meta-limestone intercalations. The volcanoclastic rocks are composed, mainly, of lithic fragments set in a fine-grained groundmass of plagioclase, quartz and chlorite. The groundmass typically forms in excess of 85% of the rocks. The andesitic lavas are composed mainly of plagioclase phenocrysts set in fine-grained groundmass of mainly plagioclase laths, which show a very weak preferred orientation, epidote, chlorite and rare apatite, zircon and limonite. A typical sample plots in the field of andesite (Sabine 1989; Fig. 3.9) in the field of arc-lavas (Pearce 1980; Fig. 3.9), and

gives a similar LREE enrichment pattern to that of a back-arc environment, of calc-alkaline type (Pearce & Cann 1973).

3.4 Um Relan Succession

This distinct assemblage of meta-sedimentary rocks with some meta-volcaniclastic intercalations occurs structurally above the Atshani Formation of the Filat Succession (Figs. 1.4 & 3.10) and is contained within the Allaqi Shear zone in the area. The primary sedimentary structures are occasionally preserved in many of these rocks, but it has not proved possible to deduce a convincing internal sequence because of the intensity of the deformation which locally has produced mylonites (see section 2.9). The thickness is in the order of 1.5 km. Although it is difficult without distinct marker beds to restore the original stratigraphical relationship of the Um Relan Succession to the Kholoud Formation of the Filat Succession, because of the affinity of the lithological units of the Kholoud Formation to that of the Atshani Formation either the Um Relan Succession was originally intercalated within and between the two formation (Fig. 3.11b) or it lay on the top of the former formation (Fig. 3.11a). The chemical evidence tends to favour the interpretation shown in text figure 3.11b in which the Um Relan Succession occurs fringing and interdigitating with the lower and (older) volcaniclastic successions which gradually intercalate the lowest unit of the succession. Such a relationship is common in a developing island-arc adjacent to a back-arc basin scenario, where basaltic rocks are gradually succeeded by progressively more acidic composition.

Metamorphosed sandstones, calcareous siltstones, limestones some with stromatolitic laminae and graphitic phyllites (Figs. 3.12, 3.13) form the bulk of the rock types. There are some distinct lithologies which are worth additional consideration. Quartzite intercalated with calcareous siltstone and

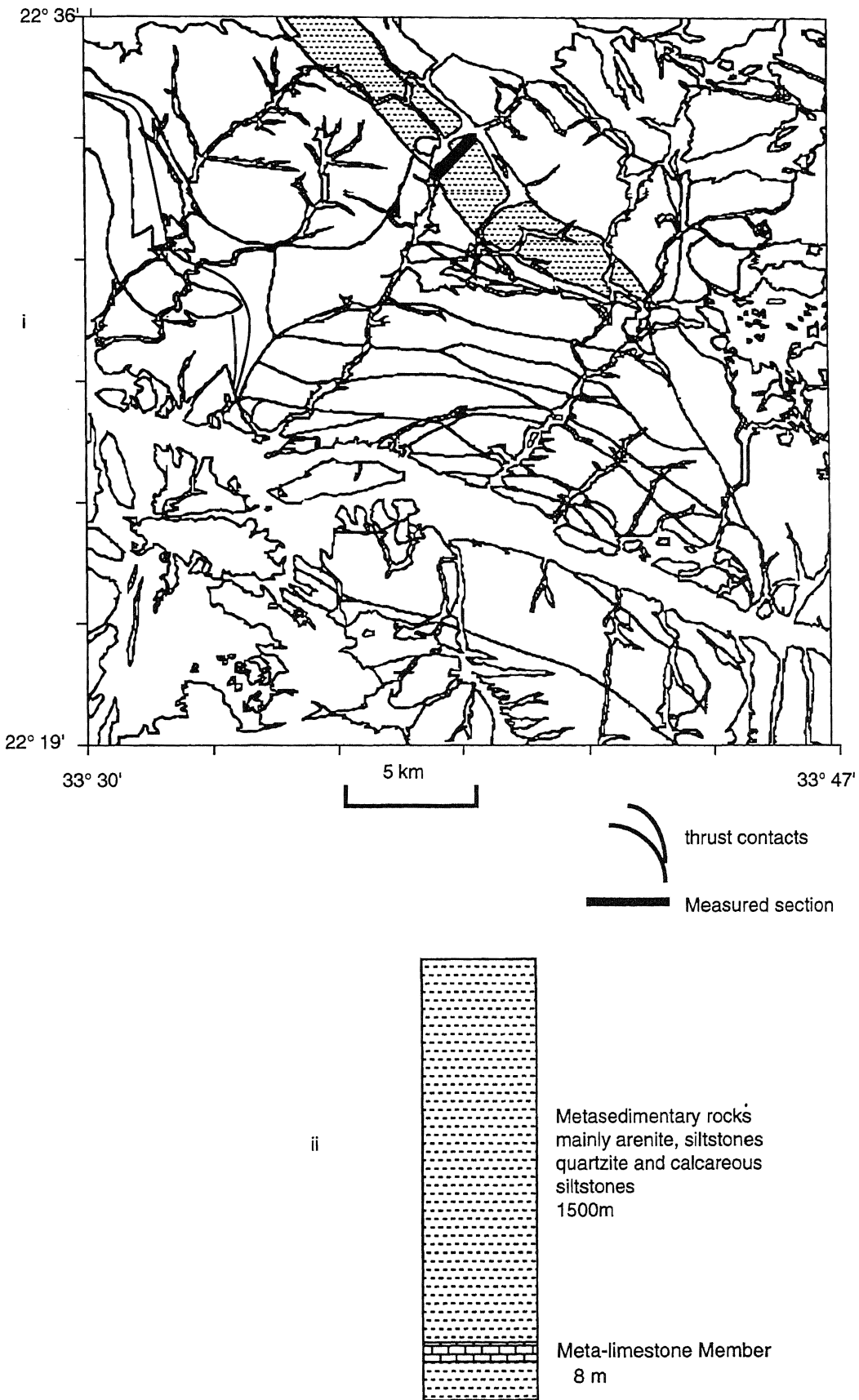


Fig. 3.10 Um Relan Succession (i) outcrop of the (ii) tectonic stratigraphic column

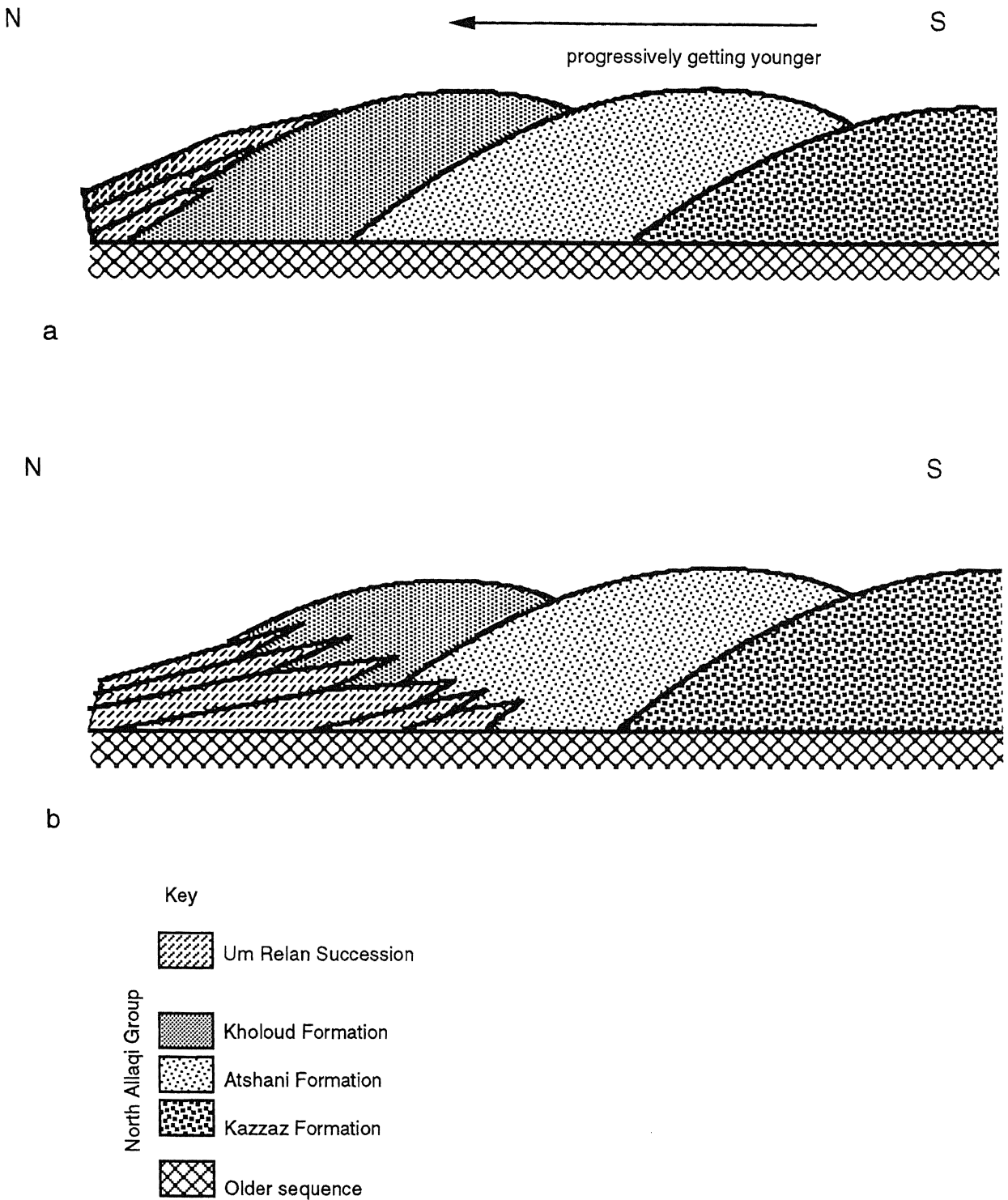


Fig. 3.11 Alternative explanations for the stratigraphical relationship of the North Allaqi Group to the Um Relan Succession: (a) Um Relan Succession younger than most of the North Allaqi Group; (b) Um Relan Succession interdigitates with the Kholoud and Atshani Formations and is gradually being over-ridden

phyllites constituent the major components of the Um Relan Succession. The cleaved, very fine-grained pale-green to greyish-green, laminated calcareous siltstones are composed chiefly of calcite and quartz with limonite, pale-green chlorite, epidote, graphite and sericite (Fig. 3.13). Clastic quartz occurs as ill-sorted subangular to slightly subhedral grains. Metamorphically-grown epidote occurs in subhedral aggregate crystals while pale-green chlorite forms irregular stretched patches. Graphite occurs as very thin laminations. Sericite-quartz phyllites with subordinate, calcite, plagioclase and chlorite occur in thinly bedded layers (Fig. 3.13b).

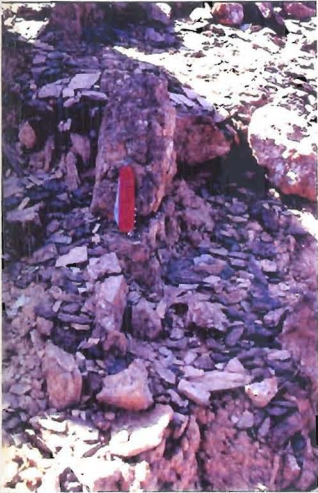
A distinctive, medium-grained, pale-grey and white *Meta-Limestone Member* occurs as laminated lenses up to 8m in thickness, and can be demonstrated to be intercalated with metavolcaniclastic rocks (GR 6700890023). The rock is composed mainly of calcite associated with minor amounts of quartz, tremolite-actinolite, chlorite, zoisite and limonite, showing stromatolitic laminae. The significance of stromatolite structures is they indicate deposition in a shallow-water (Lowe 1994). Chemical analyses for both the Allaqi Shear-zone and the Um Relan Succession plot in the field of oceanic island-arc rocks (Fig. 3.14)



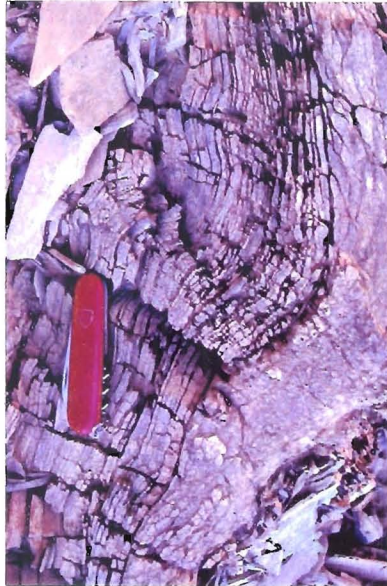
a



b



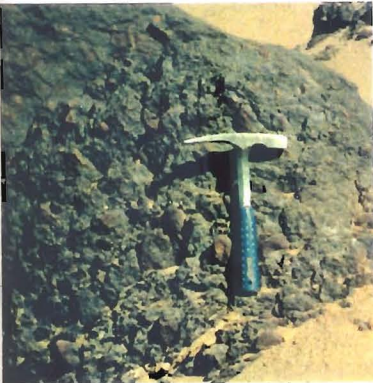
c



d



e



f



g

Fig. 3.12 Um Relan and Kilkobob Succession lithologies

(a) strike section of Allaqi shear-zone containing Um Relan Succession phyllite and quartzites (GR 7405086269), the height of the hill is 10m.

(b) Meta-limestone Member, Um Relan Succession (GR 6712489965), the height of the hill is 15m.

(c) Calcirudite unit, Um Relan Succession (GR 6712289960)

(d) close up of (b) note strong S1

(e) deformed stromatolitic laminae of Meta-limestone Member (GR 6712489962)

(f) Conglomerate unit, in Murra Formation of the Kilkobob Succession (GR 7533091042)

(g) Meta-limestone lenses, Kilkobob Succession (GR 7892090633), the height of the hill is 15m.

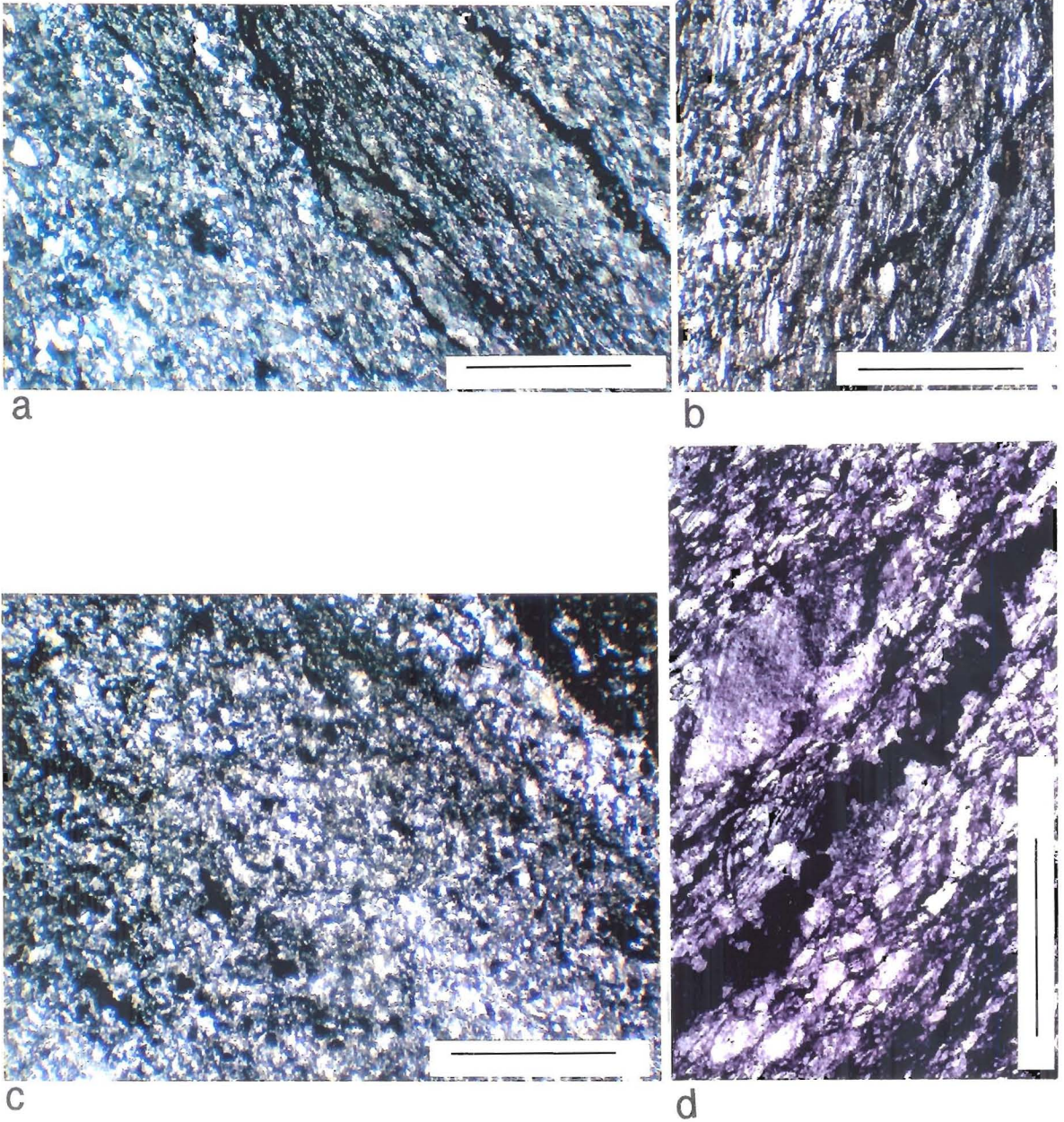


Fig. 3.13 Textures of the Um Relan lithologies

- (a) junction between bands of coarse-grained siliceous meta-limestone (left) and fine-grained meta-limestone, along which clay and graphitic stylolites developed (plane-polarized light; GR 6700890023; scale bar 1 mm)
- (b) phyllitic cleavage (S1) deformed by S2 crenulation cleavage (plane-polarized light; GR 6494292206; scale bar 1 mm)
- (c) detail of stromatolitic laminae structures growth is towards the top left associated with chlorite (green) in meta-limestone (plane-polarized light; GR 6700890020; scale bar 1 mm)
- (d) detail of stylolite structures in meta-limestone. Note general alignment of the band parallel to calcite elongation (S1 foliation) [plane-polarized light; GR 6700890023; scale bar 0.5 mm]

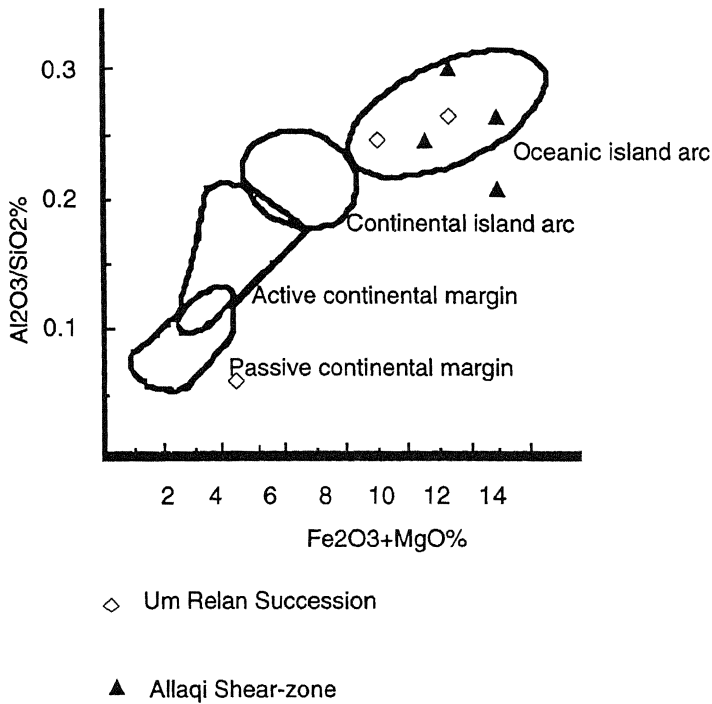


Fig. 3.14 Discrimination diagram (Bhatia 1983) for sedimentary rocks
Most of the samples plot in the field of oceanic island arc

3.5 Kilkobob Succession

The Succession crops out in the north-east of the study area within a D1 recumbent fold refolded by upright D2 folds (Figs 1.3b & 1.4), has a thickness of at least 3 km (Fig. 3.15) and is composed of pyroclastic rocks, coarse-grained volcanoclastic rocks, meta-limestones, and occasional basic lavas. The Kilkobob Succession is separated from the structurally lower Um Relan Succession by the Allaqi Shear-zone and consists of three formal tectonic-stratigraphical formations each of which has tectonic boundaries. The Kilkobob Succession is intruded by late-stage dolerite sills similar to those found in the Filat Succession (section 4.3.1) and apophyses of Kilkobob Granite. The essential features of these formations are considered below in structural order.

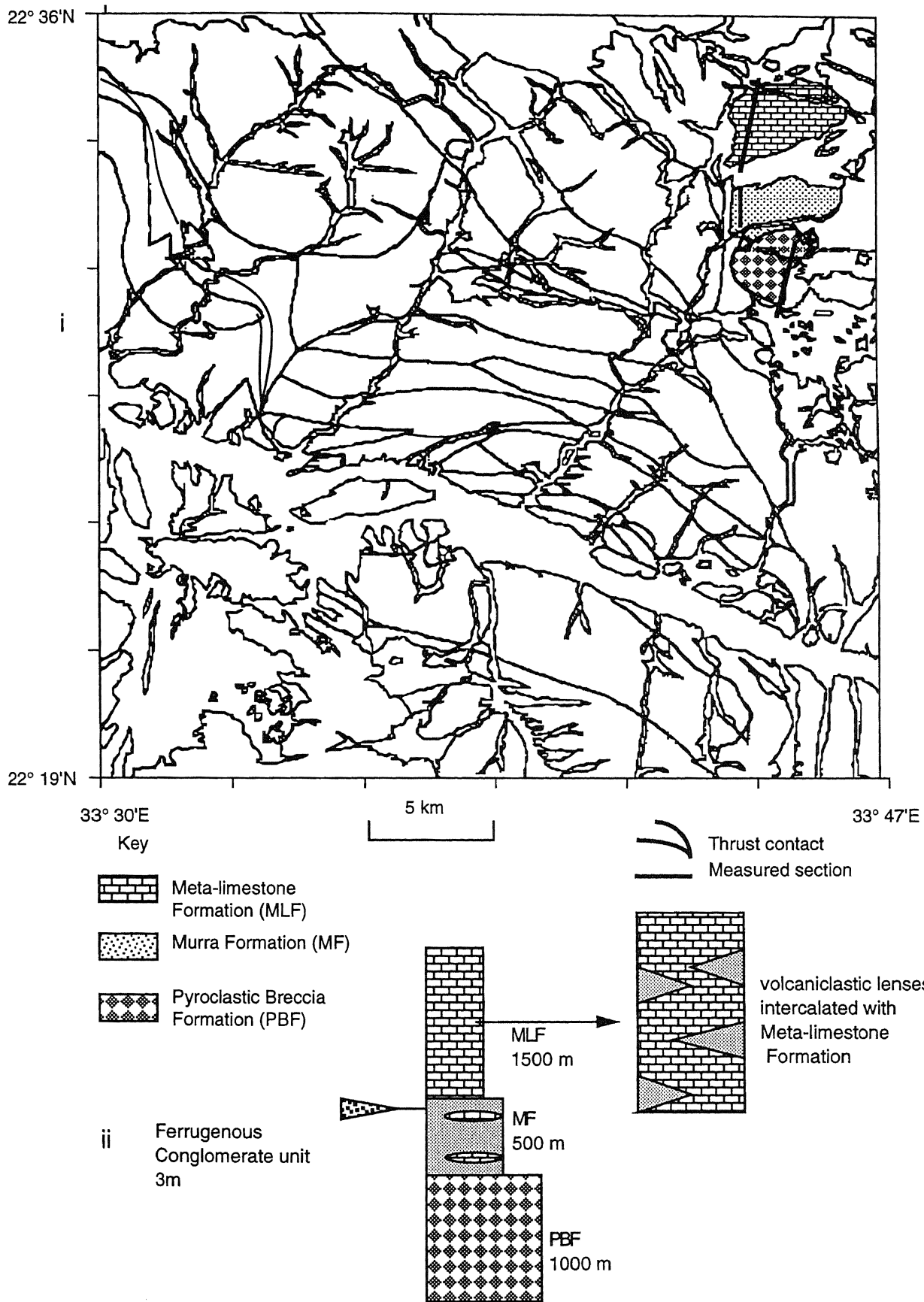


Fig. 3.15 Kilkobob Succession (i) outcrop; (ii) tectonic-stratigraphic columns (see Fig. 2.13 for structural relationships)

3.5.1 Pyroclastic Breccia Formation

This formation occupies the core of a northerly-facing, tight and refolded F1 anticlinal synform (Figs. 1.4 & 2.16), now forming the limb of an upright F2 antiform which is cross-cut by the Kilkobob Granite (Chapter 4) to the south and mainly consists of at least 1 km thick, pale to dark-grey medium- to coarse-grained breccias. Clasts include lithic and minor crystal fragments set in fine-grained groundmass which is obliterated by limonite and epidote which has developed as alteration product of plagioclase. Angular to subangular lithic fragments of basalt, andesite and metamorphic quartzite are common (Fig. 3.16a). Glassy Fiame textures are present (Fig. 3.16a) and crystal fragments slightly saussuritized plagioclase and quartz occur. Analyses of the matrix of selected samples of the formation plot in the field of andesite (Sabine 1989; Fig. 3.17) which indicates a continuation of the chemical sequence noted in the Filat Succession

3.5.2 Murra Formation

This is 0.5 km thick and bounded by thrusts and is characterized mainly by volcanoclastic rocks with intercalations of meta-limestones and hematitic rudaceous rocks in the upper portion. Poorly-sorted wacke sandstones with rare arenite bands is the predominate lithology. Modal analyses (Fig. 3.7) indicated that the majority of the volcanoclastic are greywackes, in which the matrix ranges from 34 to 47% of the rock with a mean of 35.8%.

Primary structures such as graded-bedding and cross-lamination are rarely present but when observed indicate both north-facing bedding and northerly-facing D1 structures. Texturally these rocks are similar to those of the Kazzaz Formation (Filat Succession) but a minor extensional phase (Fig. 3.16d) has been recorded in some of volcanoclastic material and evidence suggests that this is syn-depositional extensional phase. These rocks plot in the fields of andesite and dacite (Sabine 1989) and in the

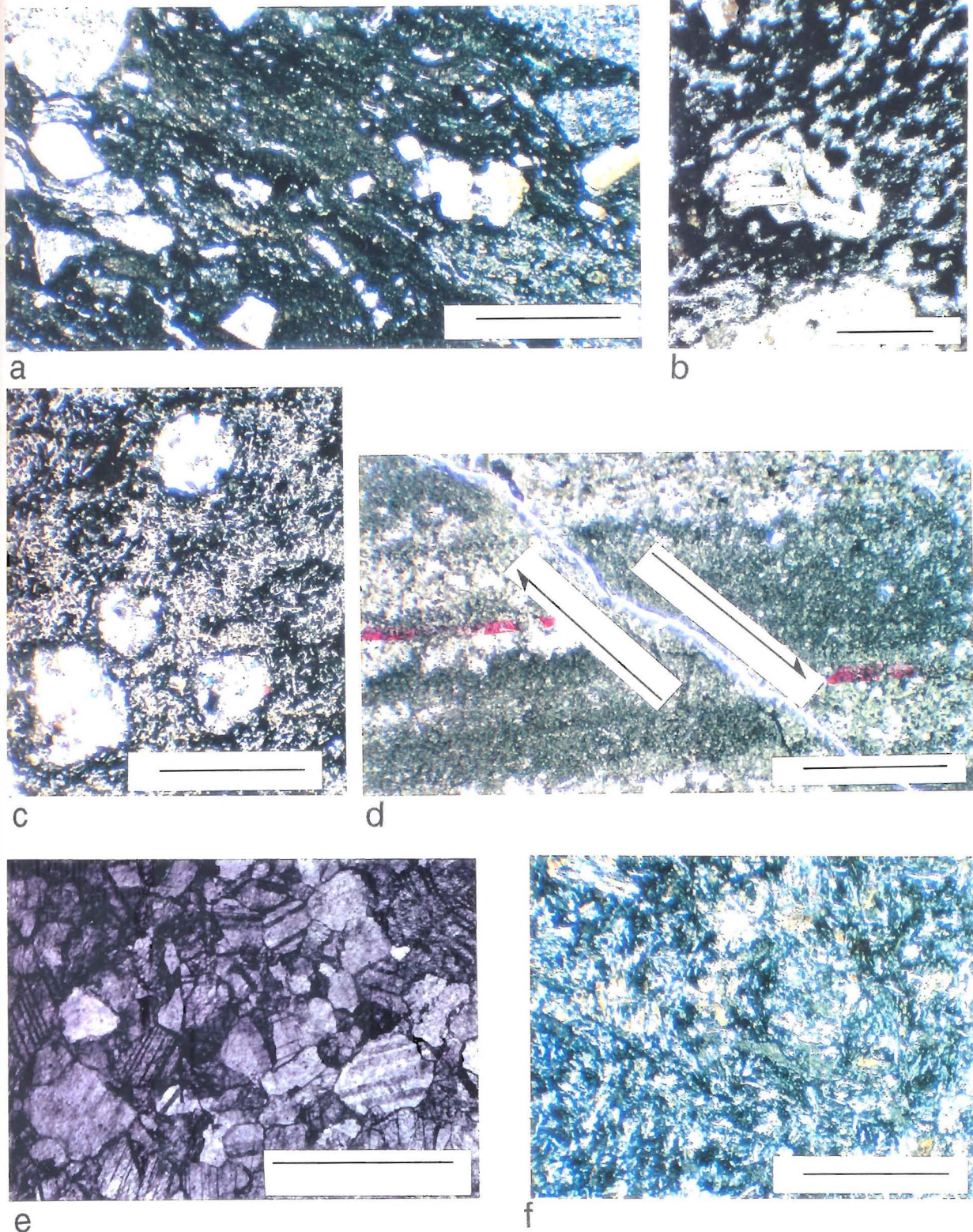


Fig. 3.16 Textures of the Killkobob Succession lithologies

- (a) plagioclase and crystals and lithic fragments in a fine-grained matrix showing flame textures, Pyroclastic Breccia Formation (plane-polarized light; GR 7640788597; scale bar 1 mm)
- (b) poorly-sorted porphyritic lithic and plagioclase crystal fragments within a ferruginous sandstone matrix, Pyroclastic and Conglomerate Member (plane-polarized light; GR 7533091042; scale bar 0.1 mm)
- (c) detail of an amygdaloidal basalt fragment within ferruginous sandstone, Pyroclastic and Conglomerate Member (plane-polarized light; GR 7533091042; scale bar 0.5 mm)
- (d) extensional micro-fault in laminated wacke and phyllites, the Murra Formation. The irregular fault-plane can be followed by the black line. Because the laminations are thicker in the hanging wall block (right) it is suggested that the extension has been taken place during deposition. Note that this is the only structure of this type which has been found in the area and no evidence has been obtained to indicate if this structure has been deformed by a D1 structure (plane-polarized light; GR 7893990634; scale bar 1 mm)
- (e) interlocking recrystallized calcite in a meta-limestones, Meta-Limestone Formation (plane-polarized light; GR 7643692962; scale bar 0.5 mm)
- (f) plagioclase flow texture, embedded in a fine-grained matrix of plagioclase, chlorite and epidote in rare basaltic rocks, Meta-Limestone Formation (plane-polarized light; GR 7719393544; scale bar 1 mm)

island-arc field (Fig. 3.17) which re-emphasises the gradual increase in the acidic component from lower to higher stratigraphic units.

A Pyroclastic and Conglomerate Member occurs as a 10 m thick distinctive marker horizon towards the top of the Murra Formation and is best exposed in an eastern branch of Wadi Kilkobob (GR 7533091042). The member can be traced for 2 km and consists of two pyroclastic units separated by a ferruginous volcanoclastic unit. Movement has occurred along the junctions of these units. Poorly-bedded brown ferruginous wacke sandstones and polymict conglomerates are the principal lithologies of the volcanoclastic unit (Fig. 3.16b) although thinly-laminated and weakly-cleaved siltstones occur. The clasts are mainly of reworked volcanoclastic rocks and quartz but fragments of micrographic aplite, andesitic porphyry, basalt (Fig. 3.16c) and sub-angular plagioclase feldspars have been rarely found (Fig. 3.16b). Typically the ferruginous matrix of fine-grained plagioclase and quartz clasts, with small amounts of calcite, forms about 75% of the rock and shows patchy development of very fine-grained epidote, sericite and chlorite. The pebbles from this horizon have been used to estimate the strain suffered by this tectonic-stratigraphic succession (Fig. 2.10b) and give a fairly low value. The pyroclastic rocks in this member are similar to those found in the Pyroclastic Breccia Formation which has described above (3.5.1).

3.5.3 Meta-limestone Formation

This at least 1.5 km thick unit of thinly-bedded lenses of metamorphosed pure, pale-grey to white limestones with intercalations of volcanoclastic rocks and lava is best exposed to the north of the Murra Formation (Figs. 1.3b, 1.4, 3.15). Petrographically the limestones are similar to those described within Um Relan Succession (Fig. 3.16e) except that stromatolitic varieties have not been observed. A dark-green massive, meta-basalt lava unit, 4m thick and composed of plagioclase and hornblende (probably

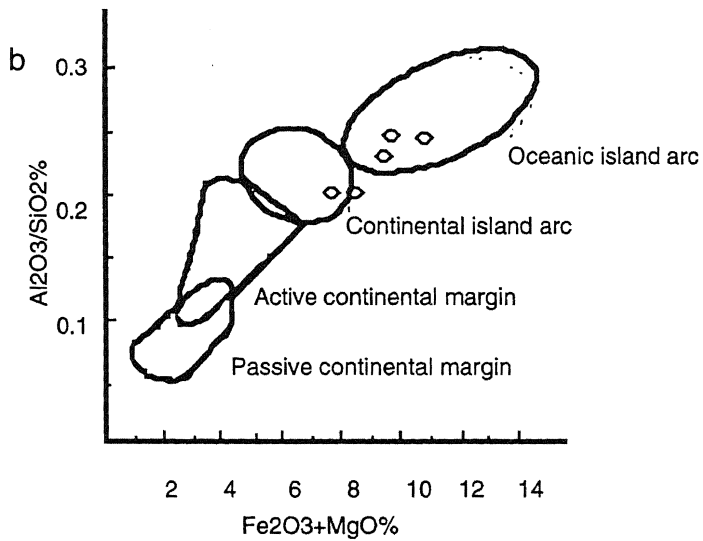
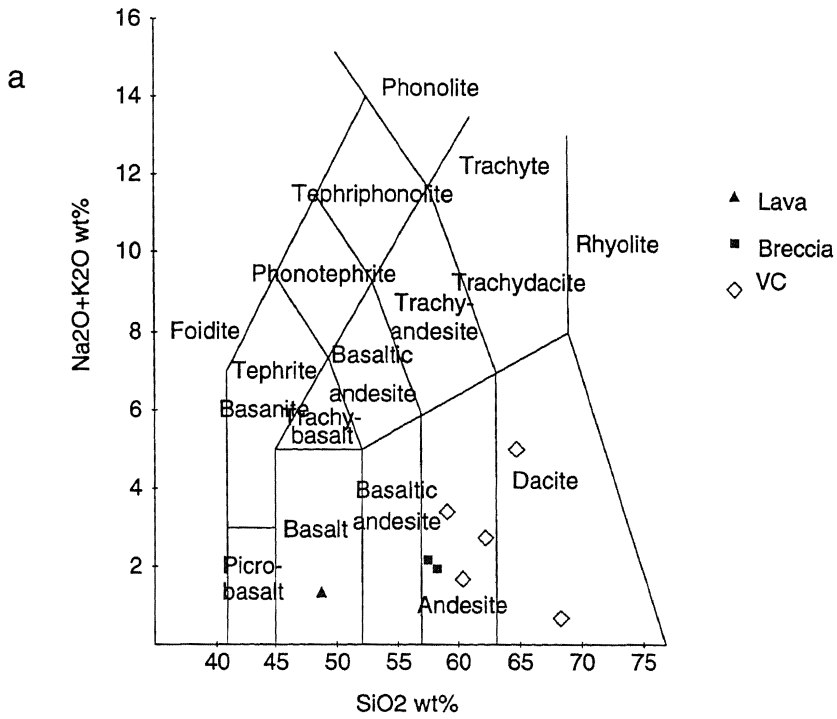


Fig. 3.17 (a) Composition of analysed rocks (Sabine 1989). Lava plot in the field of basalt, breccia fall in the field of andesite and volcanoclastic rocks (Vc) lay in the field of andesite and dacite.
(b) Discrimination diagram (Bhatia 1983) for volcanoclastic rocks
Volcanoclastic rocks plot in the fields of oceanic island arc and continental island arc.

altered from pyroxene) phenocrysts, set in a fine-grained groundmass of mainly plagioclase, chlorite and epidote (Fig. 3.16f). A single analysis of the lava plots in the calc-alkaline basalt field (Sabine 1989, Fig. 3.17) showing trace element similar to those of back-arc environments. The tectonic relationship of this formation to the structurally lower formations is not clear and it requires additional work to elucidate the relationships.

3.6 Gebel Taylor Wedge.

A distinctive 1 km thick thrust slice composed mainly of metamorphosed ultrabasic- and basic-igneous rocks (Figs. 1.3b, 1.4 & 3.18), which may be part of a E-W-trending ophiolite occurs between the Neiqit Formation and the North Allaqi Group. Three distinct rock units can be distinguished (Fig. 3.18, 3.19). A lower ultra-basic unit with schists, a middle tremolite-actinolite schist unit, and an upper meta-gabbroic unit. The *ultrabasic unit* consist of dunites and serpentinites which when highly-strained are converted into talc-carbonate schist with net-vein streaky textures, magnesite veinlets and occasional fibrous asbestos. Coarse-grained dunites are coarse-grained composed of interlocking anhedral olivine crystals, sometimes strongly altered to serpentinite along the cracks (Fig. 3.20a,b), and disseminated chromite. Massive, fine-grained and greenish-green serpentinites consist essentially of antigorite, tremolite and olivine with occasional, altered orthopyroxene (Fig. 3.20c) calcite, talc. The olivine is usually altered to antigorite which is occasionally intersected with thin veinlets of chrysotile associated with chromite minerals and display mesh texture. Replacement of antigorite by aggregates of talc occurs occasionally. Randomly oriented tremolite is formed at the expense of talc and antigorite. A pale-blue schist (GR 6174174397) composed mainly of chlorite and with some deformed glaucophane (Fig. 3.20d) within more common chlorite schist in the ultrabasic unit. Chlorite clearly overprints the formation of glaucophane.

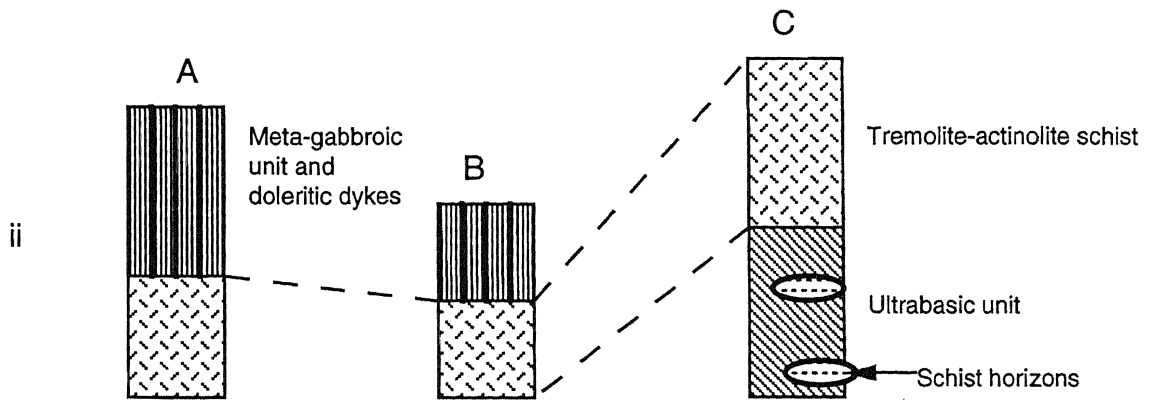
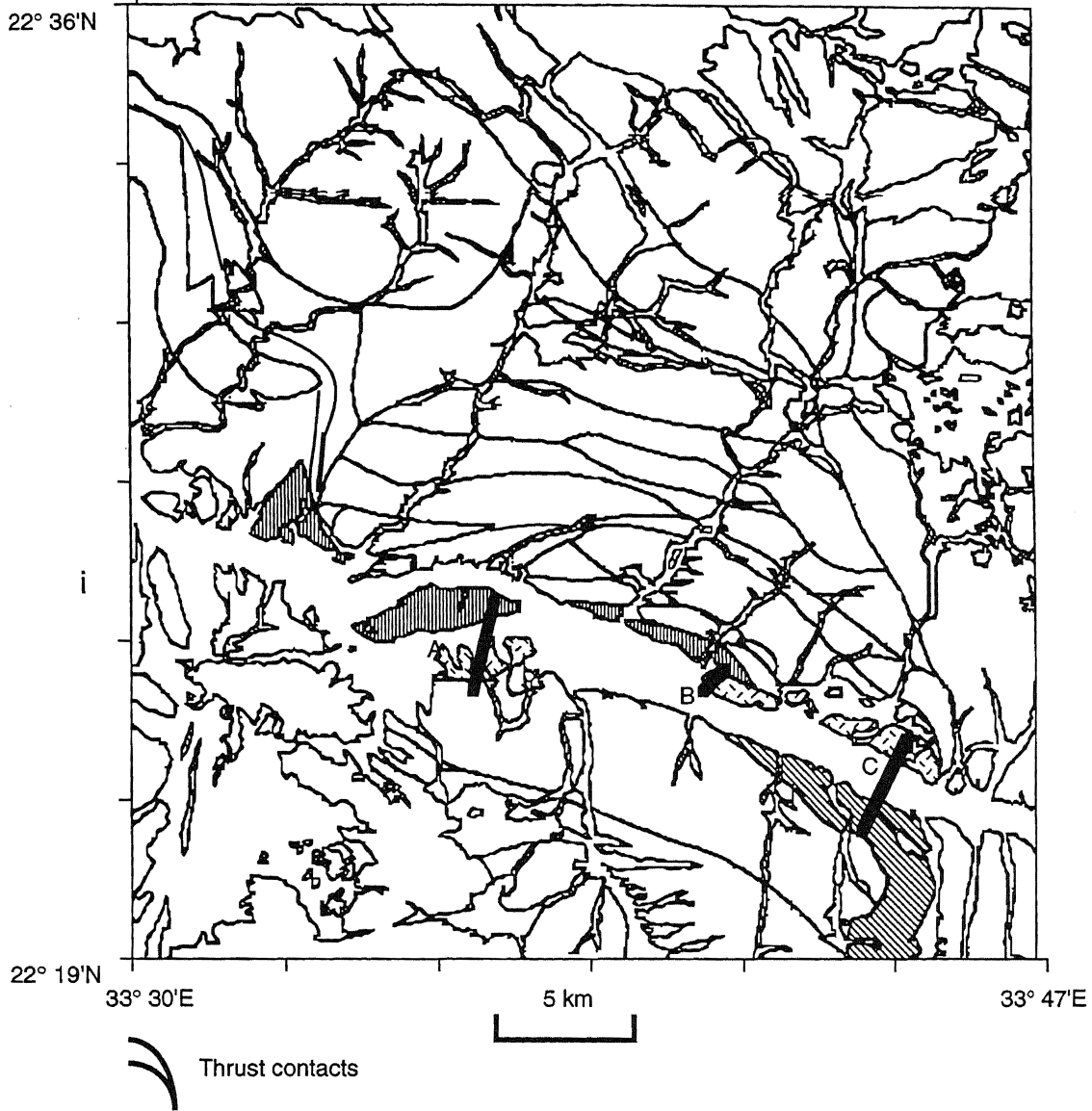


Fig. 3.18 Gebel Taylor Wedge (i) outcrop; (ii) tectonic-stratigraphic columns

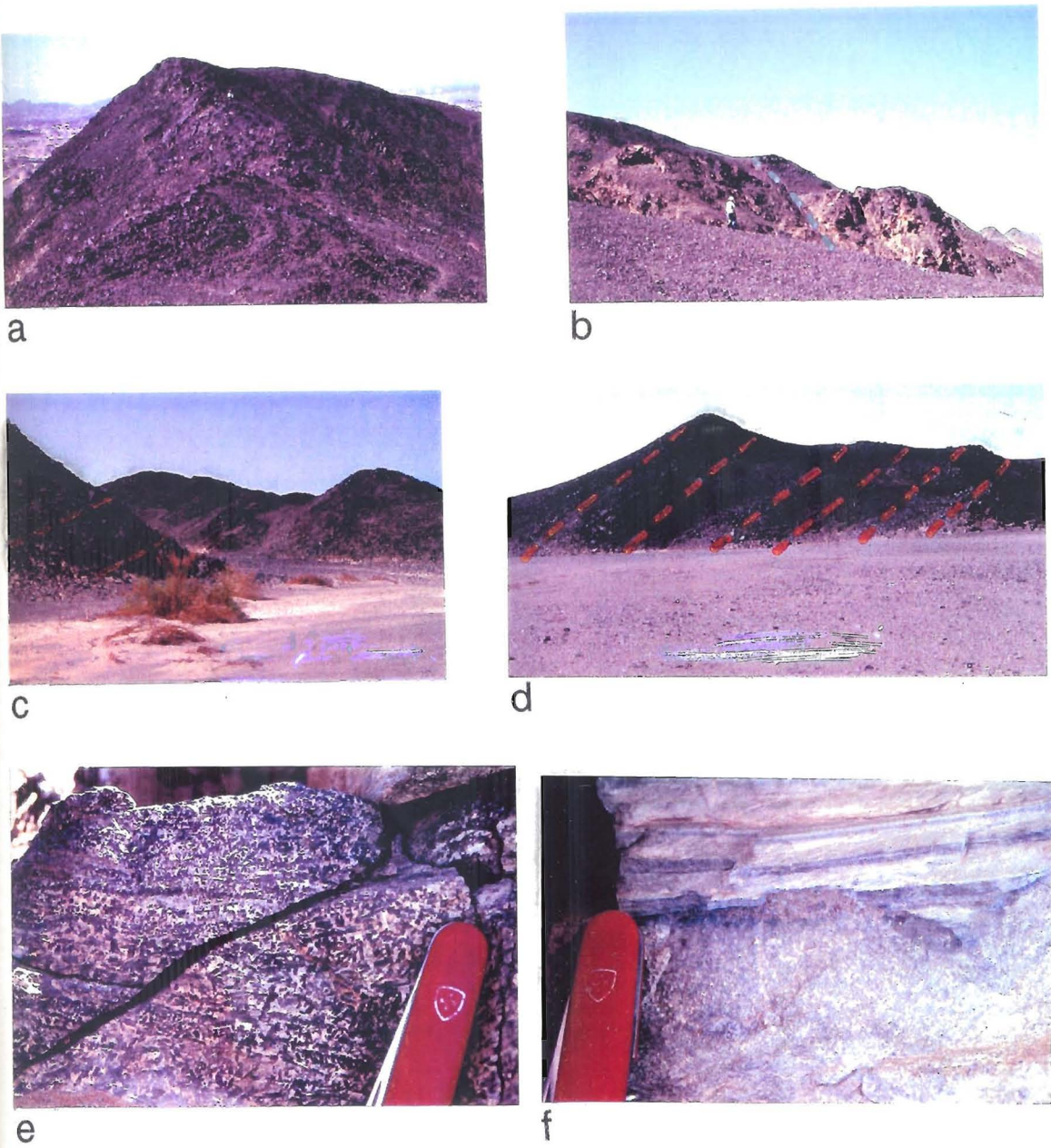
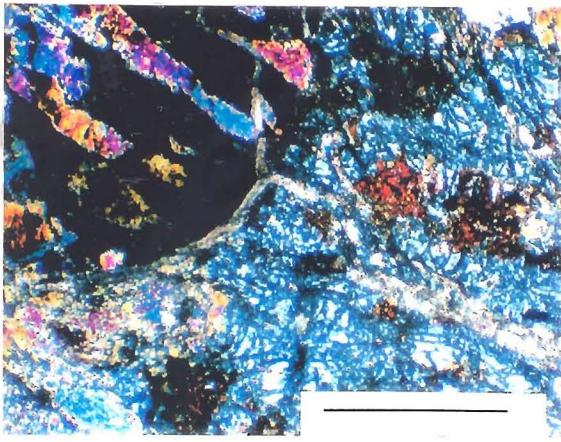
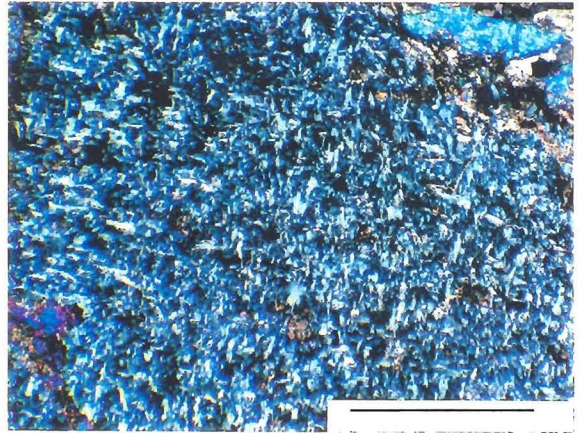


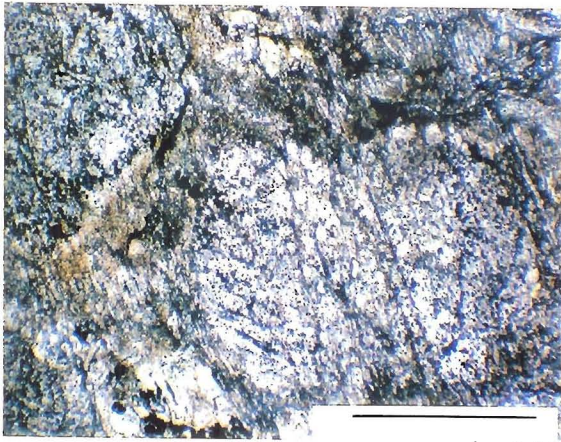
Fig. 3.19 Field relations of the lithologies of Gebel Taylor Wedge
 (a) peridotite and serpentinite exposures, looking west towards Gebel Filat (GR 7387573145), height of the peak to col (foreground) 35m.
 (b) alternating metabasites and schists (GR 7396373611)
 (c) dunite and serpentinitized horizons (GR 7387573155), height of the hill is 15m.
 (d) sheeted dyke complex of intruded meta-gabbroic and volcanoclastic country rocks (GR 6677278851) height of the hill is 8m
 (e) foliated meta-gabbroic rocks (GR 6677578849)
 (f) intrusive meta-dolerite with contact laminated phyllites (GR 5542681410)



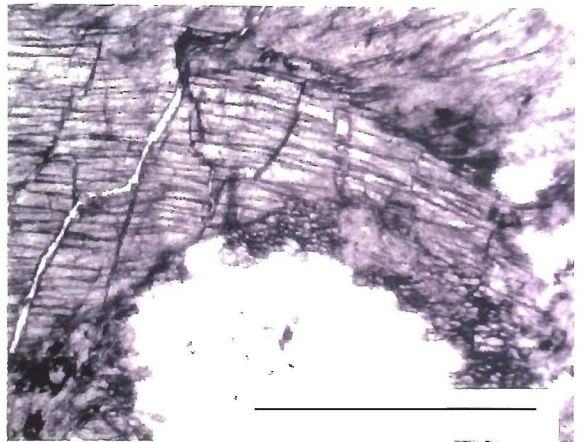
a



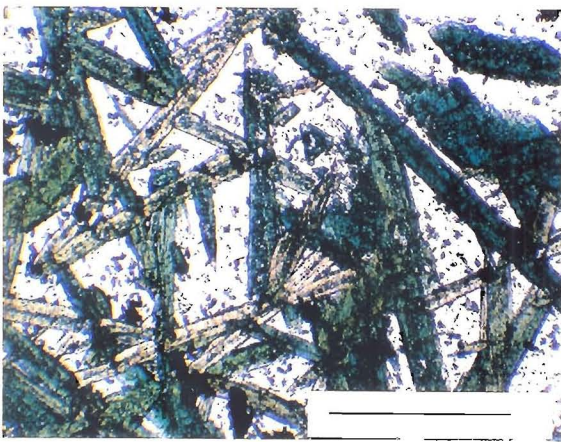
b



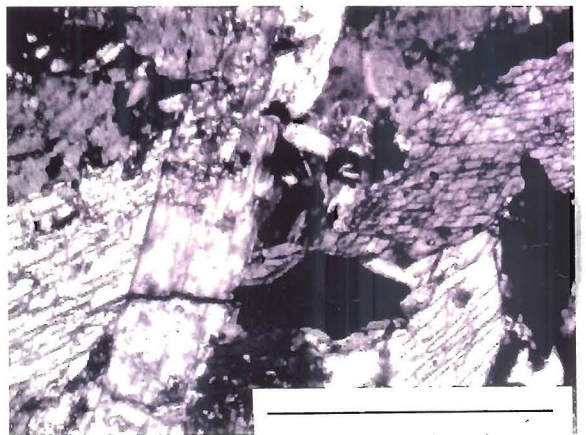
c



d



e



f

Fig. 3.20 Metamorphic textures from the rocks of Gebel Taylor Wedge

- (a) a crude foliation S1 along which serpentinite (Sps) replaces relict olivine (Ol) in dunite (cross-polarized light; GR 7387573155; scale bar 1 mm)
- (b) serpentinite showing a mesh texture as an alteration product of olivine in dunite (cross-polarized light; GR 7387373150; scale bar 1 mm)
- (c) altered pyroxene in meta-gabbro (plane-polarized light; GR 7387373150; scale bar 1 mm)
- (d) bent glaucophane partly replaced by chlorite forming S1 foliation (plane polarized light; GR 6174174397; scale bar 0.25 mm)
- (e) actinolite showing a decussate texture developed in a static phase post D1, tremolite-actinolite unit (plane-polarized light; GR 6415677801; scale bar 1 mm)
- (f) hornblende and actinolite aggregate, Meta-gabbroic unit (plane-polarized light; GR 6677578849; scale bar 0.25 mm)

Chemical analyses of meta-ultra-basic rocks (Appendix B) plot in the field of high-magnesium basalts (Fig. 3.21). A sample of the chlorite schist plots in the field of tholeiitic basalts (Fig. 3.21) and therefore, might be demonstrating an origin from either a highly sheared basalt or a sedimentary rock derived from basalt. The LREE depleted pattern can be demonstrated with positive values for Ni and Cr (Fig. 3.21) which is necessary for either the partial melting process or the early olivine-dominated crystallization in the formation of Back-arc ultra-basic rocks (Pearce *et al.* 1994). LREE depletion has been recorded for the back-arc Lau Basin of the SW Pacific where there is a gradual change from depletion to enrichment toward the subduction zone (Pearce *et al.* 1994) as an island arc is approached (Fig. 3.21). This would indicate that any subduction zone in the central Wadi Allaqi area would be a considerable distance away (probably well to the south).

The Tremolite-actinolite schist unit occurs in a tectonic horse overlain by the ultrabasic unit. It is overlain by Metagabbroic unit within the wedge which consists of tremolite-actinolite, quartz, plagioclase (An₃₅), calcite and chlorite with apatite and titanite as accessories. Tremolite-actinolite forms pale-green aggregates of thin prismatic aligned crystals (Fig. 3.20e). Quartz occurs as fine-grained xenomorphic elongated crystals which are aligned parallel to the schistosity. Slightly saussuritized plagioclase (An₃₅) are strewn throughout the rock. Occasionally some of samples contain minor graphite.

The Meta-gabbroic unit occurs in a tectonic horse within the wedge and consists of massive meta-gabbro which underlies volcanoclastic rocks with metamorphic dykes (Fig. 3.19d). It is underlain by the tremolite-actinolite schist unit and the Kazzaz Formation of the Filat Succession lies tectonically above. The dyke rocks and massive coarse-grained meta-

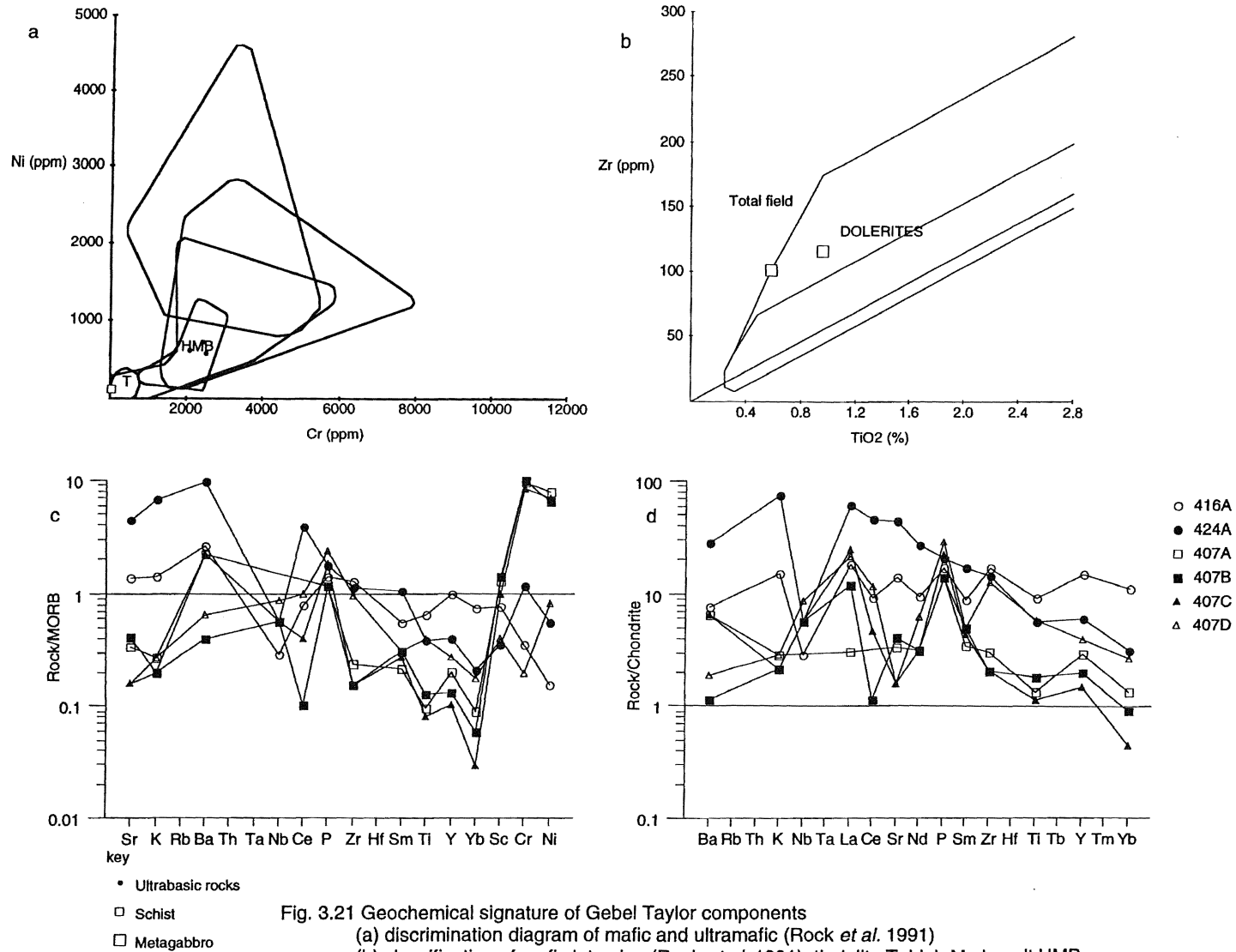


Fig. 3.21 Geochemical signature of Gebel Taylor components

(a) discrimination diagram of mafic and ultramafic (Rock *et al.* 1991)

(b) classification of mafic intrusion (Rock *et al.* 1991); tholeiite T, high Mg basalt HMB

(c) MORB-normalized (Pearce 1983)

(d) chondrite-normalized (Thompson *et al.* 1984)

416A, 424A (metagabbro), 407A, 407B, 407C (ultrabasic rocks), 407D (schist)

gabbro are petrographically indistinguishable. Coarse-grained meta-gabbros consist mainly of plagioclase, hornblende and tremolite-actinolite (Fig. 3.20f) with minor of chlorite and titanite. The plagioclase (An_{60}) is idiomorphic to sub-idiomorphic and show sericitization. Sub-idiomorphic, green hornblende megacrysts often exhibit textures similar to subophitic igneous texture indicating a possibility that they formed by alteration from pyroxene. Alteration to chlorite and tremolite-actinolite is common. A fine-grained variety of meta-gabbro with minor amount of quartz occurs as a sheared rock to the west of the outcrop (GR 5659082137). Chemical analyses of these rocks (Appendix B) plot within the dolerites field (Fig. 3.21b) by using the Zr - TiO_2 diagram (Rock *et al.* 1991). Using spider diagrams the data indicates back-arc basalt affinity.

3.7 Summary

Three tectonic-stratigraphic Successions with distinct lithologies, structures, and geochemical signatures have been established. The most appropriate tectonic environment for the deposition of the Successions, based upon petrochemical considerations, is a back-arc basin comparable to those documented in the Japan Sea [*e.g.*, Yamato Basin (Poucllet *et al.* 1994); south Aegean arc (Mitropoulos *et al.* 1987; Pe-Piper *et al.* 1994); eastern Ngatoro basin (Gamble *et al.* 1994)]. Best estimates of the thickness of the Successions are the Filat Succession 15 km, the Um Relan Succession 1.5 km and the Kilkobob Succession 3 km.

The structurally lowermost Succession, the Filat, is composed essentially of calc-alkaline, volcanoclastic rocks with rare lavas, with an upward change in composition from basalt to andesite, and meta-limestones. A lower fine-grained unit (the Neiqit Formation) is overlain by a more diverse, upward-finishing unit (the North Allaqi Group). The latter unit was likely to be a proximal

deposit to any volcanic island-arc edifice to the south of the central Wadi Allaqi area and the rudaceous units could be débris flows.

The succeeding Um Relan Succession, which crops out along the major Allaqi Shear-zone in the central Wadi Allaqi area, is formed principally of metasedimentary rocks. The presence of stromatolitic limestones and minor intercalations of fine-grained volcanoclastic rocks indicate a shallow-water marine origin probably along the fringes of an encroaching volcanic sub-aerial structure.

The Kilkobob Succession is a mixture of pyroclastic and volcanoclastic rocks. Some of the latter rocks are ferruginous and this combined with the petrochemical evidence indicates both a change to alternating basaltic and andesitic derivations and to frequent deposition from an aerial source. The tectonic environment of deposition for the Meta-limestone Formation of this Succession is some what problematic in that the basalt lavas have a back-arc affinity. This could mean that there was a volcanic edifice in a central position within the back-arc which during the collision event was caught up in the northerly-moving volcanic pile.

The Gebel Taylor Wedge is an allochthonous unit, which is composed of thin volcanoclastic cover with metadolerite dykes, metagabbros, serpentinites and dunites with schists (including a single occurrence of glaucophane), and may have originated as a fragment of an obducted back-arc basin sea-floor (Dewey 1976; Saunders *et al.* 1979; Oberhänsli 1994).

Chapter Four

Igneous Intrusions

4.1 Introduction

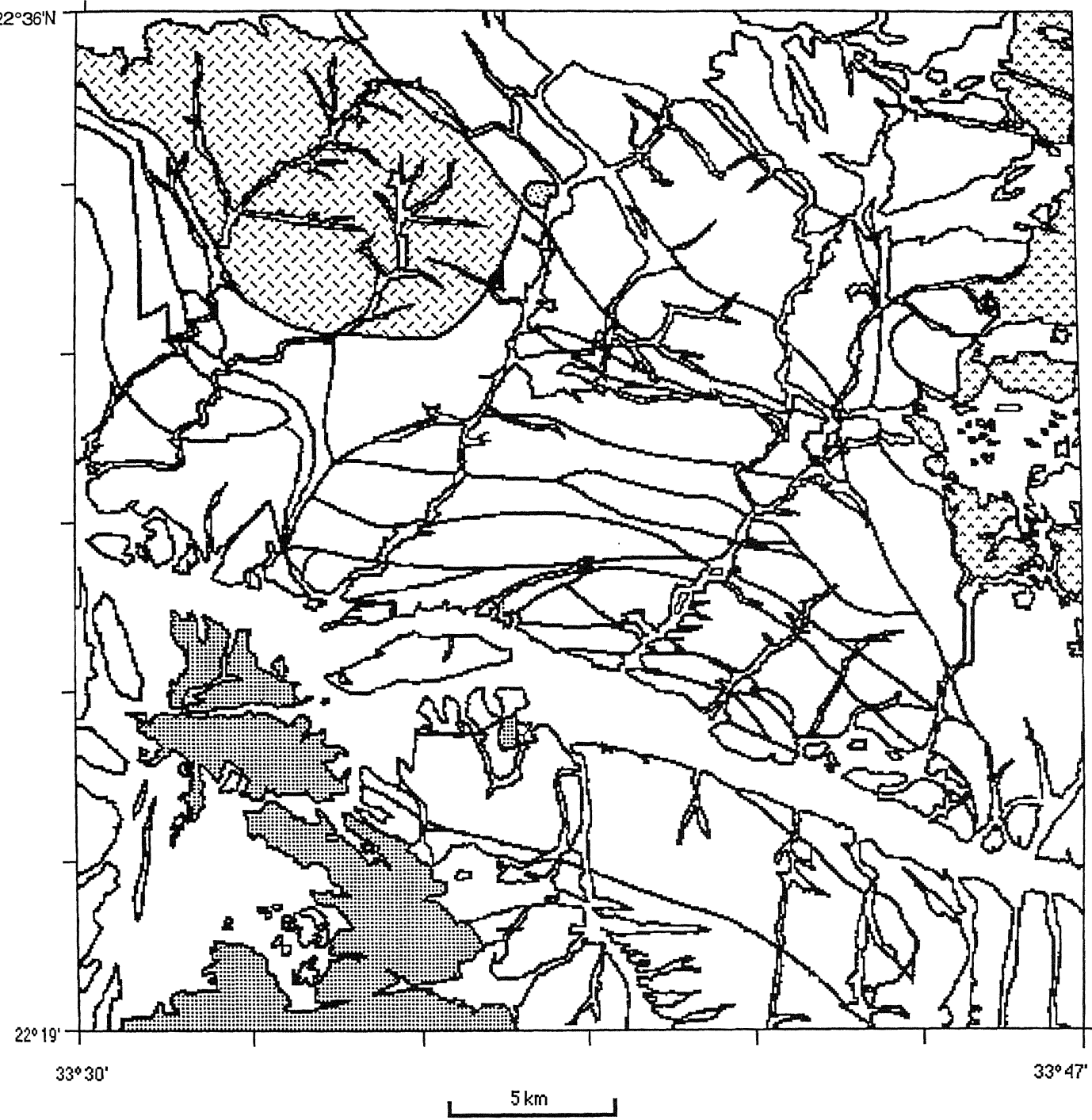
This chapter is concerned with the structural and petrochemical analysis of those igneous bodies (Fig. 4.1) which do not form an integral part of the tectonic-stratigraphical successions (see chapter three) of central Wadi Allaqi. The emphasis has been on deducing the correct tectonic setting of the granitic plutons, minor sills and dykes with respect to the structural history (chapter 2); and, although it is recognised that the igneous bodies are key markers of the structural and terrane evolution of the Pan-African orogeny, it was not the purpose of this study to determine radiometric ages.

4.2 The granitic plutons

Although the tectonic relationships are complex, broadly the four granitic plutons may be divided into syn- and late-tectonic types. The granitic intrusions show a great range in size (Figs. 1.3b, 1.4, 4.1); from the small elliptical Um Relan Granite to relatively large intrusions of batholithic proportions, *viz.*, the Filat and Kilkobob Granites. They will be described in putative order of their relative age of intrusion (Table 2.2). The study is based upon copious field observations supplemented by analyses of a necessarily restricted number of samples in which the sample closest to the mean modal composition of each pluton was used for a full geochemical analysis.

4.2.1 Atshani Granite

Almost the whole of the elliptical Atshani Granite is exposed within central Wadi Allaqi and is about 90 km² in area (Figs. 1.3b, 4.2). The northern margin of the pluton is a tectonic junction in which the original intrusive



Key

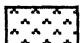


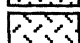
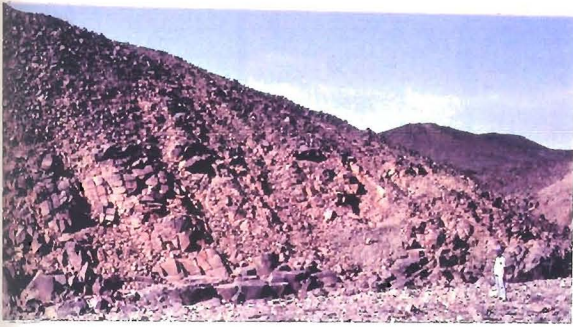
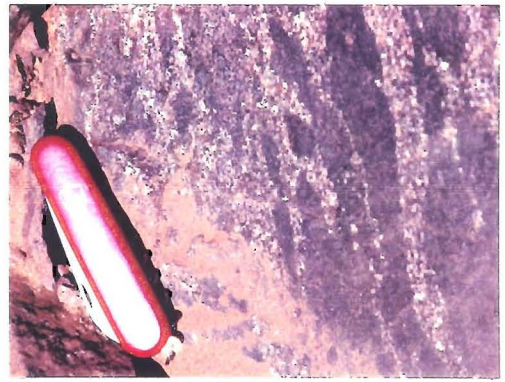
-  Kilkobob Granite
-  Filat Granite
-  Um Relan Granite
-  Atshani Granite

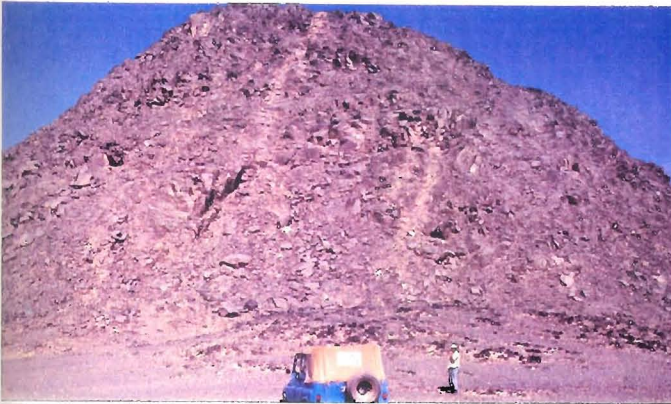
Fig. 4.1 Outcrop of granite intrusions



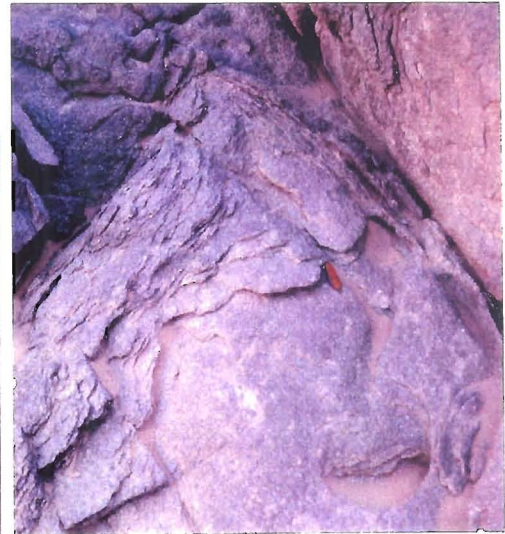
a



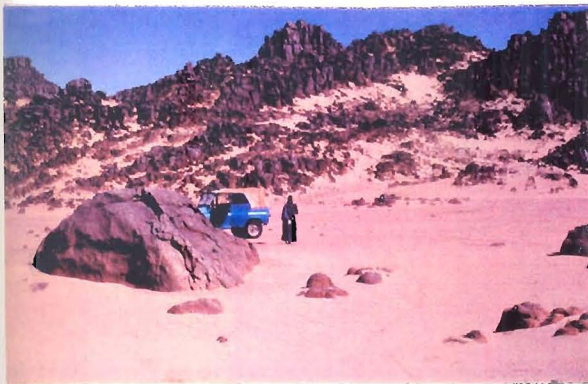
b



c



d



e



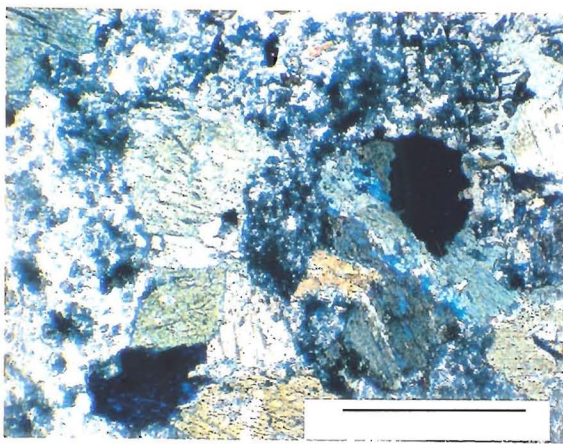
f

Fig. 4.2 Field relations of the Atshani, Um Relan and Filat Granites
 (a) panoramic view of southern edge of Atshani Granite showing jointing and crude S1 (GR 5926792089)
 (b) xenoliths in Atshani Granite showing alignment parallel to S1 (GR 5589291158)
 (c) outcrop of the Um Relan Granite (GR 6531892648)
 (d) sigmoidal shear in Um Relan Granite (GR 6532092642)
 (e) panoramic view of part of Filat Granite showing typical jointing (GR 5720178121)
 (f) xenoliths in Filat granite showing lack of alignment (GR 5478674280)

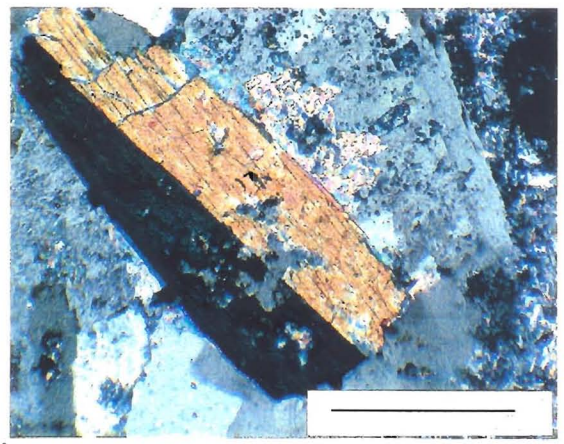
contact has been sheared and obliterated during the compressional D2 regional phase. Elsewhere the junction between the pluton and the volcanoclastic country rocks of the Filat Succession is sharp, relatively smooth and regular. A contact aureole is not recognised from field and petrographic observations. Frequent small xenoliths (Fig. 4.2b) and large enclaves, up to a kilometre in length (Fig. 5.6), of the country rocks are aligned with a mean 300° azimuth (Figs. 4.2, 5.6). The large enclaves contain S1 and associated gold-bearing quartz-veins which are truncated at the junctions with the granite.

The predominant rock is massive, medium- to coarse-grained, pale greenish-grey tonalite (IUGS nomenclature; Le Bas & Streckeisen 1991 modified from Streckeisen 1976; Appendix D, Fig. 4.4), with a calc-alkaline affinity, and is essentially composed of plagioclase, quartz, hornblende and secondary chlorite (Fig. 4.3a; Table 4.1) with minor amounts of potash feldspar, pyrite and zircon. Plagioclase (An₃₅), reaching up to 2 mm in length, is altered to sericite and epidote (Fig. 4.3d,e,f). Quartz occurs as subhedral to anhedral aggregates with undulose extinction interstitial to the plagioclase. Unaltered green hornblende occurs as euhedral crystals, elongate, occasionally showing lamellar twinning and zoning (Fig. 4.3b). Chlorite, probably formed secondarily from biotite, is frequently bent into microfolds of the D2 phase (Fig. 4.3c). Textural evidence (Fig. 4.3) indicates the following order of crystallization : plagioclase-->biotite-->quartz-->hornblende followed by chlorite as a secondary alteration mineral.

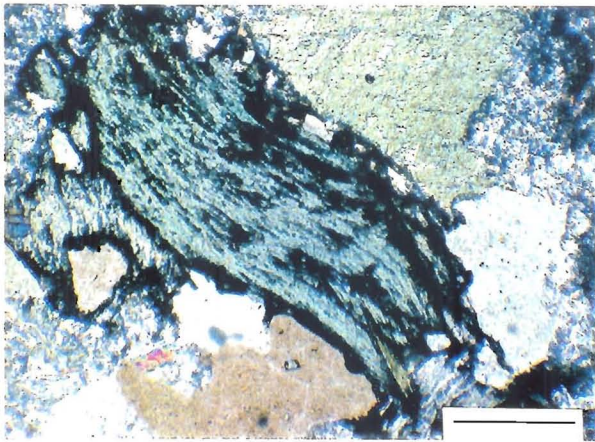
Three fine- to medium-grained, unmetamorphosed, undeformed, thin doleritic dykes intrude the Granite near its southern margins (GR 6191571312).



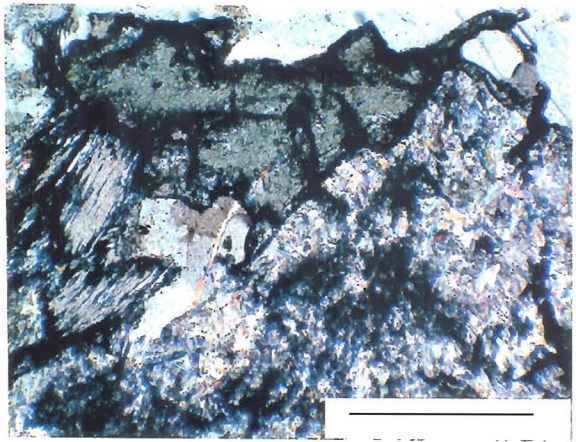
a



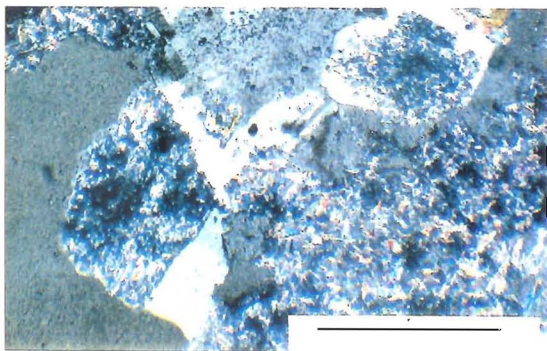
b



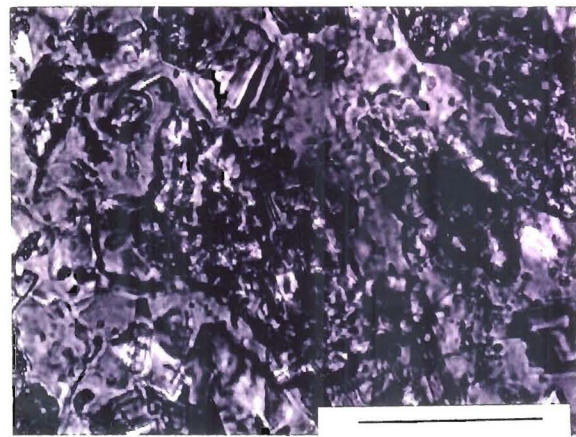
c



d



e



f

Fig. 4.3 Atshani Granite: textures and mineralogy

(a) typical textures showing hornblende and chlorite aggregates set in a coarse matrix of altered plagioclase and quartz (cross-polarized light; GR 5496090780; scale bar 0.1 mm)

(b) euhedral twinned hornblende phenocryst set within a relatively unaltered plagioclase crystal abutting quartz and altered plagioclase. Note weak zoning of plagioclase (cross polarized light; GR 5589291158; scale bar 0.1mm)

(c) chlorite aggregate deformed by F2 open microfold adjacent to hornblende, quartz and sericitized plagioclase (cross-polarized light; GR 5589291158; scale bar 0.1 mm)

(d) interstitial chlorite in an interlocking texture of altered plagioclase and quartz (cross-polarized light; GR 5589291158 scale bar 0.1 mm)

(e) sericitized plagioclase abutting clear quartz (cross-polarized light; GR 5589291158; scale bar 0.1 mm)

(f) detail of the alteration products of sericite and epidote within plagioclase (cross-polarized light; GR 5496090780 scale bar 0.05 mm)

	Atshani Granite		Um Relan Granite		Filat Granite		Kilkobob Granite	
Number of samples	4		3		7		6	
Minerals	Mean %	Range %	Mean %	Range %	Mean %	Range %	Mean %	Range %
Quartz	30	±5	30	±1	33	±4	34	±5
K-feldspar	1	±0.5	32	±2	22	±2	45	±5
Plagioclase	28	±7	35	±5	39	±5	17	±5
Hornblende	10	±2	-	-	-	-	-	-
Chlorite	8	±2	-	-	trace	-	trace	-
Biotite	-	-	-	-	2	±1	2	±1
Muscovite	-	-	3	-	-	-	-	-
Other minerals (e.g. zircon)	trace	-	trace	-	trace	-	trace	-

Table 4.1 Modes of the Granite intrusions

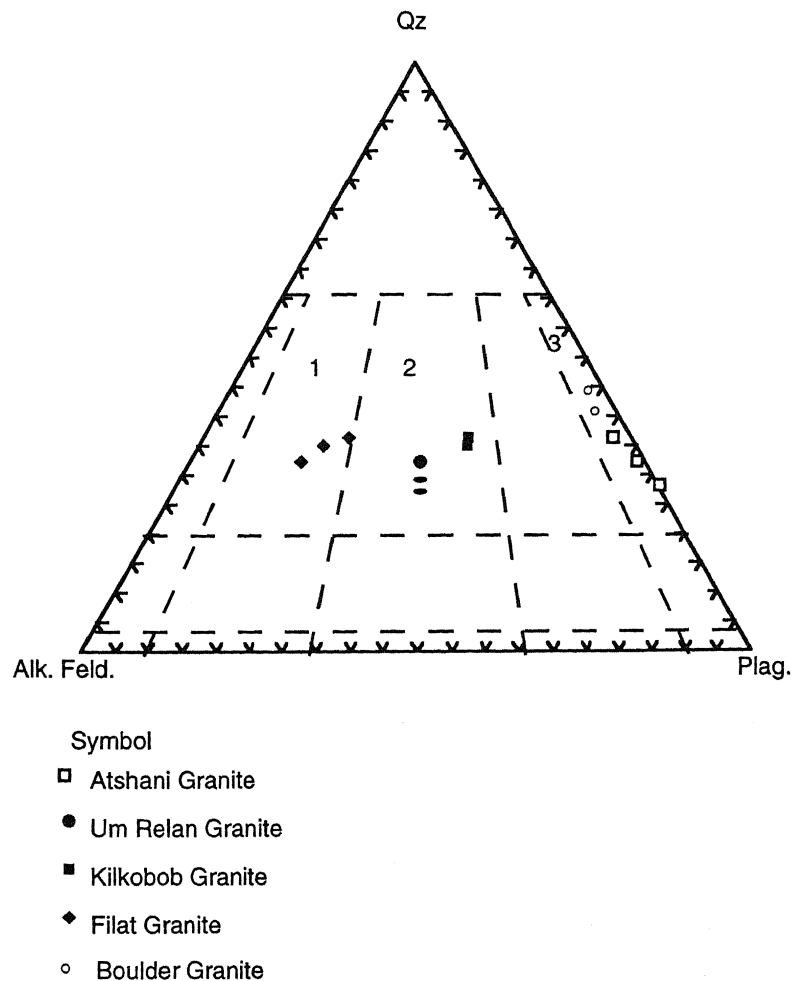
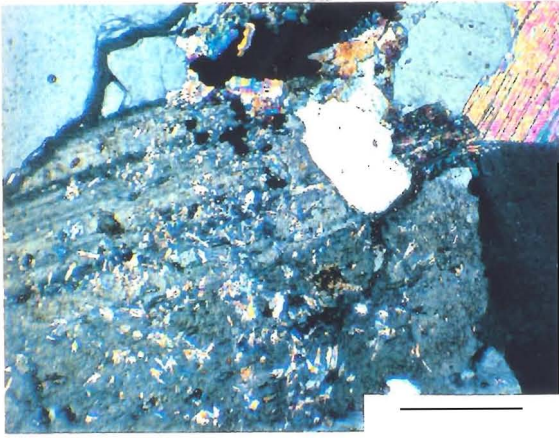


Fig. 4.4 Modal plots (Le Bas & Streckeisen 1991) for the granite plutons (1 syenogranite; 2 monzogranite; 3 tonalite)

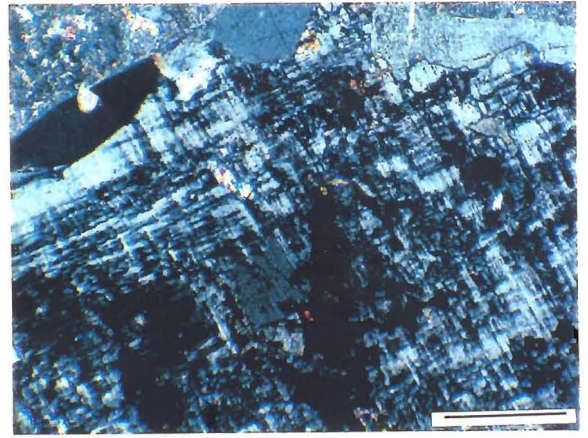
4.2.2 Um Relan Granite.

An oval-shaped granite body (Fig. 4.1, 4.2c), of about 0.25 km² area, intrudes the Um Relan Succession along a prominent shear-zone. The length of the granite outcrop (Fig. 1.3b), which is orientated sub-parallel to S₁, is about 900m and the width is about 400m. The granite has sharp and irregular intrusive contacts and a 100 m wide zone of marked discolouration, from dark to light grey, is exposed within largely unresponsive quartzite country rocks on the northern side. In thin section the quartz shows a conspicuous granoblastic and polygonized texture which might represent the effects within a limited contact metamorphic aureole. The southern margin of the body is affected by strong shearing, which has obliterated any evidence for intrusion, and individual shears can be traced into the granite body (Fig. 4.2d).

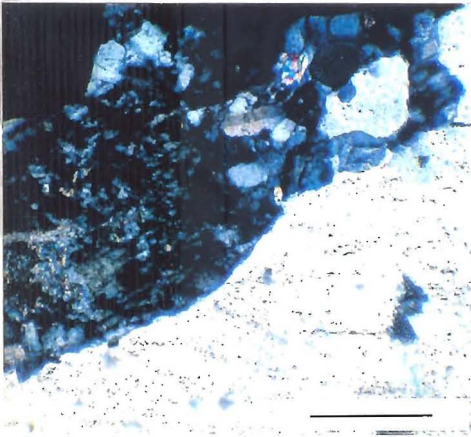
This granite is an homogeneous, massive, pale-grey, well-jointed and sigmoidally sheared (Fig. 4.2d) muscovite-bearing monzogranite (IUGS nomenclature Le Bas & Streckeisen 1991 modified from Streckeisen 1976; Appendix D, Fig. 4.4). The rocks are composed essentially of quartz, feldspars and muscovite (Table 4.1) with zircon and limonitized pyrite as the main accessories. Large (reaching to 4 mm in length and 3 mm in width), albitic plagioclase (An₇), which are slightly altered to sericite (Fig. 4.5a), and subordinate microcline-perthite phenocrysts (Fig. 4.5b) form the framework of the rock. Quartz, containing small prismatic crystals of zircon, usually forms in interstitial patches enclosed by the feldspars with some granulation along margins adjacent to feldspars (Fig. 4.5c). Biotite is rare and usually shows partial alteration to chlorite with opaque minerals aligned parallel to the cleavage (Fig. 4.5e). Muscovite occurs as clear interstitial plates which appears to have replaced pre-existing phyllosilicates and is deformed by D₃ kink folds (Fig. 4.5d & e). Textural evidence (Fig. 4.5) indicates the following order of crystallization : biotite-->feldspars with some quartz-->quartz and at



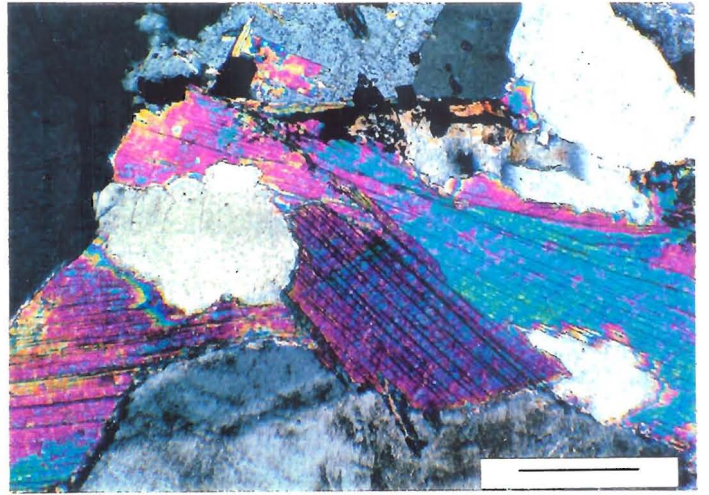
a



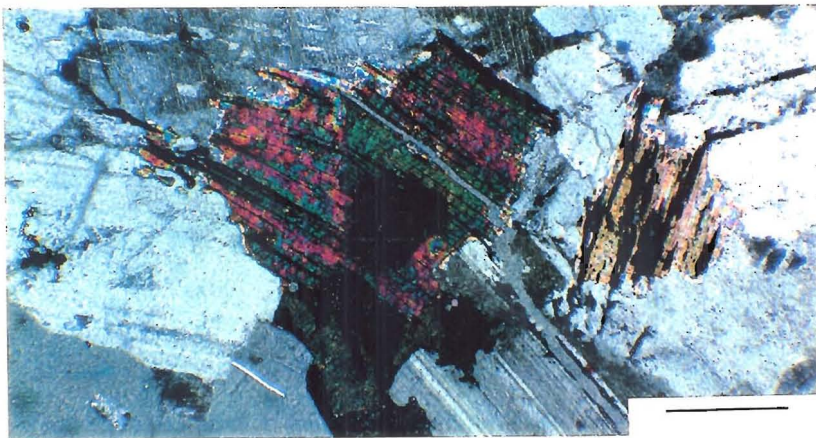
b



c



d



e

Fig. 4.5 Um Relan Granite: textures and mineralogy

(a) slightly sericitized plagioclase adjacent to quartz, demonstrating smooth boundary, and white mica plates (cross-polarized light; GR 6532092642; scale bar 0.1 mm)

(b) microcline phenocryst with inclusion of quartz and plagioclase showing irregular boundary with quartz and plagioclase (cross-polarized light; GR 6532092642; scale bar 0.1 mm)

(c) granulated quartz around the margin of an alkali feldspar indicating that brittle shear occurred after crystallization (cross-polarized light; GR 6532092642; scale bar 0.1 mm)

(d) large undeformed plates of interstitial muscovite with plagioclase and quartz indicating that the muscovite developed at a late stage (cross-polarized light; GR 6531592639; scale bar 0.1 mm)

(e) typical texture of the granite showing juxtaposition of plagioclase, biotite and perthitic alkali-feldspar. Note deformation of the mica and feldspars and alteration of the biotite with opaques parallel to the cleavage (cross-polarized light; GR 6531592639; scale bar 0.1 mm)

later stages chlorite replaced biotite and sericite replaced feldspar followed by widespread development of muscovite. Muscovite commonly develops in rocks found in shear-zones during the decompression stage following high strain. In the case of the Um Relan Granite this could be as late as the period following the D2 phase of deformation.

4.2.3 Filat Granite

The northern two-thirds (about 70 km²) of this locally triangular granitic pluton is exposed in central Wadi Allaqi (Fig. 1.3b). The country rocks are of volcanoclastic rocks of the Neiqit Formation of the Filat Succession and no contact aureole has been recognized for this granite. All of the exposed junctions are steeply-faulted and no unambiguous intrusive contacts have been observed. The granite is a pink, coarse-grained, non-foliated, massively-jointed syenogranite (Figs. 4.2e, 4.4) and contains randomly-oriented xenoliths only of the country rock (Fig. 4.2f). The syenogranite is composed of an assemblage of microcline-perthitic feldspar, plagioclase (An₁₀), quartz and biotite which shows a small amount of alteration to chlorite (Table 4.1; Fig. 4.6a,b). The microcline-perthite grains are usually in excess of 2 mm in diameter and contain quartz and plagioclase as inclusions. Plagioclases are frequently zoned and affected by D5 brittle deformation (Fig. 4.6c). Occasionally secondary reaction zones with a median suture occur along the boundaries of adjacent plagioclase grains and are related to exsolution of silica during the late-stages of crystallization (Fig. 4.6d,ef). Textural evidence (Fig. 4.6) indicates the following order of crystallization : plagioclase+quartz--> microcline-perthite-->biotite-->quartz.

4.2.4 Kilkobob Granite.

Only the western 50 km² of this pluton is exposed in central Wadi Allaqi. The Granite is a pale-pink, medium- to coarse-grained, mainly unfoliated

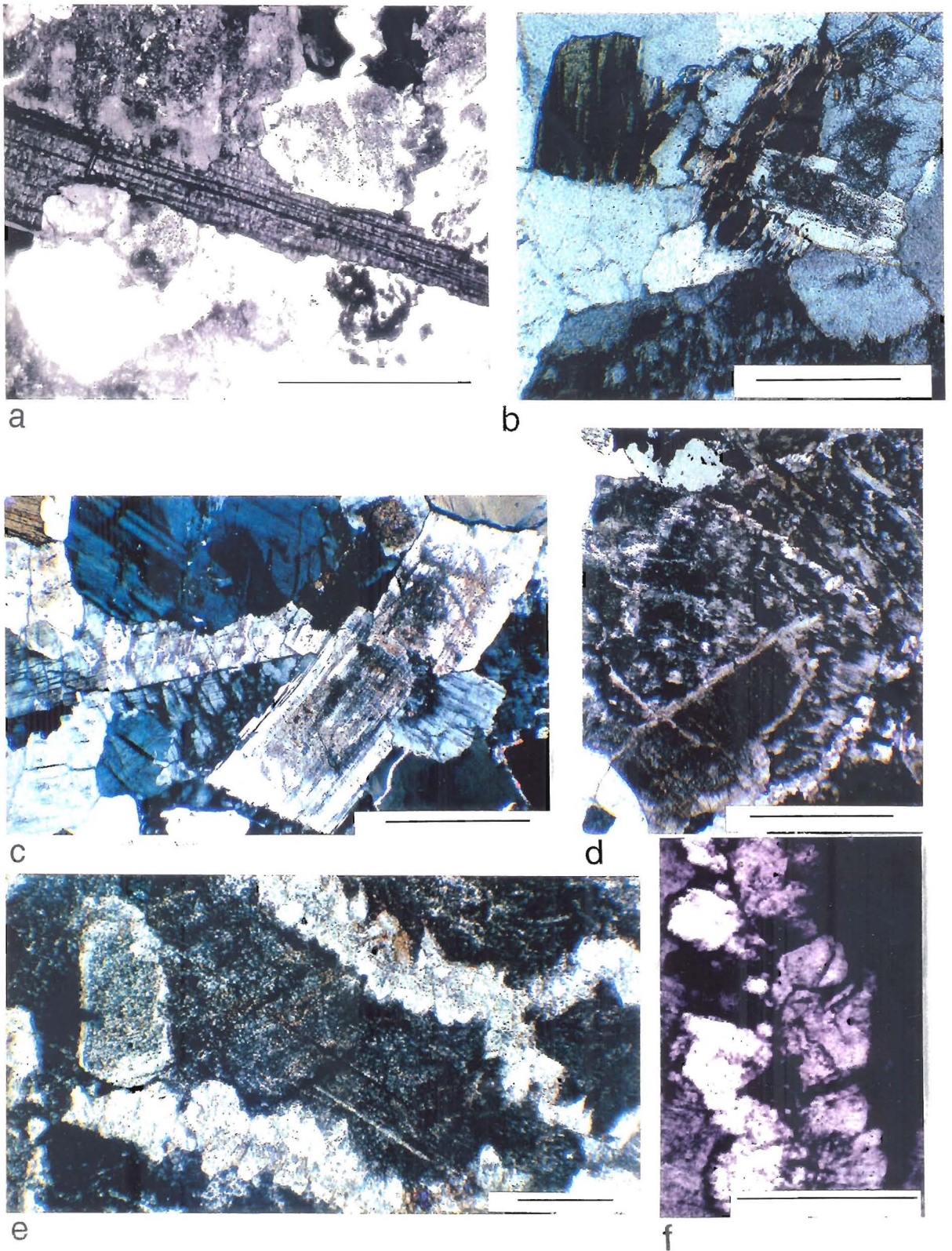
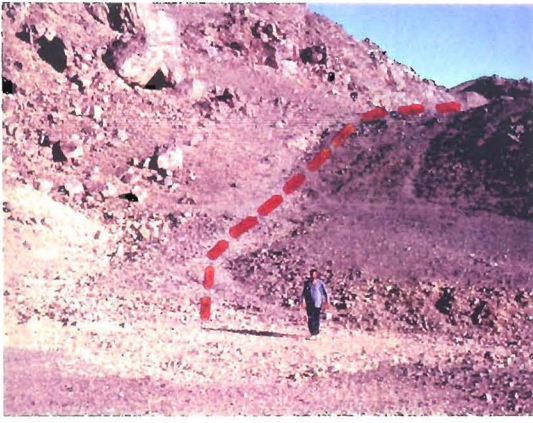
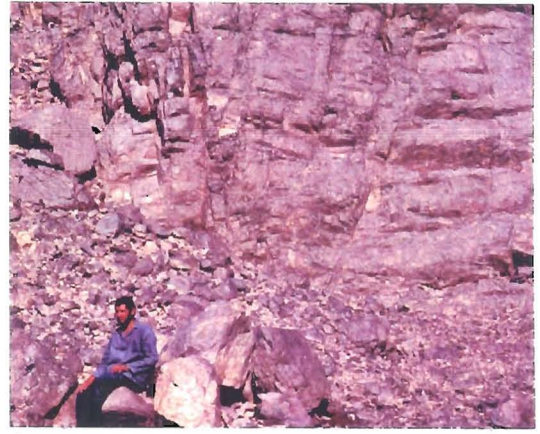


Fig. 4.6 Filat Granite: textures and mineralogy

- (a) altered alkali-feldspar, clear quartz and biotite plate interconnecting fabric (cross-polarized light; GR 6191571312; scale bar 0.5 mm)
- (b) plagioclase, quartz and chloritized biotite with opaques parallel to the cleavage. (cross-polarized light; GR 6191571312; scale bar 1 mm)
- (c) brittle deformation of plagioclase (?D5) adjacent to quartz (plane polarized light; GR 6191571312; scale bar 1 mm)
- (d) reaction texture along the boundary of highly altered feldspar crystals suggesting that the reaction leads to exsolution of silica (cross-polarized light; GR 5478674280; scale bar 1 mm)
- (e) reaction zones along grain boundaries of plagioclase (cross-polarized light; GR 5478674280; scale bar 0.1 mm)
- (f) enlargement of the quartz within the reaction zone showing a median suture (cross-polarized light; GR 5478674280; scale bar 0.25 mm)



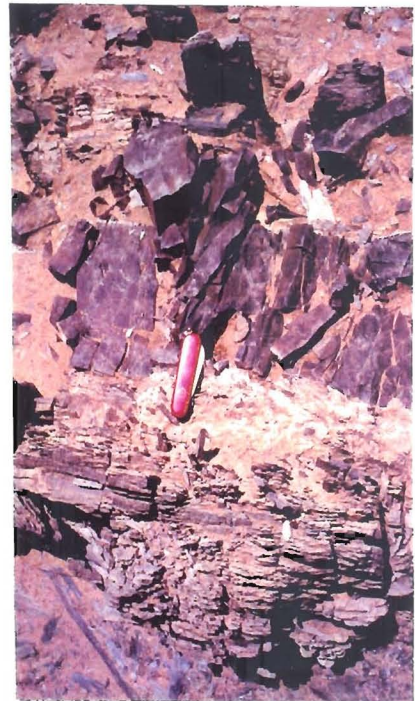
a



b



c



d

Fig. 4.7 Field relations of the Kilkobob Granite and late basaltic sills
 (a) junction with country rock and contact aureole of the Kilkobob Granite (GR 7736780333)
 (b) conjugate kink folds near the margin of the Kilkobob Granite (GR 7756780335)
 (c) basaltic sill showing slight transgression (GR 7300282108)
 (d) close up of (c) showing that the sill has been affected by late-stage joints

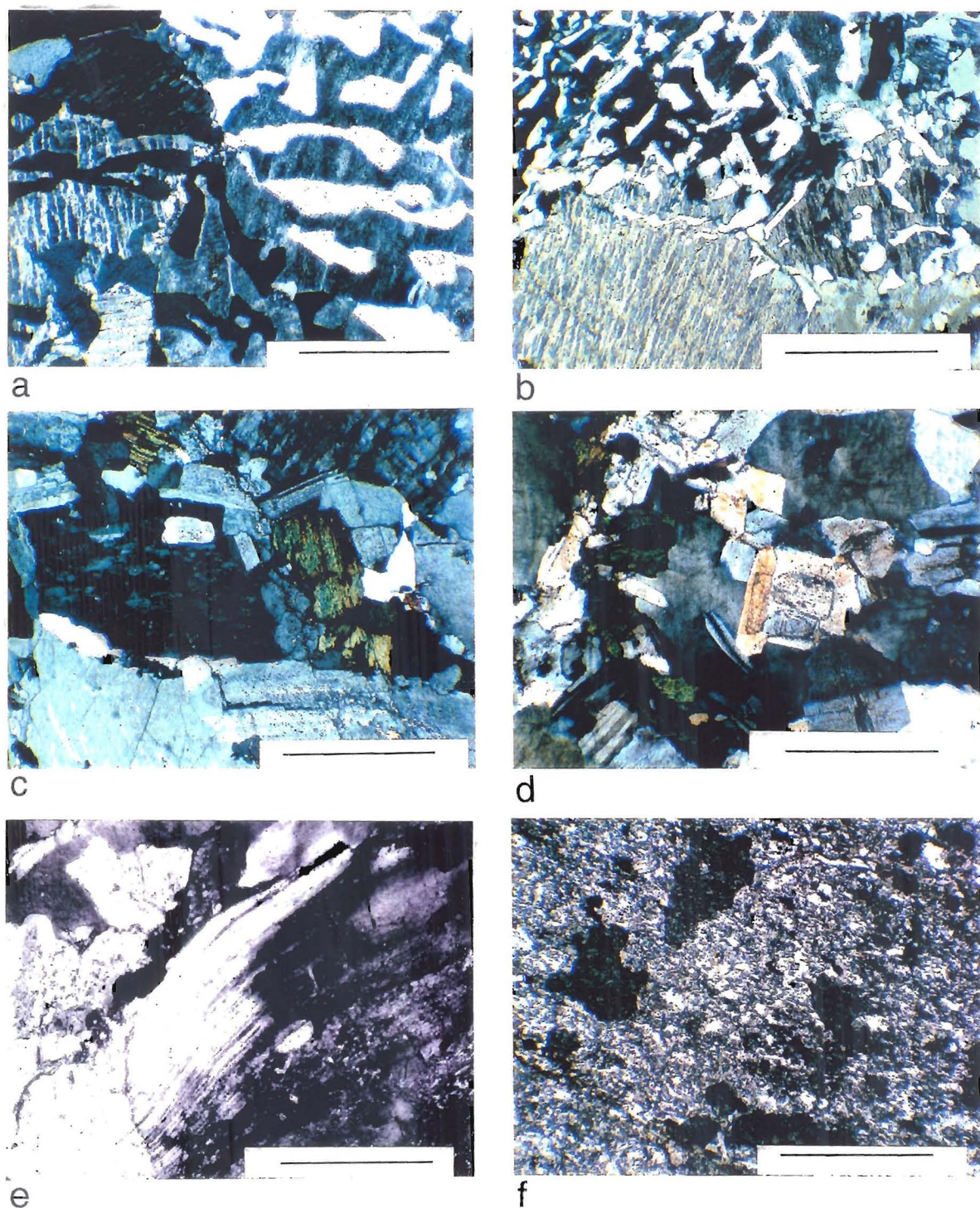


Fig. 4.8 Kilkobob Granite: textures and mineralogy

- (a) graphic intergrowth of quartz and alkali feldspar (cross-polarized light; GR 7736780333; scale bar 1 mm)
- (b) graphic texture adjacent to an alkali-feldspar with perthitic texture (cross-polarized light; GR 7736780333; scale bar 1 mm)
- (c) zoned plagioclase, alkali-feldspar, quartz and chlorite intergrowth (cross-polarized light; GR 7742686589; scale bar 1 mm)
- (d) interlocking quartz, alkali-feldspar and plagioclase showing variations in grain size (cross-polarized light; GR 7789188103; scale bar 1 mm)
- (e) bent plagioclase set in a quartz grains showing undulose extinction, all produced during D3 phase (cross polarized light; GR 7742686589; scale bar 0.5 mm)
- (f) carbonaceous spots in a calcareous phyllite within the contact metamorphic aureole of the Kilkobob Granite (plane-polarized light; GR 7736780333; scale bar 1 mm)

monzogranite (Table 4.1, Fig. 4.4) locally grading into a marginal granodiorite and intruded by rare E-W-trending, aplitic dykes (see section 4.4). Some small unorientated xenoliths of the country rocks are found near sharp, vertical intrusive contacts (Fig. 4.7a) with the rocks of both the Kilkobob Succession and Allaqi Shear-zone (Fig. 1.3b). Near to the contact a crude foliation has been developed and is deformed by D4 kink bands (Fig. 4.7b). Around the western margin of the pluton there is a contact metamorphic aureole, at least hundred metres wide, (Fig. 4.7a) in which thermally altered calcareous siltstones and semi-pelitic phyllites have developed small irregular spots formed, in part, by the segregation of carbonaceous material (Fig. 4.8f).

The granite is composed of an intergrowth of microcline-perthitic feldspar, quartz, plagioclase and chloritized biotite with rare tourmaline (Fig. 4.8c,d). Granophyric and graphic textures between the microcline-perthite and quartz are common in the granite (Fig. 4.8a,b) and indicate eutectic melt conditions. Small zoned plagioclases are common as inclusions within the alkali-feldspars (Fig. 4.8d). Isolated plagioclase grains are frequently buckled (Fig. 4.8e) and microcline-perthite is granulated along grain margins. Deep-blue tourmaline rosettes replace plagioclase. Textural evidence (Fig. 4.8) indicates the following order of crystallization : plagioclase-->microcline-perthite+quartz-->biotite-->tourmaline

4.2.5 Petrochemistry of the granitic bodies

All of the samples of all of the bodies plot in the field of "I-type granites" (Hine *et al.* 1978, Fig. 4.9a). On an alkalinity-variation diagram (Wright 1969) the sample of Atshani Granite falls within the field of calc-alkaline and the samples of the Um Relan, Filat and Kilkobob Granites plot in the field of alkaline (Fig. 4.9b).

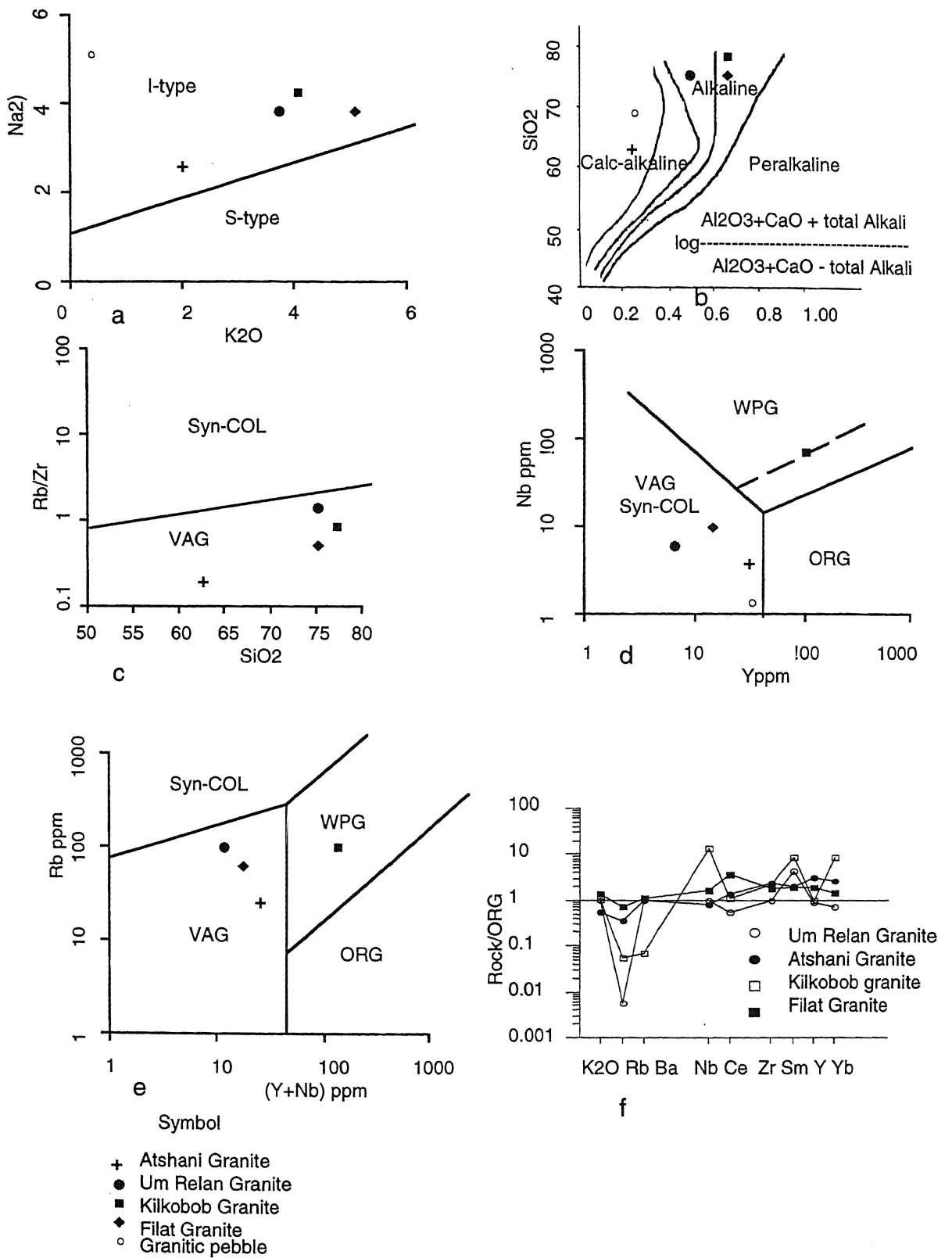


Fig. 4.9 Geochemical signatures of the Granites Plutons

(a) discrimination diagram of "I" and "S" types granites (Hine *et al.* 1978)

(b) alkalinity variation ratio (Wright 1969)

(c) Rb/Zr-SiO₂ discrimination diagram (Harris *et al.* 1986)

(d) Nb-Y discrimination diagram (Pearce *et al.* 1984)

(e) Rb-(Nb+Y) discrimination diagram (Pearce *et al.* 1984)

(f) distribution pattern of granites normalized by oceanic ridge granite (ORG; Pearce *et al.* 1984)

Consideration of the tectonic scenarios of the granite bodies from the geochemical data is confusing. Using the Y/Nb discrimination diagram (Pearce *et al.* 1984), the majority of the samples occupy the field of syn-collision / volcanic-arc granites and the only exception is the Kilkobob Granite sample which lies in within-plate-granite field (Fig. 4.9d). For the (Rb/Zr)/SiO₂ and Rb / (Y + Nb) discrimination diagrams (Fig. 4.9c,e) the majority of samples fall within the field of volcanic-arc granites and the Kilkobob Granite, which lies in the within-plate-granite field, is again the exception. Data plotted on spider diagrams (Fig. 4.9f) indicate a volcanic-arc scenario for all granite bodies.

In summary, it would seem that the Atshani, Um Relan and Filat Granites demonstrate clear volcanic-arc affinities but the Kilkobob Granite geochemical signature is ambiguous and may be related to its demonstrably late-stage emplacement.

4.3 Late basaltic sills and dykes.

Occasional basaltic sills, up to 1m width with sharp margins intruded into rocks of the Kazzaz Formation of the Filat Succession (Figs. 4.7c & d), are probably related to the rare doleritic dykes which occur in both the Atshani Granite (see 4.2.1) and the Kilkobob Succession. The sills show cooling joints but are unaffected by small-scale structures of deformation phases D1 to D4. They are composed of euhedral, randomly-oriented plagioclase phenocrysts set in a very fine-grained groundmass of plagioclase, pyroxene, and a dark-brown indistinguishable glassy material (Fig. 4.10a). The chemical analysis of a selected sill sample (Appendix B) plots in the field of calc-alkaline basalt (Fig. 4.10) and therefore accords with an arc-setting for these rocks.

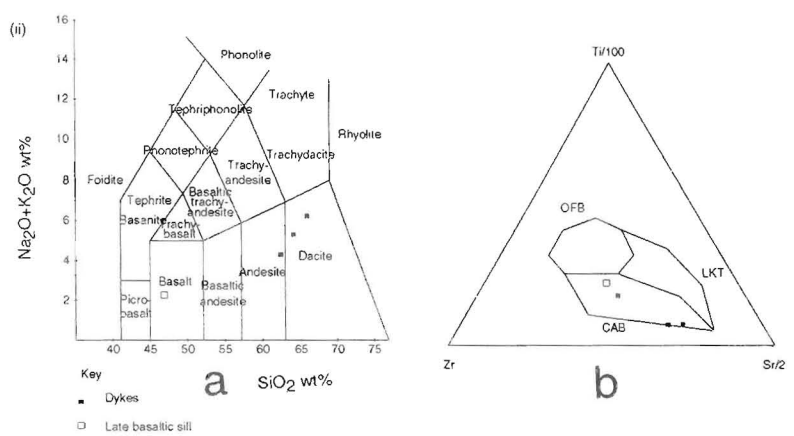
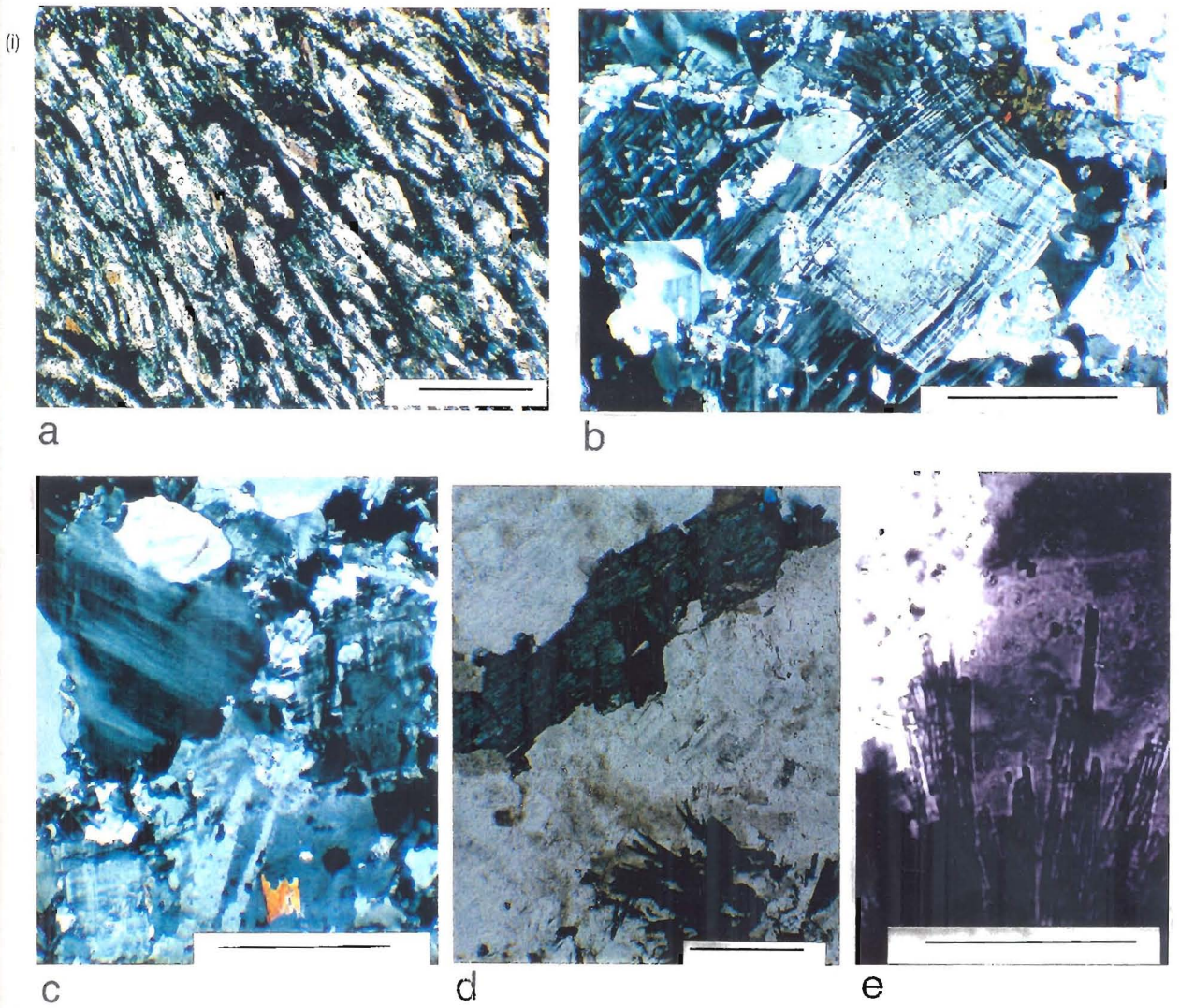


Fig. 4.10 (i) petrography of late aplite dykes and late basaltic sili
 (a) flow texture formed by aligned plagioclase laths set in a fine-grained matrix, late basic sill (plane-polarized light; GR 7300282108; scale bar 0.5 mm)
 (b) slightly deformed microcline phenocryst set in a plagioclase and quartz, aplitic dyke (cross-polarized light; GR 7754286269; scale bar 1 mm)
 (c) deformed quartz and microcline with irregular crystal boundaries, aplitic dyke (cross-polarized light; GR 7754286269; scale bar 1 mm)
 (d) tourmaline aggregates and megacryst in quartz and feldspar; aplitic dyke (cross-polarized light; GR 7754286269; scale bar 0.25 mm)
 (e) detail of tourmaline aggregates protruding into quartz with inclusions, aplitic dyke (cross-polarized light; GR 7754286269; scale bar 0.25 mm)
 (ii) Geochemical signature of late basaltic sill and dykes
 (a) composition of analysed dykes and sill (Sabine 1989)
 (b) discrimination diagram (Pearce & Cann 1973)
 OFP-ocean floor basalt, CAB-calc-alkaline basalt, LKT- low k-tholeiite)

4.4 Late aplitic dykes

Thin, up to 2m wide, aplitic dykes, composed mainly of microcline, quartz, plagioclase and tourmaline (Fig. 4.10), have intruded the western edge of the Kilkobob Granite and in one case (GR 7754286269) is presently aligned parallel to the plane of a D5a right-lateral strike-slip fault. Phenocrysts of microcline, showing slight deformation, are set in a plagioclase and quartz matrix (Fig. 4.10b). The grain boundaries of quartz and microcline are irregular (Fig. 4.10c). Tourmaline occurs as single non-aligned megacrysts and in fibrous rosettes replacing quartz and feldspar (Fig. 4.10d,e)

4.5 Discussion of the tectonics of the granites

Egyptian granites, all from the Pan-African terranes of the Eastern Desert, have been divided (Hussein *et al.* 1982) on the bases of structure, petrology, geochemistry and geochronology into three main types, *viz.*, G1, G2, and G3. G1 granites are similar to "I" types ("M" type of White 1979) of most authors (Brown 1982; Chappel & White 1974; Harris *et al.* 1984; White & Chappel 1977; Pitcher 1983). G2 granites are akin to "S" types of the above authors ("C" types of Didier *et al.* 1982). G3 granites are similar to "A" types of some geologists (Collins *et al.* 1982; Eby 1990; Pitcher 1993; Whalen *et al.* 1987). This classification developed the work of El Ramly & Akaad (1960), who divided the granites into two types, *viz.*, "older grey" and "younger red", El Shazly (1964), who recognised that the two granite types were respectively synorogenic and late-orogenic, and El Gaby (1968, 1975) who demonstrated that the synorogenic, grey granites, have calc-alkaline to alkaline affinities.

Although there is ambiguity in the use of classifications according to chemical affinity Fig. 4.9b shows that Atshani is calc-alkaline whilst the others are alkaline however a classification recommended by Pearce & Gale (1977) would make all the granites calc-alkaline types since they have low

values of Rb, Nb, and Y and Nb is less than 15 ppm. All of the Pan-African granites of central Wadi Allaqi are "I" type, broadly synorogenic. The Atshani, Um Relan, and Filat Granites are "I" type but the Kilkobob Granite is more akin "A" type granites to (Eby 1990). However emplacement of the Kilkobob Granite does not appear to be directly related to post-tectonic rift, nor is it similar to the majority of post-tectonic "A" type granites in the Arabian-Nubian Shield that are associated with ring complexes (Pitcher 1993). It has been stated (Atherton 1993) that different tectonic settings do not always produce significantly distinctive source rock assemblages because granites are the last product of mantle advection. So it is likely the Kilkobob Granite is the last stage of magmatic crystallization within a volcanic-arc.

4.6 Summary

The Atshani, Um Relan, Filat and Kilkobob Granites have broadly similar characteristics, although only the Atshani Granite demonstrates undoubted calc-alkaline affinities. The intrusions vary in modal composition from tonalites to syenogranites and the Atshani, Um Relan and Filat are "I" type granites of volcanic-arc tectonic setting. The signature of Kilkobob Granite is ambiguous but on balance is thought to be the latest to be emplaced.

Minor basaltic sills, with a volcanic-arc petrochemical signature, invaded the volcanoclastic country rocks. Late-stage emplacement, possibly after D5, of aplitic dykes occur within the Kilkobob Granite.

The structural relationships indicate that the Atshani Granite has been emplaced between the D1 and D2 phases, the Um Relan during the early stages of D2, the Filat Granite post-D2, and the Kilkobob Granite between the D3 and D4 phases.

Chapter Five

Gold mineralization and its tectonic setting

5.1 Background

During the nineteenth dynasty (2500 BC.; Trigger 1976) the ancient pharaonic Egyptians established several productive mines and pits along the Wadi Allaqi and its tributaries (the ancient region of *Akita*; Fig. 5.1a). Although mining records for this area are sparse and very cursory references are confined to regional maps (*e.g.*, Fig. 5.1a) and lists (*e.g.*, Afia & Imam 1979), Hume (1937) suggested that early production (see Fig. 5.1b for production figures for Egypt) came from more easily exploited alluvial and surficial vein sources with higher grades and that later production came increasingly from more complex underground veins. A major ancient mine at Um Garayat in the western Wadi Allaqi was sporadically worked until 1948 (Fig. 5.2) and recent geochemical investigations (Ivanov & Hussein 1972) have not led to re-opening or extending the mine. Bean & Hudson (1983) reported the results of geochemical surveys of Wadi Allaqi, on rocks and wadi sediments for lead, tin, niobium, molybdenum, copper, zinc, nickel, cobalt and chromium as part of an exploration programme of the British Geological Survey, in co-operation with the Egyptian Geological Survey and Mining Authority. The results showed good copper prospects, reasonably good nickel prospects, insignificant chromium and cobalt results, and only a few isolated results for the other five elements.

5.2 Objectives of this investigation

The gold deposits of Wadi Allaqi are poorly documented and the paragenesis has not been studied. The main purpose of this study was to produce evidence for the relationship of the gold-bearing veins in the tectonic history of the area and in particular the objectives were to:

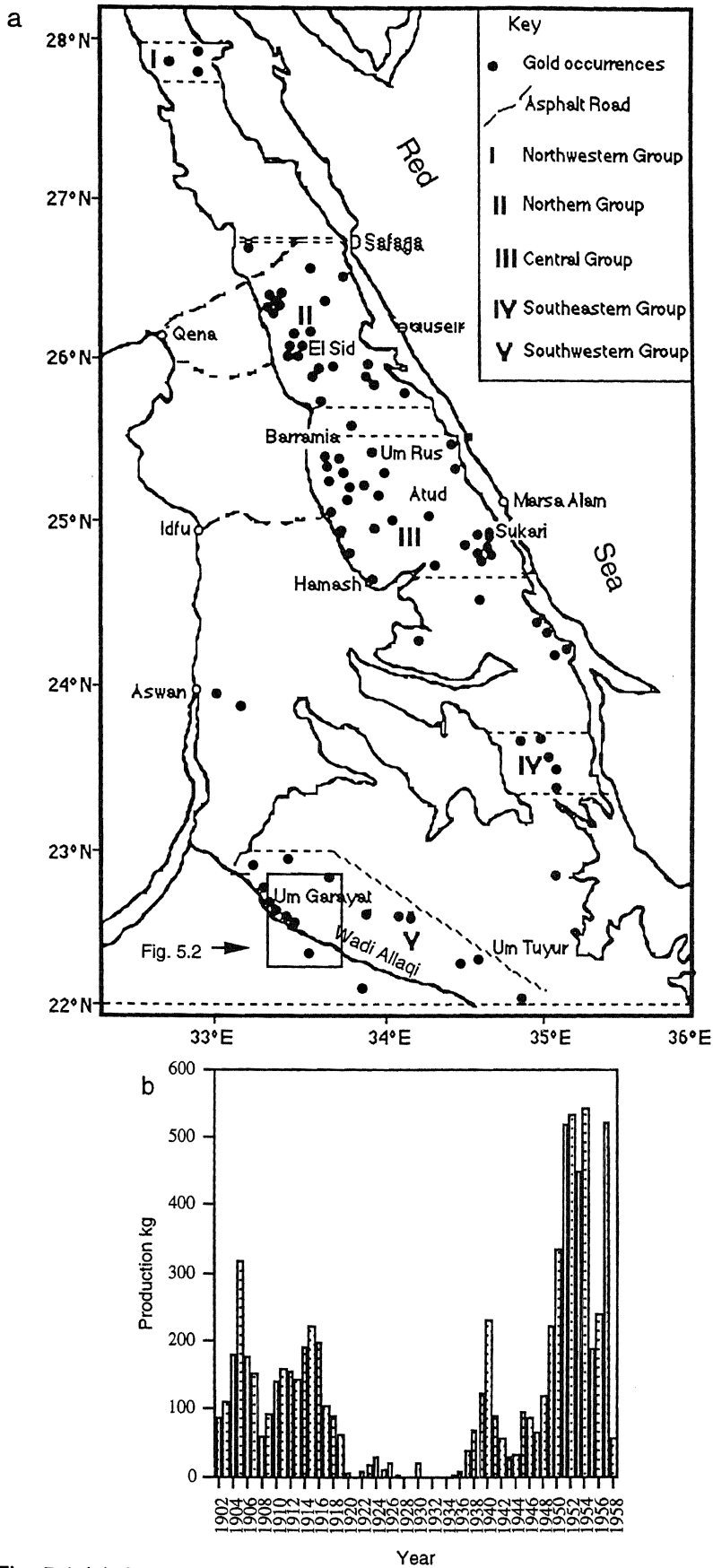


Fig. 5.1 (a) Gold occurrences in the Eastern Desert
 (b) Production from 1902 to 1958 in the Eastern Desert (after El Ramly *et al.* 1970)

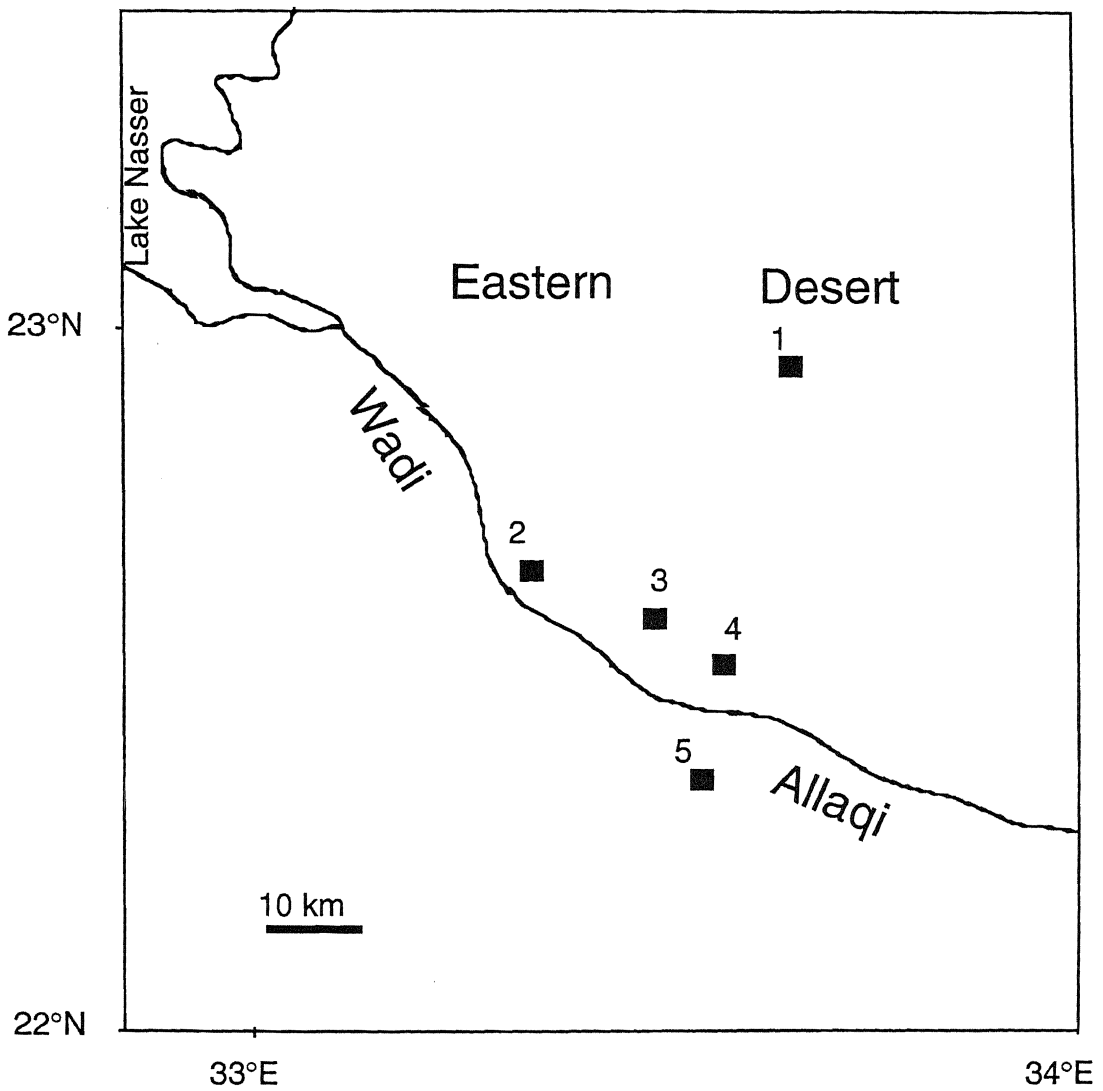


Fig. 5.2 Wadi Allaqi mineralized occurrences and former mines
 1- Nagib, 2- Um Garayat gold mine, 3- Atshani pit;
 4- Allaqi Shear-zone, 5- Um Geir

- 1) document the mode of occurrence of the deposits,
- 2) understand the geological processes which may have controlled the development of the gold-bearing veins,
- 3) obtain data on the temperature of trapping of the fluids and the likely sources of the fluids associated with the gold mineralization,
- 4) produce a model for the formation of the deposits.

The following techniques were used to achieve these objectives:

- a) remotely-sensed aerial photographs and ground structural geology,
- b) gold geochemistry,
- c) vein / gangue and wall-rock petrography,
- d) fluid inclusions,
- e) stable isotopes.

5.3 Structural setting

Preliminary investigations using remote-sensed images (Fig. 5.3) with ground control showed that potential mineralized areas in central Wadi Allaqi were only associated with the ubiquitous shear-zones. On the ground (Fig. 5.4) the mineralized zones are several metres wide showing distinct alteration zones, up to 5m in width, either side of white and smoky quartz veins. Volcanic rocks of every type are the only hosts although a prominent mineralized vein set occurs within the associated volcanoclastic enclaves rock of the Atshani Granite (Figs. 5.4, 5.6) and mineralized quartz veins are not found in the Um Relan, Kilkobob and Filat Granites. The veins vary in thickness from a few centimetres to over a metre (Fig. 5.4), crop out over several tens of metres (GR 5560191798), and the spatial and temporal structural relationships indicate that they have developed synchronously with the D1 structures (see Chapter 2).

The veins can be demonstrated as part of a brittle-ductile shear sequence. The kinematics and sequence of emplacement of the quartz-veins within the

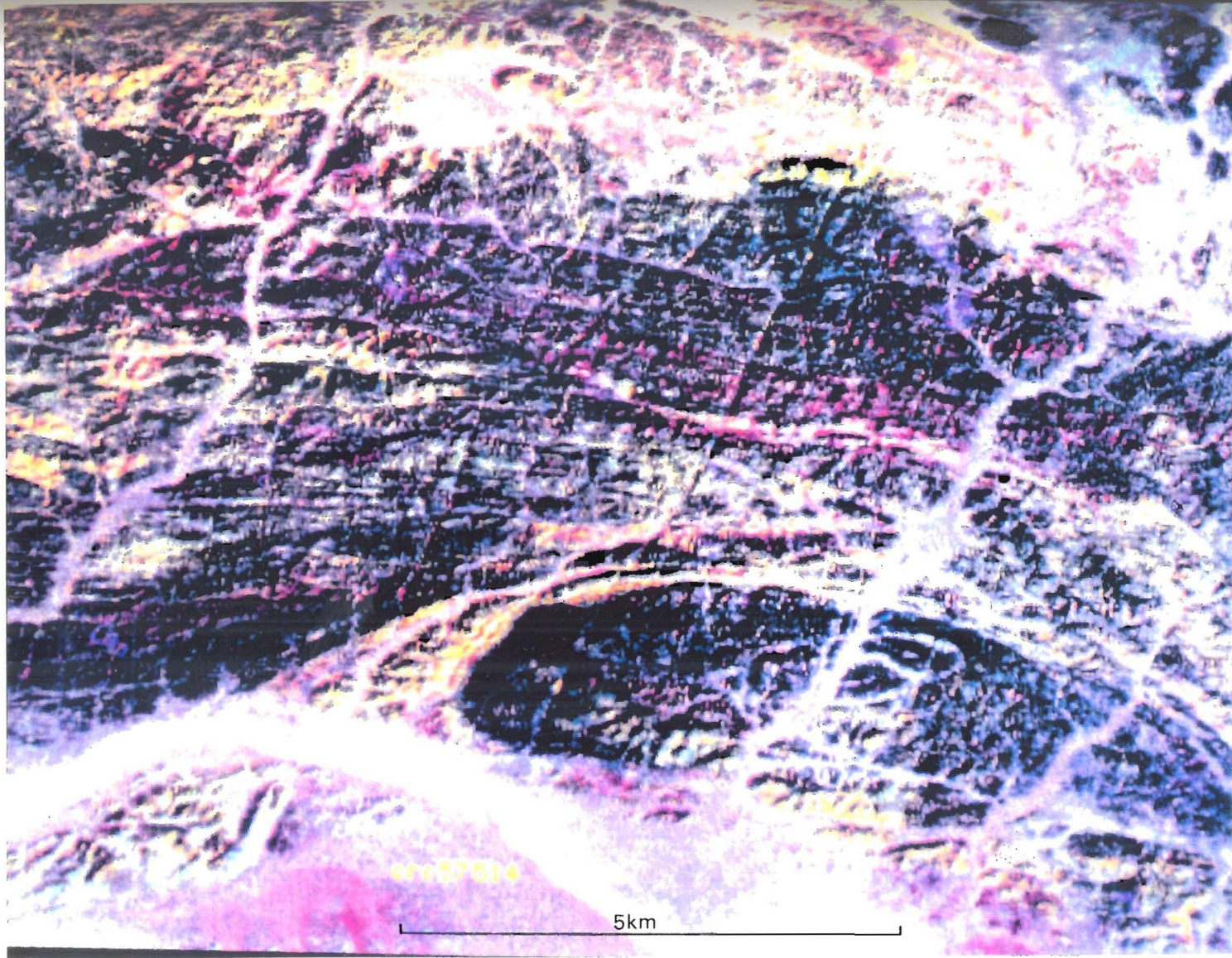
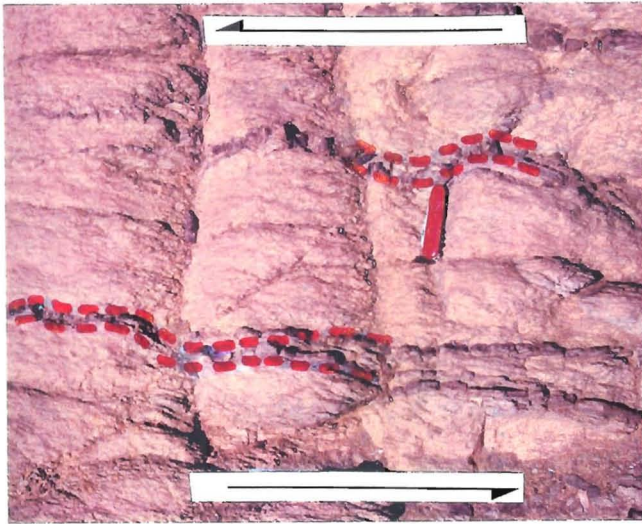
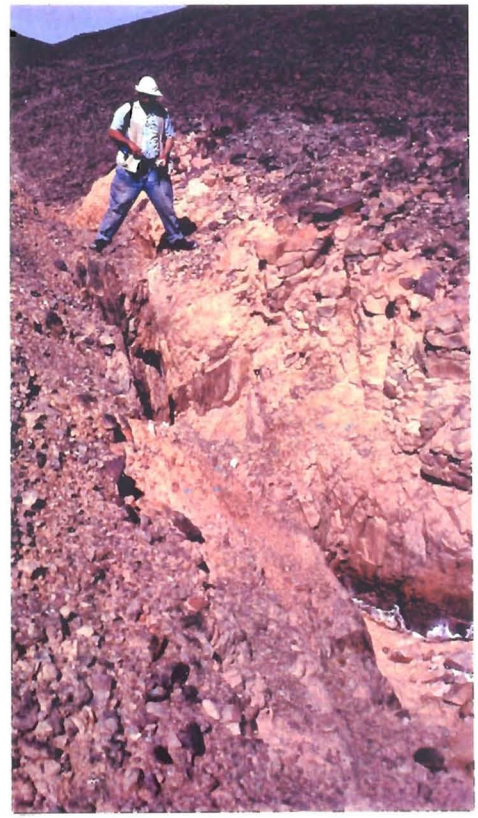


Fig. 5.3 T-M imagery of the central part of the area (see Fig. 2.1) showing the shear-zones and possible mineralized zones in yellow



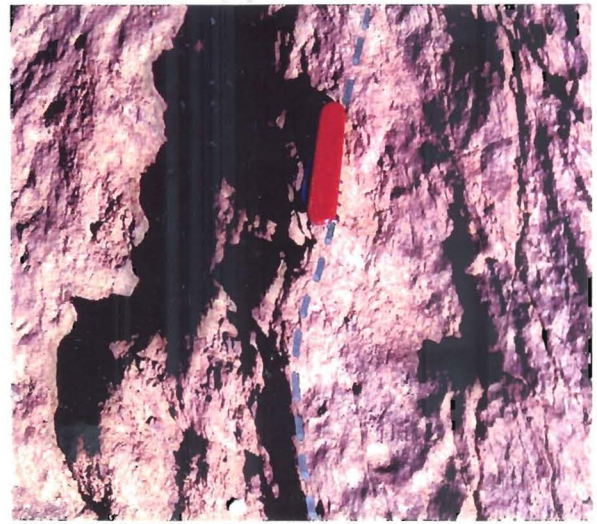
a



b



c



d

Fig. 5.4 Field relations of mineralized zones

(a) quartz veinlets showing a sinistral sense of shear and oblique-foliation (compare Fig. 5.5b; GR 7847378762)

(b) mineralized vein within a shear-zone of a volcaniclastic enclave within the Atshani Granite (Fig. 5.6; GR 5560191798)

(c) junction of mineralized zone (right) within Kazzaz Formation (viewing to the north-west; GR 7774673698)

(d) close up of the junction on the north-east side of locality (c)

shear-zones are shown schematically in text-figure 5.5. The S1 foliation in the outer part of the mineralization zones is subparallel to the shear walls and material forms in narrow open spaces gradually created by shearing movements along undulating and irregular foliation planes in the central part of the shear-zones. Early sigmoidal veinlets developed in the shear-zones in the more competent rock types. These fractures dilated sinistrally and filled with quartz veinlets becoming folded or boudinaged during the infinitesimal strain stages of D1.

5.4 Gold geochemistry

Hume (1937) reported auriferous veins from the Eastern Desert of a thickness up to 15m in which gold-rich pockets, with a gold content ranging from 7.75-15.5 g/t and average values of 12.9 g/t, were separated by low-grade to barren quartz. The ratio of silver to gold was given as 1: 6.5.

In the central Wadi Allaqi gold occurrences are restricted to the quartz veins and immediately adjacent wall-rock alteration zones. ICP-MS analyses of a carefully selected variety of thirty-nine potential gold host-rocks (twenty two samples from wall rock alteration and seventeen from quartz veins) have been carried out (Appendix B). Six samples were gold bearing-quartz (Fig. 5.7) vein and one samples from wall rock alteration gave a range of gold values from 0.07g/t to 6.98 g/t .

5.5 Petrography of the mineralized zones

The quartz veins are composed mainly of strained quartz, pyrite and chlorite (Fig. 5.8a,b,d,f) with minor amounts of ankerite. Gold minerals (Fig. 5.7a) were difficult to isolate. Where native gold has been found (*e.g.*, Atshani, GR. 6165385687) it occurs in the quartz veins, associated with chlorite and other phyllosilicates which have been formed during the D1 phase, and occasionally attached to pyrite. Two phases of pyrite growth have been recognised (Fig. 5.10b) but gold grains have only been

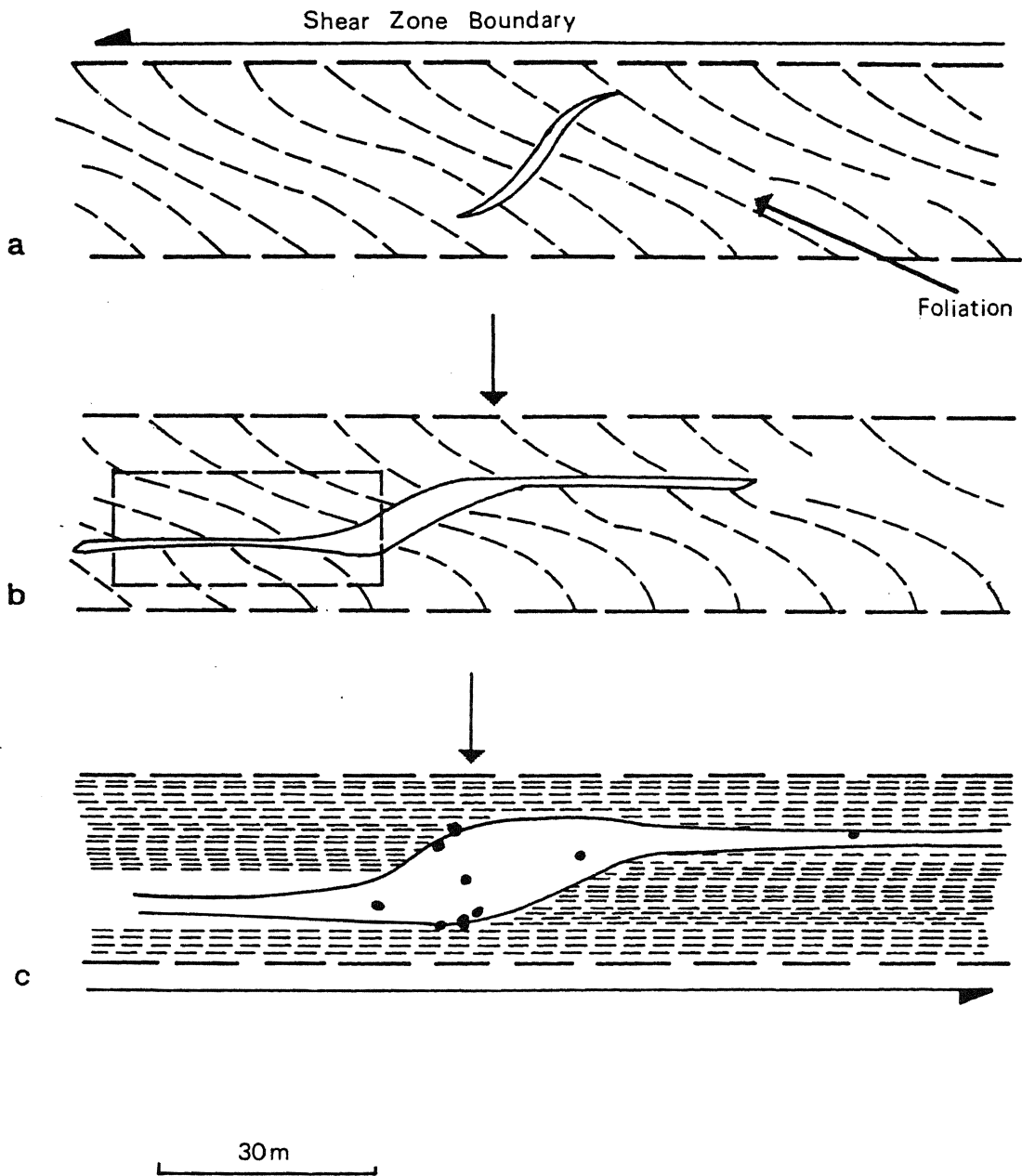
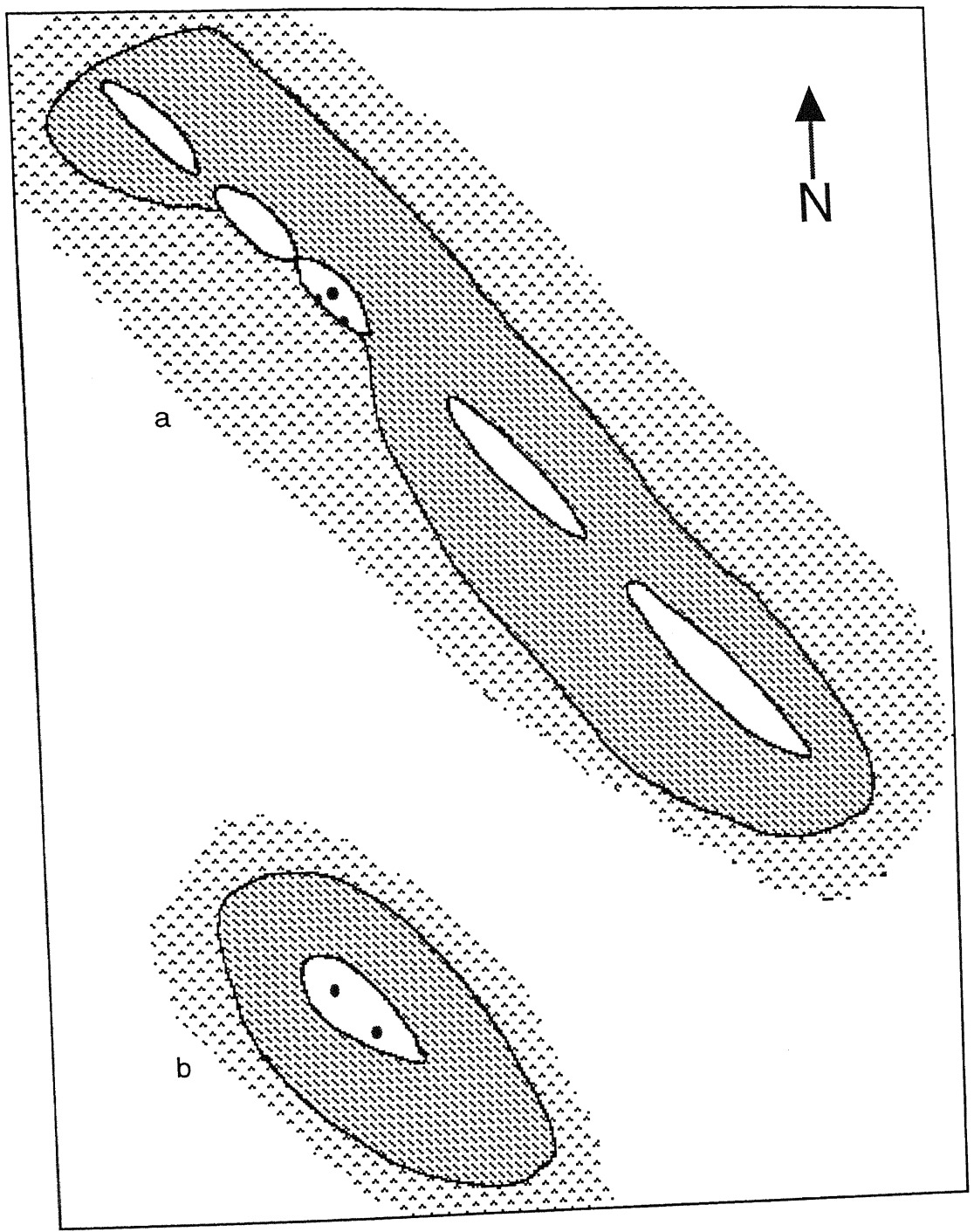
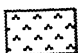
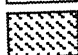
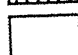


Fig. 5.5 Schematic development of mineralization in the vein systems
 (a) subhorizontal fractures developed between the ductile shear-zone in more competent rocks,
 (b) increment of sinistral oblique opening fractures (outlined area is comparable to Fig. 5.4a),
 (c) increment increased, black spots mark likely gold precipitation zone



Key

-  Atshani Granite
-  Volcanic rocks
-  mineralized quartz veins

3m

Fig. 5.6 Mineralization at Atshani Occurrences
 (a) Atshani north gold bit (GR 5560191798)
 (b) Atshani south gold pit (GR 5548491507)
 Gold mineralization localities represented by black as terisks

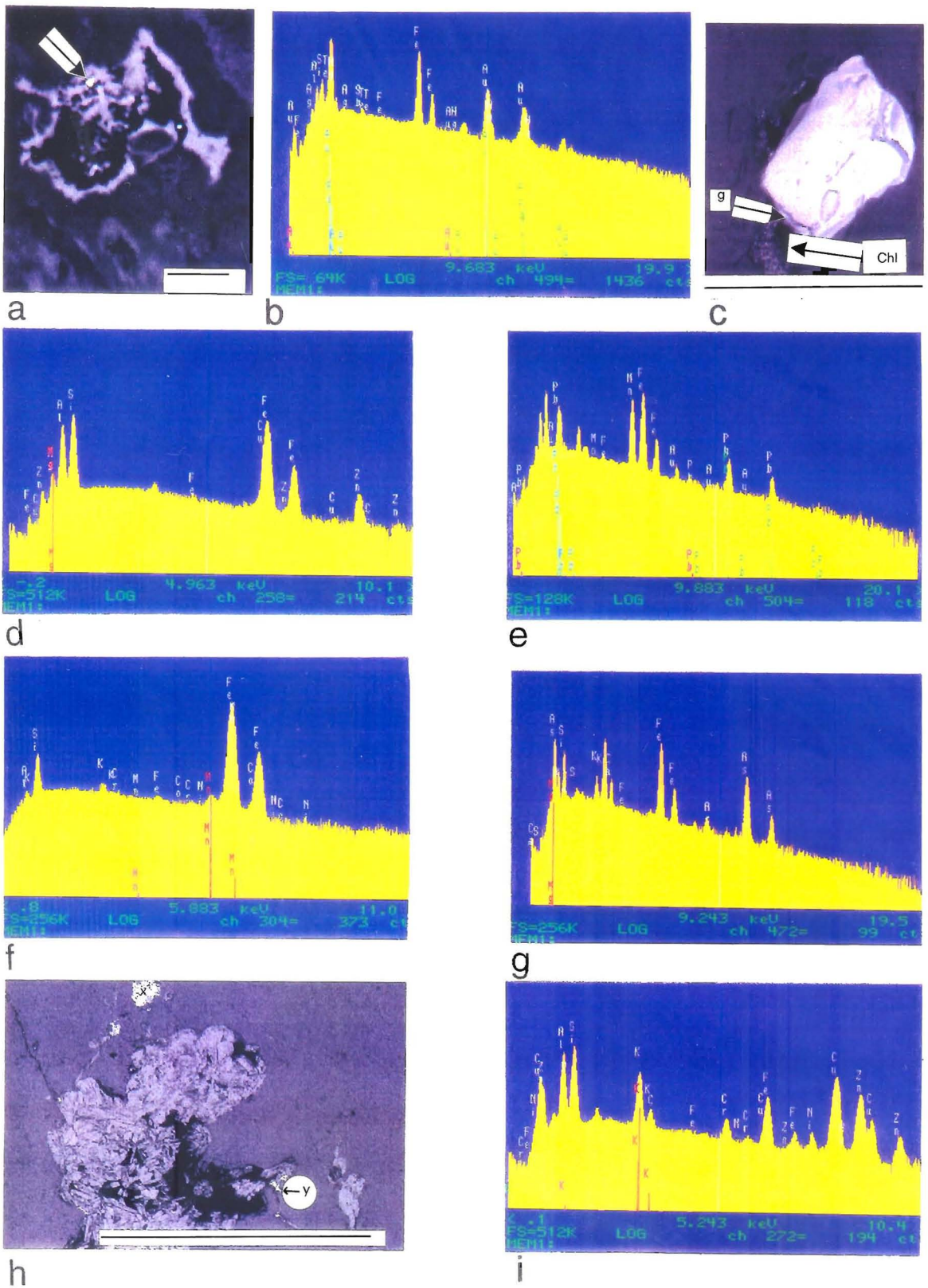


Fig. 5.7 Early mineralization petrography

- (a) backscatter SEM image showing gold (g) located with chlorite (chl) set in an inclusion within quartz indicating gold formed during D1 under low-grade metamorphic conditions, Atshani gold-bearing quartz veins (GR 5560191798; scale bar 10 μ m)
- (b) analytical spectrum of the gold grain seen in a)
- (c) pyrite (py), with a piece of gold (g) attached adjacent to an early-formed chlorite indicating that pyrite and gold formed together, Um Garayat gold mine (for location see Fig. 5.2; scale bar 100 μ m)
- (d) analytical spectrum of the chlorite adjacent to pyrite grain in (c) containing an unusual amount of Zn
- (e) analytical spectrum obtained from the gold particle in (c). Note the interference by the adjacent minerals which are relatively, rich in Mn, Fe and Pb.
- (f) analytical spectrum of mineral X in (h) indicating an iron-rich phyllosilicate (?chlorite)
- (g) analytical spectrum of mineral Y in (h) indicating an Fe-As-Ca rich phyllosilicate (?chlorite)
- (h) backscatter SEM image of a chlorite aggregate; note highly reflectant associated minerals (f) and (g), Nagib gold-bearing quartz vein (for location see Fig. 5.2; scale bar 0.5 mm)
- (i) analytical spectrum of the central mass of chlorite Z in (h); note high Cu, Cr, Zn and Fe values with some Ni.

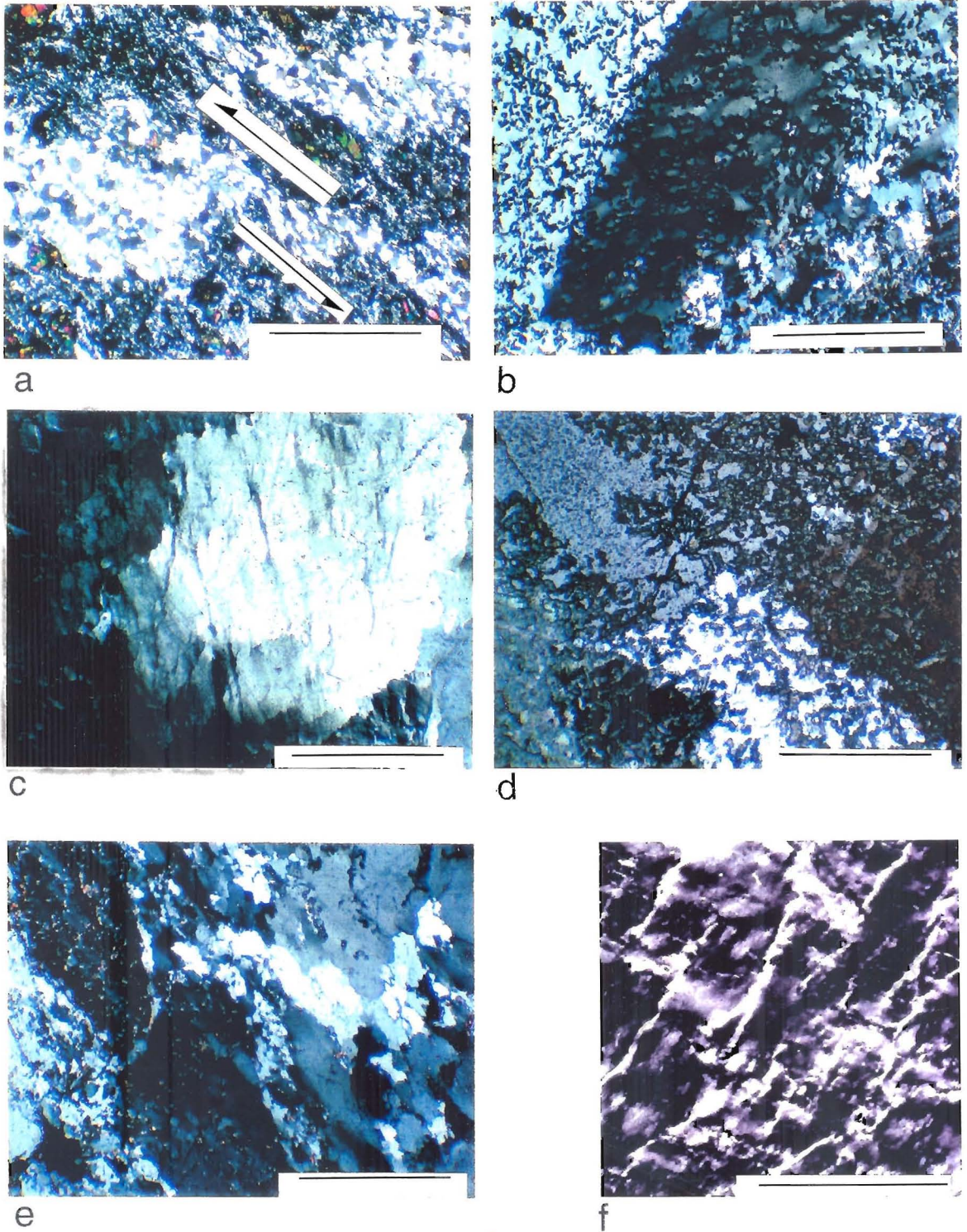
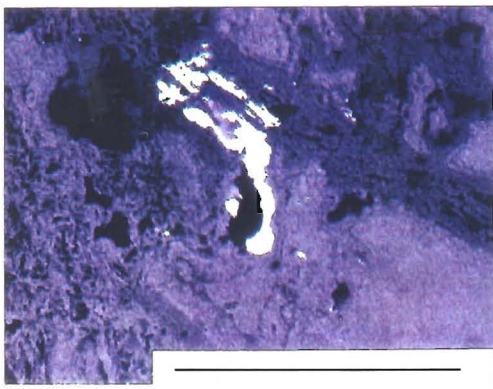


Fig. 5.8 Quartz fabrics in quartz-veins formed during the early mineralization
 (a) quartz vein set in phyllite and formed during the D1 phase indicating sinistral sense of shear, Filat Succession (cross polarized light; GR 5301193050; scale bar 1 mm, see Fig. 5.5 for formation of vein system and Shelley 1993 sections 5.3.4, 5)
 (b) D1 strained quartz, chlorite and sericite, Atshani gold-bearing quartz-vein (cross-polarized light; GR 5560191798; scale bar 1 mm)
 (c) D1 highly-strained quartz, Um Garayat gold-bearing quartz-vein (cross polarized light; for location see Fig. 5.2; scale bar 0.5 mm)
 (d) D1 strained quartz, chlorite and sericite, Atshani gold-bearing quartz-vein (cross-polarized light; GR 5548491507; scale bar 1 mm)
 (e) deformed quartz, chlorite, biotite and sericite, Nagib gold-bearing quartz-vein (cross-polarized light; for location see Fig. 5.2; scale bar 1 mm)
 (f) D1 highly-strained quartz vein, Nagib-gold bearing quartz-vein (cross-polarized light; for location see Fig. 5.2; scale bar 0.5 mm)

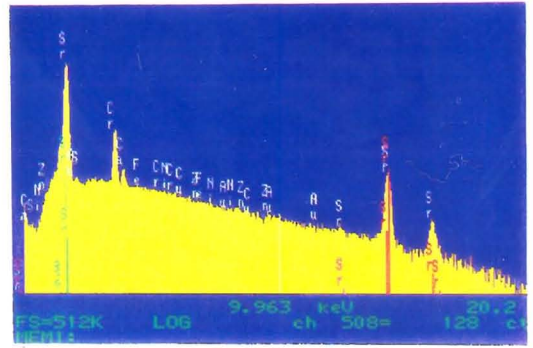
distinguished in the earlier phase. The earlier pyrites occur as anhedral small grains which are aligned parallel to S1. Pyrites of the later phase (Fig. 5.10b,c,d,e,f & h) are generally euhedral, cut S1 and only show evidence of brittle deformation (Fig. 5.10h) typical of the later stages of the deformation history (*i.e.*, D3, D4 and D5, see Chapter 2). Microprobe analyses indicate that the earlier-formed pyrite is associated with phyllosilicate minerals, which have unexpectedly high amounts of copper, chromium, iron, lead, nickel, and zinc (Fig. 5.7), and rare iron- and calcium-rich arsenate minerals (Fig. 5.7g). The ICP-MS chemical analyses revealed the presence of some unusual mercury compounds within the samples of both quartz veins and the wall-rock which may be associated with these latter minerals, but individual mercury minerals have not been identified

Evidence for a third, and latest, phase of mineralization (Fig. 5.9) has been distinguished by the alteration of pyrite to goethite (Fig. 5.9c,e) with the formation of minor amounts of xenotime and monazite (Fig. 5.9a,b,c,e,f). The formation of the latter minerals suggests alteration under weathering or diagenetic conditions (Deer *et al.* 1962, pp 200, 339).

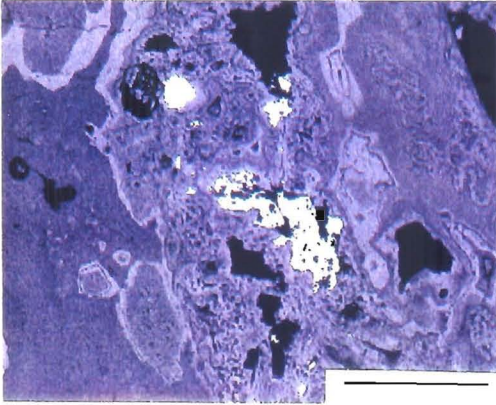
In the zone of wall-rock alteration in the volcanoclastic enclaves of the Atshani Granite (GR 5560191798, GR 5548491507), plagioclase is altered to epidote and sericite (Fig. 5.10a), and biotite to chlorite. In other mineralized zones, the wall-rock alteration shows similar mineral changes with the predominant production of calcite, epidote and chlorite as the quartz vein is approached. Carbonatization is marked in its initial stages by disseminated fine-grained calcite in the matrix of the volcanoclastic wall-rock which are commonly disposed along or wrapped around by the S1 foliation planes. Sericitization and chloritization is co-eval with this process. Fine-grained white mica replaces plagioclase feldspar (Fig. 5.10a) and chlorite forms from the alteration of relict Fe-Mg minerals (*e.g.*, biotite; Fig. 5.10f)



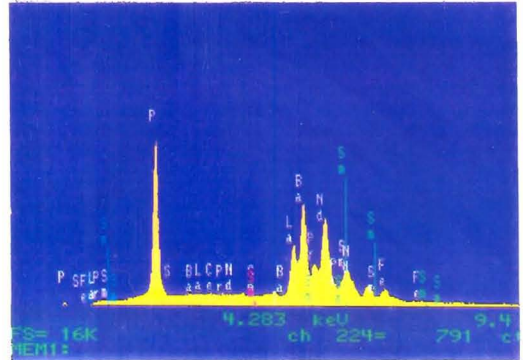
a



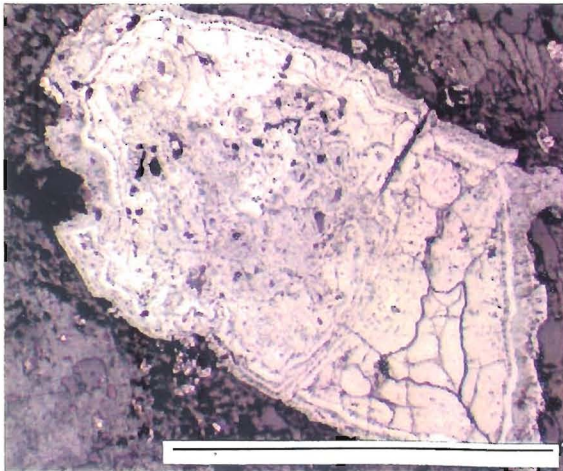
b



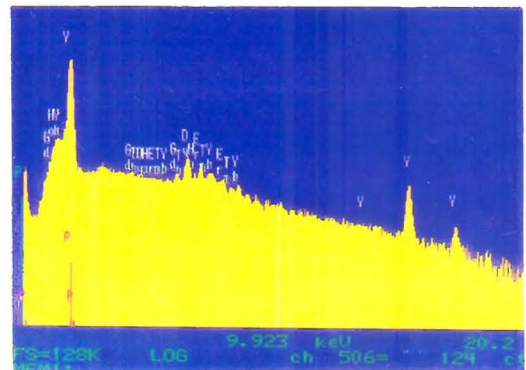
c



d



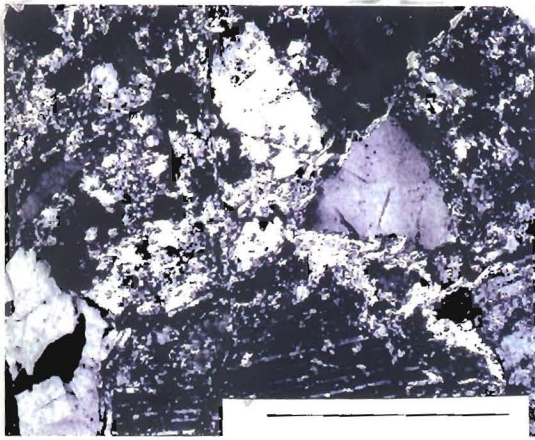
e



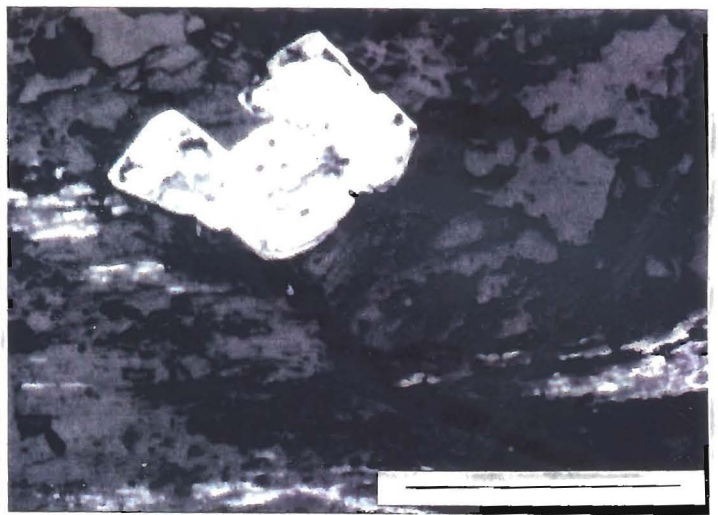
f

Fig. 5.9 Petrography of the residual / diagenetic phase

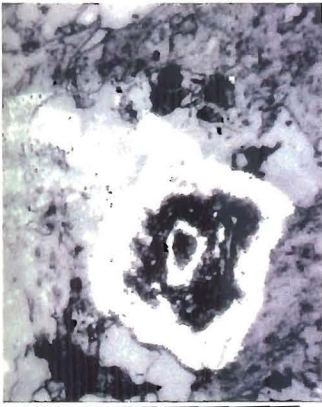
- (a) backscatter SEM image of monazite and celestine within altered pyrite and formed under residual diagenetic processes, Atshani gold-bearing quartz-vein (GR 5560191798; scale bar 100 μ m)
- (b) analytical spectrum of celestine in (a)
- (c) backscatter SEM image of xenotime formed within pyrite altered to goethite, Atshani gold-bearing quartz-vein (GR 5560191798; scale bar 100 μ m)
- (d) analytical spectrum of monazite in (a)
- (e) goethite formed as residual alteration of pyrite, Atshani wall rock alteration (reflected light; GR 5560391800; scale bar 1 mm)
- (f) analytical spectrum of xenotime in (c)



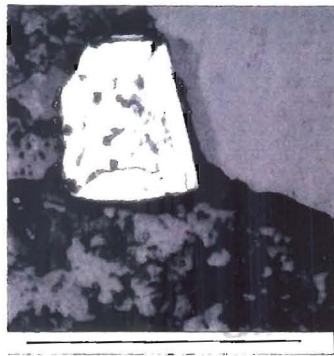
a



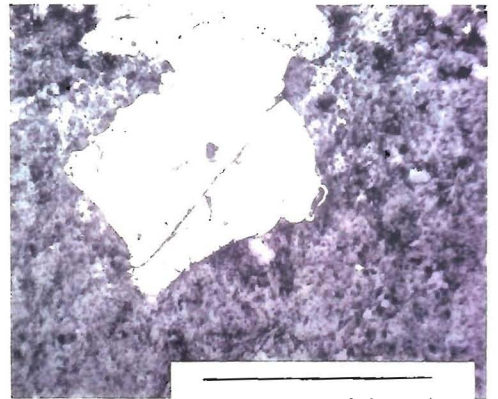
b



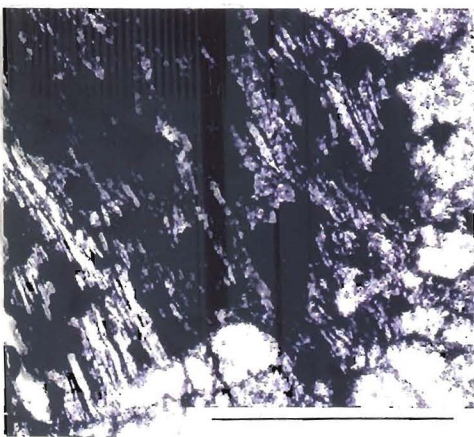
c



d



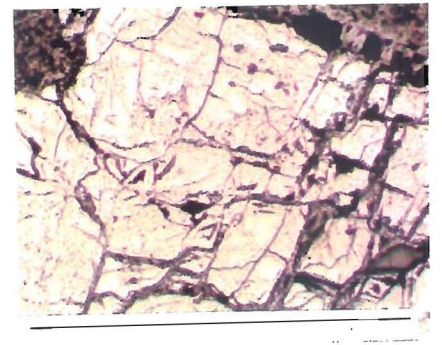
e



f



g



h

Fig. 5.10 Wall rock petrography

- (a) deformed sericitized plagioclase and granulated quartz during D1 phase altered to sericite, Atshani volcanoclastic enclave (cross polarized light; GR 5560191798; scale bar 0.5 mm)
- (b) early pyrite affected by ductile stretching parallel to S1 within chlorite and the later euhedral pyrite affected by brittle deformation, Atshani volcanoclastic enclave (reflected light; GR 5560191798; scale bar 0.25 mm)
- (c) late subhedral pyrite showing zonal alteration to late goethite mineral Atshani volcanoclastic wall rock alteration (reflected light; GR 5548491507; scale bar 0.25 mm)
- (d) late euhedral pyrite, Atshani volcanoclastic enclave (reflected light; GR 5560091798; scale bar 0.25 mm)
- (e) late pyrite crystal affected by D5 brittle deformation, Atshani volcanoclastic wall rock alteration (reflected light; GR 6165385687; scale bar 0.5 mm)
- (f) chlorite formed from the alteration of relict biotite and goethite opaque developed within chloritized biotite and cross-cutting the cleavage, Nagib volcanoclastic enclave (cross-polarized light; for location see Fig. 5.2; scale bar 0.5 mm)
- (g) deformed early pyrite parallel to chloritized biotite (S1) affected by D1 deformation, Nagib volcanoclastic rock (cross-polarized light; for location see Fig. 5.2; scale bar 0.5 mm)
- (h) residual/diagenetic goethite replacing late pyrite, Middle Volcanoclastic Formation (reflected light; GR 6133385775; scale bar 1 mm)

during the greenschist metamorphism. Both types of pyrite are recognised in the wall-rock alteration zones (Fig. 5.10b,c,d,e,f,g).

5.6 Fluid inclusions

Fluid inclusions occur in the quartz and calcite of both the veins and the wall-rocks but this preliminary study has concentrated upon the abundant primary types in the quartz of the quartz veins. The intention of this study was to deduce evidence for the nature of the ore-forming fluids and their conditions of formation. Data was obtained from mainly mineralized samples (Appendix A) although a study of a limited number of non-mineralized samples, for comparative purposes, gave identical results.

The external shapes of the primary inclusions (Fig. 5.11a,b,c) show a great variety. Oblate, cylindrical, negative cubic and irregular forms are common and most occur isolated. Secondary inclusions are generally aligned along conjugate fractures associated with D4 structures (Fig. 5.11d). All types of inclusions are relatively small (diameters $<15\ \mu\text{m}$) but the secondary inclusions are particularly minute.

Using the criteria of Roedder (1984), and on the basis of petrography and fill types, five main types of primary inclusions have been distinguished (Table 5.1). Subdivision of types 1, 2 and 3 were mainly based on the proportion of the different H_2O and CO_2 phases. Type 4 are two phase liquid dominated aqueous inclusions always associated with chlorite which is a syn-D1 formed mineral. Type 5 have fills of immiscible, heterogeneous fluids composed of three phases, *viz.* aqueous solution (L_1), liquid CO_2 (L_2) and CO_2 vapour (V).

Microthermometric measurements were made only on the primary inclusions since the small size of the secondary inclusions precluded such analyses. The data is summarised in Appendix E and Plots of the data for

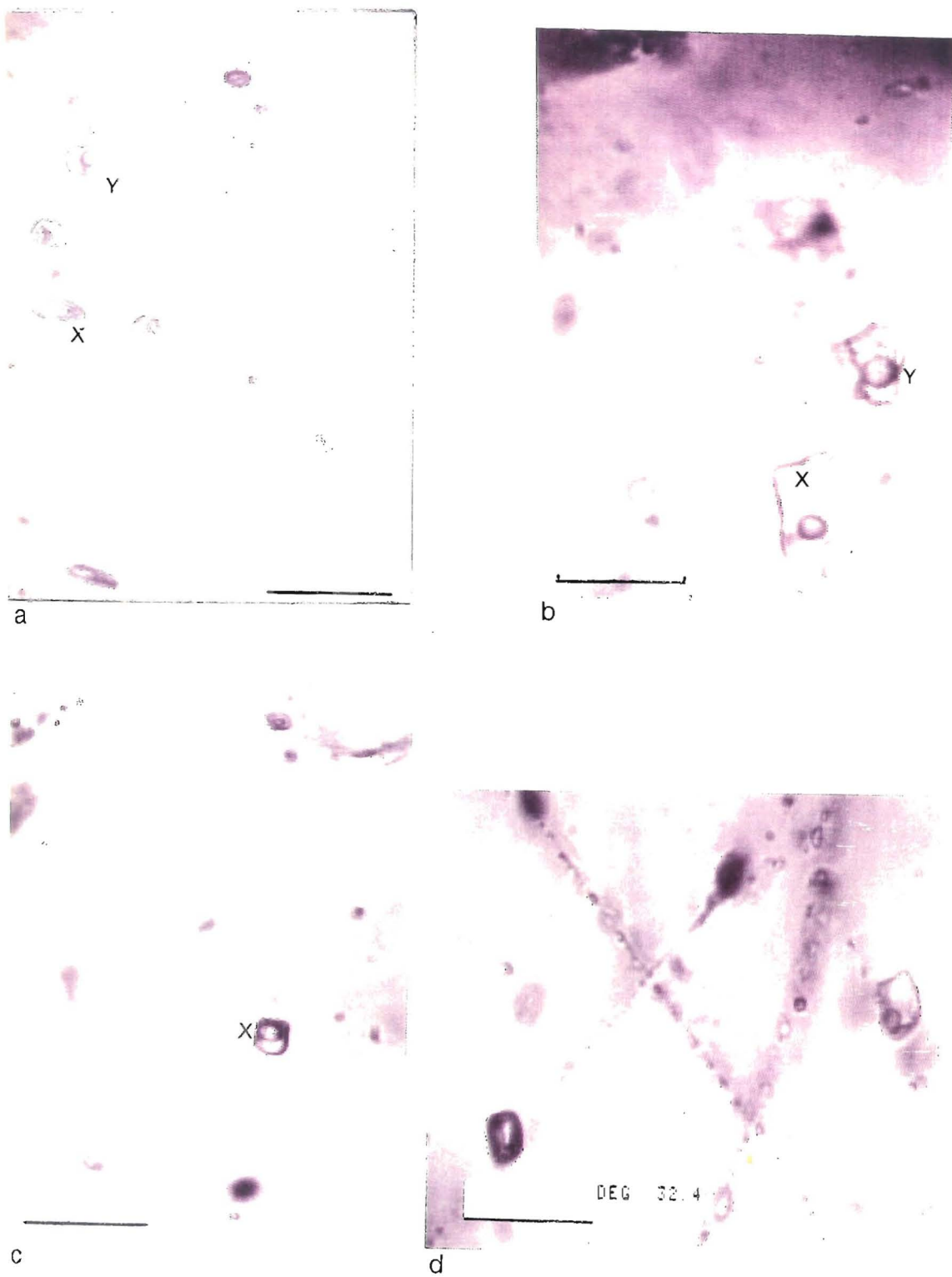


Fig. 5.11 Photomicrographs of fluid inclusion types (bar scale=15 µm)






(a) oblate type 1 inclusions (x) and type 2 inclusions (y) containing aqueous solution (H_2O) and vapour (CO_2), Atshani gold bearing-quartz vein (GR 5560191798)

(b) irregular type 3 inclusions (x) and type 4 inclusions (y) containing two phase aqueous solution (H_2O) and vapour (CO_2). Type 4 is associated with chlorite (dark), quartz vein in Filat Succession; (GR 5979182137)

(c) equant type 5 inclusions (x) containing heterogeneous immiscible inclusions fluids and three phases : water or aqueous solution (H_2O ; L_1), liquid (CO_2 ; L_2) and (CO_2) vapour (V), Atshani gold bearing-quartz vein (GR 5560191798)

(d) secondary inclusions parallel to D3 fractures, Atshani gold bearing-quartz vein (GR 5560191798)

Table 5.1 Fluid inclusion types

Type	Inclusion type	Proportion of phase	Form
1	Vapour (V)-rich two phases	V = 80 % L = 20 %	
2	Liquid (L)-rich two phases	L = 70 % V = 30 %	
3	Liquid (L)-rich two phases	L = 60-50 % V = 40-50 %	
4	Liquid (L)-rich two phases associated with chlorite	L = 70 % V = 30 %	
5	Immiscible aqueous liquid, gas liquid and vapour gas	L = 75 % V = 25 %	

homogenization temperatures (T_H) of the inclusions (Fig. 5.12) showed four main concentrations; type 1 about 29°C, types 2 and 3 about 100°C, type 5 about 165°C, and type 4 about 180°C. Freezing data for type 2 and 4 inclusions indicate that the salinity is about 25 wt % equivalent NaCl. For the fluids in type 5 inclusions, the melting temperatures (T_m) were -3 ± 1 °C and the freezing temperatures (T_e) were -22 ± 2 °C which are close to pure CO₂.

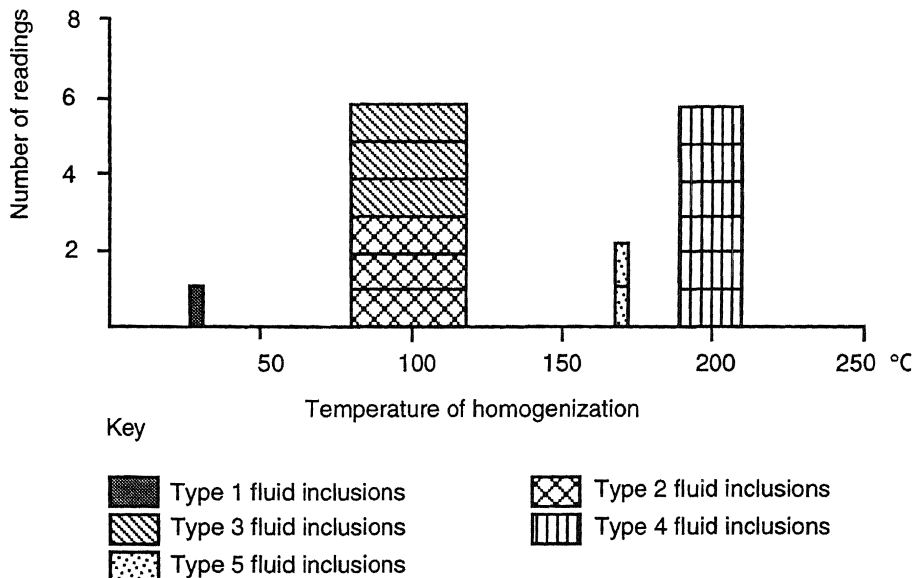


Fig. 5.12 Homogenization temperatures of fluid inclusions for gold-bearing and barren quartz vein. The width of each column is related to the uncertainty of the data

Taking into account pressure estimates of about 2 Kbar (see Chapter 2) this would yield tentative trapping temperatures (T_t) of approximately 320°C for type 4 inclusions and 280 °C for type 5 inclusions (Shepherd *et al.* 1985 pp155-165; Barker 1990 pp151). It is more difficult to ascertain the trapping temperatures for types 1, 2, and 3 since there was a great variation in T_m and T_e and this aspect is worthy of a more detailed study.

5.7 Stable isotopes

The oxygen and hydrogen stable isotopes, from carefully selected samples of pure vein quartz which clearly demonstrated the early mineralization, were investigated in order to distinguish a likely source for the initial mineralizing fluids. Six samples were gold-bearing, contained chlorite, which was formed during the D1 phase of deformation, and type 4 fluid inclusions were predominant. A further four barren samples, two from known gold deposits, but which had similar specifications were selected for comparison. The samples were prepared at Luton University and the analyses were carried out by Dr. Fallick at the Scottish Universities Research and Reactor Centre at East Kilbride. Standard methodology was followed and the data are given in full in Appendix F. For one gold-bearing sample (399) three attempted runs to determine the $\delta^{18}\text{O}$ gave yields of 10.8 to 11.3 instead of the theoretical $16.7 \mu \text{ moles mg}^{-1}$ and so are not included within the data set. Moreover these samples did not behave as expected for isotopically homogeneous pure silica, in particular the oxygen yields were consistently low. This behaviour could not be explained by the presence of any impurities in the system. The yields in the determination for δD are not typical for fluid inclusions in quartz. But in sample 601 about 70% of the $11 \mu \text{ moles H}_2$ was released as H_2 and not H_2O . This is highly unusual although appreciable H_2 release sometime occurs in iron-bearing minerals because of the reduction of H_2O during release (Dr Fallick, written communication). However because the samples are very pure quartz the meaning of this is not clear. For these reasons the data must be treated with some caution.

Plots of the data of oxygen and hydrogen isotopes (Fig. 5.13) show that there is an overlap of $\delta^{18}\text{O}$ values for gold-bearing and barren quartz-veins. Both the δD and $\delta^{18}\text{O}$ data lie within the ranges which have been reported (Sheppard *et al.*, 1969; Taylor 1974; Sheppard 1981) from waters in the metamorphic field but close to the magmatic field. Meteoric and epithermal

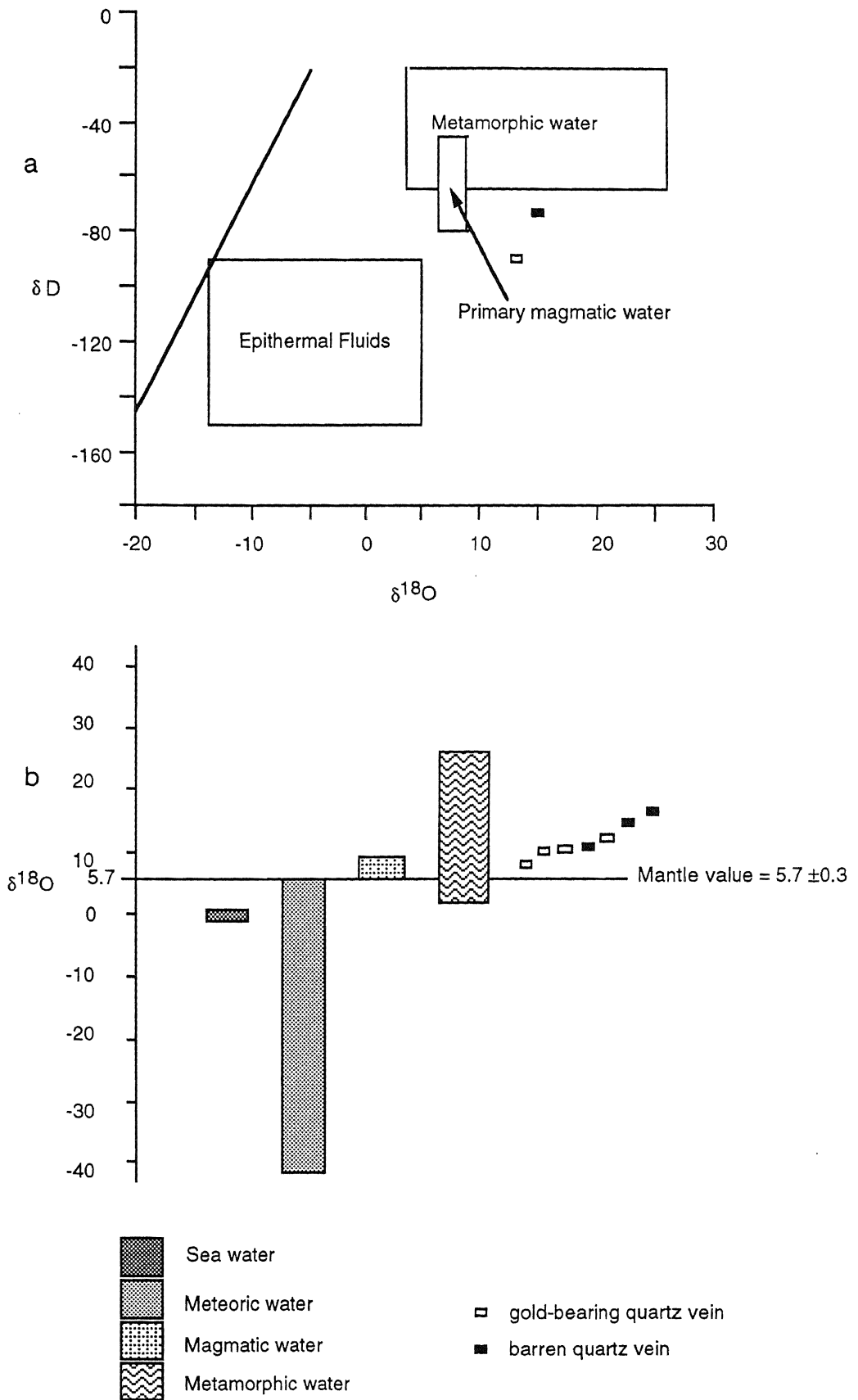


Fig. 5.13 (a) Oxygen and hydrogen stable isotope data for quartz vein (after Xavier 1991)
 (b) Comparison of $\delta^{18}\text{O}$ with the compiled data by Rollinson (1993)

waters show a much wider range of δD and $\delta^{18}O$ values (Fig. 5.13) due mainly to variations in altitude and time (Epstein *et al.* 1970).

The attempt to use analyses of the ^{18}O and D isotopes in the quartz-vein material does not provide a definitive identification of the source of the respective elements since the evidence from the study of the fluid inclusions has indicated that complex mixing of fluids is highly likely. On balance the original source of the ore-forming fluids was probably derived from metamorphic water during the formation of the D1 shear-zones.

5.8 Paragenesis

The evidence from above analyses has enabled a sequence of the timing of the mineralization events relative to the deformation, metamorphic and intrusive events to be established (Fig. 5.14). Gold-pyrite mineralization occurs, in quartz veins associated with relatively narrow zones of wall-rock alteration, as a single event related to the D1 deformation accompanying greenschist facies metamorphism and before the emplacement of the granitic intrusions. At a later stage formation of euhedral pyrite with little or no gold content is restricted to the wall-rocks. During the last stage pyrite, of both the wall-rocks and the quartz veins, is transformed to goethite with a range of minerals normally associated with residual or diagenetic deposits.

Presently there are two schools of thought regarding the origin of Precambrian lode gold deposits, one favouring a metamorphic origin and the other favouring a Mantle origin. Kerrich & Fyfe (1988) have shown, by isotopic studies of an Archaean greenstone belt in Canada, an important genetic link between mineralization and metamorphism of shear-zones which indicates that mineralizing fluids may have a metamorphic source. Others (notably Groves *et al.* 1988) using a $\delta^{13}C$ tracer confirmed this conclusion and added that the CO_2 in the gold-bearing fluids was metamorphic in origin although in some instances could have been

Minerals	Early mineralization event	Late mineralization event	Residual/Diagenetic event		
gold	██████████				
pyrite	██████████	██████████			
goethite		██████████	██████████		
quartz	██████████				
chlorite	██████████	██████████			
biotite	██████████				
monazite			██████████		
xenotime			██████████		
celestine			██████████		
Structural Phases	D1	D2	D3	D4	D5

Fig. 5.14 Summary of the mineralization history in the central Wadi Allaqi

reworked during metamorphism from an original Mantle source. Fluids in shear-zones were most likely generated by tectonic dewatering and metamorphic dehydration reactions (e.g. Phillips & Groves 1983; Foster 1985; Groves & Phillips 1987; Groves & Foster 1991) because of the strong relationships between deformational mechanisms and metamorphic reactions (Stel 1986). Many fluid inclusions, in the samples from central Wadi Allaqi, show a wide range in the molar ratio of CO₂:H₂O that is thought to reflect unmixing of an original CO₂-H₂O fluid to form low immiscible phases as a result of pressure decrease in the vein system during mineralization (cf. Wood *et al.* 1986). Unmixing (or boiling) of fluids carrying CO₂ can play an important factor in metal deposition (Robert & Kelly 1987; Walsh *et al.* 1988; Shelton *et al.* 1988) and also causes important changes in fluid chemistry (Murphy 1989) during metamorphism (Groves *et al.* 1988). The mineral deposits associated with shear-zones depend on the relative predominance of brittle and ductile behaviour. Fluids are commonly focused along shear-zones resulting in high concentration in the brittle-ductile transition zone but sparse dissemination within the adjacent wallrock. These conditions are favoured by low temperatures and, probably localised, high pressures (Murphy 1989). Alternating episodes of brittle and ductile behaviour are likely in this tectonic environment since the fluids are derived from the site of metamorphic reactions and subsequently removed (Stel 1986; Sibson *et al.* 1988). Excess fluid pressures may activate or re-activate weaknesses (Sibson *et al.* 1988) and allow fluids to escape.

The general form of the mineralization in central Wadi Allaqi bears a close resemblance to the gold-vein mineralization recorded by Piroshco & Hodgson (1988) in Ontario where Precambrian mafic metavolcanic rocks form the wall-rocks and have been regionally metamorphosed to greenschist facies and also by Worku (1993), for the Adola belt, where the host rocks have been regionally metamorphosed to greenschist facies. If this

comparison is valid then it should be expected that the mineral assemblages grew under the influence of different CO₂ concentrations in the interstitial fluid during greenschist facies metamorphism. The mineral assemblage of the least altered facies would have had the lowest CO₂ concentration and the other assemblages grew in environments having successively higher CO₂ concentrations.

The genesis of the Egyptian Pan-African gold mineralization has been discussed by many geologists (*e.g.* Hume 1937, Amin 1955; El Shazly 1957; Sabet *et al.* 1976; Hilmy & Hussein 1978; Sabet & Bondonov 1984; Hussein 1990; Takla *et al.* 1990) all of whom favoured an epigenetic hydrothermal model with granitic intrusions providing the heat source. The preliminary data coupled with the structural evidence presented above indicates that this is an oversimplification of the paragenesis for the deposits. Mesozoic and Cenozoic epithermal geothermal systems in volcanic terranes (Henley & Ellis 1983; Henley 1991) are characterized by acidic to intermediate volcanic wall-rocks, intense and pervasive alteration haloes, and widespread presence of hydrothermal breccia (Grindley & Browne 1976; Browne 1978; Berger & Eiman 1983). Locally (*e.g.*, from Indonesia and Philippines; Simmons & Browne 1990; Van Leeuwen *et al.* 1990; Cooke & Bloom 1990) the wall-rocks of epithermal gold deposits are porphyritic and normally are unmetamorphosed (Buchanan 1981). Most of epithermal deposits have formed from alkaline chloride solutions (about 0.5 - 5 wt % NaCl; Vikre 1981). Henley (1991) has suggested that such deposits may exist in more ancient (even Precambrian) volcanoclastic rocks and have developed before deformation and metamorphism. None of the criteria indicated above fit the central Wadi Allaqi gold deposits which are restricted to relatively narrow shear-zones formed during the D1 phase close to the acme of greenschist facies metamorphism.

Recently Harraz & El Dahhar (1993) have obtained T_h values in the range of 250-300° C for fluid inclusions from gold-bearing quartz veins from the Um Rus gold mine of the central Eastern Desert (Fig. 5.1a) and have questioned the previous interpretations for the Egyptian gold deposits. The preliminary fluid inclusion, stable isotope, petrochemical, and structural data, presented above and in the preceding chapters, favour a metamorphic origin for the gold-quartz vein deposits of central Wadi Allaqi during the earliest tectonic deformation phase (D1) of the Pan-African orogeny. This interpretation is advanced with some caution because of the overall complexity of the duration and nature of both the probable mineralizing fluids which formed the gold mineralization and the associated tectonism.

5.9 Summary

The main features of the quartz vein gold deposits of central Wadi Allaqi may be summarized as follows:

- (a) *Tectonostratigraphic setting* : Quartz-veins restricted to ubiquitous D1 shear-zones and, within the Atshani Granite, preserved in the D1 shear-zones of volcanoclastic rock enclaves.
- (b) *Regional depositional environment* : The veins were formed along fractures in brittle-ductile shear-zones, the mineralizing fluids were released during deformation and metamorphism.
- (c) *Age range* : The host rocks of the veins are Neoproterozoic and mineralization commenced during the earliest deformation phase (D1) of the Pan-African orogeny.
- (d) *Host rocks.* : Exclusively volcanoclastic rocks .
- (e) *Associated rocks* : Granite intrusions are associated in space but not in time (Chapter 4).
- (f) *Ore mineralogy* : Pyrite, native gold (rarely); secondary alteration to goethite and other diagenetic minerals.

(g) *Gangue minerals* : Quartz, chlorite, sericite.

(h) *Structure* : Sigmoidal-shaped, gold-bearing quartz veins hosted within shear zones. The quartz in the veins shows varying intensities of strain and frequently stained with iron oxide. There are no open space structures.

(i) *Isotopic signatures* : Very complex. Data for O¹⁸ stable isotope gives a metamorphic water range and data for hydrogen (D) plots in an intermediate position between metamorphic and magmatic water.

(j) *Fluid inclusions* : Very complex, most fluids rich in varying amounts of CO₂ and the T_h ranges from 29°-165°C. Probably the initial fluids were metamorphic in origin since inclusions associated with chlorite gave T_h ranges from 170-195°C.

In conclusion a metamorphic rather than an epithermal origin is favoured for the formation of the gold-bearing quartz veins because :

(a) the host rocks are of Neoproterozoic volcanoclastic types in which epithermal type mineralization is unknown or rare;

(b) the host rocks are affected by low-grade greenschist facies metamorphism (*i.e.*, about 2 Kbar pressure and 350°C) and strong, complex deformation;

(c) the widespread vein system is part of the complex deformation history and is formed by an overall compression régime within brittle-ductile shear-zones containing metamorphic minerals (*i.e.*, chlorite and biotite);

(d) the vein system pre-dates the intrusion of the Atshani Granite which was emplaced as a stopped pluton into relatively cold country rocks and does not form mineralized haloes;

(e) petrographic data indicates that the gold is associated with complex phyllosilicates which were formed during an earlier metamorphic event coeval with the D1 deformation;

- (f) supporting data from both the fluid inclusion and oxygen and hydrogen stable isotope investigations indicate that the trapped fluids have a metamorphic affinity;
- (g) the composition of the trapped fluids are very complex and some are rich in CO₂ which is typical of metamorphic reactions in volcanoclastic rocks;
- (h) the typical pre-tectonic mineralization in a back-arc setting (chapter 3) would be polymetallic or kuroko type massive-base-metal deposits and would be concentrated in specific locations (*e.g.*, Okinawa Trough, Sakai *et al.* 1990) not as widespread veins along shears which have been formed during a distinct phase of deformation as in central Wadi Allaqi.

Chapter Six

Discussion and Conclusions

6.1 Broader considerations

The Pan-African Neoproterozoic supra-crustal rocks (termed *juvenile crust*) throughout north-east Africa and Arabia are characterized by the abundance of volcanoclastic successions with ophiolitic rocks and occasional sedimentary intercalations (Bakor *et al.* 1976; Shackleton *et al.* 1980) which have been metamorphosed to the greenschist facies (Vail 1983) in the main. In Arabia there are remnants of pre-Pan-African microcontinents (Stoeser & Camp 1985; Stoeser & Stacey 1988) whereas in Egypt and the Sudan the deformed passive continental margin, which some workers (*e.g.* Hepworth 1979; Delfour 1980) think is a continuation of the Mozambique belt, was partly transformed into an active margin along which there are ophiolites and inter-thrust volcanic arc rocks (Kröner 1985).

The duration of the Pan-African orogeny in the Arabian-Nubian shield has gradually been refined to 950-450 Ma (Kennedy 1964; Greenwood *et al.* 1976; Kröner 1984), but the precise timing of individual events are still poorly constrained and many of the details of the events which led to the accretion of the Neoproterozoic juvenile crust of the Arabian-Nubian Shield are continuous. Alternative tectonic scenarios for the development of the Arabian-Nubian Shield have been proposed:

a) the formation and accretion of ensimatic island arcs with marginal basins (Al Shanti & Mitchell 1976; Al Shanti & Gass 1983; Bakor *et al.* 1976; Greenwood *et al.* 1976; Frisch & Al Shanti 1977; Gass 1977 & 1981; Schmidt *et al.* 1979; Kröner 1983, 1984, 1985; Vail 1983; Camp 1984; Stoeser *et al.* 1984; Stoeser & Camp 1985);

b) rifting of an older sialic basement (Garson & Shalaby 1976; Hepworth 1979; Engel *et al.* 1980; Delfour 1981; Stern 1981; Kemp *et al.* 1982).

At present there is a general consensus that the Arabian-Nubian Shield represents an assemblage of accreted island-arcs, ophiolitic belts, and probable microcontinents and oceanic plateaus, and thus provides good evidence of processes of lateral crustal-growth and obduction-accretion tectonics (Kröner 1985; Stoesser & Camp 1985). Disrupted ophiolites (Shackleton 1979; Fig. 6.1) occur in linear belts up to 900 km in length and are thought by some people to define so-called "sutures" between island-arcs and microplates (Kröner 1985; Pallister 1988). Rarely a complete ophiolite succession is exposed (*e.g.*, Wadi Ghadir, El Sharkawy & El Bayoumi 1979). It is probable that different parts of the Pan-African belt represent different tectonic scenarios, for example some authors interpret the rocks variously as arc-back-arc basin systems (*e.g.*, Bakor *et al.* 1976; Frisch & Al Shanti 1977), continent-continent collisions (*e.g.*, Rogers *et al.* 1978; Fleck *et al.* 1980) or the sites of smaller intracontinental oceanic basins that quickly opened and closed (*e.g.*, Kazmin *et al.* 1978; Kröner 1979; Engel *et al.* 1980).

A great deal of the published evidence on the development of the Arabian-Nubian Shield has come from Arabia. The work of relevance to the Wadi Allaqi area would come from the Midyan and the Hijaz terranes with the intervening southerly verging Yanbu "suture" if one accepts the pre-Red Sea rift assemblage of the Arabia and Nubian shields (Stoesser & Camp 1985). Data from the Yanbu and Bir Umq "sutures" supports three distinct periods of island arc formation at probable sites of plate convergence:

(1) the earliest arc (900-800) Ma rocks are chemically immature bimodal suites of low-K tholeiites and sodic dacites / rhyolites lavas which are depleted in lithophile elements and have chemical characteristics similar

to immature island arcs such as the present-day Tonga-Kermadec and Lesser Antilles arcs (Stoeser & Camp 1985). At 805 Ma (U / Pb zircon data of Hedge 1984) these were intruded by plutons of diorite and trondhjemite;

(2) intermediate-aged (800-900 Ma) lavas of predominantly calc-alkaline and low-K arc tholeiites, andesites, dacites and tuffs (Camp 1984; Jackson *et al.* 1984; Stoeser & Camp 1985), which were intruded by granitic batholiths, U / Pb zircon dates (Hedge 1984) indicate the magmatism had ceased by 715 Ma.

(3) youngest (700-800 Ma) basaltic and andesitic subaerial volcanics. U/Pb zircon age date for granitic rocks that the magmatic was active between 680-615 Ma (Aldrich 1978; Duyverman *et al.* 1982; Hedge 1984). As study of both exposures and TM - imagery (Fig. 6.3) of the area adjacent to the central Wadi Allaqi clearly indicate the sinuous nature and extent of the Allaqi Shear-zone. The Allaqi Shear-zone is the most northerly major fault of a wide (> 70 km) fault-duplex zone. This may support the speculative interpretation of a tectonic boundary (between the Gabgaba and Aswan terranes of Greiling *et al.* 1994) and this matter will be further discussed at a later stage.

6.2 Tectonic evolution and setting

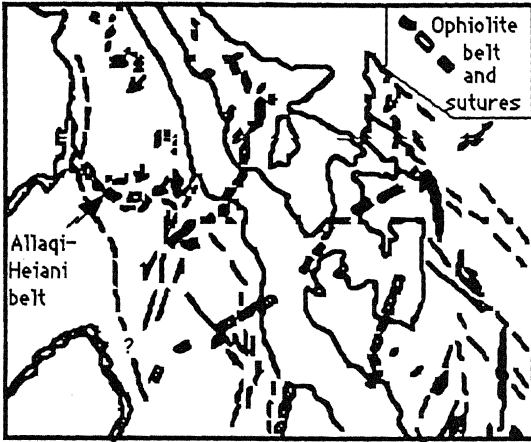
It has been admirably pointed out by Miller & Dixon (1992) that the tectonic setting must be inferred from independent lines of evidence such as the relationship between deformation history and magmatic evolution. A number of issues require some discussion before an holistic scenario of the tectonic setting for the south Eastern Desert may be proposed.

6.2.1 Limits of the Nile Craton and the Arabian-Nubian volcanic pile. The occurrence of the Nile Craton (pre-Pan-African rocks) in the Arabian-Nubian Shield is highly disputed. Many authors (*e.g.*, Dixon & Golombek 1988; Abdelsalam & Dawoud 1991; Schandelmeier *et al.* 1988,1994; Sultan *et al.*

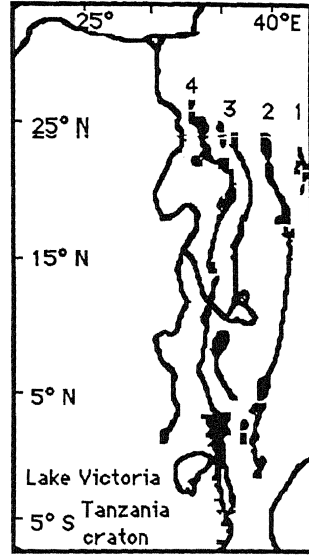
1993; Greiling *et al.* 1994) concur that the boundary between the juvenile crust of Arabian-Nubian Shield and the Eastern Sahara Craton (termed locally the Nile Craton by some of these authors) in Egypt and northern Sudan occurs as a north-south-trending line (Fig 6.2) and central Wadi Allaqi lies to the east of this line. Sultan *et al.* (1993) produced evidence from radiometric age dates (U-Pb and Pb/Pb on single and multi-grain zircons in gneisses) to support this position of the boundary.

The occurrence of pre-Pan-African basement rocks (*i.e.*, >1.0 Ga according to Kröner 1985) within the Arabian-Nubian Shield of the Eastern Desert is highly disputed. El Gaby *et al.* (1984, 1988) from a synthesis of available geological, geochemical and radiometric age data initially for the central Eastern Desert and later for the entire Egyptian Pan-African rocks, supported an hypothesis that the continental cratonic crust extended eastwards into the Eastern Desert underneath the Pan-African cover and is now exposed in several tectonic windows (*e.g.*, at Meatiq, Sibai, Hafafit and Beitan; Fig. 6.2) where the junction between the basement and the cover is always tectonic (Abdel-Khalek *et al.* 1992). Others, on the basis of structural analyses (*e.g.*, Shackleton *et al.* 1980; Ries *et al.* 1983; Greiling *et al.* 1988), isotopic geochemistry and radiometric ages (*e.g.*, Harris *et al.* 1984; Stern & Hedge 1985; Stern & Kröner 1993; Kröner *et al.* 1988; Kröner *et al.* 1994), dispute that a Pre-Pan-African basement is not present in the Eastern Desert and interpret the gneisses as altered rocks related to derivatives from the Pan-African oceanic crust.

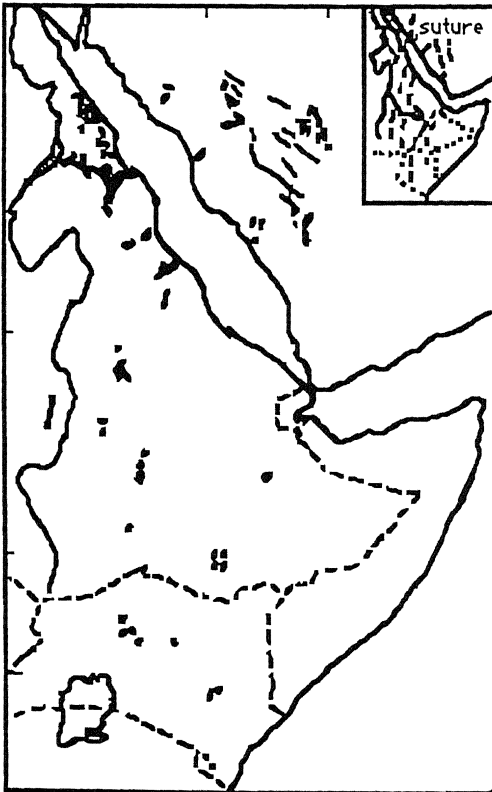
6.2.2 Ophiolite belts. The significance of the ophiolite is to infer the probable position of sutures and direction of obduction and subduction (Shackleton 1994). Berhe (1990) argued that the ophiolite belts in southeastern Desert and north-east Sudan represent sutures. Although the ophiolite belts may mark sutures between collided crustal plates, it is possible that they may be the site of ancient convergent margins which do



Kroner *et al.* 1987

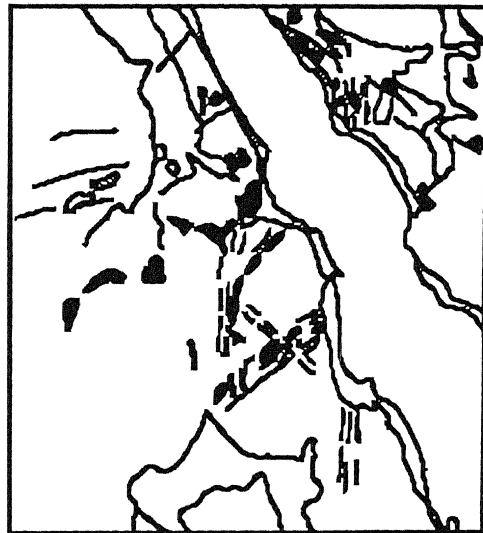


Shackleton 1979



Berhe 1990

● Ophiolites



Schandelmeier *et al.* 1993

Fig. 6.1 Various interpretations of the distribution of ophiolitic rocks in the Pan-African belt

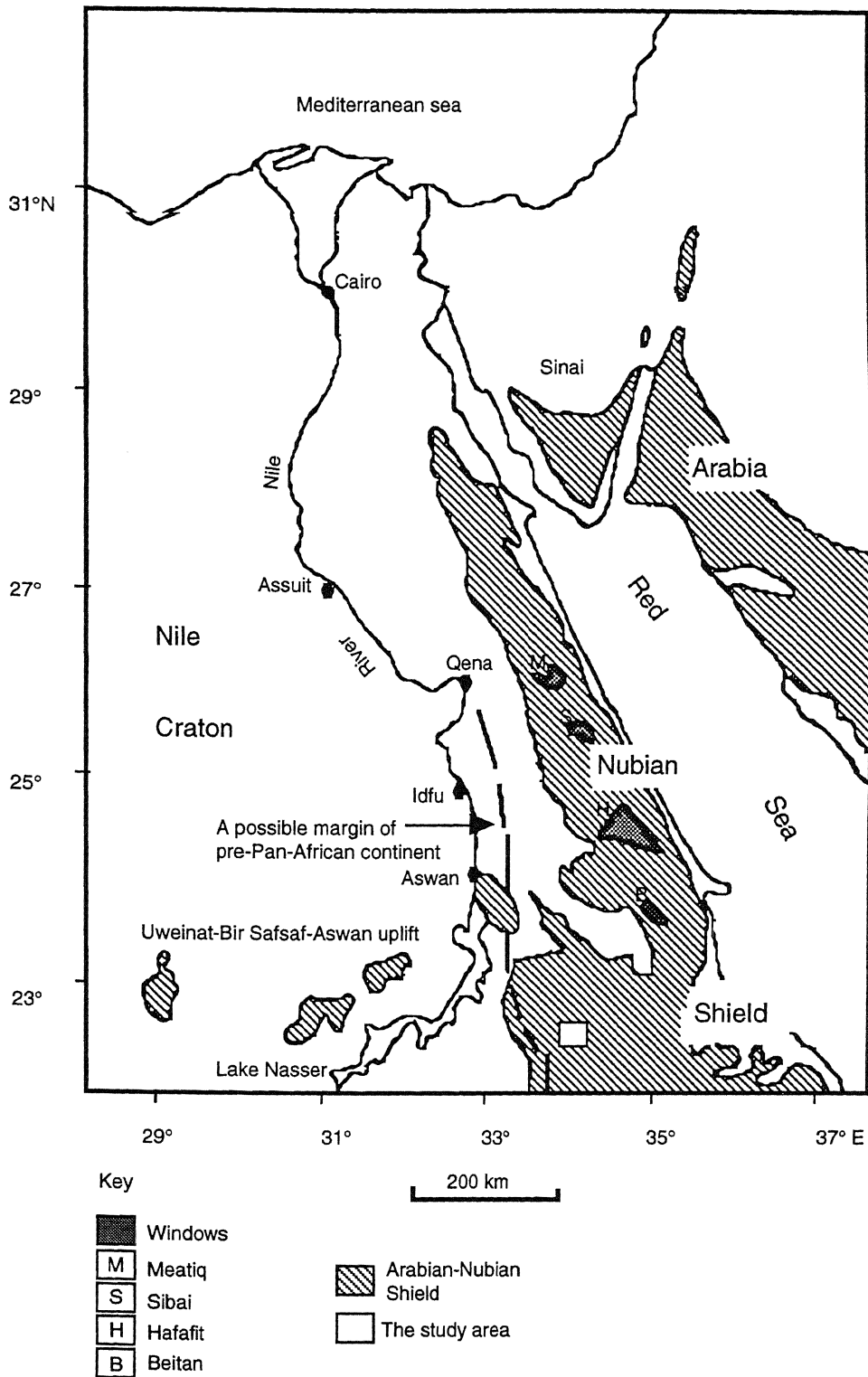


Fig.6.2 Map showing the generally accepted division between the Nile Craton and the rocks of the Pan-African belt and the tectonic windows (compiled from El Gaby *et al.* 1988; Abdel Khalek *et al.* 1992; Greiling *et al.* 1994)

not necessarily lead to vigorous collision. Shackleton (1986) termed such accretionary processes as 'gentle' collision and indicated that they might occur prior to collision events. The significance of the Gebel Taylor Wedge is important in this context. It is not certain whether the wedge is a remnant of an *in situ* subduction site, a piece of obducted ophiolitic back-arc, or an allochthonous remnant of a subduction site. If either of the latter two suggestions are correct it is certain that the wedge has come from the South and the direction of transportation is towards the north. North of the present area there are several klippen of mainly ultra-basic igneous rocks (*e.g.*, around Shilman, Fig. 6.3), which have been interpreted as pieces of obducted ophiolitic rocks, and if these are related to the Gebel Taylor Wedge it would support a regional northerly transportation perhaps similar outcrops situated to the north of the Heiani and Onib - Sol Hamed ophiolite belts might also be northerly-obducted oceanic crust.

The ophiolitic rocks in the Arabian-Nubian Shield have been subject to a number of different interpretations (Fig. 6.1). Berhe (1990) identified five major ophiolitic belts in NE Africa. These ophiolite belts are dismembered remnants of supra-subduction zones and back-arc basins with different structural relationships. Shackleton (1988) pointed out that many ophiolite occurrences are transported far from the site of the original sutures.

6.2.3 Suture zones / shear-zones and their sense of movement in Wadi Allaqi. Although there is no general agreement in the use of the term *suture zone* (*cf.* Howell 1995) and it is not easy to apply in the field, according to Karig (1989) the term may be defined as belts of ophiolite, melange and sometimes blue-schist metamorphic rocks that mark the site of an ocean closure during a collision event. On the other hand, a collision involving an oceanic arc with a continental margin might show a belt of ophiolitic material, but this belt would represent the earlier pre-collision forearc. For example the young Banda collision zone near Timor (Underwood & Moore

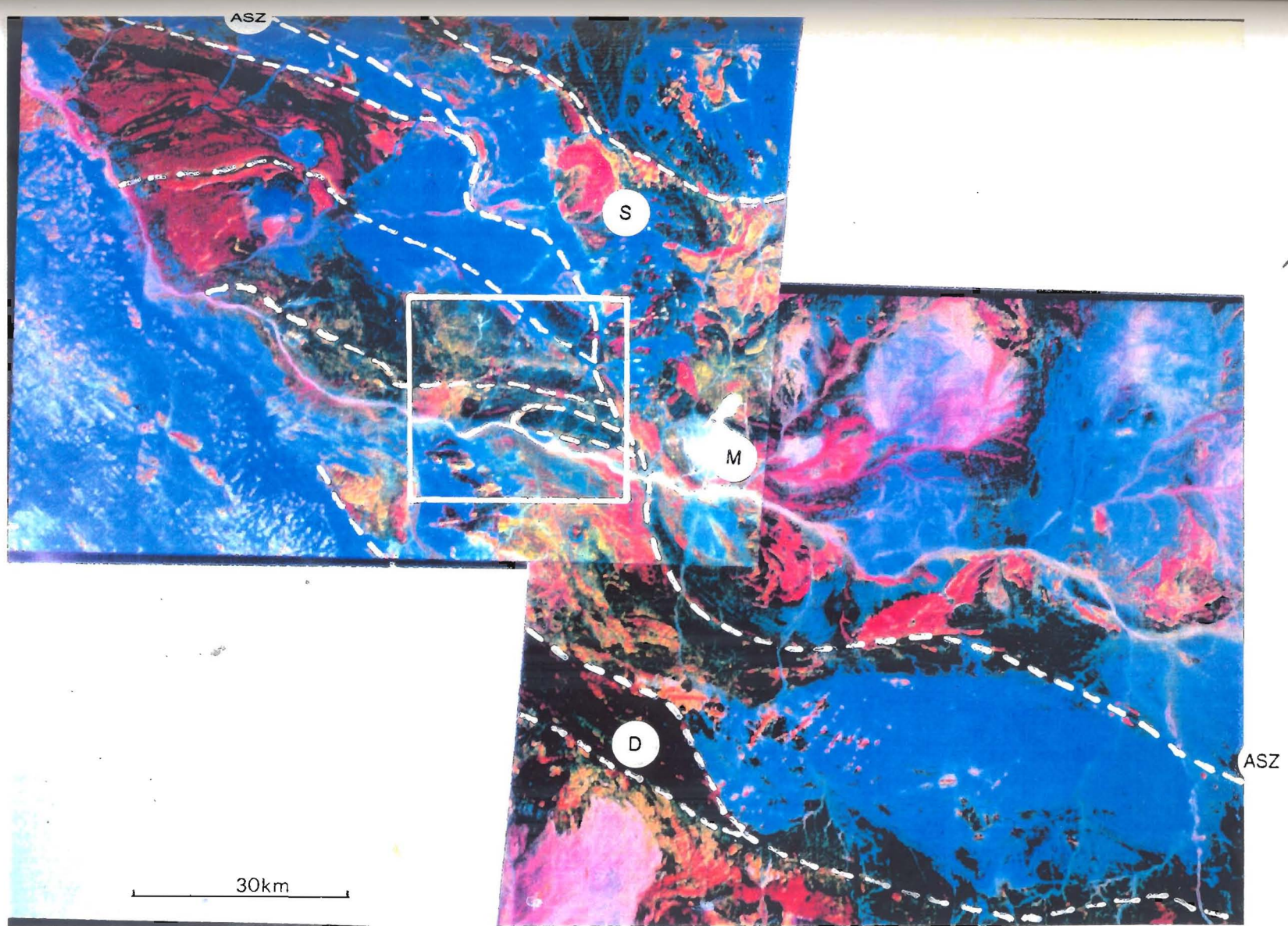


Fig. 6.3 Thematic Mapper image of the western Wadi Allaqi area showing major shear-zones including Allaqi Shear-zone (ASZ) and a large-scale duplex to the south (D), [the outline of the location for Fig. 2.1 shown, Gebel Shilman (S), Wadi Murra (M)]

1995) has not produced a suture zone where an ocean basin closed, accretion in the fore-arc changed from a complex of highly deformed oceanic sediments to a foreland fold-thrust belt. Also the Indus suture zone in Ladakh (Dickinson 1995) also fails to conform to a simple model. North of a pile of south verging foreland thrust sheets is a north-verging thrust stack of volcanoclastics, turbidites, and molassic conglomerates that appear to represent a collapsed fore-arc basin. Except for several ophiolite sheets that now lie well south of the suture (and may represent basement of a fore-arc basin), ophiolite and melange, with minor high P-T components lie in narrow belts, usually along unit-bounding faults which are possible strike-slip zones. In short, there is no simple relationship between suture zones and plate collisions.

Several geologists (Kröner *et al.* 1987; Stern *et al.* 1989, 1990; Sultan *et al.* 1992; Abdelsalam & Stern 1993a,b) consider Wadi Allaqi as a suture zone during the Pan-African orogeny and, on a regional scale, compressional shear-zones are common in subduction-related environments (Murphy 1989). That the Allaqi Shear-zone is a major tectonic structure is not disputed. Its sinistral shear-sense criteria and predominantly oblate strain fabric are well developed throughout and lineations are not as common, but the predominant movement pattern in this shear-zone is oblique compressional thrusting rather than strike-slip motion. The principal deformation mechanisms within the Allaqi Shear-zone are identified as grain-size reduction, mineral phase changes, development of planar anisotropies and localization of fluids. Appearance of pore fluids (?mineralizing fluids) lead to fracturing within the shear-zones which tend to concentrate in the finer-grained material due to their relatively high strength. This deformation pattern is similar to many other middle- to lower-Crustal structural régimes (Coward 1990).

The ophiolitic rocks of the Gebel Taylor Wedge are clearly allochthonous and appear to have travelled from a southerly direction but have been emplaced as a quasi-obducted slab with a back-arc basin geochemical signature. Observations of these types of rocks from a wider area (*e.g.*, Fig. 6.3) indicate both that they have been involved in some element of obduction and that the evidence for a *suture zone* is not proven.

6.2.4 Regional sense of movement. The Allaqi Shear-zone is generally accepted as related to the collision of the Arabian-Nubian shield with the Nile Craton to the west which was part of the consolidation of east- and west-Gondwana. However there is divergent evidence regarding the sense of movement of the Pan-African Belt in the surrounding area (Greiling *et al.* 1994; Kröner *et al.* 1987; Fig. 6.4). This data is poorly constrained because adequate radiometric ages and paleolatitude data are not available and published information is of variable quality.

Ries *et al.* (1983) stated that the extension in a NW-SE direction, is so large that it must indicate the direction of tectonic transport. Shackleton & Ries (1984) suggested that, the relative plate motion is oblique to the ophiolitic sutures, because there are consistent NW-SE oriented stretching lineations although they are not easy to recognize. Berhe (1990) also supports an oblique collision, which caused juxtaposition of the Pan-African-Mozambique terranes along a NW-SE trending strike-slip transpressive craton margin. If the continuity of the ophiolitic sutures is established for NE Africa then sutures like plate margins, must continue until replaced by another type of plate boundary, either a transform fault or a constructive margin. Hence ophiolite belts which have been interpreted as forming sutures must continue further south into the Mozambique belt of East Africa but only if no terrane margin has been crossed. Greiling *et al.* (1990) indicated that thrusting is invariably directed north-westerly towards the Nile Craton from the evidence of stretching lineations, the asymmetry of shear minerals and

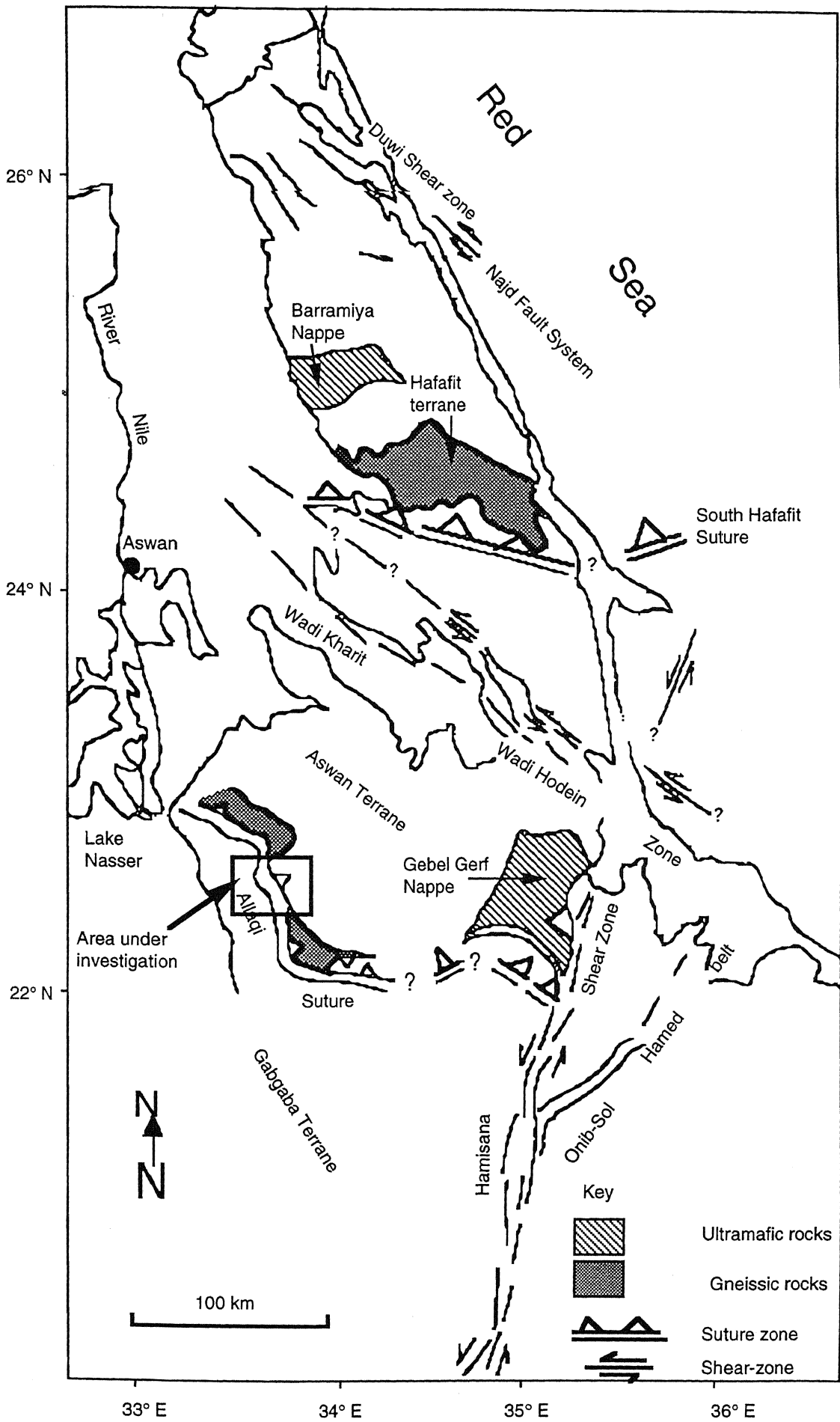


Fig. 6.4 Postulated terrane boundaries and "Sutures" of the eastern Egyptian part of the Neoproterozoic East African Orogen (after Greiling *et al.* 1994)

pressure shadows. Greiling *et al.* (1994) interpreted the E-W trending folds as being transported to the NW. From stretching lineations the overall general direction of movement of the ophiolitic thrust belts is NW (Greiling *et al.* 1994) this is clearly obvious in the areas adjacent to the study area to the south and to the northwest but in the study area the direction of movement is towards the NE (Fig. 2.12). Stern & Kröner (1993) concluded that the boundary developed as due to collision of the Arabian-Nubian Shield with the pre-Pan-African continental crust to the west as part of consolidation of East and West Gondwana at c.670-610 Ma ago.

6.2.5 Radiometric dating of the Pan-African Orogeny. Radiometric analyses have shown that some of the rocks of the Pan-African Belt are derived, in part at least, from Archean sources (probably the Nile Craton). Kröner *et al.* (1992) on the basis of single grain zircon evaporation technique provided evidence for the existence of Archean crust (3017 ± 3 Ma) in metasedimentary rocks from the eastern Wadi Allaqi region. Wust *et al.* (1987b) reported a detrital zircon age of 2390 Ma from metagreywackes in the same area. Wust *et al.* (1987a) in Abu Swayle 20 km to the north of the central Wadi Allaqi area, reported 2300 Ma ages from detrital zircon in a meta-sandstone and 2300 Ma from zircon in granitic pebbles (Dixon 1981). About 250 km to the north Abdel-Monem & Hurley (1979) reported a 1770 Ma age from detrital zircons from the Hafafit Gneiss. Harris *et al.* (1984) reported ages of 1900-1600 Ma from Wadi Mubarak and Wadi Nugrus (detrital zircon from metasedimentary rocks).

6.2.6 Reconstruction of the assembly of Gondwana. Although much effort has been expended on studying the disaggregation of *Pangea*, it is only in recent years that geologists have begun to study the assembly of terranes forming the Neoproterozoic supercontinent (termed *Rhodinia* by McMenamin & McMenamin 1990) which was disaggregated and parts reassembled to form *Laurasia* and *Gondwana*. *Gondwana* was assembled

from its constituent cratons during the Pan-African orogeny at the end of a Neoproterozoic-early Palaeozoic Wilson cycle. Largely on the basis of geological and paleolatitude evidence some interesting reconstructions (Fig. 6.5) of the formation of both the Rhodinia and Gondwana supercontinents have been published recently (*e.g.*, Hoffman 1991; Kröner 1991,1993; Dalziel 1992; Stern 1994; Rogers *et al.* 1995). On the basis of palaeomagnetic evidence Piper (1982) suggested that Rhodinia remained intact until after 570 Ma. This view is confirmed by ages of about 500 Ma widespread within the Pan-African belt which may represent an event post-dating the *initial suturing stage* of Gondwana (Stern & Bloomer 1992). Several major early Neoproterozoic sutures in Western Gondwana (South America-Africa), along the boundaries between the Brazilian-West Africa, Rio de la Plata, and Sao Francisco-Congo-Kalahari cratons and particularly along the Mozambique belt between West Gondwana and East Gondwana (Hartnady *et al.* 1985; Ramos 1988; Porada 1989; Fig. 6.5a), have been used as evidence to support this contention. However, there is a growing body of evidence which suggests that the Arabian-Nubian ocean basins (part of the *Mozambique Ocean* of Dalziel 1992) probably closed during the final amalgamation stages of the Neoproterozoic supercontinent (*cf.* the conclusions of Stoesser & Camp 1985) and may have been accompanied by the separation of *Laurasia* from the Neoproterozoic supercontinent (Dalziel 1992; Soper 1994). Dixon & Golombek (1988) estimate the growth rate of Arabian-Nubian Shield between 900-600 Ma at about 20% of the modern global rate. The evolution of the rocks of what is now the Arabian-Nubian shield probably started by rifting with the supercontinent Rhodinia which formed about 1000 Ma and broke up during the late Neoproterozoic (Bond *et al.* 1984; Moores 1991; Dalziel 1991, 1992; Hoffman 1991; Powell *et al.*

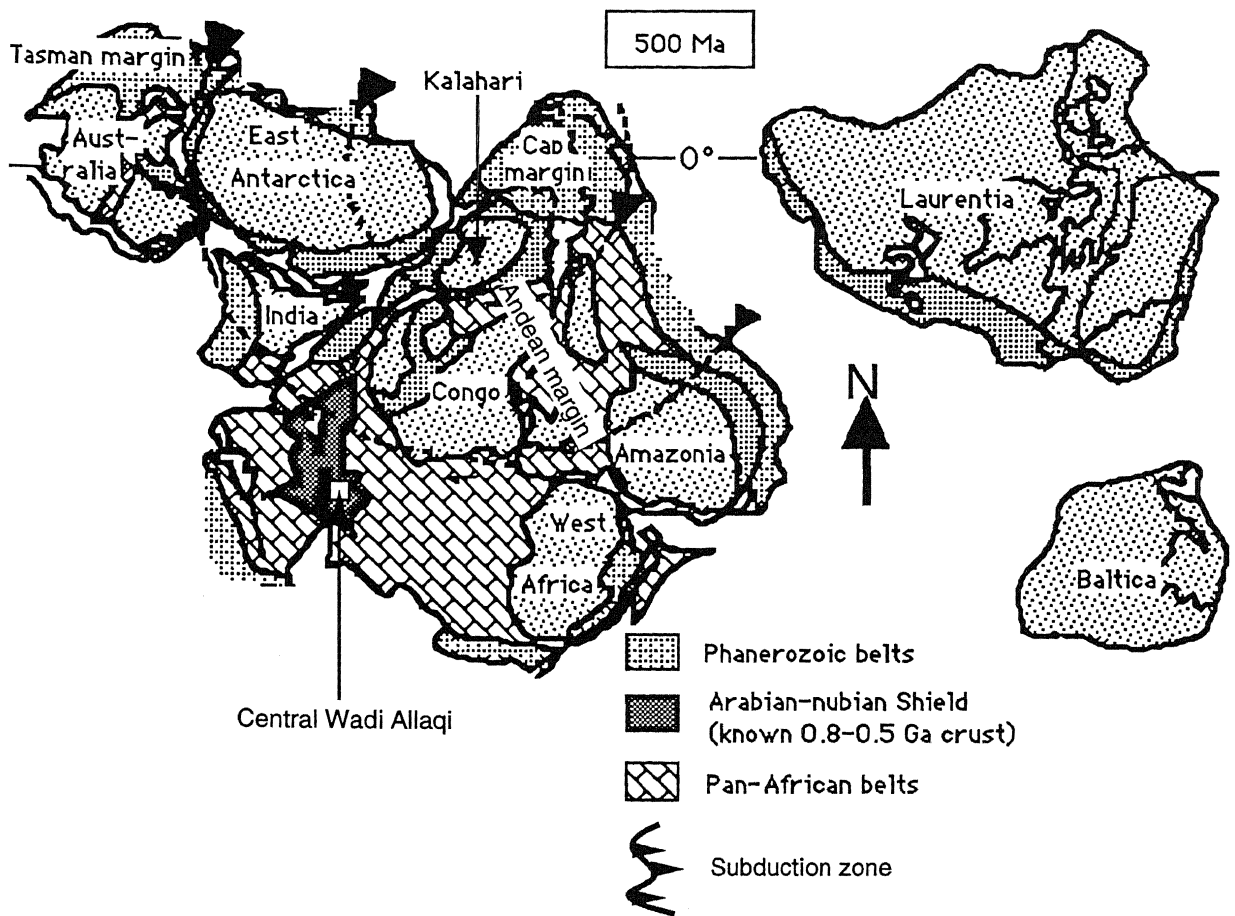
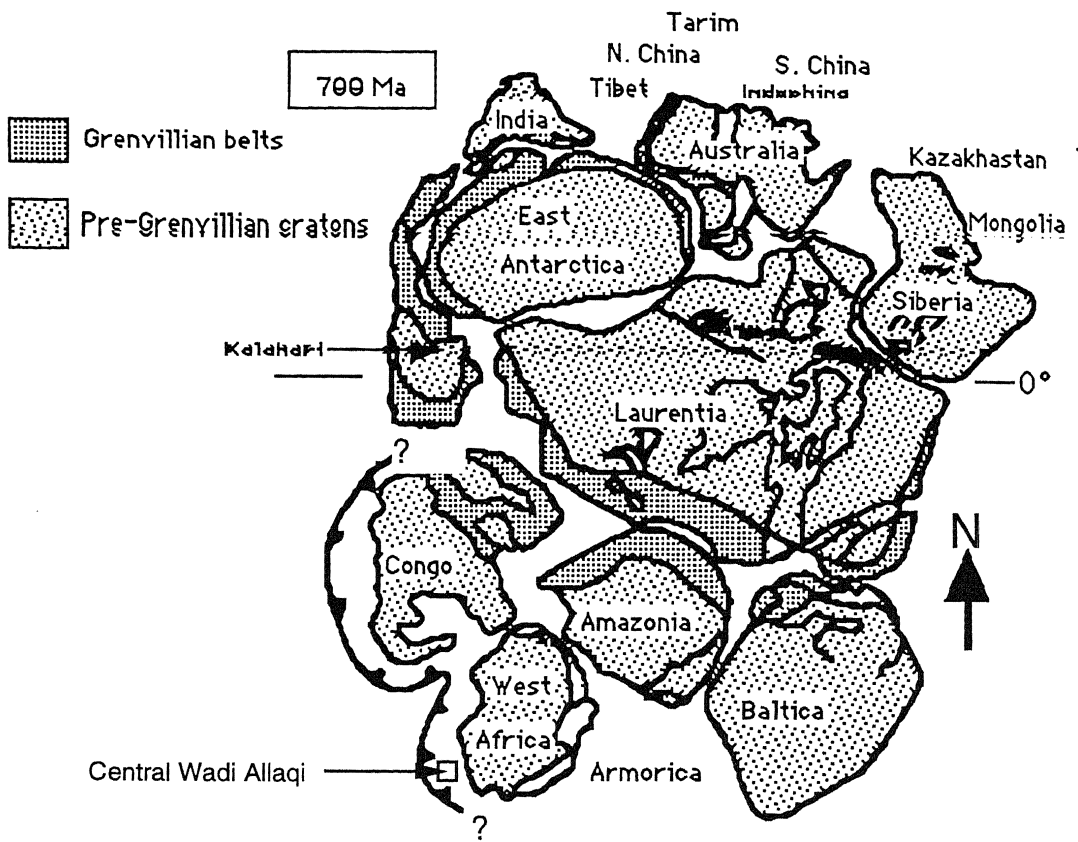


Fig. 6.5 A reconstruction of the continent disposition in the period 700 Ma (a) and 500 Ma (b) (after Hoffman 1991)
 Note that in (b) Africa's orientation is the reverse of the present day orientation.

1993) and this was followed by sea-floor spreading. The events affecting the rocks of central Wadi Allaqi can now be placed in a plate tectonic context (see 6.3)

6.3 A model for the development of the central Wadi Allaqi

Three main development stages in a Wilson Cycle can be identified from the rocks of central Wadi Allaqi : (a) an early rock-forming volcano-sedimentological stage, which has involved some extension; (b) an accretion stage involving contraction, the formation of thrust-duplexes, and orogenies which may be related to collision of east and west Gondwana at about 550 Ma (Stern 1994); and (c) a collapse of the tectonic pile (*cf.* Table 2.2).

Reconstruction of the early stage (a-above), and in particular the basin architecture, is difficult because of the later tectonic overprint and the relative lack of marker horizons in the Successions. Indeed little can be said about the non-tectonic (*e.g.*, eustatic changes in sea-level), tectonic, volcanic, and rift location controls on the sedimentation (*e.g.*, Karig 1985). For example, an upward transition from biogenetic pelagic carbonates to pelagic clays can not be confirmed and, as has been mentioned in chapter 3 for the upper part of the Filat Succession and Um Relan Succession (Fig. 3.11), the relationship may be more complex. Also because complete sequences for each of the three Successions are not exposed in the central Wadi Allaqi it is impossible to give a definitive statement on the accumulation rates within the basin. However, from a general consideration of the lithostratigraphical successions (chapter 3) and geochemical signatures of both the, largely volcanoclastic, successions and intrusive granite plutons (chapters 3 and 4 respectively) it is possible to discuss the likely development of the central Wadi Allaqi pile in terms of a plate tectonic scenario.

At present only a few detailed stratigraphical sequences are available for comparison (Marsaglia 1995 and references contained therein) but the overwhelming evidence indicates that the volcano-sedimentary pile has initially developed as a distal facies in a back-arc environment (Klein 1985) and that from time-to-time a few localized and distinct *débris* flows have been intercalated within the successions. The main lithological components of the central Wadi Allaqi Successions match those of typical back-arc basins (Klein 1985, Marsaglia 1995), *i.e.*, reworked volcanoclastic rocks of varying grain-size, *débris* flow deposits, lava flows (mainly basaltic), and pyroclastic rocks although carbonate and siliciclastic sedimentary deposits are not unknown. The stratigraphical sequences and geochemical signatures of the central Wadi Allaqi are broadly comparable with those of present-day back-arc basins (see chapter 3) such as the Mariana (Taylor 1992) and Lau Basins (Jenner *et al.* 1987, Pearce *et al.* 1994) both of which are extremely elongated with lengths in excess of 500 km. The main difference between modern back-arc sequences and that found in the central Wadi Allaqi is the thickness. The Filat Succession has an estimated thickness of about 15 km whilst modern sequences rarely exceed 2 km, *e.g.*, DSDP Site 451 on the West Mariana Ridge (Scott & Kroenke 1980), which spanned 6 Ma, has a thickness just below 1 km. Although sediment accumulation rates are known to be variable, Scott & Kroenke (1980) report very high rates for the first 2 Ma and then a gradual decrease for the remaining 4 Ma, it would seem that if the rates were comparable that the early rock-forming volcano-sedimentological stage of the Filat Succession should have occupied about 90 Ma. Comparison with more ancient back-arc sequences (*e.g.*, the Middle Jurassic Gran Cañon Formation on Cedros Island, Baja Californian; Busby-Spera 1987) indicate similar rates of sedimentation and accumulation of volcanic material.

In addition, Cas & Wright (1987) have stated that ancient back-arc basins should contain evidence of an ophiolitic sequence since the back-arc floor would have been segmented during any later collision stage. The Gebel Taylor Wedge, from geochemical data presented in chapter three, could be interpreted as a segment from the central Wadi Allaqi back-arc.

Although the mechanisms of back-arc basins are not entirely understood back-arc basins have been classified into four main types (Ingersoll 1988) :

1) *extensional*, which formed by rifting and sea floor spreading (Tamaki & Honza 1991) and may be initiated by rifting within or behind either a continental-margin arc (*e.g.*, Japan Sea) or an intra-oceanic arc (*e.g.*, Mariana Basin)

2) *non-extensional*, composed of trapped old ocean basins (Tamaki & Honza 1991) causing a sudden shift to the subduction zone during plate reorganisation (*e.g.*, Bering Sea)

3) *non-extensional*, transitional with retroarc foreland basins (Jordan 1995) and develops on continental crust (*e.g.*, Sunda Shelf and Java Sea)

4) *boundary*, (Taylor & Karner 1983) in which basins are produced by extension along plate boundaries with translational components (*e.g.*, Andaman Sea) and contemporaneous magmatism may or may not be associated.

The presence of a limited number of E-W-trending early-formed dykes, discovery of extensional structures in the Kilkobob Succession, and the lithostratigraphical and geochemical signatures of the pile suggest that the extensional stage in the development of the central Wadi Allaqi back-arc basin was akin to that of the Mariana Basin (*i.e.* in 1) above; Fig. 6.6c).

The accretion stage of the development of the central Wadi Allaqi area has been discussed at length in chapter 2 and probably lasted from 750 Ma to 650 Ma (according to Stern 1994). In the area the complex polyphase

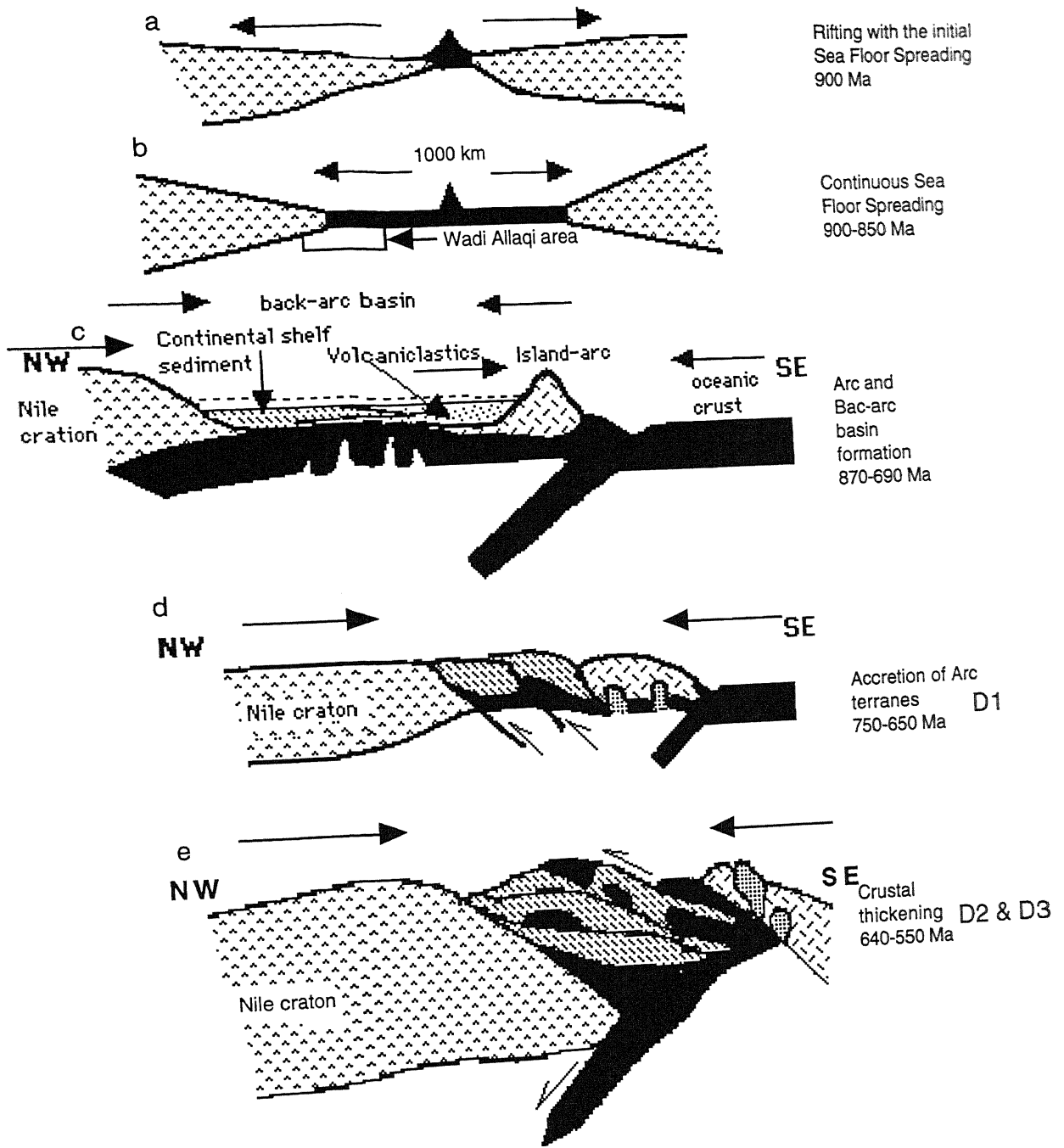


Fig. 6.6 Proposed reconstructions of the development of the Pan-African rocks in the central Wadi Allaqi area

deformational history was dominated by a hinterland-dipping thrust duplexes (Boyer & Elliott 1982; Fig. 6.6d), formed during the earliest phase (D1), and was associated with strong fluid movement which formed the quartz-vein gold mineralization under greenschist facies metamorphism.

The collapse or crustal-thickening stage (Fig. 6.6e) is represented in the area by horizontally arranged kink-bands (D4) and strike-slip faulting (D5). Elsewhere in the Pan-African outcrop post-depositional inter-mountain pull-apart basins develop (*e.g.*, the Iqla Basin, Rice *et al.* 1993) and are deformed by NNE-SSW-trending strike-slip faults.

6.4 Outcomes and Conclusions

The main outcomes of the, first, detailed investigation of central Wadi Allaqi illuminates some of the protracted problems of the Pan-African tectonics and mineralization :

- 1) production of structural and lithological maps using a modern UTM grid reference system (Figs. 1.3a & 1.3b)
- 2) establishment of a detailed and complex structural history related to regional metamorphism (summarised in Table 2.1, and Fig. 2.25)
- 3) production of an interpretation of the geometry of the large-scale structures (chapter 2 and Fig. 1.4)
- 4) production of a detailed tectonic stratigraphical sequence (chapter 3 and Fig. 1.3b)
- 5) establishment of the timing of emplacement of the four granitic plutons relative to the structural history (chapter 4, and summarised in Table 2.2)
- 6) production of an interim model for the paragenesis of the gold mineralization and its relationship to the structural history (summarised in Fig. 5.14)
- 7) proposal for a working model of the plate tectonic development of central Wadi Allaqi (summarised in Fig. 6.6).

The main conclusions of this investigation are :

a) detailed structural study of the central Wadi Allaqi area showed five phases of deformation and a major Shear-zone (the Allaqi Shear-zone) which has formed as the result of early thrusting. The rocks have been affected by low-grade greenschist facies metamorphism which reached a peak during the D1 deformational phase and was maintained beyond the D2 deformational phase.

b) three major tectonic stratigraphic Successions, Filat, Um Relan and Kilkobob have been established and the lithostratigraphical and geochemical evidence support formation in a back-arc basin as distal deposit.

c) Gebel Taylor Wedge represents a piece of ophiolitic rocks which was obducted during the closure of the back-arc basin. The site of the ophiolitic rocks has not been proven to be a suture zone but the Allaqi Shear-zone represents the northernmost extent of a complex thrust-duplex structure.

d) the relative timing of emplacement of the granite intrusions have been established: Atshani Granite (post- D1 and pre-D2 phase) followed by Um Relan Granite (early D2 phase), Filat Granite (post-D2 phase) and Kilkobob Granite (post-D3 phase). The geochemical signatures of the granites indicate that the first those have been derived in a volcanic-arc tectonic setting although the Kilkobob Granite is ambiguous the chemical evidence supports a within-plate derivation.

e) widespread gold-bearing and barren quartz veins were emplaced during D1 deformation within the country rocks of the Filat Succession and the Allaqi Shear-zone accompanying greenschist facies metamorphism. Both the wall-rocks and the veins were subsequently altered by a residual/diagenetic event.

f) three principal tectonic stages in the development of the rocks of the central Wadi Allaqi are recognised. Initially, an island-arc with an extensional back-arc basin towards the Nile Craton and a subduction-zone in the opposite direction (Fig. 6.6c) was formed. This was followed by closure, accretion, obduction, thrusting and crustal thickening with movement towards the Nile Craton (D1-D3; Fig. 6.6d,e). The final stage involved the collapse of the orogen and faulting (D4-D5).

6.5 Suggestions for further work

These outcomes and interpretations provide a reasonable basis for further more specialized investigations. The interpretation of the Pan-African events in the rocks of central Wadi Allaqi area could be further refined and better constrained by additional studies as follows:-

- a) extension of the structural work of central Wadi Allaqi in order to deduce a well-constrained north-south, tectonic profile of the Pan-African rocks throughout Egypt, in part using seismic profiling, so that the controversy of the correct position of the Nile Craton, and whether it originally extended as far as the present-day Red Sea, may be resolved.
- b) a programme of radiometric-age determination to better constrain the structural history. Rb-Sr, U-Pb and $^{40}\text{Ar}/^{39}\text{Ar}$ techniques on recrystallized minerals of the granitic intrusions and/or single grain zircon evaporation technique for metasedimentary rocks should yield good results and negotiations with the staff of the NERC Isotope Geoscience Laboratory for a joint programme have been opened.
- c) the exact nature of the source of fluids which formed the gold mineralization would be better defined by detailed fluid inclusion and stable isotope studies.

d) Palaeomagnetic/palaeolatitude studies of the volcano-sedimentary pile would provide important corroborative data for plate tectonic reconstruction.

References

- Abdel Khalek, M. L., Takla, M. A., Sehim, A., Hamimi, Z. & El Manawi, A. W. 1992. Geology and tectonic evolution of Wadi Beitan area, SE Desert, Egypt. In Sadek, a (ed.) *The First International conference on geology of the Arab World*. Cairo. 369 - 394.
- Abdel Monem, A. A. & Hurley, P. M. 1979. U-Pb dating of zircon from psammitic gneisses, Wadi Abu Rusheid-Wadi Sikait area, Egypt. *Bulletin of the Institute of Applied Geology, King Abdulaziz University, Jeddah*. **3**, 165 - 170.
- Abdelsalam, M. G. & Dawoud, A. S. 1991. The Kabus ophiolitic melange, Sudan, and its bearing on the western boundary of the Nubian Shield. *Journal of the Geological Society, London*, **148**, 83 - 92.
- Abdelsalam, M. G. & Stern, R. J. 1993a. Tectonic evolution of the Nakasib suture, Red Sea Hills, Sudan: evidence for a late Precambrian Wilson Cycle. *Journal of the Geological Society, London*, **150**, 393 - 404.
- Abdelsalam, M. G. & Stern, R. J. 1993b. Structure of the late Proterozoic Nakasib suture, Sudan. *Journal of the Geological Society, London*. **150**, 1065 - 1074.
- Afia, M. S. & Imam, I. 1979. *Mineral map of Egypt, scale 1 : 2000,000, with explanatory notes and lists*. Geological Survey of Egypt.
- Akaad, M. K. & El Ramly, M. F. 1960. Geological history and classification of the basement rocks of the central Eastern Desert of Egypt. *Geological Survey of Egypt, Paper No. 9*.
- Akaad, M. K. & El Ramly, M. F., 1963 The cataclastic-mylonitic gneisses north of Gabal El Maiyit and the origin of the granite of Shaitian type. *Geological Survey of Egypt, Paper No. 26*.
- Akaad, M. K. & Moustafa, G. A. 1963. The Shaitian granite, cataclastic mylonitic granodiorite. *Geological Survey of Egypt, Paper No. 19*.
- Akaad, M. K. & Noweir, A. M. 1980. Geology and Lithostratigraphy of the Arabian Desert Orogenic belt of Egypt between Latitude 25° 35' N

and 26° 30' N. *Bulletin of the Institute of Applied Geology, King Abdulaziz University, Jeddah*, **3**, 127 - 134.

- Aldrich, L. T. 1978. Geochronologic data for the Arabian Shield. Section 1. Radiometric age determinations of some rocks from the Arabian Shield. *US Geological Survey-Saudi Arabian Project Report 240*.
- Al Shanti, A. M. & Gass, I. G. 1983. The upper Proterozoic ophiolite melange zones of the easternmost Arabian Shield. *Journal of Geological Society, London*, **140**, 867 - 876.
- Al Shanti, A. M. S. & Mitchell, A. H. G. 1976. Late Precambrian subduction and collision in the Al Amar-Idsas region, Arabian Shield, Kingdom of Saudi Arabia. *Tectonophysics*, **30**, T41 - T47.
- American Geological Society. 1970. *Rock-Color Chart*.
- Amin, M. S. 1955. Geological features of some mineral deposits in Egypt. *Bulletin of the Institute of Desert, Egypt*, **5**, 209 - 239.
- Atherton, M. P. 1993. Granite magmatism. *Journal of the Geological Society, London*, **150**, 1009 - 1023.
- Bhatia, M. R. 1983. Plate tectonic and geochemical composition of sandstones. *Journal of Geology*, **91**, 611 - 627.
- Bak, J., Korstgard, J. & Sorensen, K. A. 1975. Major shear zone within the Nagssugtoqidian of west Greenland. *Tectonophysics*, **27**, 191 - 209.
- Bakor, A. R, Gass, I. G., & Neary, C. R. 1976. Jabal al Wask, northwest Saudi Arabia: an Eocambrian back-arc ophiolite. *Earth and Planetary Science Letters*, **30**, 1 - 9.
- Barker, A. J. 1990. *Introduction to metamorphic textures and microstructures*. Blackie & Sons Ltd, Glasgow.
- Bates, R. L. & Jackson, J. A (eds) 1987. *Glossary of Geology* (3rd Edition). American Geological Institute.
- Bean, J. H, & Hudson, J. M. 1983. Geochemical reconnaissance of the Wadi Allaqi-wadi Haimur Area, south Eastern Desert, Arab Republic of Egypt. *Institute of Geological Sciences/Geological Survey of Egypt, Internal Report 27/83*.

- Berger, B. R. & Eimon, P. L. 1983. Conceptual models of epithermal precious metal deposits. In Shanks, W. C. (ed), *Cameron volume on unconventional mineral deposits* 191 - 205.
- Berhe, S. M. 1990. Ophiolites in Northeast and East Africa: implications for Proterozoic crustal growth. *Journal of the Geological Society, London*, **147**, 41 - 57.
- Berthe, D., Choukroune, P. & Jegouzo, P. 1979. Orthogneiss, mylonite and non coaxial deformation of granites: the example of the south Armorican shear zone. *Journal of Structural Geology*, **1**, 31 - 42.
- Blenkinsop, T. G. & Treloar, P. J. 1995. Geometry, classification and kinematics of C-S and S-C' fabrics in the Mushandike area, Zimbabwe. *Journal of Structural Geology*, **17**, 397 - 408.
- Bond, G. C., Nickeson, P. A. & Kominz, M. A. 1984. Breakup of a supercontinent between 625 Ma and 555 Ma: new evidence and implications for continental histories. *Earth and Planetary Science Letters*, **70**, 325 - 345.
- Boyer, S. E & Elliott, D. 1982. Thrust systems. *Bulletin of the American Association of Petroleum Geologists*, **66**, 1196 - 1230.
- Brown, G. C. 1982. Calc-alkaline intrusive rocks: their Diversity, evolution and relation to volcanic arcs. In Thorpe, R. S. (ed.), *Orogenic andesites and related rocks*. Wiley & son Ltd, London. 437 - 461.
- Browne, P. R. L. 1978. Hydrothermal alteration in active geothermal fields. *Annual Review of Earth Planetary Sciences*, **6**, 229 - 250.
- Buchanan, L. J. 1981. Precious metal deposits associated with volcanic environments in the southwest. *Arizona Geological Society Digest*, **14**, 1 - 26.
- Burke, K. C., & Dewey, J. F., 1972. Orogeny in Africa. In Dessauvagie, T. F. J. & Whiteman, A. J. (eds.), *African Geology*. University Ibadan, 583 - 608.
- Burrows, D. R., Wood, P. C., & Spooner, E. T. C. 1986. Carbon isotope evidence of a magmatic origin for Archean gold-quartz vein ore deposits. *Nature, London*, **321**, 851 - 854.

- Busby-Spera, C. J. 1987. Lithofacies of deep marine basalts emplaced on a Jurassic backarc apron, Baja California (Mexico). *Journal of Geology*, **95**, 671 - 686.
- Busby, C. J & Ingersoll, R. V (eds) 1995 *Tectonics of Sedimentary Basins* Blackwell Science, Oxford.
- Camp, V. E. 1984. Island arcs and their role in the evolution of the western Arabian Shield. *Bulletin of Geological Society of America*, **95**, 913 - 921.
- Cas, R. A. F. & Wright, J. V. 1987. *Volcaniclastic successions, modern and ancient*. Chapman & Hall, London.
- Chappel, B. & White, A. J. R. 1974. Two contrasting granite types. *Pacific Geology*, **8**, 173 - 174.
- Collins, W. J., Beams, S. D, White, A. J . R. & Chappell, B. W. 1982. Nature and origin of A- type granites with particular reference to southern Australia. *Contributions to Mineralogy and Petrology*, **80**, 189 - 200.
- Condie, K. C. & Hunter, D. R. 1976. Trace element geochemistry of Archaean granitic rocks from Barberton region, South Africa. *Earth and Planetary Science Letters*, **29**, 389 - 400.
- Conoco 1987. *Geological map of Egypt, NF 36 NE Bernice*, scale 1:500,000. Geological Survey of Egypt.
- Cooke, D. R. & Bloom, M. S. 1990. Epithermal and subjacent porphyry mineralization, Acupan, Baguio District, Philippines: a fluid-inclusion and paragenetic study. In Hedenquist, J. W. White, N. C. & Siddeley, G. (eds), *Epithermal gold mineralization of the circum-pacific*, 1. Special Publication, Journal of Geochemical Exploration, **16a**, 297 - 340.
- Cox, S. F. & Etheridge, M. A. 1983. Crack-seal fibre growth mechanisms and their significance in the development of oriented layer silicate microstructures. *Tectonophysics*, **92**, 147 - 170.
- Cox, S. F. & Etheridge, M. A. 1989. Coupled grain-scale dilatancy and ass transfer during deformation at high fluid pressures: examples from Mount Lyell, Tasmania. *Journal of Structural Geology*, **11**, 147 - 162.

- Coward, M. P. 1990. Shear zones at the Laxford front, NW Scotland and their significance in the interpretation of lower crustal structure. *Journal of the Geological Society, London*, **147**, 279 - 286.
- Dalziel, I. W. D., 1991. Pacific margins of Laurentia and East Antarctica-Australia as a conjugate rift pair: evidence and implication for an Eocambrian supercontinent. *Geology*, **19**, 598 - 601.
- Dalziel, I. W. D., 1992. On the organization of the American plates in the Neoproterozoic and the breakout of Laurentia. *GSA Today*, **2**, 240 - 242.
- Deer, W. A., Howie, R. A. & Zussman, J. 1962. *Rock-forming minerals: Volume 5, non-silicates*. Longman, London.
- Delfour, J. 1980. Geologic, tectonic and metallogenic evolution of the Northern part of the Precambrian Arabian shield (Kingdom of Saudi Arabia). *Bulletin Bureau des Recherches Geologiques et Minières*, **11**, 1 - 20.
- Delfour, J. 1981. Geologic, tectonic and metallogenic evolution of the Northern part of the Precambrian Arabian shield (Kingdom of Saudi Arabia). *Bulletin Bureau des Recherches Geologiques et Minières*, **11**, 1 - 19.
- Dewey, J. F. 1976. Ophiolite obduction. *Tectonics*, **31**, 93 - 120.
- Dewey, J. F. 1988. Extensional collapse of orogens. *Tectonics*, **7**, 1123 - 1139.
- Dickinson, W. R. 1995. Forearc basins. In Busby, C. J & Ingersoll, R. V (eds), *Tectonics of Sedimentary Basins* Blackwell Science, Oxford. 221 - 261.
- Dickinson, W. R. & Suczek, C. A. 1979 Plate tectonics and sandstone compositions. *Bulletin of the American Association of Petroleum Geologists*, **63**, 2164 - 2182.
- Didier, J., Duthou, J. C. & Lameyre, J. 1982. Mantle and crustal granites: genetic classification of orogenic granites and nature of their enclaves. *Journal of Volcanology and Geothermal Research*, **14**, 125 - 132.

- Dixon, T. H. 1981. Age and chemical characteristics of some pre-Pan-African rocks in the Egyptian Shield. *Precambrian Research*, **14**, 119 - 133.
- Dixon, T. H. & Golombek, M. P. 1988. Late Precambrian crustal accretion rates in north-east Africa and Arabia. *Geology*, **16**, 991 - 994.
- Dunnet, D. 1969. A technique of finite strain analysis using elliptical particles. *Tectonophysics*, **7**, 117 - 136.
- Dunnet, D. & Siddans, A. W. B. 1971. Non-random sedimentary fabrics and their modification by strain. *Tectonophysics*, **12**, 307 - 325.
- Duyverman, H. J., Harris, N. B. W. & Hawkesworth, C. J. 1982. Crustal accretion in the Pan-African: Nd Sr isotope evidence from the Arabian Shield. *Earth and Planetary Science Letters*, **59**, 315 - 326.
- Eby, G. N. 1990. The A-type granitoids: a review of their occurrence and chemical characteristics and speculations on their petrogenesis. *Lithos*, **26**, 115 - 134.
- Egyptian Geological Survey and Mining Authority. 1981. *Map of Egypt scale, 1 : 2.000,000*.
- Egyptian Survey. 1945. *Elba Topographic sheet 12, scale 1:250,000*.
- El Gaby, S. 1968. Plagioclase-potash feldspar relation and the origin of porphyritic granite. *Abstract of the Sixth Annual Meeting; Geological Society of Egypt*, p7.
- El Gaby, S. 1975. Petrochemistry and geochemistry of some granites from Egypt. *Neues Jahrbuch Mineralogie Abhandlungen*, **124**, 147 - 189.
- El Gaby, S., El Nady, O. M. & Khudeir, A. A. 1984. Tectonic evolution of the basement complex in the CED of Egypt. *Geologische Rundschau*, **73**, 1019 - 1036.
- El Gaby, S., List, F. K. & Tehrani, R. 1988. Geology, evolution and metallogenesis of the Pan-African belt in Egypt. In El Gaby, S. & Greiling, R. O. (eds), *The Pan-African Belt of Northeast Africa and adjacent areas; tectonic evolution and economic aspects of a late*

Proterozoic orogen. Vieweg & Sohn, Braunschweig/Wiesbaden, 17 - 65

- El Gaby, S., List, F. K. & Tehrani, R. 1990. The basement complex of the Eastern Desert and Sinai. In Said, R. (ed), *Geology of Egypt*. . Balkema, Amsterdam, 175 - 184
- El Ramly, M. F. 1972. A new geological map for the basement rocks in the Eastern and Southwestern Deserts of Egypt. *Annals of Geological Survey of Egypt*, **2**, 1 - 18.
- El Ramly, M. F. & Akaad, M. K. 1960. The basement complex in the CED of Egypt between Latitude 24° 30' N and 25° 40' N. *Geological Survey of Egypt. Paper No. 8*.
- El Ramly, M. F., Ivanov, S. S. & Kochin, G. C. 1970. The occurrence of gold in the Eastern Desert of Egypt. In Moharim, O (ed.), *studies on some mineral deposits of Egypt*. Egyptian Geological Survey and Mining Authority, Cairo, **1**, 53 - 55.
- El Sharkawy, M. A. & El Bayoumi, R. M. 1979. The ophiolite of Wadi Ghadir area, Eastern Desert, Egypt. *Annals of the Geological Survey of Egypt*, **9**, 125 - 135.
- El Shazly, E. M. 1957 Classification of Egyptian mineral deposits. *Egyptian Journal of Geology*, **1**, 1 - 20.
- El Shazly, E. M. 1964. On the classification of the Precambrian and other rocks of magmatic affiliation in Egypt, U. A. R. Abstracts/Proceeding of the *24th International Geological Congress, India*, **10**, 88 - 101.
- Engel, A. E. J., Dixon, T. H., & Stern, R. J. 1980. Late Precambrian evolution of Afro-Arabia crust from ocean-arc to craton: *Bulletin of the Geological Society of America*, **91**, 699 - 706.
- Epstein, S. 1970. Antarctic ice sheet: Stable isotope analyses of Byrd station cores and interhemispheric climatic implications. *Science*, **168**, 1570 - 1572.
- Fisher, R. V. 1961. Proposed classification for volcanoclastic sediments and rocks. *Bulletin of the Geological Society of America*, **72**, 1409 - 1414.

- Fleck, R. J., Greenwood, W. R., Hadley, D. G., Anderson, R. E. & Schmidt, D. L. 1980. Rubidium-strontium geochronology and plate tectonic evolution of the southern part of the Arabian Shield. *U.S. Geological Survey Professional Paper*, **1131**.
- Flinn, D. 1962. On folding during three-dimensional progressive deformation. *Quarterly Journal of the Geological Society, London*, **118**, 385 - 428.
- Foster, R. P. 1985. Major controls of Archaean gold Mineralization in Zimbabwe. *Transactions of the Geological Society of South Africa*. **88**, 109 - 133.
- Frisch, W., & Al-Shanti, A. 1977. Ophiolite belts and the collision of island arcs in the Arabian shield. *Tectonophysics*, **43**, 293 - 306.
- Gamble, J. A., Wright, I. C., Woodhead, J. D. & McCulloch, M. T. 1994. Arc and back-arc geochemistry in the southern Kermadec arc-Ngatoro Basin and offshore Taupo Volcanic zone, SW Pacific. IN Smelli, J. L.e (ed.), *Volcanism associated with extension at consuming plate margins, Special Publication*, Geological society, London, **81**, 193 - 212.
- Garson, M. S. & Shalaby, I. M. 1976. Precambrian - lower Palaeozoic plate tectonics and metallogenesis in the Red Sea Region. In Strong, D. F. (ed.), *Metallogeny and Plate Tectonics*. Geological Association of Canada Special Paper, **14**, 573 - 596.
- Gass, I. G. 1977. The evolution of the Pan-African crystalline basement in NE Africa and Arabia. *Journal of the Geological Society, London*, **134**, 129 -138.
- Gass, I. G. 1981. Pan-African (Upper Proterozoic) Plate tectonics of the Arabian-Nubian Shield. In Kröner, A. (ed.), *Precambrian plate tectonics*. Elsevier, Amsterdam, 388 - 405.
- Gowing, C. J .B. & Potts, P. J. 1991. Evaluation of a rapid technique for the determination of precious metals in geological samples based on a selective Aqua Regia Leach. *Analyst*, **116**, 773 - 779.
- Greenwood, W. R., Hadley, D. G., Anderson, R. E., Fleck, R. J. & Schmidt, D. L. 1976. Later Proterozoic cratonization in southwestern Saudi

Arabia. *Transactions of the Royal Society of London Philosophical*, **280A**, 517 - 527.

- Greiling, R. O., Kröner, A. & El Ramly, M. F. & Rashwan, A. A. 1988. Structural relationship between the southern and central parts of the Eastern Desert of Egypt: details of fold and thrust belt. in El Gaby, S. & Greiling, R. O. (eds), *The Pan-African Belt of Northeast Africa and adjacent areas; tectonic evolution and economic aspects of a late Proterozoic orogen*. Vieweg & Sohn, Braunschweig/Wiesbaden, Vieweg & Sohn, 121 - 145.
- Greiling, R. O., Gayer, R. A., Rice, A. H. N., El Ramly, M. F., & Rashwan, A. A. 1990. Thrust tectonics in the Pan-African of Egypt: a model for a regional sole thrust. *Abstracts of the Colloquium of African Geology*. p261.
- Greiling, R. O., Abdeen, M. M., Dardir, A. A., El Akhal, H., El Ramly, M. F., Kamal El Din, G., Osman, A. F., Rashwan, A. A., Rice, A. H. N. & Sadek, M. F. 1994. A structural synthesis of the Proterozoic Arabian-Nubian Shield in Egypt. *Geologische Rundschau*, **83**, 484 - 501.
- Grindley, G. W. & Browne, P. R. L. 1976. Structural and hydrological factors controlling the permeability of some of hot water geothermal fields. *Second United Nations Symposium on the development and use of geothermal resources*. San Francisco, 377 - 386.
- Groves, D. I. & Phillips, G. N. 1987. The genesis and tectonic control on Archean gold deposits of the Western Australian shield - a metamorphic replacement model. *Ore Geology Reviews*, **2**, 287 - 322.
- Groves, D. I., Golding, S. D., Rock, N. M. S., Barley, M. E. & McNaughton, N. J. 1988. Archean carbon reservoirs and their relevance to the fluid source for gold deposits. *Nature, London*, **331**, 254 - 257.
- Groves, D. I. & Foster, R. P. 1991. Archaean lode gold deposits. In Foster, R. P (eds), *Gold Metallogeny and Exploration*, Blackie & Sons Ltd, Glasgow, 63 - 103.

- Hallberg, J. A. 1980. *Archaean geology of the Leonora-Laverton area*. International Archaean Symposium, Northwest Yilgarn Block Excursion Guide, Geological Society of Western Australia division.
- Hanmer, S. & Passchier, C. 1991. Shear sense indicators: a review. *Geological Survey of Canada. Paper 90 - 17*, 3 - 72.
- Harraz, H. Z & El Dahhar, A. M. 1993. nature and composition of gold forming fluid inclusions in vein materials. *Journal of African and Middle East. Earth Sciences*, **17**, 341 - 353.
- Harris, N. B., Hawkesworth, C. J., & Ries, A. C. 1984. Crustal evolution in north and east Africa from model Nd ages. *Nature, London*, **309**. 773 - 775.
- Harris, N. B. W., Pearce, J. A. & Tindle, A. G. 1986. Geochemical characteristics of collision-zone magmatism. In Coward, M. P. & Reis, A. C. (eds.), *Collision tectonics*. Special Publication **19**, Geological Society, London, 67 - 81.
- Hartnady, C., Joubert, P. & Stowe, C. 1985. Proterozoic crustal evolution in southwestern Africa. *Episodes*, **8**, 236 - 244.
- Hassan, M., & Hashad, A. 1990. Precambrian of Egypt. In Said, R. (ed), *Geology of Egypt*, Amsterdam, Balkema, 201 - 245.
- Hedge, C. E. 1984. Precambrian geochronology of part of northwestern Saudi Arabia, kingdom of Saudi Arabia. *U.S Geological Survey Open File Report*, **48-381**.
- Henley, R. W. & Ellis, A. J. 1983. Geothermal systems, ancient and modern: a geochemical review. *Earth Science reviews*, **19**, 1 - 50.
- Henley, R. W. 1991. Epithermal gold deposits in volcanic terranes. In Foster, R. P (eds), *Gold Metallogeny and Exploration*. Blackie & Sons Ltd, Glasgow, 133 - 164.
- Hepworth, J. V. 1979. Does the Mozambique orogenic belt continue into Saudi Arabia? In Al-Shanti, A. M. S. (ed.), *Evolution and mineralization of the Arabian-Nubian Shield, volume 1*: Bulletin of the Institute of Applied Geology, Oxford, **3**, 39 - 52.

- Hickey, R. L. & Frey, F. A. 1982. Geochemical characteristics of boninite series volcanics: implications for their source. *Geochemica et Cosmochimica Acta*, **46**, 2099 - 2115.
- Hilmy, M. E. & Hussein, A. A. 1978. A proposed classification for the mineral deposits and occurrences in Egypt. *Precambrian Research*, **6**, Abstract, p128.
- Hippertt, J. F. M. 1993. 'V'-Pull-apart microstructures: a new shear - sense indicator. *Journal of Structural Geology*, **15**, 1393 - 1403.
- Hine, I. S., Chappell, B. W & White, J. R. 1978. Contrasts between I- and S-type granitoids of the Kosciusko batholith. *Journal of the Geological Society of Australia*, **25**, 219 - 234.
- Hoffman, P. F. 1991. Did the breakout of Laurentia turn Gondwana inside-out?. *Science*, **252**, 1409 - 1412.
- Holdsworth, R. E., Strachan, R. A. & Harris, A. L. 1994. Moine supergroup. In Gibbons, W. & Harris, A. L. (eds), *A revised correlation of Precambrian rocks in the British Isles*. Geological Society, London Special Report, **22**, 23 - 32.
- Howell, D, G. 1995. *Principals of Terrane Analysis*, Chapman & Hall, London.
- Hume, W. F. 1934. *Geology of Egypt, Vol. 2, The fundamental Precambrian rocks of Egypt and the Sudan, part 1, The metamorphic rocks*. Geological Survey of Egypt, 1 - 300.
- Hume, W. F. 1935. *Geology of Egypt, Vol. 2, part 2, The later plutonic and intrusive rocks*. Geological Survey of Egypt, 301 - 688.
- Hume, W. F. 1937. *Geology of Egypt, Vol. 2, part 3, The mineral of economic value associated with the intrusive Precambrian igneous rocks*. Geological Survey of Egypt, 689 - 990.
- Hunting Geology & Geophysics Ltd. 1967. *Assessment of the mineral potential of the Aswan region, U.A.R.*, photogeological survey, United Nation Development Program, United Arab Republic. Regional Planning of Aswan.

- Hussein, A. A. 1990. Mineral deposits of Egypt. In Said, R. (ed), *Geology of Egypt*, Balkema, Amsterdam, 511 - 566.
- Hussein, A. A. A., Ali, M. M. & El-Ramly, M. F. 1982. A proposed new classification of the granites of Egypt. *Journal of Volcanology and Geothermal Research*, **14**, 187 - 198.
- Ingersoll, R. V. 1988. Tectonics of sedimentary basins. *Bulletin of Geological Society of America*, **100**, 1704 - 1719.
- Ivanov, T. & Hussein, A. A. 1972. *Report on geological operations in the assessment of the mineral potential of the Aswan Region Project*. Geological Survey of Egypt, Unpublished report.
- Jackson, N. J., Walsh, J. N. & Pegram, E. 1984. Geology, geochemistry and petrogenesis of late Precambrian granitoids in the central Hijaz region of Arabian Shield. *Contributions to Mineralogy and Petrology*, **87**, 205 - 219.
- Jenner, G. A., Cawood, P. A., Rautenschlein, M. & White, W. M. 1987. composition of the back-arc basin volcanics, Valu Fa Ridge, Lau basins: evidence for a slab-derived component in their mantle source. *Journal of Volcanological and Geothermal Research*, **32**, 209 - 222.
- Jordan, T. E. 1995. Retroarc Foreland and related Basins. In Busby, C. J & Ingersoll, R. V (eds), *Tectonics of Sedimentary Basins*, Blackwell Science, Oxford, 331 - 362.
- Karig, D. E. 1985. Kinematic and mechanics of deformation across some accreting forearcs, in Nasu, N., Uyeda, S., Kushiro, I., Kobayashi, K., & Kagami, H. (eds), *Formation of active ocean margins*, Terra Scientific Publishing, 155 - 177.
- Karig, D. E. 1989. Suture zones: what and where are they? *EOS*, **24**, p1307.
- Kazmin, V., Shifferaw, A. & Balcha, T. 1978. The Ethiopian basement: stratigraphy and possible manner of evolution. *Geologische Rundschau*, **67**, 531-546.
- Kemp, J., Pellaton, C. & Calvez, J. Y. 1982. Cycles in the geologic evolution of the Precambrian Shield in part of northwest Saudi Arabia. *Saudi*

Arabian Deputy Ministry for Mineral Resources Professional Paper,
27- 24.

- Kennedy, W. Q. 1964. The structural differentiation of Africa in the Pan-African tectonic episode. *Annual Report 8, Research Institute of African Geology, University of Leeds*, 197-225.
- Kerrich, R. & Fyfe, W. S. 1988. The formation of gold deposits with particular reference to Archean greenstone belts and Yellowknife. *Contributions to the Geology of the Northwest Territories*, **3**, 63 - 95.
- Klein, G. D. 1985. The control of depositional depth, tectonic uplift, and volcanism on sedimentation processes in the backarc basins of the western Pacific Ocean. *Journal of Geology*, **93**, 1 - 25.
- Kretz, R. 1983. Symbols for rock-forming minerals. *American Mineralogist*, **68**, 277 - 279.
- Kröner, A., 1979. Pan-African plate tectonics and its repercussions on the crust of northeast Africa. *Geologische Rundschau*, **68**, 565 - 583.
- Kröner, A. 1983. Evolution of tectonic boundaries in the Late Proterozoic Arabian-Nubian shield of northeast Africa and Arabia. *Abstracts, International Symposium of Precambrian crustal evolution*. Beijing, China. 24 - 25.
- Kröner, A. 1984. Late Precambrian plate tectonics and orogeny: a need to redefine the term Pan-African. In Klerkx, J. & Michot, J. (eds) *African Geology*, Musée Royal de L' Afrique Central, Tervuren, 23 - 28.
- Kröner, A. 1985. Ophiolites and the evolution of tectonic boundaries in the Late Proterozoic Arabian-Nubian Shield of Northeast Africa and Arabia. *Precambrian Research*, **27**, 277 - 300.
- Kröner, A. 1991. Tectonic evolution in the Archaean and Proterozoic. *Tectonophysics*, **187**, 393 - 410.
- Kröner, A. 1993. The Pan-African belt of northeastern and eastern Africa, Madagascar, southern India, Sri Lanka and east Antarctica: Terrane amalgamation during formation of the Gondwana Supercontinent. In Thorweihe, U. & Schandelmeyer, H. (eds.), *Geoscientific Research in Northeast Africa*, 3 - 9.

- Kröner, A., Greiling, R. O., Reischmann, T., Hussein, I. M., Stern, R. J., Durr, S., Druger, J. & Zimmer, M. 1987. Pan-African crustal evolution in the Nubian segment of northeast Africa. In Kröner, A. (ed), *Proterozoic Lithospheric evolution*. American Geophysical Union, Washington D.C, 235 - 257.
- Kröner, A., Reischmann, T., Wust, H. J. & Rashwan, A. A. 1988. Is there any pre-Pan-African (>950 Ma) basement in the Eastern Desert of Egypt?, In El-Gaby, S. & Greiling, R. O. (eds), *The Pan-African Belt of Northeast Africa and adjacent areas; tectonic evolution and economic aspects of a late Proterozoic orogen*. Vieweg & Sohn, Braunschweig/Wiesbaden, 95 - 119.
- Kröner, A., Todt, W., Hussein, I. M., Mansour, M. & Rashwan, A. A. 1992. Dating of late Proterozoic ophiolites in Egypt and the Sudan using the single grain zircon evaporation technique. *Precambrian Research*, **59**, 15 - 32.
- Kröner, A., Kruger, J. & Rashwan, A. A. A. 1994. Age and tectonic setting of granitoid gneisses in the Eastern Desert of Egypt and south-west Sinai. *Geologische Rundschau*, **83**, 502 - 513.
- Le Bas, M. J., Le Maitre, R. W., Streckeisen, A. & Zanettin, B. 1986. A chemical classification of volcanic rocks based on the total alkali-silica diagram. *Journal of Petrology*, **27**, 745 - 750.
- Le Bas, M. J. & Streckeisen, A. L. 1991. The IUGS systematics of igneous rocks. *Journal of the Geological Society, London*, **148**, 825 - 833.
- Le Maitre, R. W. 1984. A proposal by the IUGS subcommission on the systematics of Igneous Rocks for a chemical classification of volcanic rocks based on the total alkali silica (TAS) diagram. *Australian Journal of Earth Sciences*, **31**, 243 - 255.
- Lister, G. S. & Snoke, A. W. 1984. S-C mylonites. *Journal of Structural Geology*, **6**, 617 - 638.
- Lisle, R. J. 1979. Strain analyses using deformed pebbles: The influence of initial pebble shape. *Tectonophysics*, **60**, 263 - 277.
- Lisle, R. J. 1985. *A Manual for the Rf/Ø Technique, Geological Strain Analysis*. Pergamon Press, Oxford.

- Long, C. B. & Max, M. D. 1977. Metamorphic rocks in the SW Ox Mountains Inlier, Ireland; their structural compartmentation and place in Caledonian orogen. *Journal of the Geological Society, London*, **133**, 413-432.
- Lowe, D. R. 1994. Abiological origin of described stromatolites older than 3.2 Ga. *Geology*, **22**, 387 - 390.
- Mandal, N. & Khan, D. 1991. Rotation, offset and separation of oblique-fracture (rhombic) boudins: theory and experiments under layer-normal compression. *Journal of Structural Geology*, **13**, 349 - 356.
- Magaritz, M., Whitford, D. J. & James, D. E. 1978. Oxygen isotopes and the origin of high $87\text{Sr}/86\text{Sr}$ andesites. *Earth Planetary Science Letters*, **40**, 220 - 230.
- Marsaglia, K. M. 1995. Interarc and backarc basins. In Busby, C. J & Ingersoll, R. V (eds), *Tectonics of Sedimentary Basins*. Blackwell Science, Oxford, 299 - 329.
- McClay, K. R. & Insley, M. W. 1986. Duplex structures in the Lewis thrust sheet, Crowsnest Pass, Rocky Mountains, Alberta, Canada. *Journal of Structural Geology*, **8**, 911 - 922.
- McMenamin, M. A. S & McMenamin, D. L. S. 1990. The emergence of animals. *The Cambrian breakthrough*. Columbia University Press, New York.
- Miller, M. M. & Dixon, T. H. 1992. Late Proterozoic evolution of the northern part of the Hamisana zone, northeast Sudan : constraints on Pan-African accretionary tectonics. *Journal of the Geological Society, London*, **149**, 743 - 750.
- Mitropoulos, P., Saunders, A. D. & Marsh, N. G. 1987. Petrogenesis of Cenozoic volcanic rocks from the Aegean Island Arc. *Journal of Volcanology and Geothermal Research*, **32**, 177 - 193.
- Moores, E. M. 1991. Southwest U.S.-East Antarctic (SWEAT) connection: a hypothesis. *Geology*, **19**, 425 - 428.
- Morgan, P. 1990. Egypt in framework of global tectonics. In Said, R. (ed), *Geology of Egypt*. Balkema, Amsterdam, 91 - 111.

- Murphy, J. B. 1989. Tectonic environment and metamorphic characteristics of shear zones. In Bursnall, J. T. (ed.), *Mineralization and Shear zones*. Short Course Notice, Geological Association of Canada, **6**, 29 - 49.
- Oberhänsli, R. 1994. Subducted and obducted ophiolites of the Central Alps: paleotectonic implications deduced by their distribution and metamorphic overprint. *Lithos*, **33**, 109 - 118.
- Pallister, J. S. 1988. Precambrian ophiolites of Arabia: Geologic settings, U-Pb geochronology, Pb-isotope characteristics, and implications for continental accretion. *Precambrian Research*, **38**, 1 - 54.
- Passchier, C. W. & Simpson, C. 1986. Porphyroclast systems as kinematic indicators. *Journal of Structural Geology*, **8**, 831- 844.
- Peacock, D. C. P. 1991. Displacements and segment linkage in strike slip fault zones. *Journal of Structural Geology*, **13**, 1025 - 1035.
- Pearce, J. 1980. Geochemical evidence for the genesis and eruptive setting of lavas from Tethyan ophiolites. In Panayiotou, A. (ed.), *Ophiolites*. Geological Survey of Cyprus, 261 - 272.
- Pearce, J. A. 1983. The role of sub-continental lithosphere in magma genesis at destructive plate margins. In Hawkesworth, C. J. & Norry, M. J. (eds), *Continental basalt and mantle xenoliths*. Shiva Publications, Nantwich, 230 - 249.
- Pearce, J. A. & Cann, J. R. 1973. Tectonic setting of basic volcanic rocks determined using trace element analyses. *Earth and Planetary Science Letters*, **19**, 290 - 300.
- Pearce, J. A & Gale, G. H. 1977. Identification of ore-deposition environment from trace element geochemistry of associated igneous host rocks. *Geological Society, London, Special Publication*, **7**, 14 - 24.
- Pearce, J., Harris, N. B. W. & Tindle, A. G. 1984. Trace element discrimination diagrams for the tectonic interpretation of granitic rocks. *Journal of Petrology*, **25**, 956-983
- Pearce, J. A., Ernewein, M., Bloomer, S. H., Parson, L. M., Murton, B. J., and Johnson, L. E. 1994. Geochemistry of Lau Basin volcanic rocks:

- influence of ridge segmentation and arc proximity. IN Smellie, J. L. (ed.), *Volcanism associated with extension at consuming plate margins*. Geological Society, London, Special Publication, **81**, 53-75.
- Pe-Piper, G., Piper, D. J. W., Kotopouli, C. N. and Panagos, A. G. 1994. Neogene volcanoes of Chios, Greece: the relative importance of subduction and back-arc extension. IN Smellie, J. L. (ed.), *Volcanism associated with extension at consuming plate margins*. Geological Society, London, Special Publication, **81**, 213-231.
- Pettijohn, E. J. 1975. *Sedimentary rocks*. (3rd Edition), Harper & Row, New York.
- Phillips, G. N & Groves, D. I. 1983. The nature of Archean gold bearing fluids as deduced from gold deposits of Western Australia. *Journal of the Geological Society of Australia*, **30**, 25 - 39.
- Piper, J. D. A. 1982. The Precambrian palaeomagnetic record: the case for the Proterozoic supercontinent. *Earth and Planetary Science Letters*, **59**, 61-89.
- Piroshco, D. W. & Hodgson, C. J. 1988. Relationship of hydrothermal alteration to structures and stratigraphy at the Coniaurun Gold Mine, northern Ontario. *Canadian Journal of Earth Sciences*, **25**, 2028 - 2040.
- Pitcher, W. S. 1983. Granite: typology, geological environment and melting relationship. In Atherton, M. P. & Gribble, C. D. (eds), *Migmatites, Melting and Metamorphism*. Shiva Publications, Nantwich, 277-287.
- Pitcher, W. S. 1993. The nature and origin of granite. Blackie & Sons Ltd, Glasgow.
- Plumb, K. A. 1991. A new Precambrian time scale. *Episodes*, **14**, 139 - 140.
- Pohl, W. 1984. Large - scale metallogenetic features of the Precambrian in North-East Africa and Arabia. *Bulletin of Faculty of Earth Sciences, King Abdel Aziz University*. **6**, 591 - 601.
- Porada, H. 1989. Pan-African rifting and orogenies in southern to equatorial Africa and eastern Brazil. *Precambrian Research*, **44**, 103 - 136.

- Potts, P. J. 1987. *A handbook of silicate rock analysis*. Blackie & Sons Ltd, Glasgow.
- Pouclet, A., Lee, J. S., Vidal, P., Cousens, B. and Bellon, H. 1994. Cretaceous to Cenozoic volcanism in south korea and in the Sea of Japan: Magmatic constraints on the opening of the back-arc basin. IN Smellie, J. L. (ed.), *Volcanism associated with extension at consuming plate margins*. Geological Society, London, Special publication. **81**, 169 - 191.
- Powell, C. M., Li, Z. X., McElhinny, M. W, Meert, J. G. and Park, J. K. 1993. Palaeomagnetic constraints on timing of the Neoproterozoic breakup of Rodinia and the Cambrian formation of Gondwana. *Geology*, **21**, 889-892.
- Ramos, V. A. 1988. Late Proterozoic-early Palaeozoic of South America- A collisional history. *Episodes*, **11**, 168 - 174.
- Ramsay, J. G. 1967. *Folding and Fracturing of Rocks*. McGraw-Hill, New York.
- Ramsay, J. G. 1980. Shear zone geometry: A review. *Journal of Structural Geology*, **2**, 83 - 89.
- Ramsay, J. G. & Huber, M. I. 1983. *The Technique of Modern Structural Geology, Volume 1. Strain Analysis*. Academic Press, Orlando.
- Ramsay, J. G. & Huber, M. I. 1987. *The Technique of Modern Structural Geology, Volume II. Folds and Fractures*. Academic Press, Orlando.
- Rankin, A. H., Farmer, C. B., Herrington, R. J., Moser. M. & Wilkinson, J. J. 1990. Improved microthermometric measurements using a new cryogenic attachment to a conventional heating and cooling microscope stage. *Abstracts of the 3rd PACROFI Meeting, Toronto*.
- Rice, A. H. N., Sadek, M. F. & Rashwan, A. A. 1993. Igneous and structural relations in the Pan-African Hammamat Group, Iqla Basin, Egypt. In Thorweihe, U. & Schandelmeier, H. (eds), *Geoscientific Research in northeast Africa*, 35 - 39.
- Ries, A. C., Shackleton, R. M., Graham, R. H. & Fitches, W. R. 1983. Pan-African structures, ophiolites and melanges in the E. D. of Egypt, a

- traverse at 26° N. *Journal of the Geological Society, London*, **140**, 75-95.
- Robert, F. & Kelly, W. C. 1987. Ore-forming fluids in Archean gold-bearing quartz veins at the Sigma Mine, Abitibi greenstone belt, Quebec, Canada. *Economic Geology*, **82**, 1464 - 1482.
- Rock, N. M. S., Carroll, G. W., Wheatley, M. R. & Williams, K. I. L. 1991. SoftWare notice, MacSuite: an integrated compendium of geoscientific programs for the Apple Macintosh. *American Mineralogist*, **76**, 2013 - 2019.
- Roedder, E. 1984. *Fluid inclusions*. Reviews in Mineralogy. **12**, Mineralogical Society of America.
- Rogers, J. J. W., Ghuma, M. A., Nagy, R. M., Greenberg, J. K. & Fullagar, P. D. 1978. Plutonism in Pan-African belts and geologic evolution of northeastern Africa. *Earth and Planetary Science Letters*, **39**, 109 - 117.
- Rollinson, H. 1993. *Using geochemical data: evaluation, presentation, interpretation*. Longman & Scientific Technical, London.
- Rutter, E. H. 1976. The kinetics of rock deformation by pressure solution. *Philosophical Transactions of the Royal Society of London*, **283 A**, 203 - 219.
- Rogers, J. J. W., Unrug, R., Sultan, M. 1995. Tectonic assembly of Gondwana. *Journal of Geodynamic*, **19**, 1 - 34.
- Sabet, A. H. 1972. On the stratigraphy of basement rocks of Egypt. *Annals of the Geological Survey, Egypt*, **2**, 79 - 102.
- Sabet, A. H., Tsogoev, V. B., Bordonosov, V. P., Baburin, L. M., Zalata, A. A. & Francis, M. H. 1976. On gold mineralization in the Eastern Desert of Egypt. *Annals of the Geological Survey, Egypt*, **6**, 120 - 128.
- Sabet, A. H., & Bordonosov, V. P. 1984. The gold ore formations in the Eastern Desert of Egypt. *Annals of the Geological Survey, Egypt*, **14**, 35 - 42.

- Sabine, P. A. 1989. Setting standards in petrology: The commission on systematics in petrology. *Episodes*, **12**, 84 - 86.
- Sabine, P. A., Harrison, R. K. & Lawson, R. I. 1985. Classification of volcanic rocks of British Isles on the total alkali oxide-silica diagram, and the significance of alteration. *Report of the British Geological Survey*, **17**, 1 - 9.
- Sakai, H., Gamo, T., Kim, S. E., Tsutsumi, M., Tanaka, T., Ishibashi, J., Wakita, H., Yamano, M. & Oomori, T. 1990. Venting of carbon dioxide-rich fluid and hydrate formation in mid-Okinawa Trough back-arc basin. *Science*, **248**, 1093 - 1096.
- Saunders, A. D. & Tarney, J. 1979. The geochemistry of basalts from a back arc spreading centre in the East Scotia Sea. *Geochemica et Cosmochimica Acta*, **43**, 555 - 572.
- Saunders, A. D., Tarney, J., Stern, C. & Dalziel, I. W. D. 1979. Geochemistry of Mesozoic marginal basin floor igneous rocks from southern Chile. *Bulletin of Geological Society of America*, **90**, 237 - 258.
- Saunders, A. D., Tarney, J., Marsh, N. G. & Wood, D. A. 1980. Ophiolite as ocean crust or marginal basin crust: a geochemical approach. In Panayiotou, A. (ed.), *Ophiolites*. Geological Survey of Cyprus, 193 - 204.
- Schandelmeier, H., Darbyshire, D. P. F., Harms, U. & Richter, A. 1988. The East Sahara Craton, Evidence for pre-Pan-African Crust in NE Africa west of the Nile. In El Gaby, S. & Greiling, R. O. (eds), *The Pan-African Belt of Northeast Africa and adjacent areas; tectonic evolution and economic aspects of a late Proterozoic orogen*. Vieweg & Sohn, Braunschweig/Wiesbaden, 69 - 94.
- Schandelmeier, H., Küster, D., Wipfler, E., Abdel Rahman, E. M., Stern, R. J., Abdelsalam, M. G. & Sultan, M. 1993. Evidence for a new Late Proterozoic suture in Northern Sudan. In Thorweihe, U. & Schandelmeier, H. (eds), *Geoscientific Research in northeast Africa*. 83 - 85.

- Schandelmeier, H., Wipfler, E., Küster, D., Sultan, M., Becker, R., Stern, R. & Abdelsalam, M. 1994. Atmur-Delgo suture: A Neoproterozoic oceanic basin extending into the interior of northeast Africa. *Geology*, **22**, 563 - 566.
- Schmidt, D. L., Hadley, D. G. & Stoesser, D. B. 1979. Late Proterozoic crustal history of the Arabian Shield, southern Najd province, Kingdom of Saudi Arabia. In Al Shanti, A. M. S. (ed.), *Evolution and mineralization of the Arabian-Nubian Shield*. Bulletin of the Institute of Applied Geology, Jeddah, **3**, 41 - 58.
- Schurman, H. M. E. 1953. The Precambrian of the Gulf of Suez area. *Report of 19th International Geological Congress*. Algiers, **1**, 115 - 135.
- Scott, R. & Kroenke, L. 1980. Evolution of backarc spreading and arc volcanism in the Philippine Sea: interpretation of Leg 59 DSDP results. *American Geophysical Union Geophysical monograph*, **23**, 283 - 291.
- Shackleton, R. M. 1958. Downward-facing structures of the Highland border. *Quarterly, Journal of Geological Society, London*. **113** (for 1957), 361 - 392.
- Shackleton, R. M. 1979. Precambrian tectonics in north-east Africa. In Al Shanti, A. M. S. (ed.), *Evolution and mineralization of the Arabian-Nubian Shield*. *Bulletin of the Institute of Applied Geology, Jeddah*, **2**, 1 - 6.
- Shackleton, R. M. 1986. Precambrian collision tectonics. In Coward, M. P. & Ries, A. C. (eds), *Collision Tectonics*. Geological Society, Special Publication, London, 329 - 349.
- Shackleton, R. M. 1988. Contrasting structural relationships of Proterozoic Ophiolites in Northeast and Eastern Africa. In El Gaby, S. & Greiling, R. O. (eds), *The Pan-African Belt of Northeast Africa and adjacent areas; tectonic evolution and economic aspects of a late Proterozoic orogen*. Vieweg & Sohn, Braunschweig/Wiesbaden, 183 - 193.
- Shackleton, R. M. 1994. Review of late Proterozoic sutures, ophiolitic melanges and tectonics of eastern Egypt and north-east Sudan. *Geologische Rundschau*, **83**, 537 - 546.

- Shackleton, R. M., Ries, A. C., Graham, R. H. & Fitches, W. R. 1980. late Precambrian ophiolitic mélangé in the E.D. of Egypt. *Nature, London*, **285**, 472 - 474.
- Shackleton, R. M. & Ries, A. C. 1984. The relationship between regionally consistent stretching lineations and plate motions. *Journal of Structural Geology*, **6**, 111 - 117.
- Shelley, D. 1993. *Igneous and metamorphic rocks under the microscope: classification, textures, microstructures and mineral preferred orientations*. (paperback edition) Chapman & Hall, London.
- Shelton, K. L., So, C. S. & Chang, J. S. 1988. Gold-rich mesothermal vein deposits of the Republic of Korea: Geochemical studies of the Jungwon gold area. *Economic Geology*, **83**, 1221 - 1237.
- Shepherd, T. J., Rankin, A. H. & Alderton, D. H. M. 1985. *A practical guide to fluid inclusion studies*. Blackie & Sons, Glasgow.
- Sheppard, S. M. F. 1981. Stable isotope geochemistry of fluids. In Richard, D. T. & Wickman, F. E. (eds), *Chemistry and geochemistry of solutions at high temperatures and pressure*. Physical Chemistry of the Earth, **13/14**, 419 - 445.
- Sheppard, S. M. F., Nielsen, R. L. & Taylor, H. P. 1969. Oxygen and Hydrogen isotope ratios of clay minerals from porphyry copper deposits. *Economic Geology*, **64**, 755 - 777.
- Sibson, R. H. 1977. Fault rocks and fault mechanisms. *Journal of the Geological Society, London*, **133**, 191- 213.
- Sibson, R. H., Robert, F. & Poulsen, H. 1988. High angle faults, fluid pressure cycling and mesothermal gold quartz deposits. *Geology*, **16**, 551 - 555.
- Simmons, S. F. & Browne, P. R. L. 1990. Mineralogic, alteration and fluid inclusion studies of epithermal gold-bearing veins at the Mt. Muro prospect, central Kalimaantan (Borneo), Indonesia. In Hedenquist, J. W., White, N. C. & Siddeley, G. (eds), *Epithermal gold mineralization of the circum-pacific, 1*. Special Publication, Journal of Geochemical exploration, **16a**, 63 - 103.

- Simpson, C. 1985. Deformation of granitic rocks across the brittle-ductile transition. *Journal of Structural Geology*, **7**, 503 - 511.
- Simpson, C. 1986. Determination of movement sense in mylonites. *Journal of Geological Education*, **34**, 246 - 261.
- Simpson, C. 1988. Analysis of two dimensional finite strain. In Marshak, S. & Mitra, G. (eds), *Basic methods of structural geology*. Prentice Hall, New Jersey.
- Simpson, C. & Schmidt, S. M. 1983. An evaluation of criteria to deduce the sense of movement in sheared rocks. *Bulletin Geological Society of America*, **94**, 1281 - 1288.
- Soper, N. J. 1994. Was Scotland a vendian RRR junction? *Journal of the Geological Society, London*, **151**, 579 - 582.
- Soper, N. J. & England, R. W. 1995. Vendian and Riphean rifting in NW Scotland. *Journal of the Geological Society, London*, **152**, 11 - 14.
- Spry, A. 1969. *Metamorphic textures*. Pergamon Press, London.
- Stel, H. 1986. The effect of cyclic operation of brittle and ductile deformation on metamorphic assemblages in cataclastites and mylonites. *Pageophysics*, **124**, 289 - 307.
- Stern, R. J. 1981. Petrogenesis and tectonic setting of late Precambrian ensimatic volcanic rocks, central Eastern Desert of Egypt. *Precambrian Research*, **16**, 197-232.
- Stern, R. J. 1993. Tectonic evolution of the Late Proterozoic East African Orogen: Constraints from crustal evolution in the Arabian-Nubian Shield and the Mozambique Belt. In Thorweihe, U. & Schandelmeier, H. (eds.), *Geoscientific Research in Northeast Africa*, 73 - 74.
- Stern, R. J. 1994. Arc assembly and continental collision in the Neoproterozoic East African orogen: implications for the consolidation of Gondwanaland. *Annual Review of Earth and Planetary Sciences*, **22**, 319 - 351.

- Stern, R. J. & Hedge, C. E. 1985. Geochronologic and isotopic constraints on Late Precambrian crustal evolution in the E. D. of Egypt. *American Journal of Science*, **285**, 97 - 127.
- Stern, R. J., Kröner, A., Manton, W. I., Reischmann, T., Mansour, M. & Hussein, I. M. 1989. Geochronology of the late Precambrian Hamisana shear zone, Red Sea Hills, Sudan and Egypt. *Journal of the Geological Society, London*, **146**, 1017 - 1029.
- Stern, R. J., Nielsen, K. C., Best, E., Sultan, M., Arvidson, R. E. & Kröner, A. 1990. Orientation of the late Precambrian sutures in the Arabian-Nubian shield. *Geology*, **18**, 1103 - 1106.
- Stern, R. J. & Bloomer, S. H. 1992. Subduction zone infancy: example from the Eocene Izu-Bonin-Mariana and Jurassic California arcs. *Bulletin of the Geological Society of America*, **104**, 1621 - 1636.
- Stern, R. J. & Kröner, A. 1993. Geochronologic and isotopic constraints on late Precambrian crustal evolution in NE Sudan. *Journal of Geology*, **101**, 555 - 574.
- Stoeser, D. B., Stacey, J. S., Greenwood, W. R. & Fischer, L. B. 1984. *U/Pb zircon geochronology of the southern portion of the Nabitah mobile belt and Pan-African continental collision in the Saudi Arabia shield*. US Geological Survey, Technical Record USGS-TR-04-05.
- Stoeser, D. B. & Camp, V. E. 1985. Pan-African microplate accretion of the Arabian Shield. *Bulletin of the Geological Society of America*. **96**, 817 - 826.
- Stoeser, D. B. & Stacey, J. S. 1988. Evolution, U-Pb geochronology and isotope geology of the Pan-African Nabitah orogenic belt of the Saudi Arabia Shield. In El Gaby, S. & Greiling, R. O. (eds), *The Pan-African Belt of Northeast Africa and adjacent areas; tectonic evolution and economic aspects of a late Proterozoic orogen*. Vieweg & Sohn, Braunschweig/Wiesbaden, 227 - 288.
- Streckeisen, A. 1976. To each plutonic rock its proper name. *Earth Science Reviews*, **12**, 1 - 33.
- Sugden, T. 1987. Kinematic indicators: structures that record the sense of movement in mountain chains. *Geology Today*, **3**, 93 - 99.

- Sultan, M., Bickford, M. E., El Kaliouby, B. & Arvidson, R. E. 1992. Common Pb systematics of Precambrian granitic rocks of the Nubian Shield (Egypt) and tectonic implications. *Bulletin of the Geological Society of America*, **104**, 456 - 470.
- Sultan, M., Tucker, R. D., Gharbawi, R. I., Ragab, A. I. & El Alfy, Z. 1993. On the location of the boundary between the Nubian Shield and the old African continent: Inferences from U-Pb (zircon) and common Pb data. In Thorweihe, U. & Schandelmeier, H. (eds), *Geoscientific Research in northeast Africa*, 75 - 77.
- Surlyk, F. 1991. Tectonostratigraphy of north Greenland. In Peel, J. S. & SØnderholm, M. (eds), *Sedimentary basin of North Greenland*. Bulletin of GrØnlands Geologiske UndersØgelse, **160**, 25 - 47.
- Tamaki, K. & Honza, E. 1991. Global tectonics and formation of marginal basins: role of the western Pacific. *Episodes*, **14**, 224 - 230.
- Takla, M. A., El Dougdoug, A. A., Rasmy, A. A., Gad, M. A. & El Tabal, H. K. 1990. Origin of Um El-Eiga gold mineralization. South Eastern Desert, Egypt. *Egyptian Mineralogist*, **2**, 3 - 20.
- Taylor, B. 1992. Rifting and the volcanic - tectonic evolution of the Izu - Bonin - Mariana arc. *Proceedings of the Ocean Drilling Program, Scientific Results*, **126**, 627 - 651.
- Taylor, H. P. 1974. The application oxygen and hydrogen isotope studies to problems of hydrothermal alteration and ore deposition. *Economic Geology*, **69**, 843 - 883.
- Taylor, B. & Karner, G. D. 1983. On the evolution of marginal basins. *Reviews of Geophysics and Space Physics*, **21**, 1727 - 1741.
- Taylor, W. E. G. 1966. *The structural history of the metamorphic and igneous rocks of Slieve Gamph. Western Ireland*. PhD thesis, University of Sheffield.
- Taylor, W. E. G., Hamed El Kazzaz, Y. A. & Rashwan, A. A. 1993. An outline of the tectonic framework for the Pan-African orogeny in the vicinity of Wadi Um Relan area, south Eastern Desert, Egypt. In Thorweihe, U. & Schandelmeier, H. (eds) *Geoscientific Research in northeast Africa*, 31 - 34.

- Thompson, M. & Walsh, J. N. 1989. *A Handbook of Inductively Coupled Plasma Spectrometry*. (2nd Edition), Blackie & Sons Ltd, Glasgow.
- Thompson, R. N., Morrison, M. A., Hendry, G. L. & Parry, S. J. 1984. An assessment of the relative roles of crust and mantle in magma genesis: an elemental approach. *Philosophical Transactions of the Royal Society of London*, **310A**, 549 - 590.
- Trigger, B. G., 1976. *Nubia under the Pharaohs*. Thames & Hudson Ltd, London.
- Tucker, M. E. 1986. *The field description of sedimentary rocks*. Wiley & Sons, London.
- Underwood, M. B. & Moore, G. F. 1995. Trenches and trench-slope basins. In Busby, C. J & Ingersoll, R. V (eds), *Tectonics of Sedimentary Basins*. Blackwell Science, Oxford, 179 - 219.
- United Nation Department of Technical Co-operation For Development. 1986. *Mineral exploration of the Egypt/Sudan area of Integration*. New York.
- Urai, J. L., Williams, P. F. & van Roermund, H. L. M. 1991. Kinematics of crystal growth in syntectonic fibrous veins. *Journal of Structural Geology*, **13**, 823 - 836.
- Vail, J. R. 1983. Pan-African crustal accretion in north-east Africa. *Journal of African Earth Science*, **1**, 285 - 294.
- Vail, J. R. 1990. Geochronology of the Sudan. *Overseas Geology and Mineral Resources*, **66**, 1 - 58.
- Van Leeuwen, T., Leach, T., Hawke, A. A. & Hawke, M. M. 1990. The Kelian disseminated gold deposit, East Kalimantan, Indonesia. In Hedenquist, J. W., White, N. C. & Siddeley, G. (eds), *Epithermal gold mineralization of the circum-pacific*, 1. Special Publication, Journal of Geochemical Exploration, **16a**, 1 - 61.
- Vikre, P. G. 1981. Silver mineralization in the Rochester District, Pershing County. Nevada. *Economic Geology*, **76**, 580 - 609.

- Walsh, J. N., 1992. Use of multiple internal standards for high- precision, routine analysis of geological samples by inductively coupled plasma-atomic emission spectrometry. *Chemical Geology*, **95**, 113 - 121.
- Walsh, J. F., Kessler, S. E., Duff, D. & Cloke, P. L. 1988. Fluid inclusion geochemistry of high grade vein-hosted gold ore at the Palmour mine, Porcupine Camp, Ontario.
- Watterson, J. 1979. Strain and strain rate gradients at ductile levels of fault displacement. In Speed, R. C. & Sharp, R. V. (eds.), *Analysis of Fault Zones in bedrock*. U.S. Geological Survey, Menlo Park. 235 - 257.
- Whalen, J. B., Currie, K. L. & Chappell, W. B. 1987. A-type granites: Geochemical characteristics, discrimination and petrogenesis. *Contributions to Mineralogy and Petrology*, **95**, 407 - 419.
- White, A. J. R. 1979. Source of granite magmas. *Abstracts Annual Meeting of the Geological Society of America*, **11**, 539.
- White, A. J. R. & Chappel, B. W. 1977. Ultrametamorphism and granitoid genesis. *Tectonophysics*, **43**, 7 - 22.
- White, S. 1982. fault rocks of the Moine thrust zone: a guide to their nomenclature. *Textures and microstructures*, **4**, 211 - 221.
- White, S. H., Burrows, S. E., Carreras, J., Shaw, N. D. & Humphreys, F J. 1980. On mylonites in ductile shear zones. *Journal of Structural Geology*, **2**, 175 - 187.
- White, S. H., Bretan, P. G. & Rutter, E. H. 1986. Fault-zone reactivation: kinematics and mechanisms. *Philosophical Transactions of the Royal Society of London*, **317A**, 81 - 97.
- Whittaker, A., Cope, J. C. W., Cowie, J. W., Gibbons, W., Hailwood, E. A., House, M. R., Jenkins, D. G., Rawson, P. F., Rushton, A. W. A., Smith, D. G., Thomas, A. T. & Wimbledon, W. A. 1991. A guide to stratigraphical procedure. *Journal of the Geological Society, London*, **148**, 813 - 824.
- Wilson. M. 1989. *Igneous petrogenesis, a global tectonic approach*. Chapman & Hall, London.

- Winchester, J. A. & Floyd, P. A. 1977. Geochemical discrimination of different magma series and their differentiation products using immobile elements. *Chemical Geology*, **20**, 325 - 343.
- Wood, P. C., Burrows, D. R., Thomas, A. V. & Spooner, E. T. C. 1986. The Hollinger-McIntyre Au-quartz vein system, Timmins, Ontario, Canada; geological characteristics, fluid properties and light stable isotopes. In Macdonald, A. J. (ed.), *Proceedings of Gold 86*, Toronto, 56 - 80.
- Woodward, N. B., Boyer, S. E. & Suppe, J. 1989. *Balanced geological cross-sections*. Short course in geology: Vol. 6., American Geophysical Union, Washington.
- Worku, H. 1993. Implication of structural evolution of the Adola Belt. in shear zone-hosted gold mineralization. In Thorweihe, U. & Schandelmeier, H. (eds.), *Geoscientific Research in Northeast Africa*, 541 - 547.
- Wright, T. B. 1969. A simple alkalinity ratio and its application to questions of non-orogenic granite genesis. *Geological Magazine*. **106**, 370 - 384.
- Wust. H. J., Todt, W. & Kröner, A. 1987a. Conventional and single grain zircon ages for metasediments and granite clasts from the Eastern Desert of Egypt: evidence for active continental margin evolution in Pan-African times. *Terra Cognita*, **7**, 333.
- Wust. H. J., Reischmann, T., Kröner, A. & Todt, W. 1987b. Conflicting Pb-Pb, Sm-Nd and Rb-Sr systematics in late Precambrian metasediments and metavolcanics from the Eastern Desert of Egypt. *Terra Cognita*, **7**, 333.
- Xavier, R. P. 1991. *The role of microstructural and fluid processes in the genesis of gold bearing shear-zones: Fazenda Maria Preta Mine, Rio Itapicuru greenstone belt, Bahia Brazil*. PhD thesis, University of Southampton.

APPENDICES

List of Contents

- A** List of samples
- B** Geochemical methodologies and data
- C** Strain data
- D** Fluid inclusion methodologies and data
- E** Stable isotope methodology and data
- F** UTM co-ordinate methodology

Appendix A List of samples											
Sp. No.	Location	Rock Type	Tect-strat	TS	Mineral assemblage	Mod	M&T any	Au	Ref Lt	Fl	Isotopes
1.2	5827880508	andesitic dyke	KF	x	Qtz, Pl, Chl, Ep						
1.3	5827880508	phyllite	KF	x	Qz, Chl						
2	5833680566	andesitic dyke	KF	x	Qtz, Pl, Chl, Ep						
2.1	5833680566	phyllite	KF	x	Qtz, Chl						
3	5865680828	dacitic dyke	PCM (KF)	x	Qtz, Pl, Chl, Ep						
4	5871480915	Vc	PCM (KF)	x	Qtz, Pl, Chl						
4.1	5871480915	Sst	PCM (KF)	x	Qtz, Pl, Chl						
4.2	5871480915	peb (of Vc)	PCM (KF)	x	Qtz, Pl, Chl, Ep						
4.3	5871480915	Phyllite	PCM (KF)	x	Qtz, Chl, Ep						
4.4	5871480915	peb (Vc)	PCM (KF)	x	Qtz, Chl, Ep						
4.5	5871480915	Phyllite	PCM (KF)	x	Qtz, Chl, Ep						
4.6	5871480915	Phyllite	PCM (KF)	x	Qtz, Chl						
5	5868579809	andesitic dyke	PCM (KF)	x	Qtz, Pl, Chl, Ep						
5.1	5868579809	Phyllite	PCM (KF)	x	Qtz, Chl, Ep						
5.2	5868579809	peb (Vc)	PCM (KF)	x	Qtz, Pl, Chl, Ep						
6	5935580624	Ep-Chl schist	KF	x	Qtz, Ep, Ch						
7	5932580857	greywacke	PCM (KF)	x	Qtz, Pl, Chl	x					
7.1	5932580857	Sst	PCM (KF)	x	Qtz, Pl, Chl						
7.1A	5932580857	Sst	PCM (KF)	x	Qtz, Pl, Chl						
7.1B	5932580857	greywacke	PCM (KF)	x	Qtz, Pl, Chl	x					
7.2	5932580857	peb (of Vc)	PCM (KF)	x	Qtz, Pl, Chl, Cal, Ep						
7.3	5932580857	peb (of Vc)	PCM (KF)	x	Qtz, Pl, Chl, Ep						
7.4	5932580857	peb (of Vc)	PCM (KF)	x	Qtz, Pl, Chl, Cal, Ep						
7.5	5932580857	peb (of Vc)	PCM (KF)	x	Qtz, Pl, Chl, Ep						
7.7	5932580857	peb (of Vc)	PCM (KF)	x	Qtz, Pl, Chl, Ep						
7.7A	5932580857	peb (of Vc)	PCM (KF)	x	Qtz, Pl, Chl, Cal, Ep						
7.7B	5932580857	peb (of Vc)	PCM (KF)	x	Qtz, Pl, Chl, Ep						

Sp. No.	Location	Rock Type	Tect-strat	TS	Mineral assemblage	Mod	M&T any	Au	Ref Lt	FI	Isotopes
7.8	5932580857	Sst	PCM (KF)	x	Qtz, Pl, Chl						
7.9	5932580857	greywacke	PCM (KF)	x	Qtz, Pl, Chl	x					
8	5222581148	Sst	PCM (KF)	x	Qtz, Pl, Chl						
8.1	5222581148	peb (of Vc)	PCM (KF)	x	Qtz, Pl, Chl, Ep						
8.2	5222581148	peb (of Vc)	PCM (KF)	x	Qtz, Pl, Chl, Cal, Ep						
8.3	5222581148	peb (quartzite)	PCM (KF)	x	Qtz, Pl, Chl, Ep						
8.4	5222581148	peb (of Vc)	PCM (KF)	x	Qtz, Pl, Chl, Cal, Ep						
8.5	5222581148	peb (quartzite)	PCM (KF)	x	Qtz, Chl						
8.6	5222581148	peb (of Vc)	PCM (KF)	x	Qtz, Pl, Chl						
8.7	5222581148	peb (of Vc)	PCM (KF)	x	Qtz, Pl, Chl, Cal, Ep						
8.8	5222581148	peb (phyllite)	PCM (KF)	x	Qtz, Chl						
9	5918081468	mylonite	PCM (KF)	x	Qtz, Chl						
9.1	5918081468	peb (phyllite)	PCM (KF)	x	Qtz, Chl						
9.2	5918081468	peb (of Vc)	PCM (KF)	x	Qtz, Pl, Chl						
10	5999581730	andacitic	PCM (KF)	x	Qtz, Pl, Ch						
11	5984981264	andacitic	PCM (KF)	x	Qtz, Pl, Ch						
11.1	5984981264	andacitic	PCM (KF)	x	Qtz, Pl, Ch						
11.2	5984981264	peb (quartzite)	PCM (KF)	x	Qtz, Pl, Chl, Ep						
11.3	5984981264	peb (quartzite)	PCM (KF)	x	Qtz, Pl, Chl, Ep						
11.4	5984981264	peb (of Vc)	PCM (KF)	x	Qtz, Pl, Chl, Ep						
11.5	5984981264	peb (of Vc)	PCM (KF)	x	Qtz, Pl, Chl, Ep						
13	6078081992	mylonite	KF	x	Qtz, Chl						
13.1	6078081992	dacitic dyke	KF	x	Qtz, Pl, Ch, Ep						
14	6025782370	peb (of Vc)	KF	x	Qtz, Pl, Chl, Cal, Ep						
15	6066482632	Vc	KF	x	Qtz, Pl, Chl						
16	6139282428	Vc	KF	x	Qtz, Pl, Chl						
17	6130483330	Vc	KF	x	Qtz, Pl, Chl						
17.1	6130483330	meta-basalt	KF	x	Pl, Qtz, Act, Tr, Chl						

Sp. No.	Location	Rock Type	Tect-strat	TS	Mineral assemblage	Mod	M&T any	Au	Ref Lt	Fl	Isotopes
17.2	6130483330	peb (of Vc)	KF	x	Qtz, Pl, Chl						
18	6223583330	Sst	KF	x	Qtz, Pl, Chl						
19	6194483970	Vc	KF	x	Qtz, Pl, Chl						
21	6290583970	Vc	KF	x	Qtz, Pl, Chl						
23	6229484669	Vc	AF	x	Qtz, Pl, Chl						
23.1	6229484669	Vc	AF	x	Qtz, Pl, Chl						
27	6339985833	Vc	AF	x	Qtz, Pl, Chl						
28	6241085251	Sst	AF	x	Qtz, Pl, Chl						
29	6369086415	Sst	AF	x	Qtz, Pl, Chl						
31.1	6258585716	peb (of Vc)	AF	x	Qtz, Pl, Chl, Ep						
31.11	6258585716	peb (of Vc)	AF	x	Qtz, Pl, Chl, Ep						
32	6174185600	Sst	AF	x	Qtz, Pl, Chl						
34	6107185716	Sst	AF	x	Qtz, Pl, Chl						
38	5973383883	ande-basalt	KF	x	Qtz, Pl, Ch, Act						
39	6051984116	Subvolcanic	KF	x	Qtz, Pl, Chl						
43	6133386677	Vc	AF	x	qtz, Pl, Chl, Ep	x	x				
43.1	6133386677	greywacke	AF	x	Qtz, Pl, Chl	x					
44	6194486531	arenite	AF	x	Qtz, Chl						
45	6310886648	arenite	AF	x	Qtz, Chl						
46	6372086531	Sst	AF	x	Qtz, Pl, Chl						
47	6334187055	Sst	AF	x	Qtz, Pl, Chl						
50	6372087637	Vc	AF	x	Qtz, Pl, Chl						
52	6919086444	Vc	AF	x	Qtz, Pl, Chl						
55	6633987375	Arenite	AF	x	Qtz, Chl						
58	6642688103	Sst	MCM (AF)	x	Qtz, Pl, Chl						
60	6386588161	ande-basalt	AF	x	Qtz, Pl, Ch, Act						
61	6409889208	mylonite	AF	x	Qtz, Pl, Chl						
71	6494292206	phyllite	URS	x	Qtz, Pl, Chl		x				

Sp. No.	Location	Rock Type	Tect-strat	TS	Mineral assemblage	Mod	M&T any	Au	Ref Lt	FI	Isotopes
71.1	6494292206	phyllite	URS	x	Qtz, Pl, Chl						
72	6578691769	mylonite	URS	x	Qtz, Chl		x				
72.1	6578691769	phyllite	URS	x	Qtz, Pl, Chl						
73	6532092642	granite	URG	x	Qtz, Mc, Pl, Ms, Zrn	x	x				
73.1	6532092675	granite	URG	x	Qtz, Mc, Pl, Ms, Zrn	x					
73.2	6532092642	Sst	URS	x	Qtz, Pl, Chl						
73.3	6531592639	granite	URG		Qtz, Mc, Pl, Ms, Zrn	x					
75.1	6566993312	Sst	URS	x	Qtz, Pl, Chl						
95	5301193050	meta-andesite	KhF	x	Qtz, Pl, Chl, Ep						
95.1	5301193050	meta-andesite	KhF	x	Qtz, Pl, Chl, Ep						
96.2	6700893923	Sst	KhF		Qtz, Pl, Chl, Ep						
98	6837693515	Meta-andesite	KhF	x	Qtz, Pl, Chl, Ep						
99	6811494272	Vc	KhF	x	Qtz, Pl, Chl, Ep						
99.1	6811494272	metalimestone	KhF	x	Cal, Qtz						
99.2	6811494272	metalimestone	KhF	x	Cal, Qtz						
100	6878394505	Phyllite	KhF	x	Qtz, Chl, Ep						
102	7405086269	mylonite	ASZ	x	Qtz, Pl, Chl, Ep						
102.1	7405086269	graphite sch.	ASZ	x	Qtz, Gr, Chl						
103	7480786502	Vc	KhF	x	Qtz, Pl, Chl, Ep						
103.1	7480786502	Vc	KhF	x	Qtz, Pl, Chl, Ep						
106	7681587026	mylonite	ASZ	x	Qtz, Pl, Chl, Ep						
107	7742686589	granite	KG	x	Mc, Ab, Qtz, Pl						
108	7754286269	aplitic dyke	dyke	x	Mc, Qtz, Pl, Tur						
118	7684488510	breccia	PBF (KS)	x	Pl, Chl, Qtz						
123	7518591245	breccia	MF (KS)	x	Pl, Chl, Qtz						
125	7742691333	metalimestone	MF (KS)	x	Cal, Qtz						
125.2	7742691333	granite	MF (KS)	x	Mc, Ab, Qtz, Pl						
126	7760084698	breccia	MF (KS)	x	Pl, Chl, Qtz						

Sp. No.	Location	Rock Type	Tect-strat	TS	Mineral assemblage	Mod	M&T any	Au	Ref Lt	FI	Isotopes
127	7719393544	meta basalt	KS(MLF)	x	Pl, Act, Tr, Chl, Qtz						
127.1	7719393544	metalimestone	MLF (KS)	x	Cal, Qtz						
128	7643692962	meta-basalt	MLF (KS)	x	Pl, Act, Tr, Chl						
133	6788178267	meta-gabbro	MGU	x	Pl, Hbl, Tr, Act, Chl						
134	7271191042	granite	KhF	x	Mc, Qtz, Pl						
149	7399285833	CSst	ASZ	x	Qtz, Cal, Chl, Ep						
150	7387585891	metalimestone	ASZ	x	Cal, Qtz						
150.1	7387585891	Sst	ASZ	x	Qtz, Pl, Chl, Ep						
150.2	7387585891	CSst	ASZ	x	Qtz, Cal, Chl, Ep						
151	7469085833	CSst	ASZ	x	Qtz, Cal, Chl, Ep						
151	7469085833	metalimestone	ASZ	x	Cal, Qtz						
152	7495285629	CSst	ASZ	x	Qtz, Cal, Chl, Ep						
153	7637885571	granite	KG	x	Mc,Ab, Qtz, Pl						
159	7189784320	granite	AF	x	Mc,Ab, Qtz, Pl						
159.1	7189784320	andesite	AF	x	Qtz, Pl, Chl, Ep						
160	7242084611	Sst	AF	x	Qtz, Pl, Chl, Ep						
167	7399282341	granite	G B F	X	pl+qtz+chl	x	x				
167.1	6721283854	granite	G B F	x	pl+qtz+chl						
167.2	7399282341	Sst	G B F	x	Qtz, Pl, Chl, Ep						
167.3	7399282341	peb (Gr)	G B F	x	pl+qtz+chl						
167.4	7399282341	peb (Gr)	G B F	x	pl+qtz+chl						
167.4	7399282341	peb (Gr)	G B F	x	pl+qtz+chl						
171.1	7329380944	CSst	KF	x	Qtz, Cal, Chl, Ep						
173	7160680653	meta-gabbro	KF	x	Pl, Hbl, Tr, Act, Chl, Qtz						
173.1	7160680653	greywacke	KF	x	Qtz, Pl, Chl	x					
173.1A	7160680653	phyllite	KF	x	Qtz, Chl						
174	6514578441	meta-gabbro	MGU	x	Pl, Hbl, Tr, Act, Chl, Qtz						
175	6712478965	meta-basalt	Mbm (KF)	x	Pl, Tr, Act, Chl, Ep, Qtz						

Sp. No.	Location	Rock Type	Tect-strat	TS	Mineral assemblage	Mod	M&T any	Au	Ref Lt	Fl	Isotopes
176	6433175793	Tr-Act schist	GTW	x	Tr, Act, Qtz, Chl						
177	5711481788	phyllite	KF	x	Qtz, Chl						
177.1	5711481788	greywacke	KF	x	Qtz, Pl, Chl	x					
178	5659082137	granite	KF	x	Mc, Qtz, Pl						
180	5787082486	Vc	KF	x	Qtz, Pl, Chl, Ep						
185	5609584291	Sst	KF	x	Qtz, Pl, Chl, Ep						
189	5420484785	greywacke	KF	x	Qtz, Pl, Chl	x					
192	5475786269	met-basalt	Mbm (KF)	x	Pl, Tr, Act, Chl, Ep, Qtz						
192.1	5475786269	agglomerate	Mbm (KF)	x	Pl, Ch, Qtz						
192.2	5475786269	meta-basalt	Mbm (KF)	x	Pl, Tr, Act, Chl, Ep, Qtz						
196	5228384843	Sst	KF	x	Qtz, Pl, Chl, Ep						
201	5496090780	CSst	KF	x	Qtz, Cal, Pl, Chl						
201A	5496090780	Metalimestone	KF	x	Cal, Qtz						
201B	5496090780	andesitic dyke	KF	x	Qtz, Pl, Chl, Ep						
201.1	5496090780	CSst	KF	x	Qtz, Cal, Pl, Chl						
201.2	5496090780	dolerite	AtG	x	Pl, Hbl						
204	5528189208	meta-basalt	Mbm (KF)	x	Pl, Tr, Act, Chl, Ep, Qtz						
205	5565986153	Vc	KF	x	Qtz, Pl, Chl, Ep						
206	5539788626	meta-basalt	Mbm (KF)	x	Pl, Tr, Act, Chl, Ep, Qtz						
207	5449588685	Sst	KF	x	Qtz, Pl, Chl						
208	5461188219	Vc	KF	x	Qtz, Pl, Chl						
209	5397188161	Vc	KF	x	Qtz, Pl, Chl, Ep						
222	7012277976	Chl schist	GTW	x	Chl						
224	6421477568	Tr-Act schist	Tr-Act Unit	x	Tr, Act, Qtz, Chl						
224.1	6421477568	Gr schist	Tr-Act Unit	x	Gr, Qtz						
225.1	6351679285	Tr-Act schist	Tr-Act Unit	x	Tr, Act, Qtz, Chl						
225.2	6351679285	Sst	KF	x	Qtz, Cal, Chl, Ep						
227	6191571312	granite	FG	x	Mc, Ab, Qtz, Pl, Bt						

Sp. No.	Location	Rock Type	Tect-strat	TS	Mineral assemblage	Mod	M&T any	Au	Ref Lt	Fl	Isotopes
228	6121773727	meta-basalt	NF	x	Pl, Tr, Act, Chl						
230	6174174397	blue schist	GTW	x	Ch, Pl, Gln						
230.2	6174174397	meta-gabbro	MGJ	x	Pl, Hbl, Tr, Act						
234	5830776026	granite	FG	x	Mc, Ab, Qtz, Pl, Bt						
235	5720178121	granite	FG	x	Mc, Ab, Qtz, Pl, Bt						
239	6668872971	Sst	NF	x	Qtz, Pl, Chl						
241	6596074542	CSst	NF	x	Qtz, Cal, Chl						
244	6508776666	Meta-basalt	NF	x	Pl, Tr, Act, Chl						
249	7812479460	cal.s.st	ASZ	x	Qtz, Cal, Chl						
263	8001673291	quartzite	ASZ	x	Qtz, Chl						
264	8039473698	Phyllite	ASZ	x	Qtz, Chl						
266	8097676899	Sst	ASZ	x	Qtz, Pl, Chl						
301	6494291187	granite	AF	x	Mc, Qtz, Pl						
307	6511688976	phyllite	AF	x	Qtz, Pl, Chl, Tr						
308	6409888859	greywacke	AF	x	Qtz, Pl, Ch	x					
313.3	5222585513	Sst	KF	x	Qtz, Pl, Ch						
315	5577590838	meta-basalt	KF	x	Pl, Act, Ch						
316	5589291158	granite	AtG	x	Pl+Qtz+Chl+Hbl	x	x				
316A	5589291158	granite	AtG	x	Pl+Qtz+Chl+Hbl						
316.1	5589291158	dolerite sill	AtG	x	Pl, Hbl						
319	5560191798	Vc	Atshani pit	x	Qtz, Pl, Chl, Py, Gt, Bt, Cal			x			
319.3	5560191798	quartz vein	Atshani pit	x	Qtz, Chl, Py, Gt, Ank			x	x	x	x
319.4	5560191798	greywacke	FS	x	Qtz, Pl, Chl						
320	5548491507	quartz vein	Atshani pit	x	Qtz, Chl, Py, Gt			x	x		x
321	5606691566	dolerite sill	AtG	x	Pl, Hbl						
322.1	5606691566	dolerite sill	AtG	x	Pl, Hbl						
324	5926792089	granite	AtG	x	Pl, Qtz, Chl, Hbl, Gt, Zrn						
325.1	6566994010	Sst	URS	x	Qtz, Pl, Chl, Ep						

Sp. No.	Location	Rock Type	Tect-strat	TS	Mineral assemblage	Mod	M&T any	Au	Ref Lt	FI	Isotopes
327	6479690838	granite	AF	x	Mc, Qtz, Pl, Zrn						
328.1	6622288161	peb (of Vc)	MCM (AF)	x	Qtz, Pl, Ch						
329	6578687462	ande.-basalt	AF	x	Pl, Qtz, Chl. Act						
330.1	6133385775	Sst	AF	x	Qtz, Pl, Chl						
331.1	6121782254	basic sill	KF	x	Pl, Ch, Ep						
331.2	6121782254	basic sill	KF	x	Pl, Ch, Ep						
331.3	6121782254	basic sill	KF	x	Pl, Ch, Ep						
332.2	6060681817	peb (of Vc)	KF	x	Qtz, Cal, Pl, Chl						
332.3	6060681817	CSst	KF	x	Qtz, Pl, Chl						
335.1	7783373989	Graphite sch.	KF	x	Gr, Qtz, Chl						
335.2	7783373989	metabasalt	KF	x	Pl, Ac, Tr, Chl, Ep						
335.3	7783373989	Sst	KF	x	Qtz, Pl, Chl						
335.4	7783373989	CSst	KF	x	Qtz, Cal, Chl, Ep, PL						
336	7920174629	meta-gabbro	MGU	x	Pl, Hbl, Tr, Act, Qtz						
337	6415677801	Tr-Act schist	Tr-Act Unit	x	Tr, Act, Qtz, Chl						
338	5810377598	meta-gabbro	MGU	x	Pl, Hbl, Tr, Act, Qtz						
341	5504876841	granite	FG	x	Mc, Ab, Qtz, Pl, Bt						
342	5478685687	meta-basalt	Mbm (KF)	x	Pl, Act, Chl		x				
342A	5478685687	meta-basalt	Mbm (KF)	x	Pl, Act, Chl						
342.1	5478685687	breccia	Mbm (KF)	x	Pl, Chl, Ep, Qtz						
344	5629985862	Sst	KF	x	Qtz, Pl, Ch						
349	6919087288	mylonite	AF	x	Qtz, Pl, Chl, Ep						
352	7893990634	Vc	MF (KS)	x	Qtz, Chl, Tr, Act						
355	7538991071	breccia	MF (KS)	x	Pl, Qtz, Chl, Py						
355.1	7538991071	breccia	MF (KS)	x	Pl, Qtz, Chl, Py						
356.1	7527289820	breccia	MF (KS)	x	Pl, Qtz, Chl, Py						
356.2	7527289820	FerVc	MF (KS)	x	Qtz, Mc, Pl, Hem						
356.3	7527289820	Peb (of Vc)	MF (KS)	x	Pl, Qtz, Hem						

Sp. No.	Location	Rock Type	Tect-strat	TS	Mineral assemblage	Mod	M&T any	Au	Ref Lt	Fl	Isotopes
356.4	7527289820	Sst	MF (KS)	x	Qtz, Pl						
356.5	7527289820	Peb (Volcan)	MF (KS)	x	Pl, Qtz, Hem						
356.7	7527289820	breccia	MF (KS)	x	Pl, Qtz, Chl, Py						
357	7533091042	FerVc	MF (KS)	x	Qtz, Mc, Pl, Hem						
357A	7533091042	Peb (of Vc)	MF (KS)	x	Pl, Qtz, Hem						
357.1	7533091042	FerVc	MF (KS)	x	Qtz, Mc, Pl, Hem						
357.1A	7533091042	FerVc	MF (KS)	x	Qtz, Mc, Pl, Hem						
357.2	7533091042	Peb (of Vc)	MF (KS)	x	Pl, Qtz, Hem						
357.2A	7533091042	Peb (of Vc)	MF (KS)	x	Pl, Qtz, Hem						
358	7532091032	breccia	MF (KS)	x	Pl, Qtz, Chl, Py						
358.1	7532091032	breccia	MF (KS)	x	Pl, Qtz, Chl, Py						
358.2	7532091032	breccia	MF (KS)	x	Pl, Qtz, Chl, Py						
361	7879390227	grey wacke	MF (KS)	x	Qtz, Pl, Chl	x					
361.1	7879390227	grey wacke	MF (KS)	x	Qtz, Pl, Chl	x					
361.1	7879390227	Vc	MF (KS)	x	Qtz, Chl, Act						
362	7899790634	dolerite	MF (KS)	x	Pl, Hb, Act						
362.2	7899790634	grey wacke	MF (KS)	x	Qtz, Pl, Chl	x					
363	7899790518	grey wacke	MF (KS)	x	Qtz, Pl, Chl	x					
365	7800890169	grey wacke	MF (KS)	x	Qtz, Pl, Chl	x					
366	7730989820	mylonite	MF (KS)	x	Qtz, Pl, Chl						
367	7591289761	CSst	MF (KS)	x	Qtz, Cal, Pl, Chl, Ep						
368	7640788597	breccia	PBF (KS)	x	Pl, Qtz, Chl, Py						
368.1	7640788597	breccia	PBF (KS)	x	Pl, Qtz, Chl, Py						
368.1A	7640788597	breccia	PBF (KS)	x	Pl, Qtz, Chl, Py						
368.1B	7640788597	breccia	PBF (KS)	x	Pl, Qtz, Chl, Py						
368.2	7640788597	dolerite sill	PBF (KS)	x	Pl, Hb, Act						
368.3	7640788597	breccia	PBF (KS)	x	Pl, Qtz, Chl, Py						
368.3A	7640788597	breccia	PBF (KS)	x	Pl, Qtz, Chl, Py						

Sp. No.	Location	Rock Type	Tect-strat	TS	Mineral assemblage	Mod	M&T any	Au	Ref Lt	FI	Isotopes
369	7792076404	granite	KG	x	Mc, Qtz, Pl						
370	7789188103	granite	KG	x	Mc, Qtz, Pl	x	x				
370.1	7789188103	granite	KG	x	Mc, Qtz, Pl						
370.3	7789188103	granite	KG	x	Mc, Qtz, Pl						
371	7439988859	Sst	KhF	x	Qtz, Pl, Chl, Ep						
371.1	7439988859	Vc	KhF	x	Qtz, Chl, Ep						
371.2	7439988859	dolerite	KhF	x	Pl, Hb, Act						
373	7128676172	Tr-Act schist	Tr-Act Unit	x	tr, Act, Qtz, Chl						
373.1	7128676172	Tr-Act schist	Tr-Act Unit	x	tr, Act, Qtz, Chl						
373.1A	7128676172	Tr-Act schist	Tr-Act Unit	x	tr, Act, Qtz, Chl						
374	7198470235	dunite	GTW	x	Ol, Sps						
374.1	7198470235	CSst	NF	x	Qtz, Cal, Ch						
374.1A	7198470235	dunite	GTW	x	Ol, Sps						
375	7262471108	phyllite	NF	x	Qtz, Chl						
375A	7262471108	grey wacke	NF	x	Qtz, Pl, Ch						
376	7180972185	Gr schist	NF	x	Qtz, Gr, Chl						
376.1	7180972185	Gr schist	NF	x	Qtz, Gr, Chl						
376.2	7180972185	Gr schist	NF	x	Qtz, Gr, Chl						
377	7180972185	basaltic sill	NF	x	Pl, Act, Chl, Ep						
379	7285773989	Vc	NF	x	Qtz, Pl, Chl, Ep						
382	7387573145	Serpentinite	GTW	x	Sps, Ctl, Tlc, Chr						
382A	7387573145	Serpentinite	GTW	x	Sps, Ctl, Tlc, Chr						
382.1A	7387573145	Serpentinite	GTW	x	Sps, Ctl, Tlc, Chr						
383.2	Fig. 5.2	quartz vein	N.of the area	x	Qtz, Chl, Py, Bt			x	x		x
384	5792980944	andesitic dyke	KF	x	Pl, Qtz, Chl		x				
388	5920982254	quartz vein	KF	x	Qtz, Chl			x			
390	5979182137	quartz vein	KF	x	Qtz, Chl			x	x	x	x
391	6194485251	Vc	AF	x	Qtz, Pl, Chl, Ep		x				

Sp. No.	Location	Rock Type	Tect-strat	TS	Mineral assemblage	Mod	M&T any	Au	Ref Lt	Fl	Isotopes
391.1	6194485251	basalt-andesit	AF	x	Pl, Qtz, Chl		x				
392.1	6700890023	metalimestone	URS	x	Cal, Qtz		x				
393	6628088103	phyllite	AF	x	Qtz, Chl		x				
395	7809575968	phyllite	KF	x	Qtz, Chl		x				
397	7864878529	phyllite	ASZ	x	Qtz, Cal, Pl			x			
398	7888178354	phyllite	ASZ	x	Qtz, Cal, Pl			x			
398.1	7888178354	quartz vein	ASZ	x	Qtz, Chl, Py			x			
398.3	7888178354	phyllite	ASZ	x	Qtz, Cal, Pl			x			
398.4	7888178354	smoky qz vein	ASZ	x	Qtz, Chl, Py			x	x		x
398.5	7888178354	quartz vein	ASZ	x	Qtz, Chl, Py			x	x		x
398.6	7888178354	phyllite	ASZ	x	Qtz, Cal, Pl			x			
398.6	7888178354	phyllite	ASZ	x	Qtz, Cal, Pl			x			
398.8	7888178354	Mylonite	ASZ	x	Qtz, Pl, Chl, Ep		x				
398.9	7888178354	Quartz vein	ASZ	x	Qtz, Pl, Chl, Ep, Cal, Py			x			
398.9	7888178354	qz vein	ASZ	x	Qtz, Pl, Chl, Ep, Cal, Py			x			
399	7847378762	phyllite	ASZ	x	Qtz, Pl, Chl, Ep, Cal, Py			x			
399.1	7847378762	smoky qz vn	ASZ	x	Qtz, Pl, Chl, Ep, Cal, Py			x			
399.2	7847378762	phyllite	ASZ	x	Qtz, Pl, Chl, Ep, Cal, Py			x			
399.3	7847378762	phyllite	ASZ	x	Qtz, Pl, Chl, Ep, Cal, Py			x			
399.4	7847378762	qz vein	ASZ	x	Qtz, Pl, Chl, Ep, Cal, Py			x			
399.5	7847378762	Serpentinite	ASZ	x	Sps, Ctl, Tlc, Chr						
399.5	7847378762	Serpentinite	ASZ	x	Sps, Ctl, Tlc, Chr						
399.6	7847378762	CSst	ASZ	x	Qtz, Cal, Ep, Chl		x				
401	7736780333	granite	KG	x	Mc, Qtz, Pl, Zrn						
401.1	7736780333	phyllite	ASZ	x	Qtz, Chl, Ep		x				
401.2	7736780333	mylonite	ASZ	x	Qtz, Pl, Chl, Ep		x				
401.3	7736780333	Chl schist	ASZ	x	Ch, Qtz, Cal						
402	7495274979	MG	MG Unit	x	Hbl, Pl, Tr, Act, Qtz, Ep, Cal		x				

Sp. No.	Location	Rock Type	Tect-strat	TS	Mineral assemblage	Mod	M&T any	Au	Ref Lt	FI	Isotopes
402A	7495274979	Tr-Act schist	Tr-Act Unit	x	Tr, Act, Qtz, Ep, Cal						
402.1	7495274979	MG	MG Unit	x	Hbl, Pl, Tr, Act, Qtz, Ep, Cal		x				
403	7629174804	Tr-Act schist	Tr-Act Unit	x	Tr, Act, Qtz, Ep, Cal			x			
404	7780473756	Vc	KF	x	Qtz, Pl, Chl, Ep, Cal		x				
404.1	7780473756	Vc	KF	x	Qtz, Pl, Chl, Ep, Cal		x				
405	7774673698	Vc	KF	x	Qtz, Pl, Chl, Ep, Cal			x	x		
405.1	7774673698	altered vc	KF	x	Qtz, Pl, Chl, Ep, Cal			x	x		
405.2	7774673698	altered vc	KF	x	Qtz, Pl, Chl, Ep, Cal			x	x		
405.3	7774673698	altered vc	KF	x	Qtz, Pl, Chl, Ep, Cal			x	x		
405.4	7774673698	altered vc	KF	x	Qtz, Pl, Chl, Ep, Cal			x	x		
405.5	7774673698	altered vc	KF	x	Qtz, Pl, Chl, Ep, Cal			x	x		
405.6	7774673698	altered vc	KF	x	Qtz, Pl, Chl, Ep, Cal			x	x		
407	7387573155	Chl schist	GTW	x	Chl						
407.1	7387573155	dunite	GTW	x	Ol, Sps, Chr		x				
407.2	7387573155	dunite	GTW	x	Ol, Sps		x				
407.3	7387573155	serpentinite	GTW	x	Sps, Ctl, Tlc, Chr		x				
407.5	7387573155	Chl schist	GTW	x	Chl		x				
407.6	7387573155	Chl schist	GTW	x	Chl			x			
412	7300282108	basaltic sill	KF	x	Pl, Chl, Act		x				
413	7148980100	dacitic dyke	KF	x	Qtz, Pl, Chl, Ep		x				
413.1	7148980100	basic sill	KF	x	Pl, Chl, Act, Ep		x				
414	6459379198	meta-basalt	Mbm (KF)	x	Pl, Tr, Act, Chl, Ep		x				
414A	6459379198	meta-basalt	Mbm (KF)	x	Pl, Tr, Act, Chl, Ep						
415	6462279460	Vc	KF	x	Qtz, cal, Pl, Chl		x				
416	6677578849	meta-gabbro	MGU	x	Pl, Hbl, Chl, Tr, Act, Qtz		x				
416.1	6677578849	Vc	KF	x	Qtz, Pl, Chl, Ep, Cal		x				
417	6316780595	qz vein	KF	x	Qtz, Chl			x			
417.1	6316780595	Vc	KF	x	Qtz, Pl, Chl, Ep, Cal		x				

Sp. No.	Location	Rock Type	Tect-strat	TS	Mineral assemblage	Mod	M&T any	Au	Ref Lt	Fl	Isotopes
418	6313880217	Vc	KF	x	Qtz, Pl, Chl, Ep, Cal		x				
418.1	6313880217	Vc	KF	x	Qtz, Pl, Chl, Ep, Cal		x				
420	6587372709	vc	NF	x	Qtz, Pl, Chl, Ep, Cal			x			
422	6680472738	Vc	NF	x	Qtz, Pl, Ep, Chl		x				
422.1	6680472738	Vc	NF	x	Qtz, Pl, Ep, Chl		x				
424	5542681410	meta-gabbro	MGU	x	Hbl, Tr, Act, Qtz, Chl, Pl		x				
425	5461181497	Vc	KF	x	Qtz, Pl, Ep, Chl		x				
500	Fig. 5.2	qz vein	Um Geir pit	x	Qtz, Chl			x	x		x
500.1	Fig. 5.2	Vc	Um Geir pit	x	Qtz, Pl, Ch			x			
500.2	Fig. 5.2	Vc	Um Geir pit	x	Qtz, Pl, Ch			x	x		
600	Fig. 5.2	qz vein	Um Garayat	x	Qtz, Chl, Py			x	x	x	x
601	Fig. 5.2	qz vein	Um Garayat	x	Qtz, Chl, Py			x	x		x
602	Fig. 5.2	qz vein	Um Garayat	x	Qtz, Chl, Py			x			
602.1	Fig. 5.2	qz vein	Um Garayat	x	Qtz, Chl, Py						
636	7087883272	Vc	AF	x	Qtz, Cal, Chl			x			
664	6008291711	granite	AtG	x	Qtz, Pl, Hbl, Chl, Zrn						
700	5478674280	monzo gr.	FG	x	Mc, Or, Qtz, Pl, Bt, Zrn	x	x				
700.1	5478674280	granite	FG	x	Mc, Or, Qtz, Pl, Bt, Zrn						
703	6293486619	Vc	AF	x	Qtz, Pl, Cal, Chl			x			
705	6293489732	Vc	AF	x	Qtz, Pl, Cal, Chl			x			
1000	N. of the area	pelitic rocks			Qtz, Pl, Bt, Grt, Sil						

Appendix B Geochemical methodologies and data

(1) Methodologies for determination of major and trace elements.

(a) inductively coupled plasma-atomic emission spectrometry (ICP-AES) at Royal Holloway College was employed for quantitative determination of both major and trace elements in selected rocks (Appendix A). The advantages of ICP-AES for elemental analysis include: good detection limits, an excellent range of determinable elements, the ability to analyse many types of samples and cost effectiveness and speed of analysis (Thompson & Walsh 1989; Walsh 1992).

(i) Preparation of major element solutions: the rock powder was ignited in a crucible 0.5g of ignited rock powder was weighed accurately into a platinum crucible. 1.5g of lithium metaborate was added and mixed carefully. The crucible was covered partially with a clean platinum lid and fused at 900°C on a bunsen burner for 30 minutes. The crucible was gently swirled several times in the course of the fusion to ensure a complete fusion. The crucible was allowed to cool and placed upright in a polythene beaker containing 200 ml of HNO₃ (5%v/v). The material was stirred until all the fusion bead has dissolved. The beaker contents were washed into a 1000 ml volumetric flask and diluted to volume and the solutions were stored in polythene bottles.

(ii) Preparation of trace element solutions: 0.2g of sample was weighed into clean platinum crucible, 6 ml. of 1:2 mixture of perchloric acid and hydrofluoric acid was added to crucible and then evaporated to dryness. After cooling 2 ml of hydrochloric acid was added to the contents of the crucible and topped up to 3/4 full with distilled water. The mixture was warmed for no more than 15 minutes. When cooled the mixture was made up to 20 ml.

(b) X-ray fluorescence (XRF) was used in order to obtain major and minor element analyses for lava and volcanoclastic rocks to define the parent rock at the University of Luton.

(c) Determination of gold

An inductively coupled plasma-mass spectrometry (ICP-MS) at the NERC facilities, then at Royal Holloway College, capable of extending applications to samples containing parts per billion (ppb) levels was used to analyse selected samples for gold (Appendix A)

Standard procedure for the Aqua Regia Leach: Gowing and Potts (1991), freshly prepared Aqua Regia 20 ml (Aqua Regia was freshly prepared before each experiment by mixing AnalaR or Aristar grade concentrated nitric and hydrochloric acids) was added to the rock powder (10.0 ± 0.1 g) in 150 ml borosilicate glass beakers and mixed using a polytetrafluoroethylene rod until completely wetted. The beaker was covered with a watch-glass and the mixture stirred on a magnetic stirring table for 1 hour at room temperature. The contents of the beaker were then poured into a filter funnel fitted with Whatman 40 filter-paper together with washing from both beaker and watch-glass cover, rinsed with the minimum volume of de-ionized water. After filtration, the filter-paper and residue were transferred into a polythene bag and sealed for subsequent analysis, as appropriate. The filtrate was transferred into a graduated flask (100 ml) and made up to volume with de-ionized water. Beaker and storage flasks were cleaned before use by soaking in laboratory cleaner overnight and then rinsing with de-ionized water. Between runs, other glassware was rinsed with 50% nitric acid (AnalaR) and then de-ionized water. Each batch of samples included a blank Aqua Regia control (processed in the same way as the samples) and all leach experiments were performed in duplicate.

(d) the JEOL JSM-840 scanning electron microprobe at Oxford Brookes University was used for selected mineral phases from polished thin-section of the gold-bearing quartz vein samples (Appendix A). The samples were covered by a thin film of the graphite and analytical results (Figs. 5.7, 5.9) were obtained employing a LINK interface (Potts 1987, p. 364).

2) Data (see Appendix A for location)
 a) using ICP-AES at Royal Holloway College

Rock No.	43	71	72	73	167	316	342	370	384	391	391-1	392-1	393	396
SiO ₂	48.50	63.25	64.90	73.99	71.42	62.92	50.72	77.54	62.16	50.85	52.24	6.39	63.44	57.46
Al ₂ O ₃	16.67	15.59	16.31	13.98	12.99	15.12	16.97	12.64	17.56	16.21	12.29	0.35	11.69	15.54
Fe ₂ O ₃	10.14	7.51	8.42	1.22	2.70	6.03	10.86	1.47	4.51	8.69	7.19	0.48	4.79	7.72
MgO	4.59	2.54	3.24	0.22	1.18	2.98	6.93	0.04	2.79	5.90	4.98	3.77	2.13	3.63
CaO	11.68	4.50	0.72	1.28	3.76	5.09	7.82	0.25	5.62	7.32	8.66	53.36	6.48	7.83
Na ₂ O	0.74	3.78	1.31	3.88	5.22	3.08	3.06	4.26	3.91	3.85	3.55	0.05	2.97	2.39
K ₂ O	0.05	0.75	2.58	3.93	0.25	2.13	0.12	4.20	0.83	0.53	0.56	0.08	1.17	0.26
TiO ₂	0.62	0.52	0.60	0.07	0.19	0.80	0.53	0.04	0.48	1.46	0.91	0.01	0.63	0.42
P ₂ O ₅	0.15	0.16	0.15	0.05	0.11	0.18	0.15	0.03	0.17	0.26	0.21	0.19	0.18	0.14
MnO	0.15	0.10	0.09	0.05	0.05	0.09	0.18	0.01	0.07	0.11	0.17	0.03	0.15	0.14
Loi	4.34	2.38	3.14	1.45	1.98	1.59	3.19	0.15	2.54	4.52	7.23	33.8	4.50	3.03
Total	97.72	101.08	101.46	100.12	99.85	100.01	100.53	100.93	100.64	99.70	97.99	98.81	98.13	98.56
Rb				120		42		149						
Ba	16	148	342	356	57	344	36	25	271	180	144	28	290	89
Co	22	18	15	3	8	17	37	3	16	30	25	9	16	23
Cr	222	280	160	121	118	251	289	215	309	223	230	28	134	111
Cu	163	48	47	9	32	266	142	6	107	125	126	4	33	70
Li	17	16	34	22	4	9	15	5	19	6	5	24	12	9
Nb	0	3	6	5	1	4	1	67	2	2	1	4	5	2
Ni	28	34	44	4	7	33	38	8	46	112	142	30	45	20
Sc	41	21	22	3	6	15	45	0	10	19	14	1	11	28
Sr	426	301	71	98	274	336	129	9	470	662	392	431	340	193
V	340	95	174	7	40	130	283	8	87	160	120	10	89	168
Y	11	40	11	8	26	25	10	69	10	25	18	3	20	22
Zn	106	206	105	44	23	3020	118	63	160	66	49	22	49	60
Zr	44	237	186	95	221	277	47	214	107	161	139	5	119	77
La	4	24	21	18	31	23	8	37	18	11	9	63	24	10
Ce	2	40	43	33	62	46	5	51	27	21	15	34	41	14
Nd	2	19	13	11	22	22	3	22	12	14	10	20	15	6
Sm	0.2	4.8	3.6	2.5	4.5	4.9	0.5	6.6	2.3	3.4	2.5	3.1	3.3	1.7
Eu	0.3	1.2	0.6	0.3	0.7	0.9	0.4	0.1	0.7	1.1	0.8	0.5	0.7	0.5
Dy	0.6	4.8	1.1	0.5	2.9	2.8	0.5	6.2	0.6	3.1	2.1	0.6	2.1	2.0
Yb	0.7	2.8	1.2	0.7	2.3	1.8	0.7	6.7	0.5	1.4	1.1	0.3	1.4	1.8

Rock No.	398-8	399-6	401-1	401-2	402	402-1	404	404-1	407-1	407-2	407-3	407-5	412	413
SiO ₂	58.39	29.68	60.26	56.45	50.30	53.86	53.58	54.42	36.37	43.18	43.85	29.10	46.32	63.94
Al ₂ O ₃	14.37	5.17	18.48	13.47	16.23	14.91	16.43	18.94	2.46	2.13	1.82	18.41	12.78	15.71
Fe ₂ O ₃	5.77	2.64	8.53	5.73	10.04	7.40	8.25	8.05	8.62	8.92	9.70	12.46	16.15	4.37
MgO	4.04	11.32	3.57	6.49	6.33	2.44	5.40	4.44	21.29	22.99	26.53	26.43	4.06	2.27
CaO	3.91	18.30	0.72	9.50	7.39	6.73	3.64	4.92	14.73	10.82	7.61	0.62	7.47	4.51
Na ₂ O	2.99	0.50	1.59	1.98	2.79	1.53	3.50	4.11	0.08	0.07	0.04	0.09	2.12	4.31
K ₂ O	2.77	1.22	3.66	3.08	0.76	2.13	1.55	0.66	0.04	0.03	0.03	0.04	0.13	1.01
TiO ₂	0.55	0.11	0.95	0.65	0.94	0.56	0.36	0.56	0.14	0.19	0.12	0.60	3.22	0.50
P ₂ O ₅	0.23	0.20	0.21	0.25	0.22	0.17	0.18	0.19	0.14	0.14	0.22	0.29	0.84	0.15
MnO	0.08	0.06	0.09	0.12	0.17	0.13	0.14	0.12	0.17	0.15	0.18	0.20	0.24	0.08
Loi	5.63	29.70	21.9	2.01	1.88	9.91	7.05	4.7	14.67	9.93	9.91	11.52	6.62	2.45
Total	98.73	98.92	99.96	99.73	97.05	99.77	99.08	101.02	98.71	98.55	100.01	99.76	99.94	99.30
Ba	641	259	703	458	197	269	423	239	45	8	45	13	96	301
Co	17	12	20	18	29	24	23	26	72	65	79	32	26	14
Cr	98	113	209	120	292	217	201	184	2423	2486	2091	49	66	122
Cu	25	19	20	14	13	7	100	48	20	13	21	6	36	26
Li	35	6	92	26	21	21	35	34	2	1	2	3	29	11
Nb	8	2	15	14	4	4	1	3	0	2	2	3	33	2
Ni	35	7	70	39	69	46	56	38	710	586	626	74	13	21
Sc	11	6	22	13	28	21	24	24	52	56	39	16	29	9
Sr	227	175	65	217	309	180	216	459	40	49	19	19	587	534
V	91	44	167	95	185	149	172	180	129	131	85	201	214	84
Y	27	13	20	34	24	12	17	18	6	4	3	8	64	10
Zn	81	52	114	77	92	70	96	72	39	41	47	100	149	54
Zr	221	60	232	223	119	95	113	129	21	14	11	87	308	95
La	48	7	40	44	15	15	15	13	1	4	8	7	40	14
Ce	85	22	83	84	27	23	23	19	1	1	4	10	91	22
Nd	28	6	28	30	13	10	9	9	2	2	2	4	47	9
Sm	5.6	1.4	7.0	6.0	3.0	2.5	2.4	2.2	0.7	1.0	0.9	1.0	11.2	1.9
Eu	1.1	0.3	1.1	1.0	0.7	0.5	0.7	0.7	0.2	0.3	0.3	0.3	2.6	0.6
Dy	3.3	1.2	2.5	4.0	2.5	1.3	1.6	1.7	0.4	0.4	0.3	0.4	8.7	0.7
Yb	2.3	0.9	2.1	2.7	1.9	1.0	1.4	1.4	0.3	0.2	0.1	0.6	4.5	0.7

Rock No.	413-1	414	415	416	416-1	417-1	418	422	422-1	424	425	700
SiO ₂	65.70	49.46	75.55	51.59	44.05	47.22	57.65	49.85	42.39	59.65	60.15	74.42
Al ₂ O ₃	13.65	15.04	12.83	14.21	13.17	13.28	17.66	17.55	14.55	17.33	16.37	13.54
Fe ₂ O ₃	4.68	10.93	3.87	10.99	9.04	10.91	5.71	8.99	11.49	5.49	6.82	1.64
MgO	0.50	8.18	0.42	4.23	7.39	12.68	4.41	5.75	6.69	3.74	3.03	0.19
CaO	4.04	8.25	0.51	10.31	11.57	4.89	7.01	9.43	11.61	6.61	5.28	0.60
Na ₂ O	6.07	4.13	4.73	3.10	1.63	0.03	3.91	3.71	1.33	3.80	1.16	3.81
K ₂ O	0.15	0.25	1.49	0.21	0.09	0.02	0.26	0.49	0.04	1.03	0.89	5.27
TiO ₂	0.36	1.01	0.24	0.96	0.60	0.68	0.63	0.64	0.62	0.58	0.77	0.21
P ₂ O ₅	0.12	0.19	0.04	0.17	0.15	0.22	0.22	0.21	0.27	0.21	0.18	0.04
MnO	0.14	0.16	0.05	0.24	0.15	0.16	0.08	0.16	0.20	0.08	0.10	0.01
Loi	1.78	0.67	0.87	3.86	11.7	9.19	2.35	2.54	8.94	1.66	4.63	0.40
Total	97.19	98.29	100.82	100.17	99.54	99.28	99.89	99.62	98.13	100.18	99.36	100.20
Rb												86
Ba	60	34	400	52	29	9	125	103	26	194	198	390
Co	6	37	4	31	36	28	20	32	34	20	14	4
Cr	151	389	155	87	141	1161	206	278	128	290	161	223
Cu	5	30	21	10	95	5	52	61	350	59	48	8
Li	6	9	11	9	21	73	14	6	5	13	49	8
Nb	3	2	7	1	1	2	2	1	1	2	7	8
Ni	8	110	10	14	31	382	63	60	29	50	38	10
Sc	19	35	8	30	44	28	15	29	39	14	22	2
Sr	104	270	62	167	244	99	661	459	410	527	568	118
V	10	309	12	286	223	223	117	213	256	116	164	16
Y	50	28	35	30	20	9	11	18	18	12	26	15
Zn	70	70	80	83	56	95	58	65	72	56	61	22
Zr	47	126	394	116	60	63	92	38	50	101	163	171
La	14	9	21	6	4	15	17	7	7	20	23	69
Ce	25	11	59	8	5	23	32	9	9	39	41	121
Nd	13	9	29	6	4	13	16	5	6	17	16	27
Sm	4.2	2.5	9.8	1.8	1.3	3.2	3.3	1.4	1.4	3.5	4.0	4.7
Eu	1.0	0.7	1.3	0.7	0.5	0.7	0.8	0.5	0.5	0.8	0.9	0.5
Dy	5.4	3.1	4.5	3.0	2.0	1.1	1.0	1.5	1.7	1.2	2.8	1.6
Yb	4.5	1.9	5.8	2.5	1.5	0.7	0.7	1.4	1.2	0.7	2.1	1.0

(2b) Chemical analyses of selected samples from Kilkobob Succession; using XRF, University of Luton

Rock No.	118	125	127	353	357	363	365	368-3
SiO ₂	58.6	59.14	48.16	62.31	60.25	64.7	68.37	59.07
Al ₂ O ₃	14.25	14.15	10.26	12.92	15.25	12.92	13.77	12.21
Fe ₂ O ₃	8.89	8.88	10.20	6.57	10.18	6.19	7.44	10.53
MgO	1.20	1.7	5.52	2.66	1.23	1.60	1.13	2.60
CaO	5.63	3.95	8.73	8.80	6.24	5.58	6.69	6.91
Na ₂ O	0.08	2.18	1.08	0.85	0.73	2.36	0.34	0.74
K ₂ O	1.47	1.22	0.17	1.85	0.95	2.65	0.35	0.72
TiO ₂	1.60	0.84	1.46	0.57	1.54	0.75	1.18	1.70
P ₂ O ₅	0.20	0.15	0.20	0.21	0.12	0.18	0.23	0.23
MnO	0.13	0.09	0.17	0.07	0.12	0.07	0.13	0.13
Loi	9.20	6.10	11.20	2.00	3.00	1.50	0.89	3.30
Total	101.25	98.40	97.15	98.81	99.70	98.50	100.52	98.14
Sr	243	20	17	290	21	217	317	333
Zn	58	147	55	5	52	110	145	152
V	223	105	182	71	182	88	138	180
Cu	17	36	<10	18	16	16	65	15
Ni	20	100	126	77	18	59	20	10
Ba	110	340	410	405	397	86	364	390
Cr	206	160	210	120	118	163	215	218
Zr	187	54	126	165	68	124	125	176
Nb	<5	<10	65	10	<5	<5	33	<5
Rb	78	70	18	88	56	94	35	84
Co	10	9	12	8	10	8	9	13

(3b) An estimate of the measurement errors of the geochemical analyses by ICP-AES method using the standard gabbro sample

Elements	Maximum	Mean*	Minimum
SiO ₂	55.94 %	55.71 %	55.34 %
Al ₂ O ₃	16.01 %	15.46 %	14.97 %
Fe ₂ O ₃	8.71 %	8.57 %	8.43 %
MgO	3.85 %	3.73 %	3.62 %
CaO	7.14 %	7.04 %	6.85 %
Na ₂ O	3.17 %	3.02 %	2.90 %
K ₂ O	2.08 %	1.99 %	1.92 %
TiO ₂	1.11 %	1.08 %	1.06 %
P ₂ O ₅	0.33 %	0.323 %	0.32 %
MnO	0.14 %	0.14 %	0.14 %
Ba	474 ppm	455 ppm	439 ppm
Co	34 ppm	33.3 ppm	33 ppm
Cr	121 ppm	119 ppm	118 ppm
Cu	108 ppm	104 ppm	101 ppm
Li	384 ppm	367 ppm	352 ppm
Nb	19 ppm	19 ppm	19 ppm
Ni	293 ppm	287 ppm	280 ppm
Sc	24 ppm	23.2 ppm	23 ppm
Sr	383 ppm	367 ppm	354 ppm
V	214 ppm	210 ppm	206 ppm
Y	26 ppm	25.2 ppm	25 ppm
Zn	124 ppm	119 ppm	117 ppm
Zr	31 ppm	30 ppm	29 ppm
La	45 ppm	44.7 ppm	44 ppm
Ce	61 ppm	60 ppm	58 ppm
Nd	81 ppm	80 ppm	78 ppm
Sm	8.9 ppm	8.8 ppm	8.6 ppm
Eu	15 ppm	1.5 ppm	1.5 ppm
Dy	5 ppm	4.97 ppm	4.9 ppm
Yb	3.6 ppm	3.55 ppm	3.4 ppm

* of 6 measurements

Conclusion

The precision is high and the operator/machine error is low

Precision

Each sample was replicated thrice and the mean value calculated and used for plotting and discussion

Accuracy

This was carried out with reference to the standard gabbro by measurement every fifth sample so that drift and other sources of error would be corrected.

(2c) Gold analyses-using NERC ICP-MS facilities

Sample No.	sample type	Concentration	Location
319	wall-rock	0.28 ppm	Atshani
319.3	quartz vein	0.15 ppm	Atshani
320	quartz vein	0.11 ppm	Atshani
399	quartz vein	0.07 ppm	Allaqi Shear-zone
600	quartz vein	6.98 ppm	Um Garayat gold mine
601	quartz vein	5.6 ppm	Um Garayat gold mine
383.2	quartz vein	5.3 ppm	Nagib

N.B. Other samples (see Appendix A) registered a nil concentration.

Appendix C Strain data

Location 328	X	Y	Z
extracted	4.5	4	2.7
volcanic	3.5	3	1
rock clasts	6	4	1.5
set in a fine-	4	2.7	2
grained	6	2.5	2
volcaniclastic	10.5	3.1	1.5
matrix	8.5	3.5	1.5
	11	4	2.5
	7	3	1.5
	7	3	1.3
	10	6	2.5
	10	2.7	1
	3	2	0.7
	4.5	2	1
	6	4	2
	5	3	1
	5	1.5	0.7
	4	2.2	1.2
	7	2.5	1.2
	3.2	2	1.2
	3.5	1.5	0.7
	10	5.5	3
	2	2	1
	4.5	2.5	1.5
	4	2.5	1.5
	2.5	1.5	0.7
	4	2.5	1
	3	1.5	1
	7.5	2.5	1
	7	1.7	1
	3	1	0.7
	8	2.5	1.5
	4	1.5	0.6
	4	1.5	1
	6	2	1
	4.5	1	0.8
	5	1.5	1
	6.5	4.5	3
	6	2.5	2
	6	2	1.5
	5	2.5	2
	6	3	1
	2.5	1.5	1.3
	5	2.5	2
	5	1	1
	11	5.5	3.5

continued page

	5	2	1
	7	3	2
	4	2	1
	8	3	1

Location 331	X	Y	Z
	20	13	10
extracted	12	11	3
volcanic	13	8.5	1.5
rock clasts	13	7	1
set in a fine-	15	10	3
grained	25	15	2.5
volcaniclastic	28	17	1
matrix	4	3	0.7
	14	5	0.6
	9	6	0.5
	8	6.5	0.5
	5	4	0.5
	5	3	0.5
	25	17	1.5
	16	8	2
	43	15	2
	28	27	3.5
	12	7	1
	19	11	4
	2	1.5	0.3
	4	3	0.5
	4	2	0.3
	25	7	2.5
	7	3	2
	8	5	1

Location 334	X	Y	Z
	10	6	4
extracted	13	8	1
volcanic	21	9	1.3
rock clasts	15	11	1.19
set in a fine-	5.5	3.5	0.5
grained	8	4.5	0.5
volcaniclastic	9	5.2	0.69
matrix	7.5	4.5	1
	6	3	0.8
	15	9.5	1
	8	5.5	0.6
	15	6	3
	8	5.5	0.7
	9	6.5	0.5
	5.2	2.2	0.5
	2.2	1.7	0.5
	7	4.2	1
	6.9	5	2
	9	6	1
	8.5	6	1.5
	5	4	0.5
	10	5.5	0.6
	9	3.7	0.5
	6.2	2.6	2.4
	5.2	3.5	0.5
	7	3	1
	11	5	0.7
	16	6.5	1
	5.5	4	0.4
	10.5	5	1
	5.2	2	0.5
	7.5	6	0.3
	5.5	3.5	0.5
	9.5	6	1
	11	6.5	0.7
	7	5	0.5
	9	5.5	1
	9	4.5	0.6
	6.5	2.5	1
	10	6	0.6
	8.5	4	0.8
	8	2	0.6
	6	2.5	0.3
	5.5	4.5	1
	3.5	2.5	1
	6	2.5	0.7
	7	3.2	0.3
	4	2.5	0.5

Continued page

	6	3	1
	5	3.5	0.5
	5.5	2.5	1.2
	4.2	2.2	1

Location 345	8	5	3
	6	4	3
extracted	5	3.5	2.2
volcanic	4.5	2.7	2.3
rock pebbles	8	5.5	3.5
set in a fine-	10	5.5	3.5
grained	6	4	2.2
volcaniclastic	6	4	1.2
matrix	6	4	1
	7.5	4	1
	14	9.5	4.5
	6.5	5.5	1.2
	10	6	2
	10	7	2
	10	8	1.5
	8	4.5	1.5
	5	2.5	1
	8	6	3.5
	5.5	4.5	1.2
	14	7	2.5
	8	3	1.3
	6.5	4	0.5
	7	4.5	2
	17	6	4
	8	5.5	2
	7	5	0.5
	6	4	1
	10	7	2
	14	10	2.5
	10.5	6.5	1
	8.5	5	1
	21	10	3
	14	8	2
	7	4.5	1.5
	9	6	3.5
	11	7	1.8
	7	4.5	1.5
	11	6	1.5
	9	6	2
	8.5	4.2	1.3
	10	3.5	1.5
	13	8.5	3
	6	3	1
	6.2	2.5	0.7
	10	6	1
	7	3.5	0.5
	5	4	1.5
	9	3.2	1.2
	3	2	1.2

Continued page

	5	3.5	0.7
	5	3	2
	5.5	4	0.7
	9	6.5	1.5
	16	6	5
	8.5	3.5	1.5
	12	6	3

Location 167	X	Y	Z
	7	6.5	4.5
extracted	12	8.5	5
granitic	13	8.5	6
pebbles	9	6	2.5
set in	13	10	5.5
a greywacke	12	7.5	3
matrix	15	11	5
	20	7	4.5
	14	7	2
	25	10	4
	23	10	5
	17	8	3
	14	8	4
	12	9	5
	6	4.5	3
	30	22	11
	8	6.5	3.5
	10	6	3
	11	10	9
	11	9	7
	8	6	4.5
	12	7	5
	7	5	1.5
	6	4	2.5
	25	8.5	1.5
	8	5	3
	10	8	4
	10	6	2
	9.5	4	2
	8	4	2
	8	6	4
	8	6	3.5
	11	8	5
	9	5	2
	17	15	9

Rf / ϕ data

Location 167	X	Y	Rf	ϕ
	4.9	0.8	6.1	18
S1290/68NW	2.4	0.6	4	21
	1.4	0.4	3.2	33
	4.1	0.75	5.5	29
	1.5	0.3	5	20
	3.3	0.6	5.5	21
	3.3	0.6	5.5	27
	3.2	0.5	6.4	25
	2	0.4	5	21
	5.1	0.9	5.7	17
	2.3	1.1	2.1	6
	3.6	1.1	3.3	28
	1.6	0.4	4	31
	4.5	0.6	7.5	22
	1.3	0.4	3.3	30
	3.2	0.7	4.6	15
	1.9	0.5	3.8	15
	1.6	0.5	3.2	21
	1.8	0.6	3	14
	3.6	0.5	7.2	22
	2.8	0.6	4.7	25
	3.5	0.5	7	19
	1.2	0.3	4	32
	1.7	0.45	3.8	20
	4	0.6	6.7	25
	7	0.7	10	25
	1.8	0.5	3.6	21
	2.8	0.9	3.1	18
	3.2	1.1	2.9	34
	1.2	0.3	4	19
	2.5	0.7	3.6	19
	3.1	0.8	3.9	34

Location 357	X	Y	Rf	ϕ
	3.5	1.65	2.1	6
S1 272/65 N	1.8	1.5	1.2	15
	3.3	1.15	2.9	18
	1.9	1.5	1.3	90
	1	0.5	2	14
	0.6	0.5	1.2	56
	2.5	1.3	1.9	29
	0.7	0.5	1.4	58
	1.3	1	1.3	71
	1.9	1	1.9	77
	0.5	0.5	1	90
	1.9	0.7	2.7	42
	2.6	2.6	1	90
	2.4	1.3	1.8	26
	1.7	1.7	1	90
	2	1.2	1.7	10
	2	1.2	1.7	90
	2.5	2.3	1.1	53
	1.5	0.7	2.1	57
	2.8	0.8	1	90
	0.9	0.9	1	90
	2.3	2.2	1	90
	2.2	1.8	1.2	76
	1.2	0.95	1.3	17
	1.8	1.65	1.1	90
	2.45	1.5	1.6	21
	2	1.6	1.3	16

Appendix D Fluid inclusion methodology and data

(a) Fluid inclusion methodology. Carefully selected samples from quartz veins provided the predominant fluid inclusion types. Doubly polished wafers were cut from the quartz and microthermometry was carried out on an improved Linkam heating and freezing stage at Kingston University (Rankin *et al.* 1990). Measurements were taken from quartz grains represent primary inclusions, formed contemporaneously with the barren and gold-bearing vein assemblage. These inclusions were either two-phase (aqueous - liquid carbon dioxide) or three-phase (aqueous - liquid carbon dioxide - vapour) at room temperature. The fluid inclusion studies have been carried out on quartz sampled from; quartz vein from Atshani old gold working. Material for study was prepared according to the procedure described by Shepherd *et al.*, (1985). 100 - 110 μm thick polished wafers were prepared and used to examine the size, distribution and relative abundances of the different inclusion types. A classification depended on their distribution and occurrence; a) primary; b) or secondary and their phase ratios (H_2O and CO_2). Good and suitable inclusions have been selected for the heating freezing stage from the different groups of inclusions.

(b) Fluid inclusion data

Sample No.	Location	Type of inclusion	Th	Te
319	Atshani quartz vein	Type 1	29°C±2	
		Type 2	100°C±20 90°C±5 100°C±10	
320	Atshani quartz vein	Type 3	100°C±10 100°C±7 100°C±20	
		Type 5	165°C±3 1165°C	-22°C
390	quartz vein from shear-zone in the Kazzaz Formation	Type 4	190°C±10 190°C 190°C±5 198°C ±5 190°C±10 195°C±4	

Appendix E Stable isotope methodologies and data

(a) *Methodologies.* Mineral separates were obtained by hand-picking from crushed and sieved quartz veins. the separates were then cleaned in hot concentrated hydrochloric acid rinsed and dried before been powdered.

- 1) grind samples to obtain at least 50 g;
- 2) sieve and collect at least 10 g of material through a 200 mesh sieve;
- 3) wash sample with 4n HCl (placed in beaker, added 30 ml 4n HCl, left overnight, filtered, washed with hot distilled water and dried)
- 4) dry and collect at least 40 mg. material;
- 5) place into capsules with identification tags ready for transmission to SURRC, east Kilbride.

The δ values for oxygen and hydrogen stable isotopes were calculated using the following formulae :

$$\delta^{18}\text{O}\text{‰} = \left[\frac{^{18}\text{O} / ^{16}\text{O} (\text{sample}) - ^{18}\text{O} / ^{16}\text{O} (\text{standard})}{^{18}\text{O} / ^{16}\text{O} (\text{standard})} \right] \times 1000$$

$$\delta\text{D}\text{‰} = \left[\frac{\text{D} / \text{H} (\text{sample}) - \text{D} / \text{H} (\text{standard})}{\text{D} / \text{H} (\text{standard})} \right] \times 1000$$

(b) Stable isotope data (for location see Appendix A)

Sample No.	Description	Location	$\delta^{18}\text{O}\text{‰}$ SMOW	$\delta\text{D}\text{‰}$ SMOW
319.3	qz vein	Atshani	10.1	-
320	qz vein	Atshani	11.4	-
383.2	qz vein	Nagib occurrence	9.7	-
390	qz vein	Kazzaz Formation	10.3	-
398.4	qz vein	Allaqi Shear-zone	14.6	-
398.5	qz vein	Allaqi Shear-zone	15.6	-
500	qz vein	Um Geir	15.2 ; 14.8	-71
600	qz vein	Um Garayat gold mine	7.8	-
601	qz vein	Um Garayat gold mine	12.9	-89

Appendix F UTM co-ordinate methodology

Egyptian topographical maps do not have a national grid co-ordinate system. In order to locate the positions of rock samples and geological data, particularly lithostratigraphical and structural as precisely as possible, it was decided to use the globally applicable ten-figure Universal Transverse Mercator (UTM) co-ordinate system for the central Wadi Allaqi area. With the help of the Geodetic Support Branch (Geography & Geodesy Division, Production Group) of the Military Survey at Feltham a UTM graticule was prepared for the whole area using Latitude 22° 19' 00" N and Longitude 33° 30' 00" E for the south-west corner and Latitude 22° 36' 00" N and Longitude 33° 47' 00" E for the north-east corner in zone 36 using the international spheroid and the Transverse Mercator projection. The map was gridded using the following procedure :

- 1- the UTM co-ordinates were computed for the longitudes and latitudes of the four corners of the area using the expression :

$$C'' = (\lambda - \lambda_0) \cdot \sin \phi_m \quad \text{where } \lambda \text{ is the longitude of}$$

the map edge

and ϕ_m is the latitude of the mid-

point

- 2- marginal grid lines were selected to the appropriate metric scale and the difference of co-ordinates between the grid and the nearest map corner is used to calculate the *cutting distance* of the grid line along the map edge. The curvature of the parallels was ignored as in the central Wadi Allaqi area this would give no plottable error since the marginal lines are close to the map edges
- 3- using graph paper with appropriate divisions the marginal grid lines were constructed and the remainder of the grid mesh was plotted by direct measurement within this framework

For the central Wadi Allaqi area the origin was taken as longitude $33^{\circ} 00'$ E and latitude $0^{\circ} 00'$; the false co-ordinates were taken as 500000m E and 0m N, and the scale factor was 0.9996.